Strategic design of flow structures for single (bio) particle analysis using droplet microfluidic platform

by

Thu Hoang Anh Nguyen

A thesis
presented to the University of Waterloo
in fulfillment of the
thesis requirement for the degree of
Doctor of Philosophy
in
Mechanical and Mechatronics Engineering
(Nanotechnology)

Waterloo, Ontario, Canada, 2019

Examining Committee Membership

The following served on the Examining Committee for this thesis. The decision of the Examining Committee is by majority vote.

External Examiner:	**Associate Professor Carlos Escobedo** Department of Chemical Engineering Faculty of Engineering and Applied Science Queen's University, Ontario, Canada
Supervisor:	**Professor Carolyn L. Ren** Department of Mechanical and Mechatronics Engineering Faculty of Engineering University of Waterloo, Ontario, Canada
Internal Member:	**Professor David Johnson** Department of Mechanical and Mechatronics Engineering Faculty of Engineering University of Waterloo, Ontario, Canada
Internal/External Member:	**Professor Shirley Tang** Department of Chemistry Faculty of Science University of Waterloo, Ontario, Canada
Internal/External Member:	**Associate Professor Shawn Wettig** School of Pharmacy University of Waterloo, Ontario, Canada

AUTHOR'S DECLARATION

I hereby declare that I am the sole author of this thesis. This is a true copy of the thesis, including any required final revisions, as accepted by my examiners.

I understand that my thesis may be made electronically available to the public.

Abstract

Over the past two decades, a growing body of literature has recognized the importance of droplet-based microfluidics. This advanced technology shows promise in enabling large scale interdisciplinary studies that require high throughput and accurate manipulation of reagents. Each droplet acts as a micro-sized reactor where complex reactions can be carried out on the micro-scale by splitting, mixing, sorting and merging droplets. Advantages of droplet-based microfluidics include miniature sample consumption, scaled-down reaction time, high-yield manipulation, rapid mixing, and negligible cross-contamination at channel walls. As a result, instead of continuing using conventional bench-top methods, many researchers working in different fields – such as pharmaceuticals, material sciences, biochemistry, and biology – have shifted their interest towards droplet-based microfluidic devices.

The majority of these applied research studies require the encapsulation of particles or cells that range from 1 μm to 200 μm inside droplets for further studies – i.e, on bead-based nanomaterial synthesis, cell culturing, tissue engineering, and so on. Successful encapsulation of particles with such a large size range challenges the design and operation of microfluidic channel networks. It is very common that a design suitable for encapsulation of 10μm cells completely fails when used to encapsulate 1μm magnetic beads for nanomaterial synthesis or 120 to 150μm embryoid bodies for development of mini-organs. Redesigning a microfluidic channel network to accommodate a new demand often leads to an entirely new project requiring extensive experience in droplet microfluidics and trial-and-error development. The vast majority of real-world applications also require multi-step reactions, involving the integration of multiple functions such as droplet generation, merging, mixing and precise splitting for controlling the reaction environment in the droplets. This adds an extra layer of difficulty in achieving robust performance. These challenges clearly point to the need for knowledge of droplet-based encapsulation strategies that will serve as a foundation for design and operation of microchannel

networks for real-world applications. Arguably, integrating active sources (electrical components, laser supplies, etc.) could realize cell or particle encapsulation using a relatively simple channel network design, however they are often unfavorable because of the limits of laboratory micro-fabrication. As a result of those challenges, there are not many commercialized droplet microfluidic devices, despite the extensive use of droplet microfluidics reported in the literature.

This thesis is designed to meet the need for knowledge of droplet-based encapsulation strategies by carrying out systematic fundamental studies based on a double-cross configuration. This configuration has been commonly used for co-encapsulation of particles or cells with multiple reagents. Particular attention is also paid to the simplicity and robustness of the channel network for real-world applications. Proposed methods of single particle encapsulation and integration of multiple functional components are validated by two projects. The goal of the first project is to co-encapsulate a 1μm magnetic bead (MB) with multiple Quantum Dots (QDs) for further bio-decorating the QD surfaces with different molecules (i.e. single strand DNA). The goal of the second project is to integrate in a single device a two-step reaction assay for functionalizing the surface of QDs with oligonucleotide strands while QDs are immobilized on MBs. The QD-Oligonucleotide conjugate serves as bio-sensing probes for nucleic acid detection. The comprehensive experimental study is designed to span a wide range of operating parameters. Since the validation of the proposed methods, namely, the above two projects, are carried out in parallel with a fundamental study of the controlling parameters and completed earlier, they are then presented first in this thesis. The detailed structure of the thesis is elaborated below.

The thesis starts with a study that demonstrates the use of a double-cross junction for co-encapsulation of a single 1 μm MB and a large number of QDs in an aqueous droplet. Specifically, a stratified flow structure is formed in the first junction which is well tuned to order MBs and the droplets are formed at the second junction by using the carrier fluid (i.e. silicon oil) to pinch the stratified flow structure. The formation of droplets in the second junction causes pressure fluctuations to occur during droplet

generation. By employing a 1-D electrical circuit analogy, the stratified flow structure is decoupled from these fluctuations. A chain of serpentine channels that provide chaotic mixing inside micro-droplets is added downstream of the double cross junction. This approach quickly reduces the conjugation time, resulting in high-yield MB-QD conjugating products. Performing the conjugation process on-chip offers a degree of precision in controlling local reaction conditions beyond a level possible in bulk solution reactions. A uniform and high-density coating of quantum dots on magnetic beads is thus obtained, substantially influencing the further functionalization of quantum dots with biomolecules.

Next, in the second project, the on-chip bio-functionalization of quantum dot surfaces is achieved using oligonucleotide strands as the biomolecules of choice. The continuous and rapid immobilization of oligonucleotide strands on QD surfaces requires the integration of multiple functionalities into a single microfluidic device. These functionalities include two droplet makers in parallel; a one-to-one droplet synchronizing component; a droplet merging chamber; and a series of serpentine channels for droplet mixing. A set of criteria are developed to ensure the coupling effects caused by the integration of multiple components on one platform are eliminated. Experiments are used to verify the throughput of this platform. Not only can the design be used to conjugate biomolecules and nanoparticles, it can also be applied in many kinds of research requiring two-step chemical reactions.

The above two projects not only validate the use of a double-cross geometry integrated with other functionalities for bio-modification of nanoparticles, but also suggest the focus of the fundamental study of its controlling parameters. This study aims to provide an overview of conditions altering the hydrodynamic focusing width and droplet generation, such as the flow rate ratio between two dispersed phases; the flow rate ratio between dispersed and continuous phases; the viscosity contrast ratio and the role of an orifice. This information can offer an experimental guideline for other non-specialists (biologists, chemical engineers, and tissue engineers) who would like to apply this platform to anysingle encapsulation studies. To demonstrate this practical guideline, the same microfluidic platform

used in the experimental study is employed to encapsulate single mouse embryonic stem cells in individual droplets. This specific application is a vital step for further cell culturing and studying single cell behaviors. Moreover, the knowledge of this study is useful for creating a microfluidic device that is able to enclose single embryoid bodies (a few hundred microns) in gel-droplets. Indeed, on-chip studying of spherical cell structures instead of monolayer structures is helpful for organoid growth research that supports potential drug discoveries and cancer treatments

Acknowledgements

Initially, I would like to thank my advisor, Prof. Carolyn L. Ren, for providing me with the opportunity to work under her guidance. I sincerely admire her passion for doing research and appreciate her expertise and encouragement that have inspired me to grow into an efficient and professional researcher. As well as, I am grateful for the financial support from Prof. Carolyn L. Ren. I would like to thank my thesis committee members for their roles in the committee and their insightful suggestions and comments.

My doctoral research would not be accomplished without support from Graduate Studies and Postdoctoral Affairs in the form of an International Doctoral Student Awards.

During my graduate schooling, I would not have gained many valuable experiences without the support of other members of the Waterloo Microfluidics Lab. My gratitude goes to my colleagues – Dr. Xiaoming Chen; Dr. Ning Qin; Dr. Gurkan Yesiloz; Dr. Pegah Pezeshkpour and David Wong – all of whom provided good advice and offered help along the early stages of my graduate studies. Please allow me to also thank Dr. Abootaleb Sedighi, who worked closely with me in the first two of my projects, under the advice of Prof. Ulrich Krull from the University of Toronto (Mississauga campus) and my advisor Prof. Carolyn L. Ren. It has been my great honor to work with him and learn basic knowledge about analytical chemistry. The assistance from both Dr. Abootaleb Sedighi and Dr. Xiaoming Chen during the initial stages of my thesis have been invaluable to me. I am boundlessly thankful to them for teaching me not only basic wet-lab techniques, but essentially, how to do research and think scientifically. I should also highlight here the immense role played by Prof. Evelyn Yim in the Department of Chemical Engineering, and that of her student – Sarah Chan – who helped to prepare samples in the last project affiliated with their tissue engineering research. At Waterloo, I am in awe of other great laboratory members – Marie Herbert, Jeremy Newton, Pei Zhao, Jeff Farnese, Weijia Cui,

Merve Marcali, and Matt Courtney – who attended weekly group meetings and provided beneficial input to my study.

I would not have made it this far on my research path if I had not received mental support from my family. I am absolutely grateful for the aid of my parents. I am also very thankful to my sister, Lavie Nguyen, and my fiancé, Johnny Truong, who have been behind me all the way. They have constantly reminded me how far I have come and why I am pursuing my Ph.D. research. Thanks to their reminders, I have kept chasing my dream to be a professional researcher in spite of the multiple challenges that I have faced. Lastly, I would like to extend my appreciation to many friends, especially Lucky Nguyen, Kate Nguyen, Linh Do, Vivian Nguyen, and Brian Pham who I have met and shared enjoyment with during many years at Waterloo.

Dedication

To my father, Nhuan Nguyen and my mother, Anh Hoang,

my sister, Lavie Nguyen and my Fiance, Johnny Truong,

for their lifelong endless love and hard work.

Table of Contents

List of Figures

List of Tables

Chapter 1: Introduction

1.1 The developing world of microfluidics

Since the early 2000s, Lab-on-a-chip (LOC) technology (Figure 1-1) has been driven by the desire of many bio/chemistry researchers to perform high throughput and low-cost bio/chemical reactions (Reyes et al. 2002; Stone, Stroock, and Ajdari 2004; Ziaie et al. 2004; Whitesides 2006; El-Ali, Sorger, and Jensen 2006; Y. Liu and Jiang 2017). The underlying idea is to scale down the sample volumes and dimensions of laboratory devices to improve the performances of conventional bench-top assays. Microfluidics, belonging to LOC technology, refers to a platform that allows researchers to control and to manipulate fluids on the length scale of microns. Many microfluidic platforms have played a significant role in life-sciences research diversity, including biology, drug discovery, clinical diagnostics, genetics research, chemical synthesis, biosensors, and so on (Squires and Quake 2005; El-Ali, Sorger, and Jensen 2006; Sackmann, Fulton, and Beebe 2014; Shembekar et al. 2016; Feng, Sun, and Jiang 2016; Miller et al. 2012; Faustino et al. 2016) The inherent advantages of these platforms include low-cost, shorter analysis times, as well as, reduced reagent consumption, minimized waste, and increased production capacity. Microfluidic devices are typically small enough to be hand-held, advancing their portability. More importantly, microfluidic chips contain micro-channels with length scales comparable to those of cells and biomolecules, making them useful in bio-related studies and chemistry (Vreeland et al. 2010; Whitesides 2006; Jayaraj, Kang, and Suh 2007; Dressler, Casadevall i Solvas, and DeMello 2017). Therefore, researchers benefit greatly from microfluidics devices. For instance, using microfluidic devices, they can investigate the kinetics of chemical reactions; do drugs screening; develop bio-sensing platforms, etc. and obtain high yields but at low cost (Shui, Eijkel, and van den Berg 2007; Rivet et al. 2011; Sesen, Alan, and Neild 2017; Dressler, Casadevall i Solvas, and DeMello 2017). As yet, microfluidic devices have not fully replaced conventional bench-top assays due to certain current limitations (Abgrall and Gué 2007).

Microfluidic devices include several components – mixers, valves, detectors, pumps, etc. that are connected by micro channels, which usually are on the order of 10 to 500 micrometers. The initial microfluidic devices were fabricated in glass or silicon by using microfabrication techniques; however, the cost was too high to be practical. Thanks to the novel fabrication process introduced in 1998, known as soft lithography, the fabrication cost has reduced dramatically (Xia and Whitesides 1998). Since then, the growth of LOC research, microfluidics in particular, has been exponentially increased. Generally, soft lithography is a micro-molding technique, where a polydimethylsiloxane (PDMS) pre-polymer mold is cast against a master with raised relief structures, representing the fluidic network. The mold is peeled from the master, cut off, and holes for injecting fluids are punched in it. To complete the microfluidic chip, the mold is bonded to another substrate, usually a glass slide coated with a thin layer of PDMS. Polydimethylsiloxane is optically transparent, largely insensate, bio-compatible, and can be withstand large temperature ranges in spite of its high rate of adsorption and absorption. Furthermore, by employing various surface treatments, users can modify the properties of PDMS; plus, a clean-room setting is not required for using PDMS and soft lithography. Therefore, in research, soft lithography and PDMS are preferred for making microfluidics chips – a part of LOC devices (P. Kim et al. 2008; Ren, Zhou, and Wu 2013; Faustino et al. 2016).

In the early days of microfluidics, most microfluidic devices were based on single phase systems consisting of various miscible aqueous phases (Papautsky and Frazier 2001; DeMello 2006). Fluids are mainly controlled by syringe pumps or pressure systems. A major concern in using single phase microfluidic devices is that samples come in direct contact with microchannel walls, resulting in wall-contamination which may cause sample impurities. The well-defined nature of laminar flow, such as its stability and sensitivity to channel geometries, does allow for the formation of unique working environments (Singh et al. 2002; Steinke and Kandlikar 2004; Vreeland et al. 2010). Nevertheless, the laminar flows inside micro channels, where viscous forces dominate inertial forces, impart significant

physical limitations in controlling reagents. For example, mixing two or more reagents together is uncontrollable because the mixing mainly depends on diffusion. Although a few studies have solved a mixing problem in single-phase microfluidic systems (Jacobson, McKnight, and Ramsey 1999; Vreeland et al. 2010; Ward and Fan 2015a), researchers have been attracted to another microfluidic system–known as two-phases microfluidics, specifically droplet-based microfluidics, which offers rapid mixing, plus no wall-contamination (Zhao and Middelberg 2011). Compared to single-phase microfluidics, two-phase microfluidic technology offers novel abilities, such as; targeted coalescence between droplets; mixing droplets in high throughput; providing tools for multi-step reactions by integrating different functions in one platform; manipulating individual droplets, and so on (Shui, Eijkel, and van den Berg 2007; Teh et al. 2008; Baroud, Gallaire, and Dangla 2010; Tomasz S. Kaminski, Scheler, and Garstecki 2016; Vladisavljević, Al Nuumani, and Nabavi 2017; Shang, Cheng, and Zhao 2017). Additionally, generated droplets – oil-in-water or water-in-oil – are separated from the channel walls by a very thin film of carrier fluid, which prevents adsorption and cross-contamination between those droplets as well as wall-contamination. The carrier fluid also transports individual droplets to desired processing locations for mixing, splitting or merging. Practically, droplets can be generated and manipulated at rates between 1 Hz to 20 kHz, depending on the need for throughput; thus, the technology provides researchers with greater flexibility and scales-up products effectively (Chong, Tan, Gañán-Calvo, et al. 2016; P. Zhu and Wang 2017). Compared with the state-of-the-art 96-well plates and robotics technology (i.e. digital microfluidics (K. Choi et al. 2012)), droplet microfluidics has demonstrated hundred-to-thousand-fold throughput and millions in cost reduction for applications. Thanks to these advantages, droplet microfluidic devices are recommended widely in numerous applications, specifically, screenings, chemical synthesis and diagnostics (Shestopalov, Tice, and Ismagilov 2004; Nisisako et al. 2006; B. W. Tan and Takeuchi 2007; Köster et al. 2008b; M. C. W. Chen, Gupta, and Cheung 2010; Courtney et al. 2016; Zubaite et al. 2017;

Giuffrida, Cigliana, and Spoto 2018; C. Liu et al. 2018).

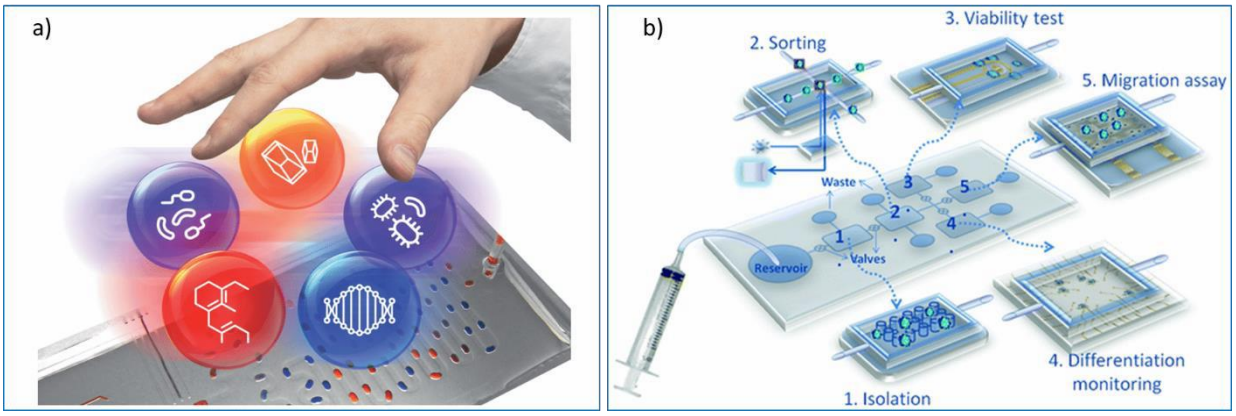

Figure 1-1. (a) Idea of controlled droplet microfluidic systems for multistep chemical assays (Kaminiski et al. 2017); (b) Cell chips as new tools for cell biology (Primiceri et al. 2013)

Although droplet microfluidic devices have been advocated for other life-science research, several challenges need to be solved (Shui et al. 2008; Casadevall I Solvas and Demello 2011). To design a multifunctional droplet-based LOC device that processes robustly is a significant obstacle, especially, when a passive droplet microfluidic platform is made to function only by the use of pressure sources (a syringe pump or pressure system). Many research groups have investigated the phenomena of droplets in micro-channels by fundamentally studying droplet formation (D R Link et al. 2004; G F Christopher and Anna 2007; Glawdel, Elbuken, and Ren 2012; van Loo et al. 2016; L. Wu et al. 2017), droplets coalescence (Aarts et al. 2005; K. Liu et al. 2007; X. Niu et al. 2008; X. Z. Niu et al. 2009), the resistance of droplets in micro-channels (Labrot et al. 2009; Parthiban and Khan 2013; Glawdel, Elbuken, and Ren 2011), etc., to provide the information needed for making robust passive droplet microfluidic designs. In contrast, integrating other active sources (acoustic waves, electrical signals, etc.) to manipulate droplets in a microfluidic platform would provide more flexibility. However, at this moment, the soft-lithography fabrication at laboratory scale does not allow for fabricating *perfect* polymer complex droplet-based LOC

devices integrated with external sources, making the devices complicated to micro-fabricate and scale up (Mukhopadhyay 2007).

In order to achieve the main objective of applying *passive* droplet microfluidics to other fields, particularly single cell engineering and single particle studies, an ideal microfluidic design should have the following features. First, the essential functions – generating droplets, encapsulating either single or multiple cells/particles and consistently injecting multiple reagents into droplets – should be included. Indeed, most bio/chemical applications and tissue engineering studies and analytical chemistry require those functions. Second, the design should be simple to fabricate by using the economical soft-lithography technique, leading to an expansion of droplet microfluidics' uses. Although soft lithography using PDMS is not an ideal fabrication technique to use in commercializing microfluidic devices, it still attracts researchers largely because alternatives, such as silicon micromachining, are more expensive. Lastly, in some applications that need more functionality, the integration of extra components – droplet splitting, sorting, or merging functions– should be less burdensome. To address these requirements, a double-cross geometry with stratified flow forming in between the two junctions is proposed.

This thesis focuses on applying the double-cross configuration and stratified flow structure occurring between the two cross junctions in different studies; specifically, (1) analytical chemistry and (2) tissue engineering. Additionally, the ability to passively integrate other functions, such as parallel droplet generation followed by droplet merging and mixing, with a current design is also achieved throughout this thesis work. This integrated microfluidic network shows the prospective applications in chemical or biological involving two-step reactions. Throughout this thesis, the physical parameters influencing the width of the hydrodynamic focusing (the inner stream of stratified flow) are comprehensively studied to provide an experimental guideline so that non-specialists can further utilize this research knowledge for achieving the single/multiple (bio) particles encapsulation. Hypothetically, a stratified flow structure occurring in between the two cross junctions allows researchers to generate monodispersed droplets

containing two to three miscible reagents and simultaneously to encapsulate multiple/single (bio) particles within those droplets. By the end of this thesis research, the double-cross geometry combining with a stratified flow structure will meet the three prerequisites: (1) to be simple, such that uncomplicated fabrication is capable, (2) to accomplish multiplex feasibility at the same time without external applied forces (electrical/optical) and (3) to be able to combine with the other compartmentalized functions, thus extending the capability of the droplet microfluidics.

1.2 Thesis outline

The rest of this thesis is organized as follows. Chapter 2 has two subsections. The first one provides an overview of droplet microfluidics showing the benefits of scaling-down current chemical and biological systems. The fundamentals of microfluidics, such as the various mechanisms used to generate, combine, mix, transport, and split droplets through microfluidic networks, are also discussed. The second presents a brief summary of basic concepts related to several applications that have used droplet microfluidic platforms.

Chapter 3 describes the fabrication technique and the laboratory setup for all experiments throughout this research.

Chapter 4 and Chapter 5 apply droplet microfluidics in an analytical chemistry study to achieve rapidly immobilize oligonucleotide strands on the surfaces of nanoparticles, synthesizing quantum dot oligonucleotide conjugates. After being released from solid phases, these conjugates act as bio-nano-probes which are used for nucleic acid detection. In particular, Chapter 4 describes the first step of the immobilization process, involving the conjugation between semiconductor nanoparticles and magnetic beads inside droplets using a double-cross geometry integrated with a series of serpentine channels. The design and flow conditions needed to achieve the single 1 μm magnetic bead encapsulated with multiple quantum dots in aqueous droplets are also discussed in detail. Chapter 5 covers the next step of the

conjugation, in which oligonucleotide strands are loaded onto the nanoparticle's surfaces. This step is conducted using a multifunctional microfluidic device that includes two droplet generators, a droplet synchronized component, a merging chamber and a mixer. The oligonucleotide strands conjugating with quantum dots are collected at the outlet and released from the magnetic beads serving as solid-based holders. The nucleic acid detection is used to characterize the quality of these conjugation products. Overall, this study suggested an approach to achieving bio-nano-sensors by using a magnetic solid-phase method combined with a passive droplet microfluidic device.

Chapter 6 presents the fundamental project that studies the impacts of experimental parameters on the formation of a hydrodynamic focusing formed by viscosity contrast stratified flow, occurring in between two cross junctions. In detail, the flow rate ratios, the viscosity contrasts, and the geometry of a double-cross junction are investigated. Therefore, the information obtained throughout this project provides experimental guideline for non-specialists to apply this approach in their studies involving the single (bio) particle encapsulation; for instance, the single encapsulation of single stem cells in aqueous/hydrogel droplets.

Chapter 7 summarizes the contribution of this thesis research to the academic research and briefly mentions potential future research toward manufacturing commercial products.

Chapter 2: An overview of microfluidics and its applications

Two-phase flow, which has been studied since the early 1800s, is a complex phenomenon in fluid mechanics. This short review chapter cannot cover the entire subject of two-phase flow, and it would be impractical to review all the aspects that are not related to this research. Hence, I narrow the topic to the scope of two-phase flow at micro-scale, specifically, segmented flow in micro-channels. The two-phase microfluidic flows is formed inside micro-channels when two immiscible fluids come into contact with each other. The most common two-phase flow systems in microfluidic devices are gas-liquid and liquid-liquid systems, known as bubbles and droplets, respectively. This chapter is divided into two main sub-sections: the first one covers the fundamentals of two-phase flow – droplet microfluidics and some features used to manipulate droplets/bubbles. The second part describes the potential applications of droplet microfluidics. Then, my personal motivation is briefly mentioned, connected to the research presented in Chapters 4-6.

2.1 Fundamentals of two-phase flow micro-system

2.1.1 Dimensionless number

In droplet microfluidics, two immiscible fluids both exist within the same device and come into contact with each other. In a confining channel, one phase (the dispersed phase) forms discrete bubbles/droplets that are surrounded by the other phase (the continuous phase) due to surface/interfacial tension. A balance between viscous, inertial, interfacial and gravitational forces dictates a two-phase microfluidic flow system (Dreyfus, Tabeling, and Willaime 2003; Stone, Stroock, and Ajdari 2004; Teh et al. 2008; Rosenfeld et al. 2014). The relative information represents the relationship among these forces, characterized by dimensionless numbers consisting of the Reynolds (*Re*), Capillary (*Ca*), Grashof (*Gr*), Bond (*Bo*), Weber (*We*) (Baroud, Gallaire, and Dangla 2010; P. Zhu and Wang 2017). Table 2.1.1 summarizes the scaling of these numbers with size. In microfluidics, the inertia and gravity force are

negligible in comparison to the viscous and interfacial forces because of the low flow velocity and high surface-to-volume ratio in flows at micro-scale. Thus, the Capillary number (viscous/interfacial) is the most important dimensionless number for analyzing micro-scale two-phase flow systems, such as droplet formation, coalescence, transportation, and so on. The Reynolds number (inertia/viscous) is another important dimensionless number, which is regularly low in microfluidics where the viscous force dominates the inertia force. The Grashof number (buoyancy/viscous), Bond number (gravitational/interfacial) and Weber number (inertia/interfacial) are not important in most microfluidic studies. In summary, the three independent variables that form the Capillary number: viscosity (Pa.s), flow velocity (m/s), surface tension (N/m), are employed to control overall droplet processing inside a systematic microfluidic network, such as generating droplets and splitting them (Garstecki, Stone, and Whitesides 2005; De Mench et al. 2008; van Loo et al. 2016; Doonan and Bailey 2017). The properties of the continuous phase are usually used to calculate the Capillary number (Glawdel, Elbuken, and Ren 2012; Glawdel and Ren 2012c). Similarly, the Capillary number, mentioned in this thesis' work, is based on the continuous phase properties. Additionally, the viscosity ratio between the two phases, and the flow rate ratio between them are introduced to support the studies of droplet-based microfluidics.

Dimensionless #	**Definition**	**Equation**	**Scaling**
Capillary	Viscous/Interfacial	$\frac{\mu U}{\gamma}$	0
Reynolds	Inertial/Viscous	$\frac{\rho U L}{\mu}$	1
Weber	Inertia/Interfacial	$\frac{\rho U^2 \mathrm{L}}{\gamma} = \mathrm{Ca} * Re$	1
Bond	Gravitational/Interfacial	$\frac{L^2(\rho - \rho_t)g}{g_c \gamma}$	2

Grashof	Buoyancy/Viscous	$\frac{L^3\rho^2\beta\Delta T}{\mu^2}$	3
Viscosity ratio	Dispersed viscosity/Continuous viscosity	$\frac{\mu_d}{\mu_c}$	0
Flow rate ratio	Dispersed flow rate/Continuous flow rate	$\frac{Q_d}{Q_c}$	0

Table 2-1. Dimensionless numbers

2.1.2 **Wettability, carrier fluid properties, surface tension and surfactants**

Along with the dimensionless numbers representing the competition among physical forces applying in droplet microfluidic systems, wettability, surface/interfacial tension, surfactants, and carrier fluids properties also play immense roles in droplet manipulation; especially in forming droplets and transporting them along micro-channels.

2.1.2.1 Wettability

While a two-phase system operates, two fluids are injected into separate micro-channels and come in direct contact with substrates that form the channels. Either both fluids completely/partially wet the channel walls or one wets the wall and the other one does not. Therefore, wettability should be considered (G F Christopher and Anna 2007; Boruah et al. 2018). The contact angle between the fluids with the substrate represents their wettability and is determined by a force balance on the three-phase contact line. In this research, the two-phase system is a liquid-liquid system consisting of liquid 1, liquid 2 and a solid substrate (the material forming the channel walls).

$$\gamma_{l1,l2} cos\theta_{eq} = \gamma_{s,l2} - \gamma_{s,l1} \quad (2.1)$$

where γ is the interfacial tension between phases, and θ is an equilibrium contact angle. The wetting conditions strongly influence the formation and transport of droplets in micro-channels. To produce stable flow regimes, the continuous phase should wet the walls; whereas, the disperse phase should not (Dreyfus, Tabeling, and Willaime 2003; Garstecki, Stone, and Whitesides 2005; Gupta, Murshed, and Kumar 2009; Zhao and Middelberg 2011). Water-in-oil droplets are formed when micro-channels are hydrophobic – typically, oil wets the channel walls – and vice versa.

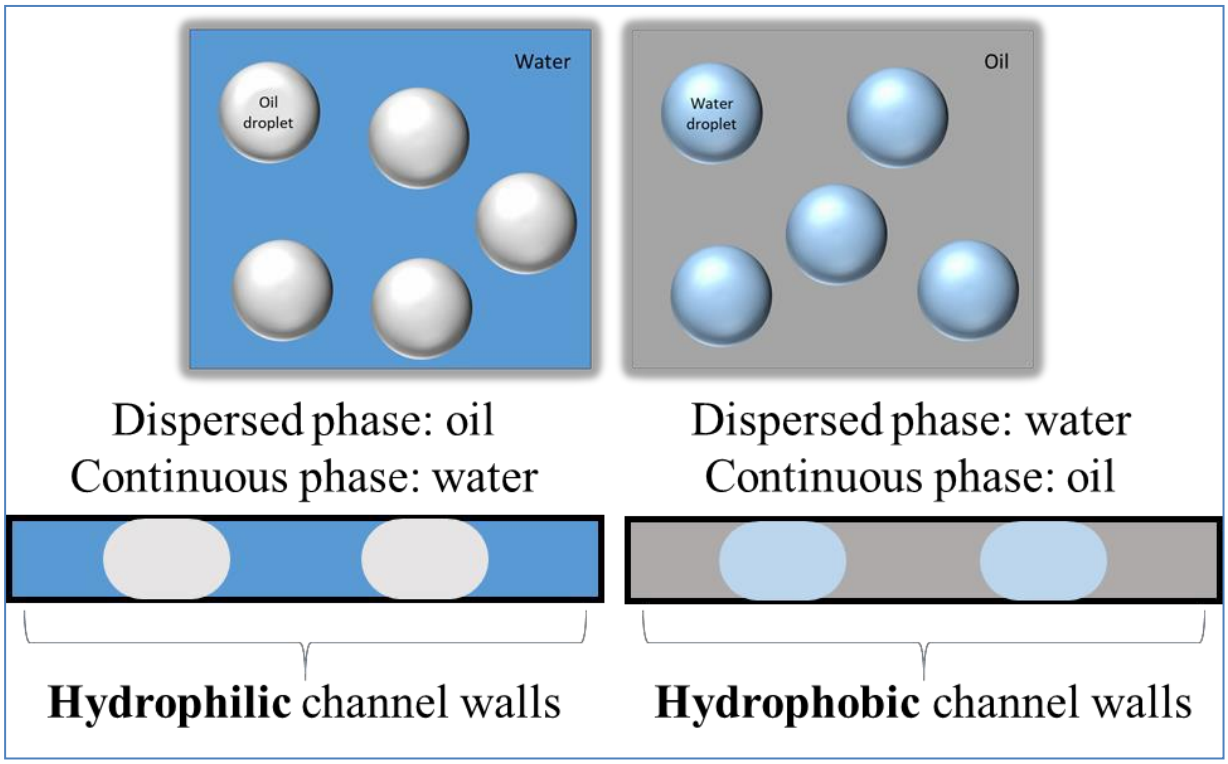

Figure 2-1. Oil-in-water droplets vs. Water-in-oil droplets and channel surfaces wettability

Hydrophobicity of the micro-channels is characterized by the contact angle between the fluids and the channels. Surfaces of micro-channels are hydrophilic when the contact angle is less than 90°; in contrast, it is hydrophobic when the contact angle is more than 90°. Throughout this thesis research, unless stated

otherwise, droplet-based microfluidic chips are operated to form water-in-oil droplets, requiring the hydrophobic microfluidic channels. Polydimethylsiloxane (PDMS) as mentioned in the beginning is the preferred material in microfluidics (Mukhopadhyay 2007; Ren, Zhou, and Wu 2013; Rosenfeld et al. 2014). It is naturally hydrophobic after cross-linking, so an oil phase wets the walls but a polar solvent, such as water does not. However, during the soft lithography fabrication process, PDMS surface chemistry transforms to hydrophilic due to Silanol group (Si–OH) on its surface introduced through the oxidation plasma that is used to bond the PDMS mold to another substrate (Darmakkolla et al. 2016; Wharton 2017). Therefore, surface treatments are required to turn the hydrophobic property back to provide suitable wettability for generating water-in-oil droplets. Details of the fabrication method and surface treatments will be discussed in the next chapter – Chapter 3.

2.1.2.2 Carrier fluids

Many types of oils have been used in microfluidic devices as carrier fluids, such as hexadecane, silicon oil, light mineral oil, perfluorinated solution, olive oil and sunflower oil. Researchers should choose compatible oils depending on the applications involved. For instance, for biological applications, a perfluorinated solution (FC 40 or FC 70) and light mineral oil are recommended because they are chemically and biologically inert, and cause less swelling of PDMS channels (Baret 2012; Rosenfeld et al. 2014). Silicon oil is also used in multiple applications, even though it does swell PDMS channels causing the changes of micro-channel dimensions over time (Rémi Dangla, Gallaire, and Baroud 2010). The swelling can reduce micro-channel sizes significantly, by up to 10%. Furthermore, a suitable oil viscosity must be chosen since it affects the continuous phase capillary number and the viscosity ratio between the two phases, as mentioned previously. The density of oil, which is usually lighter than that of the aqueous phase, should be carefully considered in some applications that require droplets to be collected and reinjected.

2.1.2.3 Surface/interfacial tension and surfactants

Unlike in single-phase microfluidics, interfacial tension is a critical factor in droplet-based microfluidics. The attractive force of fluid molecules at the interface of two fluids creates a net force that pulls those molecules inward. When two fluids meet, fluid strives to reduce its surface energy by reducing the interfacial area to resemble a spherical shape that is ideal for minimizing surface energy. In a micro-channel, the curved shape of a droplet creates pressure gradient across the interface, as defined by a Young-Laplace equation:

$$\Delta P = \gamma \mathcal{K} \quad (2.2)$$

where $\mathcal{K} = \frac{1}{R_1} + \frac{1}{R_2}$ is curvature of the interface and γ is interfacial tension. In some applications requiring droplets storage or collection, researchers need to use surfactants to stabilize droplets' interfaces and prevent them from fusing. The term "surfactant" is formed from the words: surface active agent. Each surfactant molecule contains a hydrophilic head and a hydrophobic tail, as illustrated in Figure 2-2 (Shui, Van Den Berg, and Eijkel 2009). In addition, surfactants are prepared in an oil phase or aqueous phase depending on their solubility as determined by the hydrophyl-lipophile balance (HLB) value. HLB values, presenting the balance of the size and strength of surfactant hydrophilic and hydrophobic parts, range from 0 to 20. Surfactants in the range of 3.5 to 6 are appropriate for generating water-in-oil droplets; whereas, ones in the range of 8 to 18 are common in oil-in-water droplets applications. Thus, the right surfactant needs to be chosen carefully beforehand. Furthermore, the concentration of surfactant plays a role in droplet formation and stabilization, as well as, in the dynamics transportation of surfactant molecular at the interface of droplets (Baret 2012). To determine the effect of a surfactant on droplet generation, Glawdel and Ren (2012) carefully performed an experimental study, finding that at high concentrations, surfactant molecules rapidly transport to the interface between two phases and stay there, resulting in an equilibrium interfacial tension during the expansion of the interface through droplet

formation. As a result, to avoid the problem of interfacial tension gradients at the interface, a high surfactant concentration approximately ten times higher than the critical micelle concentration (CMC) is suggested to use (Glawdel and Ren 2012a).

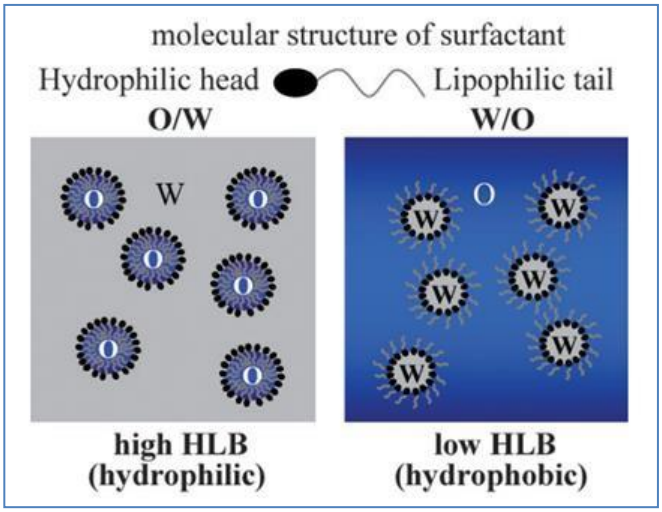

Figure 2-2. Surfactant structure and emulsion types in macroscale emulsion preparation corresponding to HLB values. O and W subscript oil and water phases, respectively (Shui et al. 2009)

2.1.3 **Droplet manipulation**

Droplet manipulation is a consequence of competition between forces, especially viscous force and interfacial tension. In particular, the competition between these two forces is represented by using the Capillary number which involves several independent variables: viscosity, interfacial tension, flow speed. These variables can be flexibly tuned. For instance, the viscosity can be changed by thermal manipulation, while interfacial tension can be altered by adding surfactants or by applying thermal effects. The shear stress on droplets can be changed by changing the flow speed (applied for Newtonian fluids). Overall, passive microfluidic systems are influenced by systematically changing flow rates, viscosity contrast between fluids, interfacial tension between phases, or locally changing the geometries of channels. As a result, researchers can design droplet microfluidic systems that consists of compartmentalized features: droplet generation, droplet break-up, droplet merging, etc. and implement them in different applications.

2.1.3.1 Droplet generation

Under laminar flow conditions, droplets are stably generated with controlled sizes at a range of frequencies from 1 Hz to 20 kHz. Droplet generation can be categorized: (1) *passive* droplet generation and (2) *active* droplet generation. This section mainly focuses on the passive methods to generate droplets which are Co-flowing, Flow-focusing and T-junction. Depending on the channel wettability, flow velocities, fluid viscosities, interfacial tension between phases and channel geometries, the two immiscible fluids that are injected into micro-channels can create either droplets or stratified flow patterns.

Co-flowing

The Co-flowing approach generating droplets is formed within two capillaries, where the inner capillary is used for a dispersed phase and the outer one is used for a continuous phase. The continuous phase stretches the interface of the dispersed phase when they come into contact; then, droplets are generated via viscous stresses between the two immiscible fluids. Co-flowing approach can be designed 2D planar or 3D coaxial configurations (Guillot et al. 2009; P. Zhu and Wang 2017; G F Christopher and Anna 2007; P. Zhu, Tang, and Wang 2016). Droplet generation using this method was first introduced by Umbanhowar et al. (Umbanhowar, Prasad, and Weitz 2000). Two droplet generation regimes achieved by using this method are dripping and jetting. Briefly, the dripping regime happens when droplets are broken up near the capillary orifice; in contrast, when they are formed at the end of an extended thread, the droplet generation is under a jetting regime. In a follow-up study, Utada et al. experimentally investigated the dripping-to-jetting transition occurring in the co-flowing geometry, in which they found that the critical *Ca* was ~ 0.1 for the transition to start (Utada et al. 2008). Another study, characterizing sizes of bubbles generated using a co-flow geometry, was carried out by Hoeve and colleagues using the Navier Stokes equation (Van Hoeve et al. 2011; Castro-Hernández et al. 2011). They reported that the flow rate ratio of the inner phase to outer phase and their viscosity ratio strongly influenced the bubble radius.

Specifically, the diameter of bubbles was reduced and proportional to the flow rate ratio, $Q_{in}/Q_{out} \to 0$, and was independent of the viscosity ratio between the inner and outer phases. A liquid-liquid droplet formation in co-flowing geometry was studied by Crammer et al. (Cramer, Fischer, and Windhab 2004). The authors considered the influence of the velocity of the continuous phase and that of the dispersed phase, as well as the effect of the dispersed viscosity. Experiments in this study suggested that the viscosity of the dispersed phase and the *Ca* number of the continuous phase are crucial to generate sequences of droplets. Lately, Taassob et al. investigated the generation of monodispersed non-Newtonian droplets using a co-flow geometry. The results presented that the volumes of droplets are less influenced by the viscosity of the dispersed phase; however, they are significantly affected by the flow rate of the continuous phase (Taassob et al. 2017). As yet there is no physical model to explain the non-Newtonian droplet generation using co-flowing approach which the model would be useful in advancing microfluidics applications, such as biology and food industry. Although small sizes of droplets/bubbles can be generated using co-flowing geometry, the 3D co-flowing microfluidic device is not practical because of the challenging fabrication, which requires researchers to carefully insert a tapered cylindrical glass capillary into a rectangular micro-channel or into a square glass capillary.

Step emulsification, first introduced by Priest et al., is a modified configuration of co-flowing geometry (Priest, Herminghaus, and Seemann 2006b). Both phases are injected into a high aspect ratio channel where they flow beside each other. A sudden expansion of the micro-channel is applied to trigger droplet formation. Continuing Priest's work, Dangla and Baroud investigated the physical mechanisms of step emulsification by introducing model for drop breakup based on a quasi-static balance between the curvature of the thread inside the inlet channel and the curvature of the stream at the step (Rémi Dangla et al. 2013). In detail, a sudden removal of the stabilizing walls at the step disturbs the co-flow thread resulting in breaking up into droplets. Droplets can be generated before/at/after the step depending on flow conditions that consist of the ratio between the flow rates and their magnitudes. Furthermore, the

droplet size decreases with an increasing step height and is independent of the continuous flow rate.

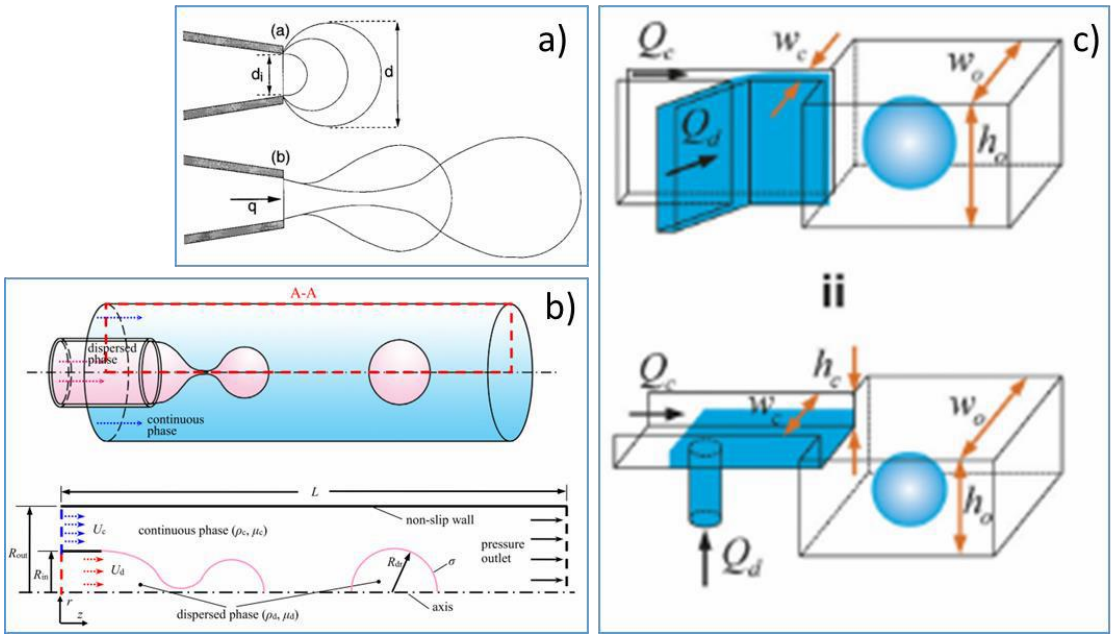

Figure 2-3. (a) Stage of drop evolution (Umbanhowar et al, 2000); (b) Schematic and simulation domain of droplet formation in co-flow (Wu et al., 2017); (c) Step emulsification (top) Horizontal step, (bottom) Vertical step.

Flow-focusing

Flow-focusing configuration, first studied by Anna et al, is a well-highlighted method for generating monodispersed droplets (Anna, Bontoux, and Stone 2003). The planar flow-focusing usually consists of a cross-junction where both phases meet and flow coaxially. The continuous phase squeezes the dispersed phase to a critical point at which droplets are pinched off. The symmetric shearing caused by the continuous phase flowing on both sides of the dispersed phase improves the stability and controllability of droplet formation. In general, droplet formation using this configuration depends on the Capillary number, viscosity ratios, flow rate ratios, wettability of channels, and geometries (Garstecki, Stone, and Whitesides 2005; Zhou, Yue, and Feng 2006; Ong et al. 2007; Cubaud and Mason 2008; W. Lee, Walker, and Anna 2009; Derzsi et al. 2013; X. Chen et al. 2015). Adding an orifice would create a singular point of high shear stress (Zhou, Yue, and Feng 2006; Ong et al. 2007). As a result, the two immiscible fluids pass

through the orifice and consistently form very small droplets. Cubaud et al. provided a flow map showing four flow patterns in the flow focusing configuration. Specifically, the three primary regimes that form droplets are: (1) squeezing, (2) dripping, and (3) jetting (Cubaud and Mason 2008). Studying the transitional regimes (squeezing to dripping or dripping to jetting) is interesting because the transitions of the dominant force in droplet generation show up clearly (J K Nunes; S S H Tsai; J Wan; and H A Stone 2009).

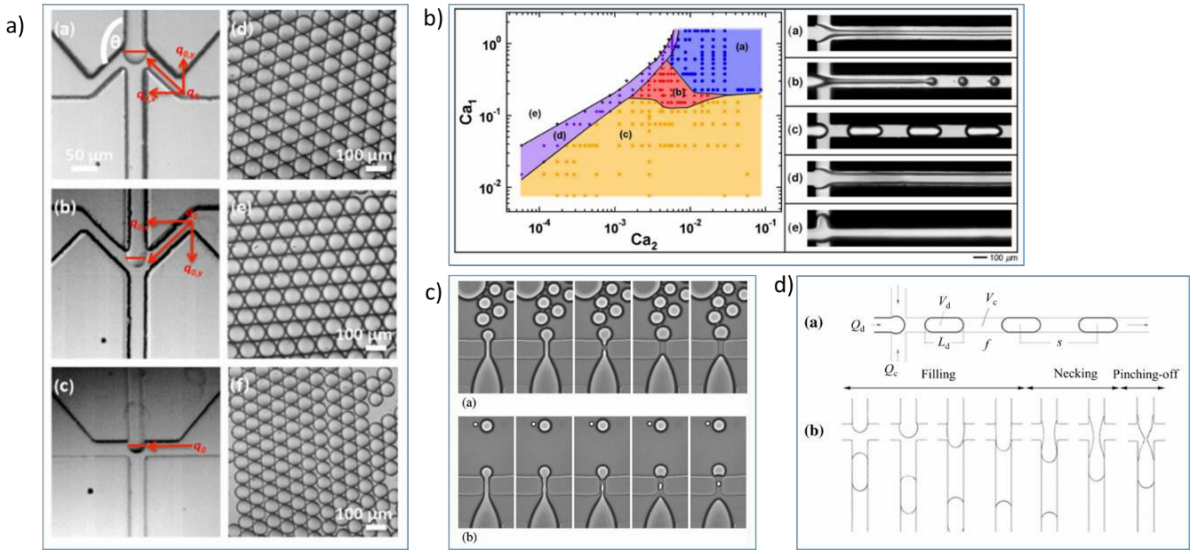

Figure 2-4. (a) Optical micrographs of microfluidic flow focusing devices. The angle between the inlet of the outer phase and the main channel is varied (Amstad et al. 2017); (b) Typical capillary number-based flow map with flow patterns (Cubaud et la. 2008); (c) Experimental images of drop breakup sequences occurring inside the flow-focusing orifice (Anna et al. 2003); (d) Droplet generation cycle in the flow focusing generator with three stages (Chen et al. 2015)

A large and growing body of literature has investigated droplet generation under the squeezing, dripping and jetting regimes. Those regimes mainly depend on the flow rate ratio between two phases and the Capillary numbers (W. Lee, Walker, and Anna 2009). In detail, the breakup process under squeezing regime happens when the dispersed phase dominates the continuous phase and the flow rate ratio of both phases is usually high $\varphi>1$. The interface enters the orifice, expands and blocks the flow of the continuous phase. As a result, the upstream pressure increases; then, the continuous phase begins to

squeeze the dispersed phase and pinches off droplets. The interfacial tension dominates the viscous force, so the *Ca* is typically small. The droplets generated under the squeezing regime are confined in the micro-channels and the size of droplets are slightly bigger than the width of the orifice. Under dripping regime, when the dispersed phase is at the junction, the front interface enters the orifice and transforms into a bulb-end. The competition of interfacial tension and deceleration of the fluid play a role in breaking up droplets. The flow rate ratio slightly reduces to approximately $\varphi \sim 1$. Both squeezing and dripping regimes are defined as upstream processes because droplets are usually generated before or inside the orifice. In the upstream operation, the droplet generation follows a power law curve of a dimensionless diameter versus the Capillary number ($\frac{d}{D_h} \propto Ca^{-\frac{1}{3}}$) (W. Lee, Walker, and Anna 2009; Zhao and Middelberg 2011). In contrast, the jetting regime, considered as downstream process, occurs when the viscous shear force from the continuous phase overcomes the interfacial tension and the flow rate ratio is usually less than 1, $\varphi \ll 1$ (W. Lee, Walker, and Anna 2009; Rosenfeld et al. 2014). The jet thread is irregular at the interface that breaks off and forms droplets; consequently, droplets generated under the jetting regime are usually non-uniform. Under dripping close to jetting regime, very small satellite droplets are usually produced behind the main droplets; whereas, under the squeezing and transition to dripping regimes, no satellite droplets are produced and main droplets are highly monodispersed (Zhou, Yue, and Feng 2006).

The droplet formation and breakup dynamics from the dripping to jetting regimes were recently studied by Fu et al. (Fu et al. 2012) The Micro-PIV technique was applied to quantify the flow field around a droplet and captured the dynamic changes during droplet formation. The results from this work consistently agreed with the blocking-pinching hypothesis before final pinch-off, as put forward by Guillot and Collin in 2005 and Garsteki et al in 2005 (Guillot and Colin 2005; Garstecki, Stone, and Whitesides 2005). Moreover, the authors also concluded that in jetting regime the stable jet width is a

function of the viscosity ratio and flow rate ratio when the viscosity contrast of both phases is low; whereas, that width is a function of only the flow rate ratio when the viscosity contrast between phases is high. Most studies of flow focusing droplet generation have presented the scaling laws or correlations based on the experimental data. Therefore, the 3D curvature of droplets during the formation, which has an impact on the accuracy of droplet volume, has been ignored. In 2014, Chen et al. modeled droplet generation in flow-focusing configuration, concentrating on generation under the squeezing regime (X. Chen et al. 2015). The model covered the 3D droplet shape during the formation process, as well as, a semi-analytical model predicting pressure drop over the 3D gutter between droplet curvature and channel walls. Other researchers were thus able to accurately determine droplet sizes, their spacing and the formation frequencies. As mentioned above, the geometry of the junction, where droplets form, also influences the volumes of droplets and their monodispersity. Amstad et al. investigated the role of the angle between the dispersed phase and the continuous phase, influencing droplet size uniformity experimentally (Amstad et al. 2017). Research, done by Yu et al., used a numerical simulation method to study the droplet formation (W. Yu et al. 2019). Follow up, a very fresh publication from Zheng's group provided a 3D numerical simulation of droplet formation in a microfluidic flow-focusing device using Level-set method (W. Han et al. 2019). The filling stage, necking stage and pinching off stage are clearly shown via 3D numerical simulation, but the simulation does not capture the effects of altering the geometry dimensions, such as varying the channel width and channel height. Overall, the further work is needed to capture all factors related to droplet generation using flow-focusing.

T-junction

At a T-junction, the continuous phase is perpendicular to the dispersed phase. When the dispersed phase is injected into the main channel and the shear force created by the oil phase elongates the interface downstream, a droplet breaks off (Guillot and Colin 2005; Gupta et al. 2011). The T-junction design is widely implemented to generate droplets because a wide range of droplet sizes can be produced with this

configuration (X. Li et al. 2012). There are two operational regimes for the T-junctions, defined as: (1) when droplets are sheared off before the dispersed phase fills the main channel, and (2) when the dispersed phase is confined to the main channel and the breaking-off process happens. Similar to the flow-focusing configuration, droplet generation using a T-junction depends on the flow rate ratio, the viscosity ratio, the interfacial tension and the dimensions of geometries (aspect ratios and width ratios) (D R Link et al. 2004; Glawdel, Elbuken, and Ren 2012; Glawdel and Ren 2012a; Boruah et al. 2018; Loizou, Wong, and Hewakandamby 2018). Confinement will not happen when the inverse width ratio of the dispersed phase to the continuous phase is more than 5 and the flow rate ratio is really small (Glawdel and Ren 2012c).

At a very low flow rate ratio and high width ratio, droplet sizes are smaller than the channel width, defined as a dripping regime. Under this regime, droplet breakup is governed by the balance between the viscous continuous phase dragging on the emerging droplet and the interfacial tension resisting deformation (De Mench et al. 2008). In another regime – known as the squeezing regime – droplets are physically confined in micro-channels and generated at typically low *Ca* (De Mench et al. 2008; Gordon F. Christopher et al. 2008; Jullien et al. 2009). Under the squeezing regime, the dispersed phase first penetrates to the main channel, then the interface expands until it fills and blocks that channel. During the process, pressure upstream builds up, subsequently causing the continuous phase to squeeze the disperse phase to a thin neck. Eventually, a droplet is pinched off. The droplet moves downstream carried by the continuous phase and the remaining interface pulls back into the perpendicular channel to be ready for a new generation cycle. Droplets produced in this regime have a slug-like shape with the lengths of droplets usually being greater than their widths. Typically, confined droplets are generated at $\mathrm{Ca} \leq 0.002$, when the width ratio between two phases is ~ 1 (Gupta and Kumar 2010). In early research on generating droplets using the T-junction configuration, the physic of the process was expressed by using the scaling law, $V^*_{drop} = \alpha + \beta\varphi$, where φ is flow rate ratio, V^*_{drop} is a dimensionless droplet volume, and α, β are

constants respectively related to the initial fill volume and the rate of droplet growth during the necking stage (De Mench et al. 2008).

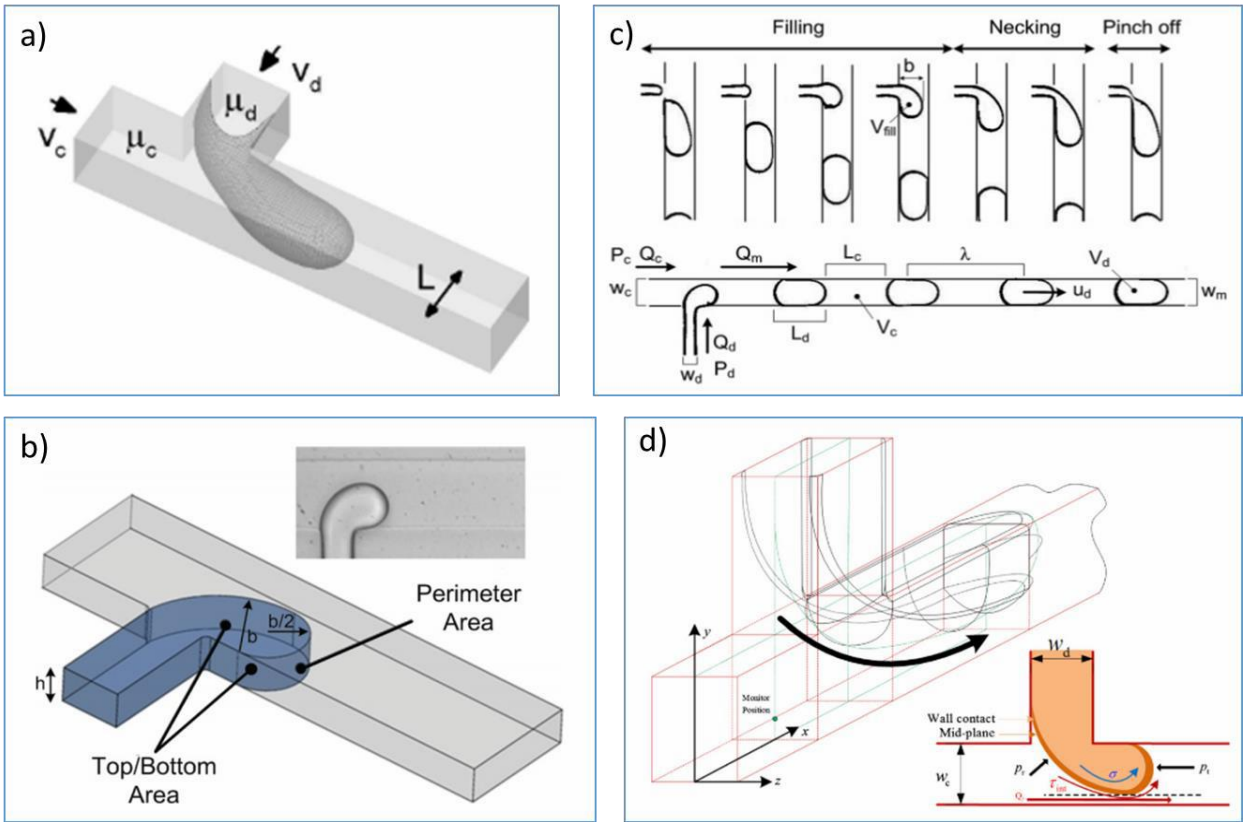

Figure 2-5. (a) Diagram of a T-junction with cross flow (Menech et al. 2008); (b) Diagram of the approximated area of the droplet from the projection of the 2D image (Glawdel et al. 2012); (c) Droplet formation cycle in the T-junction generator consisting of three stages (Glawdel et al. 2012); (d) Sketch of emerging droplet prior to detachment and the related force competition (Li et al. 2012).

Later, another study by Christopher et al. covered the effects of viscosity ratio in the droplet generation process (Gordon F. Christopher et al. 2008; G F Christopher and Anna 2009). In 2012, Glawdel et al. fully developed a model of droplet generation in the squeezing to transition regime using a T-junction and published their works in a series (Glawdel and Ren 2012a; Glawdel, Elbuken, and Ren 2012; Glawdel and Ren 2012b). The physical model was developed from the experimental observations, including the effect of surfactants on interfacial tension during the droplet formation. Until now, this model has been

considered as the most comprehensive physical model that covers most of the parameters influencing droplet generation under the transition regimes.

Active droplet generator

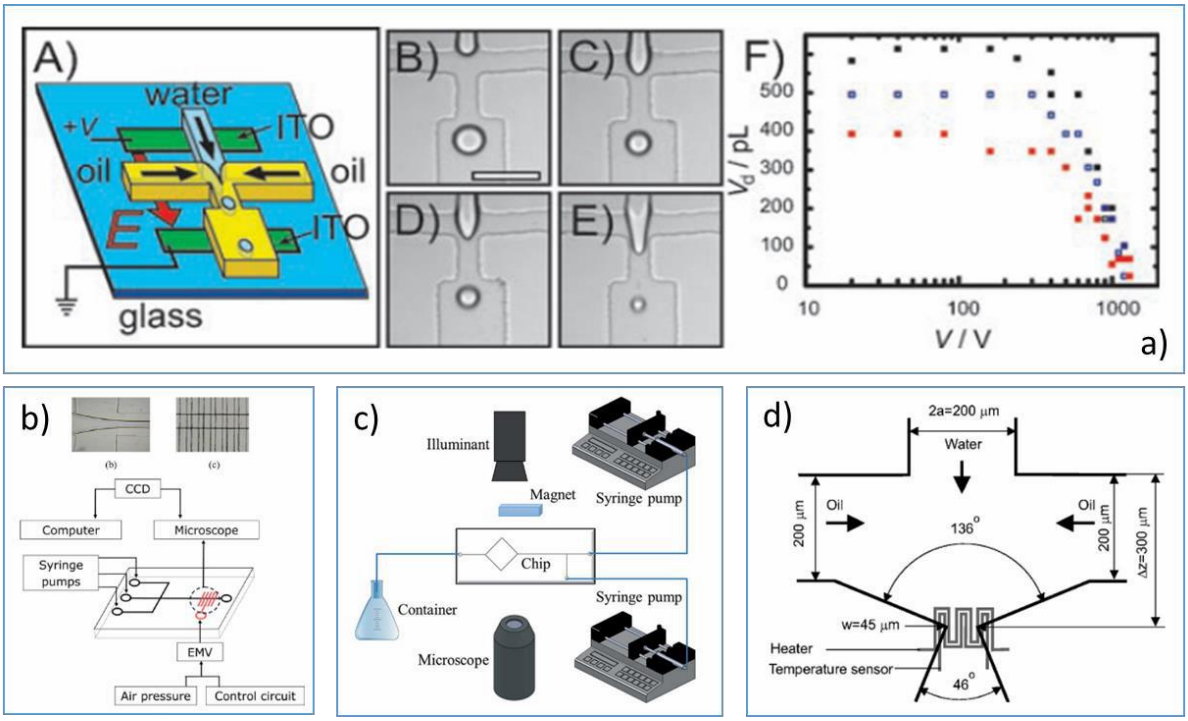

Figure 2-6. (a) Charged-droplet generation (ITO electrodes on glass produces an E field) (Link et al. 2006); (b) Experimental setup for droplet formation using hydrodynamic pneumatic choppers (Chen et al. 2006); (c) Schematic of experimental set up integrated with the permanent magnet for using generating ferrofluid droplet (Li et al. 2015); (d) Schematic concept of the microfluidic for the temperature dependency of the droplet formation (Nguyen et al. 2007)

In contrast to the above technologies, the active methods involve external components that provide the local external energy to form droplets, such as mechanical, thermal, electrical, magnetic or optical energy (Cheng-Tso Chen and Gwo-Bin Lee 2006; Darren R. Link et al. 2006; Ting et al. 2006; Zeng, Shin, and Wang 2013; Chong, Tan, Ganan-Calvo, et al. 2016). For example, droplet formation processes can be mechanically manipulated by using either pneumatic/hydraulic valves or piezoelectric actuation (Zeng, Shin, and Wang 2013; Cheng-Tso Chen and Gwo-Bin Lee 2006). Not only can droplets be produced via

mechanical approaches, they can also be generated via thermal ones (N. T. Nguyen et al. 2007). The temperature that influences the change of fluid viscosity and interfacial tension can be varied to tune droplets sizes. Electric fields are also used to generate droplets (H. Kim et al. 2007). This approach is usually used when dispersed phases contain electrorheological fluids. Applying magnetic and optical forces to produce droplets offers other options (Pamme 2006; H. Li et al. 2016). For instance, several articles have shown the formation of ferrofluid droplets by integrating an electromagnet (or a permanent magnet) into a T-junction (or a flow-focusing geometry) to change the viscosity of the ferrofluid. In some applications, researchers combine more than one method to generate droplets. Overall, the active droplet generators require extra steps during the fabrication procedure, thereby increasing the cost of complex microfabrication. The number of scale-up products for devices is also limited. Thus, most of these methods are barely employed in microfluidic applications.

2.1.3.2 Droplet fusion

The capacity to merge droplets together is one of the essential qualities integrated in droplet microfluidic platforms, because it allows researchers to combine at least two reagents together for further chemical/biological reactions (Gu, Duits, and Mugele 2011; X. Chen and Ren 2017a; Wong and Ren 2016; Jin et al. 2010; Um et al. 2008; Baroud, Gallaire, and Dangla 2010; Mashaghi and van Oijen 2015). Mixing between reagents is also achieved when two/three droplets collide (Y. C. Tan, Ho, and Lee 2007; X. Chen and Ren 2017a). Droplets must be paired and synchronized before they fuse together. Uncontrolled droplet pairing, however, influences droplet fusion. Therefore, to pair droplets, researchers either alternatively generate droplets or synchronize two separate droplet-streams.

Droplet pairing and synchronization

In passive droplet microfluidics, the alternative droplet formation methods usually rely on the hydrodynamic coupling effects of multiple droplet generators; whereas, alternative droplets generated by

active methods depend on the controlling of micro-valves or electric/optic/magneto fields. Hong et al. introduced a platform consisting of two passive components to achieve controllable and alternative droplet generation (Hong et al. 2010). The system included a droplet-pair generator, a simple Y-junction for droplet fusion, and a winding channel for mixing. In the droplet-pair generator, the two important passive components were: (1) a pressure oscillator and (2) an oil regulator. The authors implemented the pressure oscillator to manipulate the time between two separated droplet generators via a fluidic network; and, the oil regulator was integrated into a platform to passively control pressure differences at the furcate junction. Other research by Zheng et al. showed alternative droplet formation at two opposing T-junctions sharing the same continuous phase (Zheng 2004). The same configuration, reported by Fidalgo et al, was also used to alternatively generate droplets from two opposite streams (Fidalgo, Abell, and Huck 2007). Similarly, Hung et al. also presented a platform that has three inlet channels joined at a double T-junction; however, the authors introduced two triangular wings between the inlets and each T-junction (Hung et al. 2006). The purpose of the wings is to reduce flow instability and prevent back flow. The alternating droplet generation was the result of a "push-pull" mechanism. Saqib et al. replaced the double opposite T-junctions with two opposite tapered channels (Saqib, Şahinoğlu, and Erdem 2018). The optimized design demonstrated the ability to controllably produce a sequence of alternating droplets. Specifically, by measuring the radius of droplet curvature at the necking and pinching-off times, and calculating the Laplace pressure during the necking stage, the researchers analyzed how the angle formed between the tapper dispersed phases and the continuous phase affects pattern repetition and droplet uniformity and spacing. In addition, Frenz et al. researched a dual nozzle for the production of droplet pairs (Frenz et al. 2008). The size of paired droplets was manipulated by the flow rates of dispersed phases and the

continuous phase.

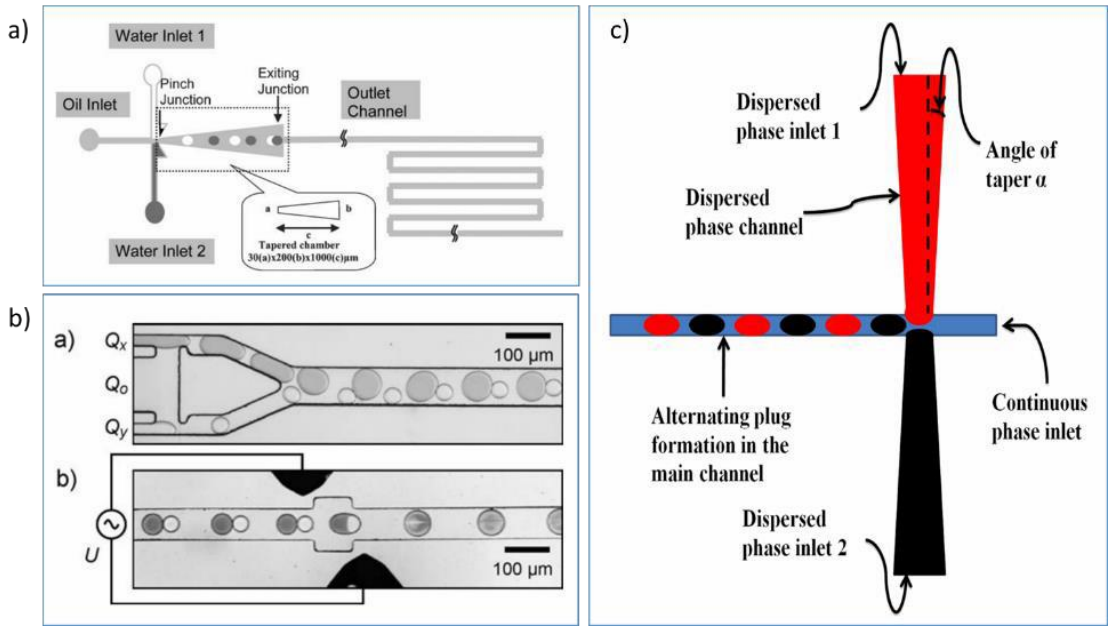

Figure 2-7. (a) Schematic diagram of the tapered microchannel pattern for alternating generate droplets (Hung et al. 2006); (b) Pairing module. Two aqueous phases are injected by the outer channels and are synchronously emulsified by the central oil channel (Frenz et al. 2008); (c) Schematic of the droplet generation device. The continuous phase inlet and the two dispersed phase inlets are shown. The angle of taper is denoted by α. (Saqib et al. 2018)

Despite their different geometries meant to minimize instability, these methods introduced so far have problems with irregular fluid flow rates and pressure fluctuations because of the coupling effects of the microfluidic network. Thus, achieving uniform droplet formation is problematic. To avoid the coupling effect caused by sharing the same oil stream/oil bridge, another strategy is to synchronize pre-formed droplets that are generated with separated droplet generators. A ladder structure (Figure 2-8) is favored for that purpose, as was introduced by Prakash and Gerhenfeld (Gershenfeld and Prakash 2007). In their work, two streams of bubbles, which were produced separately by using two disconnect oil, streams entered into two micro-channels. The pressure difference between those channels guided the carrier oil flowing through the vertical micro-channel, connecting the two channels. Eventually, the resistance induced by the existence of bubbles in each channel balanced so that the two streams of bubbles were

passively synchronized. To use this design, bubbles must be slug-shape to avoid the carrier oil flowing across them. In a follow-up study, Ahn et al. applied the same geometry to experimentally synchronize two trains of water droplets in oil (B. Ahn et al. 2011). From a numerical study of the transportation of droplets in the ladder geometry conducted by Song et al., a theoretical model was discovered based on the effects of network geometry, flow rates, and droplet resistances (K. Song, Zhang, and Hu 2012). Using the electronic-hydraulic analogy, the analytical model described the hydrodynamic behavior of the droplets in interconnected microfluidic ladder devices.

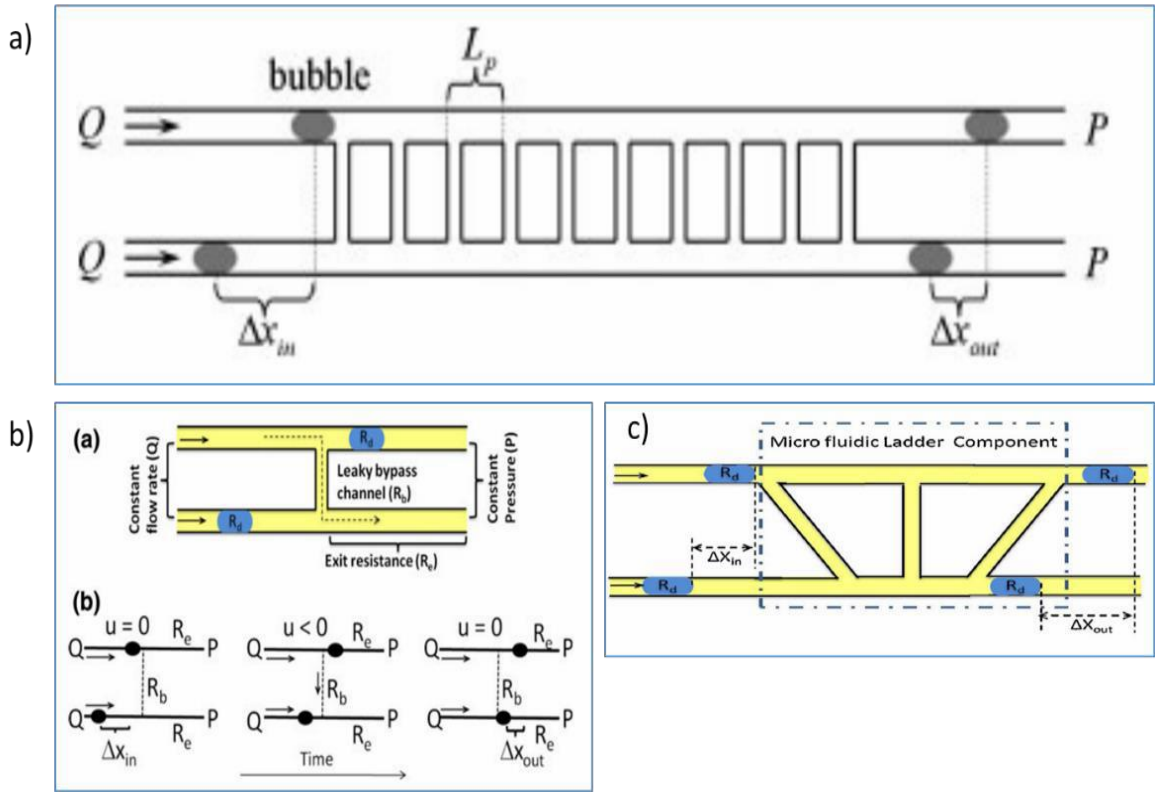

Figure 2-8. (a) A microfluidic ladder device for droplet synchronization (Song et al. 2012); (b) Ladder with a vertical bypass with a constant flowrate (Q)at inlets and constant pressure (P) at outlet channels and Three distinct configurations are possible when a pair of drops traverses through a symmetric ladder network (Maddala et al. 2013); (c) Asymmetric ladder design (Maddala et al. 2014)

The authors concluded that the pressure drop along the droplets had an impact on the droplet synchronization. Later, the dynamics of aqueous droplets travelling in an asymmetric ladder network was

investigated by Maddala et al. The research group found that temporary control of droplet spacing was achieved using the asymmetric ladder network instead of symmetric ladders (Maddala et al. 2013; Maddala and Rengaswamy 2014).

Droplet coalescence

When the oil thin film separating droplets is shortened or drained off, the eventual result is droplet collision, and subsequent fusion. Similar to droplet generation, droplet fusion in microfluidic networks has been achieved by means of passive methods or active methods.

In passive methods, microchannel geometries must be properly designed to control droplet fusion. The most common configuration is to transport droplets to an expanding area where they slow down so that the carrier oil can draw off droplets. The next droplet comes and merges with the one that has been waiting inside the expanding location. Hung et al. and Bremond et al. both studied droplet fusion in an expanding channel. In Hung's work, a tapered outlet was placed at the exit of a dual T-junction generator to merge the droplets (Hung et al. 2006). The tapered design was used to gradually slow the speed of the first droplet so that the next droplet would eventually come in contact with it. When the two surfactant-free droplets touched, they merged. However, the efficiency of pairing droplets and merging them was low, with 50% random droplet coalescence. In 2007, Tan and Lee pioneered to study the phenomenon of merging of two droplets travel at the same velocity in a micro-channel (Y. C. Tan, Ho, and Lee 2007). The authors concluded that to merge the droplets at the junction, the oil drainage time must be shorter than transport time of droplets. Instead of using the tapered channel, Bremond et al. used a divergent-convergent chamber (Bremond, Thiam, and Bibette 2008). Their study demonstrated that the droplets did not actually fuse into each other when they stayed in the expanding area; surprisingly, they merged closer to an exit site. Many fundamental investigations have predicted the positions where droplets merge and their behaviors in an expanding chamber. For example, a model by Lai et al. was used to study the

positions of droplets merging (Lai, Bremond, and Stone 2009). Lately, an experimental study involving the flow behavior of a droplet train in an expansion chamber under different viscosities and flow rates conditions was done by Jose et al. (Jose and Cubaud 2012).

In a modified expanding chamber introduced by Niu and colleagues, two arrays of pillars in parallel were placed inside a merging chamber (X. Z. Niu et al. 2009). The arrays of pillars temporarily held the first droplet until the next droplet came into contact with it. The oil separating the droplets drained through the gaps between the pillars; thus, the distance between the droplets was shortened, causing them to collide and fuse. In 2017, Chen et al. published an article describing the relationship between the numbers of droplets merged, the length of input droplets and the length of output droplets (X. Chen, Brukson, and Ren 2017). Those parameters were considered key in the design of a merging chamber. The authors concluded that droplet merging events depend on the proportional relationship between Ca_{crit} and the bypass resistance ratio (BRR), as well as on the ratio of the droplet length to the length of the merging chamber. Another geometry used for droplet coalescence is a T-junction, undertaken by Christopher et al. Droplets from two side streams were brought together at the junction where they merged after the collision (G F Christopher et al. 2009). The process of collision was governed by the timing of the droplet contact and the rate of oil film drainage. Droplets collided when they moved at low speeds; in contrast, they either split or slipped when they moved at higher speeds. Yang and Luo et al. also experimentally studied micro-bubble coalescence at a T-junction (L. Yang et al. 2012). Their study agreed with the one done by Christopher et al., in that the fluid dynamic conditions, such as characteristic contact time and film drainage time, influenced the efficiency of merging. Furthermore, the degree of viscosity influenced droplet merging.

Droplet fusion can also be manipulated by partial-hydrophilic micro-channels (Fidalgo, Abell, and Huck 2007). To use this approach, managing the surface wettability is a critical step because carefully treating a part of a channel to be hydrophilic is required to provide the best control over the process.

Specifically, the pattern hydrophilic poly(acrylic acid) – PAA was placed on a planar PDMS substrate via UV photo-polymerization. Selective grafting was enhanced by exposing PDMS to UV through a photomask. The mechanism for merging droplets can be understood as two steps. The first step is trapping the droplet – the coalescence between droplets and the hydrophilic pattern. In sequence, the next droplet also comes into contact with the hydrophilic pattern. The contents of both droplets mix. When the viscous drag force overcomes the surface energy stabilization, the second step occurs – known as droplet detaching. The trapped droplets are released, forming a merged droplet. However, wall-contamination is a practical concern in using this method.

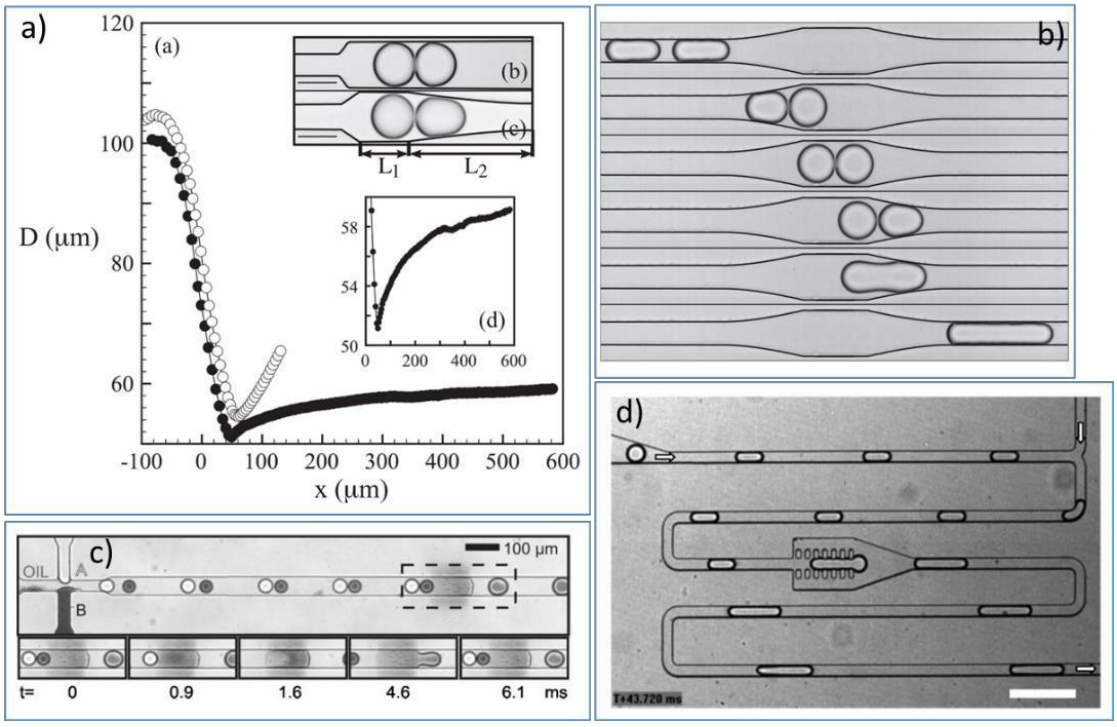

Figure 2-9. (a) (b) De-compression merging (Bremond et al. 2008); (c) Sequence of surface induced droplet fusion (Fidalgo et al. 2007); (d) CCD image showing the merging of two droplets (Niu et al. 2008)

Overall, the advantages of passive techniques are that they are easy to implement on a microfluidic platform, and can also be integrated with other components. However, they have the following drawbacks (X. Chen, Brukson, and Ren 2017): (1) they cannot be used for microfluidic systems involving

surfactants; (2) each design has a limitation in their operational range, such as in the speed of droplets and the spacing between droplets before they enter a chamber. Thus, in some applications, researchers need to use active methods.

Active methods enable droplets to be manipulated regardless of whether microfluidic systems are using surfactants to stabilize the droplets or not, and they provide researchers with the flexibility to merge droplets by triggering external forces. The most common method for actively fusing droplets is to use electrofusion by applying either DC or AC fields (Chabert, Dorfman, and Viovy 2005; Priest, Herminghaus, and Seemann 2006a; Zagnoni, Baroud, and Cooper 2009; Zagnoni, Le Lain, and Cooper 2010). Electro-coalescence is a popular active method for merging droplets. Under the non-uniform electric field, droplets tend to deform due to the electrical (Maxwell) stress. The imbalance between the total stress, consisting of electric and viscous stress, and the interfacial tension play a role in merging droplets. Therefore, the electro-coalescence is mainly influenced by the strength of the applied electric field. Another approach is called thermal-coalescence, in which droplet fusion is controlled by thermos-capillary effects (Köhler et al. 2004). A laser is employed to heat the interface of adjacent droplets until they merge (Baroud, Robert de Saint Vincent, and Delville 2007). The temperature gradient induces Marangoni effect at the droplet surfaces because of the temperature dependent properties of the interfacial tension and the viscosity of fluids. Additionally, the optical tweezer offer another tool with which to selectively merge droplets (Jung et al. 2015). Furthermore, the mechanical pneumatic actuator integrated in pillar structures also allows users to control the number of merged droplets having a wide range of droplet volumes (Yoon et al. 2014). Not only can droplets be merged by applying electrical or thermal forces, they can also be merged by utilizing acoustic waves. For instance, Sesen et al. experimentally demonstrated that multiple droplets can be trapped and immediately merged on-demand using surface

acoustic waves (SAWs) (Sesen, Alan, and Neild 2014).

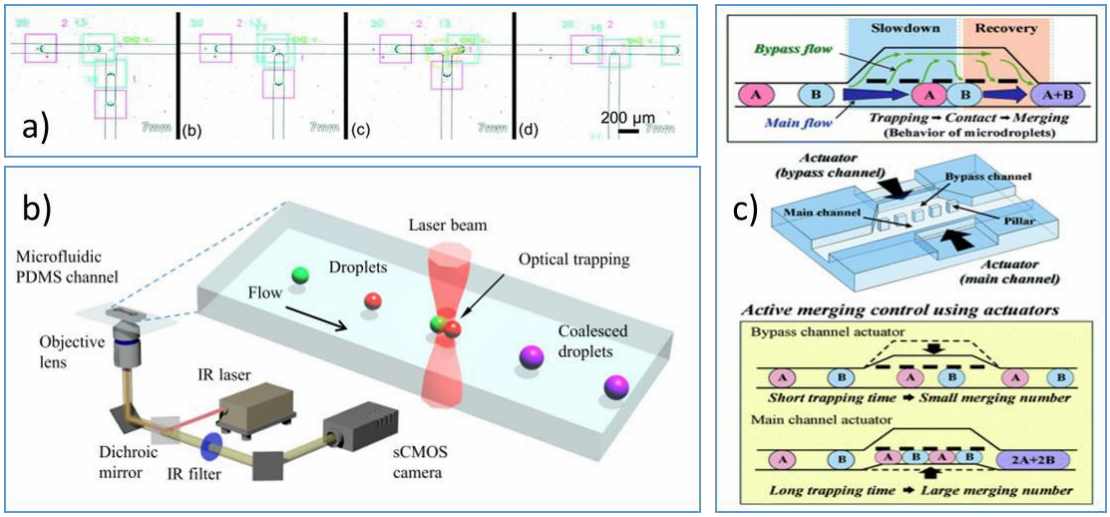

Figure 2-10. (a) Droplet merging process using Semi-automated system (Hebert et al. 2019); (b) Schematic illustrations of the optofluidic droplet coalescence device (Jung et al. 2015); (c) Active control of droplet merging using horizontal pneumatic actuators (Yoon et al. 2014)

Lately, Wong et al. and Hebert et al. have developed a controller for manipulating droplets, such as by generating or merging them, etc. (Wong and Ren 2016; Hébert, Courtney, and Ren 2019). This approach is considered to be a combination of passive and active methods. Specifically, the controller uses information from images taken in real time as feedback signals for updating the controller on the current positions of droplets; as a consequence, the controller automatically tunes the pressure source to manipulate the droplets. The research seems promising for droplet on-demand manipulation, but so far the platform's use has been limited by the processing frequency, around 10Hz.

2.1.3.3 Droplet mixing – a micro-mixer

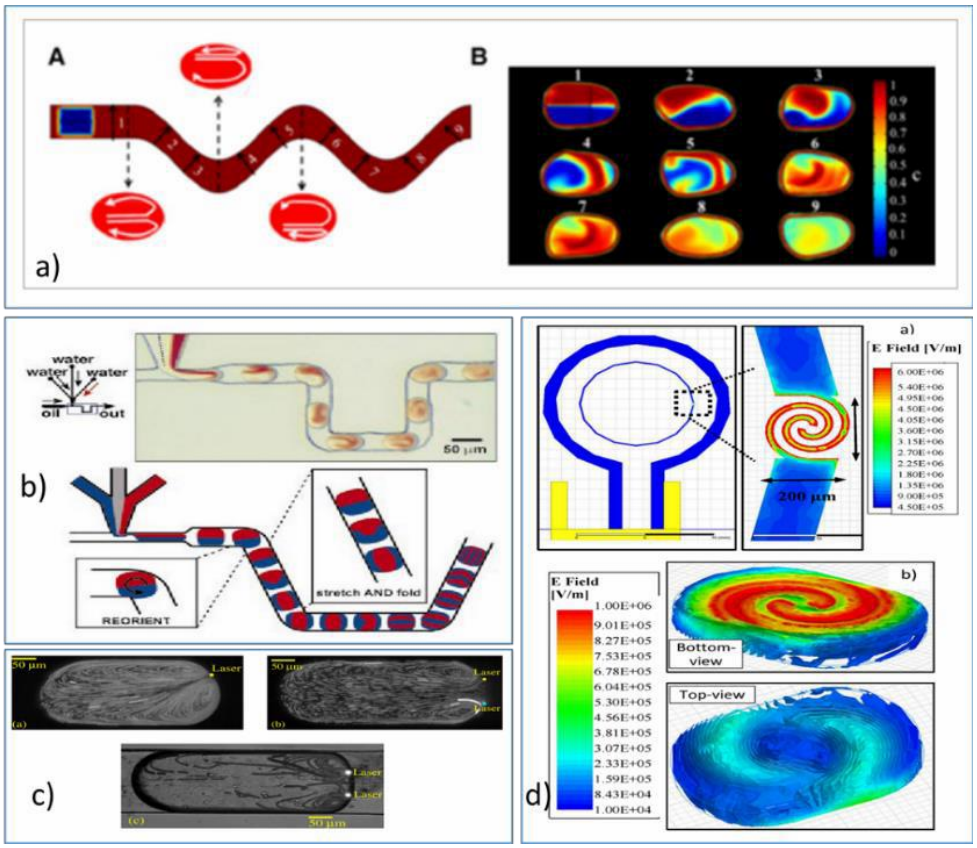

Figure 2-11. (a) Schematic of asymmetric vortices formed in droplets moving through the bent channels (Jiang et al. 2012); (b) Rapid mixing inside plugs moving through winding channels at the same flow velocity (Song et al. 2003); (c) Using laser spot to achieve droplet mixing (MCGloin 2017); (d) Using microwave resonator to induce the asymmetric vortices inside droplet for mixing (Yesiloz et al. 2017)

Under the low *Re* condition, that is the unlikely Stoke flow of single phase microfluidics in which two streams flow side-by-side and the mixing depends on diffusion, the mixing of two reagents that are enclosed inside micro-bubbles/droplets using two-phase microfluidics is achieved via 3D flow circulation (Whitesides 2006; Jayaraj, Kang, and Suh 2007; Teh et al. 2008). Thus, the mixing is highly homogeneous and rapid. When droplets carry reagents inside and are transported inside channels, each droplet performs as an individual micro-mixer (Tice et al. 2003a; Shui et al. 2008; Ward and Fan 2015b; Vladisavljević, Al Nuumani, and Nabavi 2017). Compared with the bench-top methods, droplet-based

microfluidics offers high-yield products, as the latter promote fast mixing at micron scale, leading to significantly low reaction times (Sesen, Alan, and Neild 2017).

To equal recirculation vortices occur inside individual droplets when they move along a straight micro channel (Baroud, Gallaire, and Dangla 2010; Zhao and Middelberg 2011). Each half of the droplet experiences internal mixing because of this circulation, but there is not chaotic mixing happening between the two halves. The mixing between two halves later on depends on diffusion; thus, it is not as efficient as researchers had expected it to be. Investigating methods for providing fast mixing is essential. To achieve that goal, the internal flow and the recirculation of fluids inside single droplets flowing in a channel should be studied extensively (T. S. Kaminski and Garstecki 2017). In the early years of droplet mixing, the experimental study done by Tice et al. described the topology of the counter-rotating recirculation inside a droplet moving inside a micro-channel (Tice et al. 2003b; 2003a). Later, other researchers visualized the internal flow in a moving droplet by using micro Particle Image Velocimetry (Kinoshita et al. 2007; Lindken et al. 2009). From those studies, the recirculation of rotational patterns in droplets is known to be driven by differences in the speeds of droplets and the continuous phase. Generally, the internal flow patterns inside droplets relate to multiple parameters,

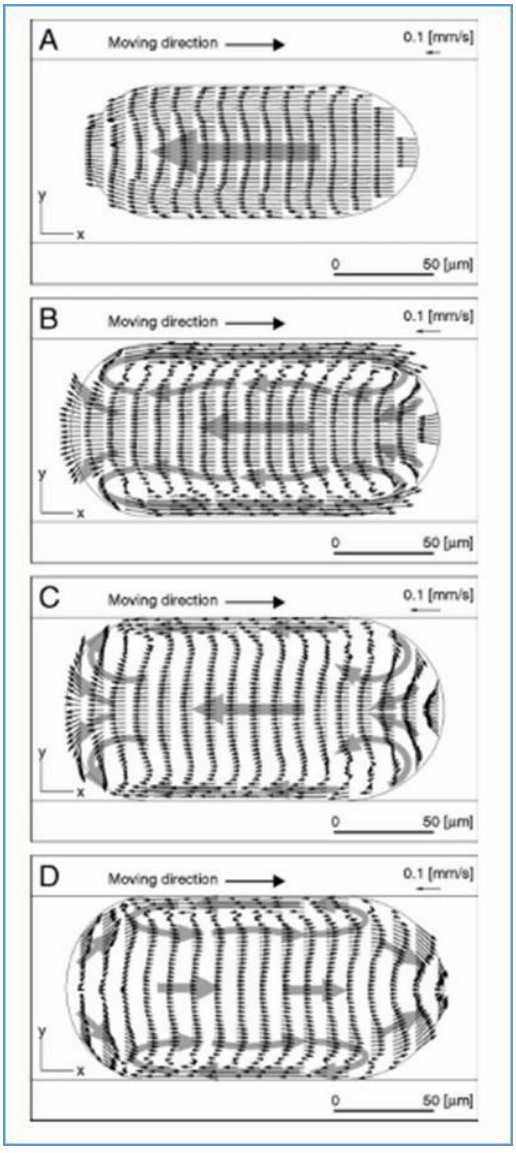

Figure 2-12. 2D velocity distribution in each cross-section at different focus position (Kinoshita et al. 2006)

including the capillary number, size of droplet relative to channels, the choice and concentration of surfactants and the viscosity ratio between the droplet and the continuous phase (Baroud, Gallaire, and Dangla 2010).

Additionally, several researchers have discussed the influences of viscosity contrast between droplets and carrier fluid and the chaotic advection inside droplets on mixing. For example, the shear stress at the liquid-liquid interface associated with droplet mixing was analyzed by Verguet et al. (Verguet et al. 2010) The authors concluded that decreasing the thickness of lubrication films between droplet and channel walls advanced greater advection velocities inside droplets, leading to the rapid mixing of reagents inside droplets. Furthermore, Song et al. observed and mentioned in their reports that rapid mixing was enhanced by passing droplets through a serpentine/winding channel as shown in Figure 2-11 (Helen Song, Tice, and Ismagilov 2003; H. Song et al. 2003; H. Song, Chen, and Ismagilov 2006). A follow-up study done by Liau et al. showed fast mixing using a serpentine channel with bumps integrated into the micro-channels (Liau et al. 2005). The results of this study agreed with those of the previous studies introduced by Verguet et al. and Song et al. that the proportional thinning of the continuous phase (in which the oil film stayed between the droplets and the channel walls) promoted the larger advection velocities inside droplets. Moreover, the asymmetric vortices induced when droplets are moving along curvy channels advanced rapid mixing. Serpentine channels are not the only way to enhance fast mixing; zigzag type structures and up-down rectangular channels also generate chaotic advection. Lately, a model showing a dynamic system for studying microfluidic mixing was presented by Balasuriya and colleagues (Balasuriya 2015). The work involved using the motion of collective fluid parcel trajectories to study crucial interior flow patterns. Its applications may eventually include several microfluidic mixing systems.

Other strategies to promote rapid mixing in droplet-based microfluidics involve integrating external sources into existed microfluidic devices. In some situations in which the device footprints are limited so that researchers cannot use a long serpentine channel to achieve homogenous mixing, they choose to use

one of the many active methods, such as by controlling electric fields (Paik et al. 2003; Hadwen et al. 2012; MCGloin 2017). Song et al. enhanced droplet mixing using electro-wetting-on-dielectrics (J. H. Song et al. 2009). Droplets were moved back and forth on a linear electrode array. The thermos-capillary methods, such as using a laser spot, can also be used to advance the mixing inside droplets (MCGloin 2017). Many studies involving this method have been done both experimentally and by using a numerical method studying parameters for mixing with laser patterns. Another active method recently introduced to the research community uses a microwave heater to speed up the mixing (Yesiloz, Boybay, and Ren 2017). The capability of microwave resonators to mix droplets was investigated by Yesiloz and his colleagues, using an electromagnetic field to provide sufficient energy to heat-up droplets passing through a capacitive gap. Thus, the Marangoni effect at the surfaces of droplets was induced, resulting in the fast mixing of reagents enclosed inside droplets. The mixing efficiency was quantified by using the mixing index, which is up to 97%. The biggest challenge that limits the use of these active methods in applications is in the micro-fabrication techniques. Small defects induced via fabrication may affect the performances of the external forces applied to droplets. The cost of fabrication is another concern (Lagus et al. 2012).

2.1.3.4 Droplet Trapping and storage

As discussed previously, droplet-based microfluidics offer rapid reaction times due to fast mixing; however, some applications require a longer residence time for storing droplets (several hours to days) (Laval et al. 2007; M. C. W. Chen, Gupta, and Cheung 2010; Miller et al. 2012; Courtney et al. 2016; Holtze, Weisse, and Vranceanu 2017; Basu and Gianchandani 2008; Hunt, Issadore, and Westervelt 2007). The simple way is to extend the length of micro-channels, but the length of micro-channels cannot be infinite due to devices' footprints. Furthermore, a long micro-channel containing thousands of droplets significantly increases the hydrodynamic resistance downstream, which may affect functionalities upstream. Expanding the outlet chamber to be wider and deeper so that droplets can be stored is another approach. For example, Courtois et al. developed a device containing a reservoir that holds up to 10^6 droplets (Courtois et al. 2008). The researchers were able to conduct the *in vitro* expression of fluorescent

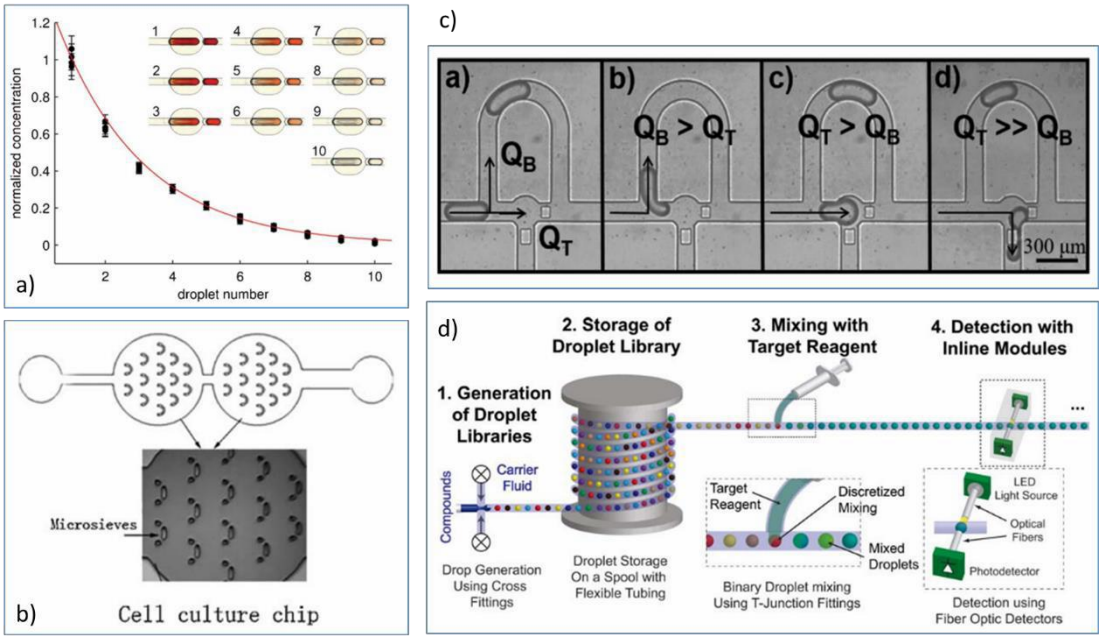

Figure 2-13. (a) Generation of a serial dilution sequence from a metering trap (Korczyk et al. 2013); (b) Cell culture microfluidic chips (Yu et al. 2010); (c) Droplet trapping scenarios (Courtney et al. 2016); (d) System concept of droplet storage in a tubing and reinject for further study (Trivedi et al. 2010)

proteins inside the microfluidic device because the droplets were kept inside the chamber for six hours. The sequence of droplets was lost when droplets moved to the reservoir. Lately, Tang's group studied the packing of droplets at the outlet and their rearrangement before they leave the chamber (Gai et al. 2016; Khor et al. 2019). Other researchers have proposed methods for trapping droplets at certain spots in the chamber, after which the droplets have the potential to be released in sequence (H. Chen et al. 2005; Shi et al. 2008; Huebner et al. 2009; Miller et al. 2012; X. Chen and Ren 2017a). In microfluidic devices, droplets move downstream following the flow of the carrier fluid. When they flow into trapping chamber arrays, as shown in Figure 2-13.b, they are kept inside these constrictions (Huebner et al. 2009; L. Yu, Chen, and Cheung 2010; Korczyk et al. 2013). Each chamber can be designed to hold one or multiple droplets, depending on the compatibility between droplet sizes and the chamber sizes (Courtney et al. 2016; X. Chen and Ren 2017a). The drop-spot design has been optimized by integrating trapping wells and bypass channels downstream of a main channel (Shi et al. 2008). Generally, the length of bypass channel is designed so that its resistance is larger than the resistance of an empty trapping well, but smaller than the resistance of a trapping well containing one droplet. Thus, droplets tend to follow the flow to where the resistance is smaller. Lately, Courtney and Chen have added diluting oil streams and modified a trapping well design so that the microfluidic devices can trap and release droplets so as to test different assays (Courtney et al. 2016). Generally, drop-spot designs provide a method for hanging droplets inside microfluidic devices, but the droplets cannot then be incubated over the long term on-chip. The biggest challenge is that PDMS is gas permeable and subject

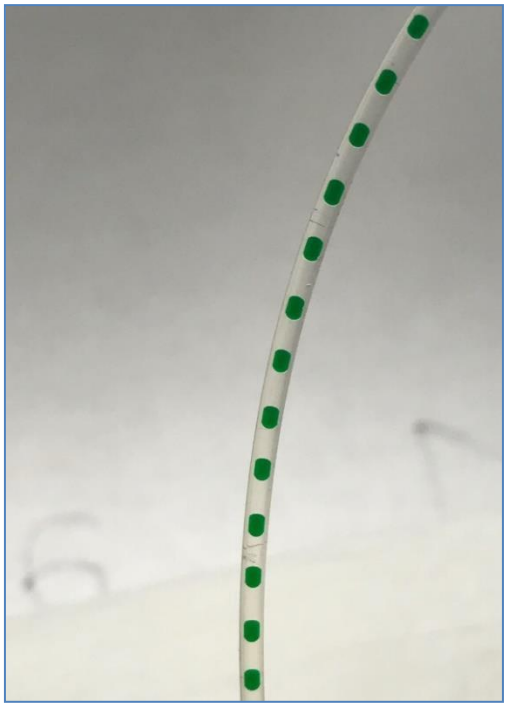

Figure 2-14. Storage droplet inside PEEK tubing

to absorption (Mukhopadhyay 2007). Therefore, the suggested solution for storing droplets long term is to collect them in a glass capillary or in small diameter PEEK tubing (Trivedi et al. 2010); then, droplets can be reinjected into a new chip for further studies (Theberge et al. 2012). To avoid droplets merging when they are stored inside the tubing or the capillaries, a suitable surfactant should be used (Theberge et al. 2012).

2.1.3.5 Splitting and sorting droplets

In addition to those functions discussed above, other functions such as splitting and sorting of droplets must be implemented in some microfluidic platforms to meet the requirements of certain applications.

Splitting droplets

Splitting droplets increases the operational capacity of microfluidic devices since these daughter droplets can be processed further by merging them with other droplets (Y.-C. Tan et al. 2004). Breaking up droplets into two either equal or more predetermined-size daughter droplets indicates the promise inherent in tuning concentration gradients or multi-step reactions on microfluidic chips (D R Link et al. 2004; Jullien et al. 2009). The majority of breakup mechanisms in micro-channels are based on using shear forces to sufficiently elongate a droplet so that its length exceeds a critical point at which it breaks up. Since water-in-oil droplets have a high relative interfacial tension, for instance, $\gamma_{silicon\ oil\ vs.water} = 35mN/m$, surfactants may be used to reduce the interfacial tension, thereby assisting droplet splitting (Leshansky and Pismen L. M. 2009). A with other functions, passive and active methods can be applied in droplet splitting. Passive methods typically use T-junction geometry (Leshansky and Pismen L. M. 2009; G F Christopher and Anna 2009; Murshed et al. 2009; D R Link et al. 2004). Droplet break-up is manipulated by varying the flow rate of the continuous phase and relative resistances of two side channels, forming an inverse T-shape. The critical capillary number plays an important role in passive droplet splitting (D R Link et al. 2004). Below a critical value, droplets move to either one of the

outlet channels, instead of

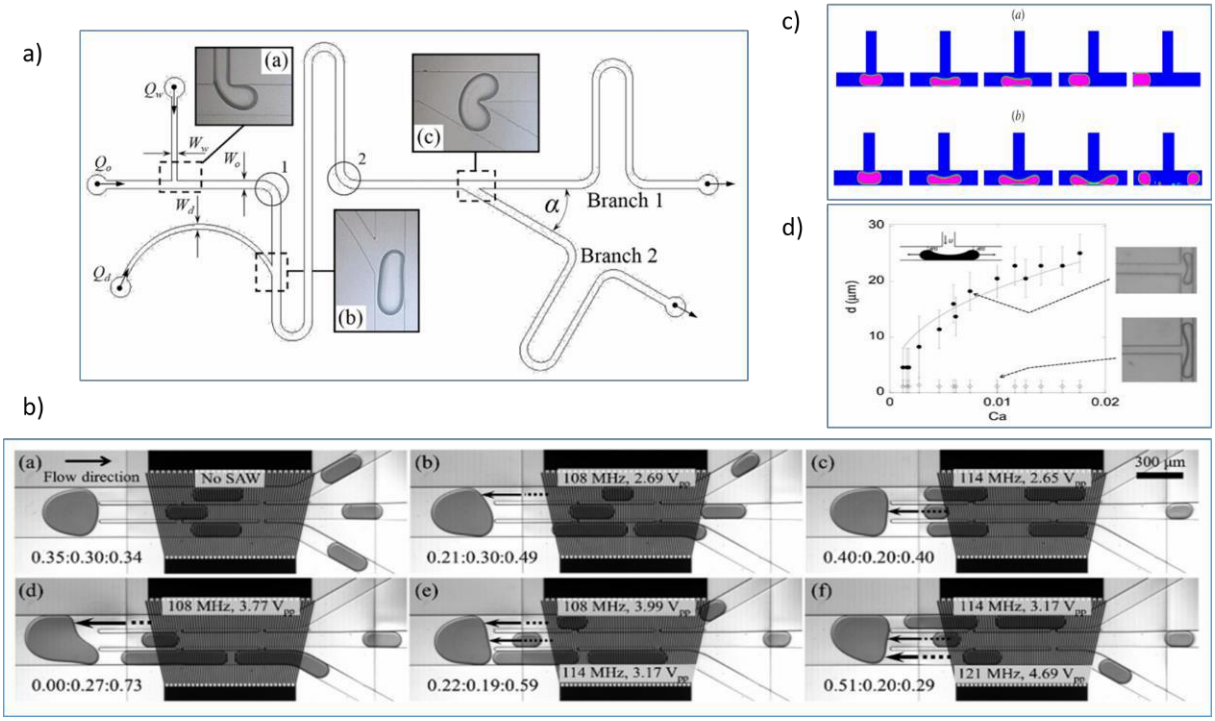

Figure 2-15. (a) The angle junction used to split droplets (Wang et al. 2018); (b) Non-breaking vs breaking droplet (Leshansky et al. 2009); (c) Droplet size vs Capillary represent droplet splitting cases (Jullien et al. 2009); (d) Images of droplet tri-splitting with varying location and magnitude of the acoustic wave (SAWs) (Park et al. 2018)

breaking up – a phenomenon termed droplet slipping. At the junction, droplets prefer to enter where the hydrodynamic resistance is smaller. A 2D analytical model worked out by Leshasky and Pismen showed that two daughter droplets were produced by the combination of the lubrication flow and the built-up pressure at the junction (Leshansky and Pismen L. M. 2009). In detail, the mother droplet elongated and blocked the main flow at the T-junction, leading to increased pressure upstream. Then, the continuous flow squeezed the mother droplet at a stagnation point until it split into two smaller droplets. This model also agreed with an experimental study done by Link et al. (D R Link et al. 2004). According to many research publications, the size of daughter droplets can be controlled by making the outlet channel asymmetric or symmetric, or by changing the flow rate and pressure at side-channels (Jullien et al. 2009).

Later research showed that droplets can also be split by using a sharp angle geometry, instead of a 90 degree one (Doonan and Bailey 2017; Xiang Wang, Liu, and Pang 2018). In summary, to use passive droplet splitting methods, the systematic critical Capillary number for break-up needs to be considered, and the influence of disturbances in the outlet channels should be minimized.

Passive methods for splitting droplets depend on the geometries involved and the local critical Capillary number; therefore, such methods may be not reliable in some applications. Active methods, however, offer better controllability. For instance, electromagnetic force (Pamme 2006) can be used to split droplets containing magnetic particles, when the droplets are shuttled across a set of six electrodes for 30 seconds at a rate of 40Hz. Another method introduced by Sung's group was applying surface acoustic waves (SAWs) to split droplets on-demand inside a straight micro-channel (Jung et al. 2016). The mechanism was interesting because the acoustic beam acted as an acoustic knife that gradually disturbed the interface of a water-in-oil droplet. Eventually, the droplet was cut into two parts. The splitting ratio was controlled by changing the SAW voltage and the flow rate of the two phases (Jung et al. 2016; Jinsoo Park et al. 2018). Electrowetting-on-dielectric (EWOD) has also been proposed to split droplets (Cho, Zhao, and Kim 2007). Recently, studies using images taken in real-time as feedback signals to control a pressure source has opened a new research direction that combines droplet-based microfluidics and micro-controllers. A report by Wong and Ren demonstrated that this platform allows droplets to be generated, split and merged easily (Wong and Ren 2016). Although the system was control manually, it has shown the potential to function automatically in the future (Hébert, Courtney, and Ren 2019).

Droplet sorting

During experiments, many un-wanted droplets may be generated, requiring that they be sorted out from the desired population (M. M. Wang et al. 2005; Cristobal et al. 2006; Y. C. Tan, Ho, and Lee 2008; Baret et al. 2009; Z. Cao et al. 2013; Hejazian, Li, and Nguyen 2015; Xi et al. 2017a; X. Niu et al. 2007;

Carlson, Do-Quang, and Amberg 2010). In passive methods, sorting mechanisms follow the principal of applying a bias to constantly differentiate droplets; whereas, active sorting uses external sources as mechanisms to both manipulate the motion of droplets and detect the sorting parameter. Passive methods have limitations in terms of droplet size (Y. C. Tan, Ho, and Lee 2008; Chabert and Viovy 2008). There are a number of designs for passively sorting droplets at a bifurcation channel (Y. C. Tan, Ho, and Lee 2008). The branches of the bifurcation are designed so that the stream lines split unevenly. The drag force on droplets exerted by the exit flows is proportion to the flow rate at the branches. The shear force imbalance applied on droplets of different sizes directs them to different channels (Y. C. Tan, Ho, and Lee 2008; Hatch et al. 2013; Pit, Duits, and Mugele 2015). Active droplet sorting methods are preferred to passive ones.

Dielectrophoresis (DEP) based devices have been developed for active sorting. In the research done by Weitz's group, droplets are dielectrophoretically sorted based on the preset fluorescent intensity threshold (K. Ahn et al. 2006). The authors note that the shear at the junction might limit the sorting rate in the design; for instance, at high flow rates, droplets might possibly split. Wang et al. also demonstrated a means of sorting droplets into five separate chambers using DEP activation (L. Wang et al. 2007). Another technique for applying electrical signals to enhance droplet sorting was introduced by Ahn et al. (K. Ahn et al. 2006). Embedded ITO electrodes were used to sort droplets at frequencies of up to 4kHz. Generally, optical detection systems have been used both to detect fluorescent signals and sort droplets (Xi et al. 2017b). Nguyen's group developed an optical detection system integrated with optical fibers for measuring droplet sizes (Hejazian, Li, and Nguyen 2015); and the system simultaneously sorted droplets based on their measured sizes. Similarly, Baret et al. developed the most complete droplet sorting system so far, based on two mechanisms: optical fluorescent detection and DEP manipulation (Baret et al. 2009). They showed that fluorescent-activated droplet sorting offered many advantages from micro-plate screening to fluorescent activated cell sorting. Magnetic sorting (Teste et al. 2015) and surface acoustic

waves are other methods that allow un-desired droplets to be isolated. Overall, despite efforts at developing multiple ways to sort droplets, droplet sorting has been hampered either by the challenges of microfabrication in active methods or by the lack of robust designs in passive methods (Casadevall I Solvas and Demello 2011; Frenz et al. 2009; Ting et al. 2006; Pit, Duits, and Mugele 2015; Y. C. Tan, Ho, and Lee 2008; Baret et al. 2009; Z. Cao et al. 2013; Lombardo et al. 2019).

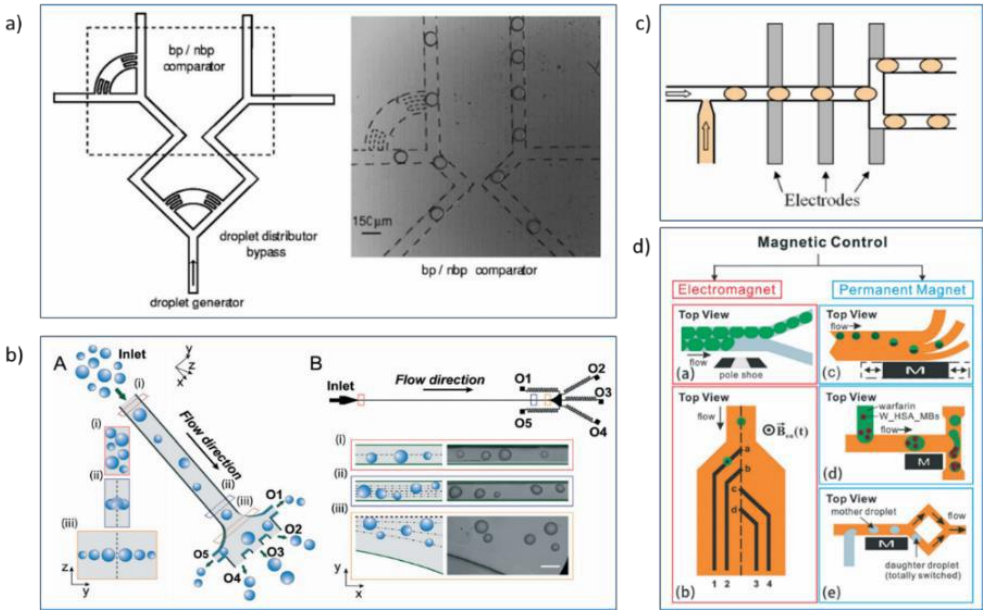

Figure 2-16. (a) Schematic and snapshot of two junctions in the same device fed by identical means with outlet branches of equal lengths (Cristobal et al. 2006); (b) Size-based sepeartion of hydrogel droplets due to size-dependent lateral inertial focusing equilibrium positions (Li et al. 2018); (c) Schematic view of the microfluidic chip (Niu et al. 2007); (d) Schematic sketch and classification of droplet sorting with a magnetic field (Xi et al. 2017)

2.2 Applications of the droplet microfluidics in other fields

Droplet-based microfluidics have offered unique functionalities, advancing research that seemed impossible to achieve with conventional bench top methods and single phase microfluidic devices. This section will present a few interesting applications of droplet-based microfluidic platforms primarily in biology and chemistry, but also in nanotechnology, and in pharmaceutical, biochemical and tissue engineering.

Nanotechnology

In nanotechnology, droplet-based microfluidic devices offer experimental environments that can help in the comprehension of crystallization and the formation of crystals (Nisisako et al. 2006; Puigmartí-Luis 2014; Xiaoguang Wang, Bukusoglu, and Abbott 2016; Yeap, Acevedo, and Khan 2019; Yoon et al. 2014). The traditional batch-based methods are labor intensive, time consuming, and suffer from their stop and start nature, leading to difficulties in determining optimal conditions for crystallization. In contrast, droplet-based microfluidic techniques allow researchers to manipulate droplets which work as micro-reactors that offer continuous chaotic mixing in tiny volumes of fluids on the order of nanoliters or even picoliters. In addition, experiments conducted in droplet microfluidic devices are not influenced by gravity and are turbulence-free. Furthermore, in using droplet microfluidics devices, the high surface-to-volume ratio environments offer excellent control of mass and heat transport.

In 2002, research by Edel and deMello established that droplet based method could be useful in investigating nanocrystalline semiconductors (Edel et al. 2002). By continuously producing small droplets containing Na_2S and $Cd(NO_3)_2.4H_2O$ and observing the impact of the flow rate on the monodispersity of the nanoparticles, the authors concluded that the small sizes of droplets and their monodispersity ensured thermal and chemical homogeneity throughout the entire reaction volume, resulting in homogenous reaction conditions for nanoparticle synthesis. Similar to Edel' study, Shestopalov et al. further investigated the multiple-step synthesis of nanoparticle performance in a microfluidic droplet system (Shestopalov, Tice, and Ismagilov 2004). In 2006, Hung and colleagues successfully demonstrated that their droplet-based microfluidic device could be used for the synthesis of CdS and CdSe core-shell nanoparticles (Hung et al. 2006). They noted that the multiple steps of the synthetic reaction would be better controlled by using the droplet-based microfluidic device. The experimental process was completely monitored under fluorescent microscopy. Another study, by Duraiswamy and Khan, reported that the sizes and shapes of functional nanocrystals could be precisely controlled using droplet-based

microfluidic devices (Duraiswamy and Khan 2009). To control the sizes and shapes of nanocrystals, the individual steps of the synthesize process, such as regent addition, diffusive mixing, reaction conditions, were carefully regulated. Other studies showing the key roles of droplet-based microfluidics in synthesizing nanoparticles have also been mentioned in many recent review articles (Valencia et al. 2012; Puigmartí-Luis 2014; Mashaghi et al. 2016).

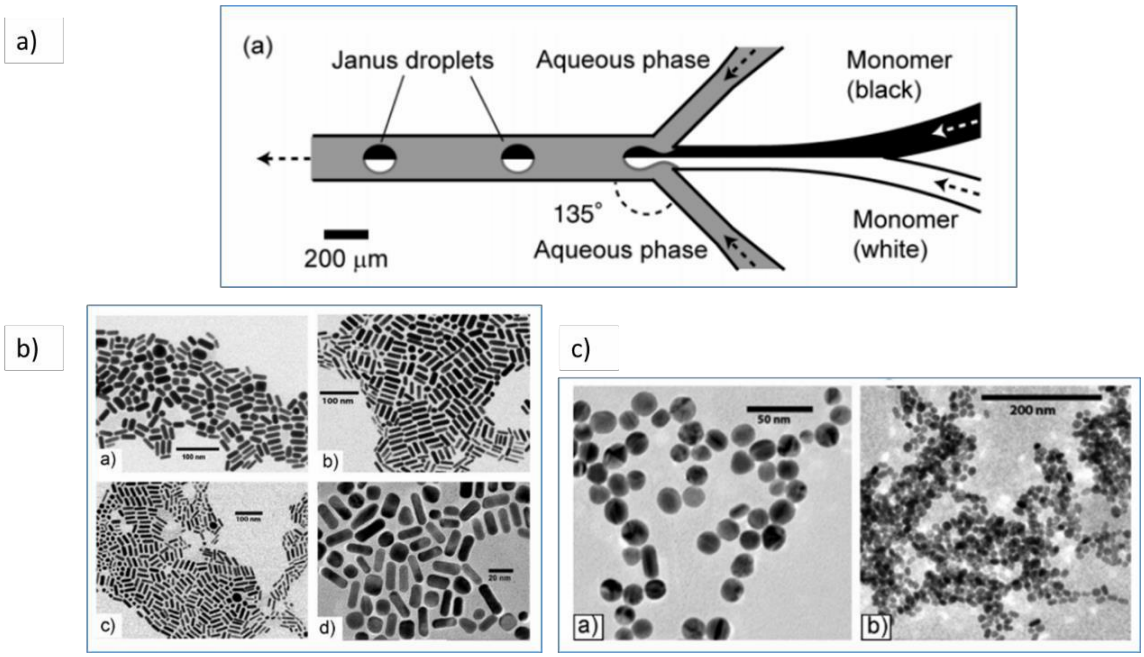

Figure 2-17. Formation of biocolored Janus droplet in a planar microfluidic geometry (Nisisako et al. 2006); (b) & (c) TEM images of rod-shaped and spherical-spheroidal particles synthesized using droplet-based microfluidic systems (Duraiswamy et al. 2009)

Biochemistry and pharmaceutical research

A major role of droplet-based microfluidic devices in pharmaceutical research and biochemistry is in improving screening performances, as the devices enable scaling down of the reaction time; meanwhile, they facilitate scaling of the numbers of assays (Goddard and Erickson 2009; Agresti 2010; Tran et al. 2012; Schneider, Kreutz, and Chiu 2013; Perozziello et al. 2014; Walsh et al. 2017; Giuffrida, Cigliana, and Spoto 2018; Yeap, Acevedo, and Khan 2019; Faustino et al. 2016). For example, the reaction and

analysis times for screening drug compounds that inhibit tau-peptide aggregation, related to Alzheimer's disease, were significant reduced using a droplet-based microfluidic device (Courtney et al. 2016). Specifically, the process was conducted with on-demand trapping of droplets that carried sample reagents. The inside micro-wells and the reaction time of drug inhibition were studied by recording the change of relative fluorescent signals. In another study, Griffiths's group showed that using a droplet-based microfluidic device achieved greater numbers of assays in the short-term, leading to increased numbers of data points that can be identified in a primary drug-screening and characterized in drug dose-response analysis (Miller et al. 2012). Thousands of independent micro-reactors have been generated, containing fixed concentrations of samples that are prepared in advance, but the concentrations of each sample inside individual droplets were varied by tuning the flow rates of individual streams. A 3D internal flow field of droplets advanced the reaction; as a result, complete mixing was achieved in milliseconds.

Moreover, microfluidic devices are well-suited for studying enzymatic reactions; for instance, droplet-based microfluidic platforms have been used to investigate the evolution of CotA laccases (Mashaghi et al. 2016). Another screening platform advanced the evolution of discovering variants of the enzyme horseradish peroxidase (HRP) (Bai et al. 2010). The platform allowed researchers to robustly screen a library of 10^8 in ~10 hours, but less than 150uL of total reagent volume was consumed. Over several years, a range of microfluidic devices for performing protein analysis have been reported. The devices are capable of extracting and processing large amounts of information in a sensitive and throughput manner. In other biochemistry studies, droplet digital PCR (DDPCR) is another example of the use of droplet-based microfluidic devices supporting the research (Mashaghi et al. 2016; S. C. Taylor, Laperriere, and Germain 2017; Baume et al. 2019; Khater et al. 2019; Ma et al. 2019). One, among thousands of other studies, has showed that high throughput DDPCR systems can be enabled to achieve absolute quantitation of DNA copy numbers (S. C. Taylor, Laperriere, and Germain 2017). DDPCR devices also offer orders of magnitude more precision and sensitivity than the older real-time PCR, which used conventional TaqMan

assays with a 96-well plate workflow (Hindson et al. 2011; S. C. Taylor, Laperriere, and Germain 2017). Researchers have also claimed that DDPCR makes it possible to explore complex genetic landscapes and discover new molecular diagnostics (Mcdermott et al. 2013; Petralia and Conoci 2017).

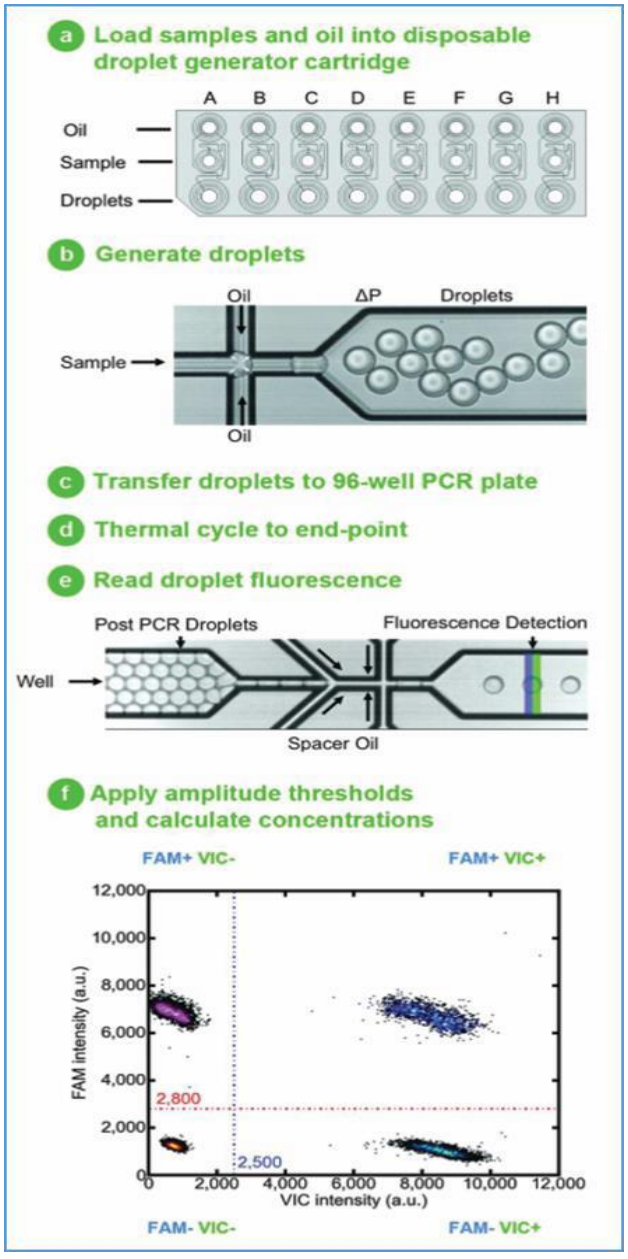

Figure 2-18. Droplet digital PCR workflow (Hindson et al. 2011)

Cell and tissue engineering

Droplet-based microfluidic technology offers a vital approach to studying single cells or single embryoid bodies, a field related to tissue engineering (Köster et al. 2008b; Shi et al. 2008; L. Yu, Chen, and Cheung 2010; Mazutis et al. 2013; Schoeman et al. 2014; Rotem et al. 2015; Blauch et al. 2017; Klein et al. 2015; Lecault et al. 2012; Lan et al. 2017) To develop new diagnostic and therapeutic approaches, the key information – molecular distributions, drug-target interactions – may be hidden at the level of single molecules or single cells (Novak, Richard; Zeng, Yong; Shuga, Joe; Venugopalan, Gautham; Fletcher, Daniel; Smith, Martyn; Mathies 2011; Fernandes et al. 2009; Heath, Ribas, and Mischel 2016a). The single-cell level data is important and significantly advances single-cell studies, such as single-cell barcoding (Lan et al. 2017), single-cell analysis in cancer research and therapy (Yin and Marshall 2012; Lecault et al. 2012; D. K. Kang et al. 2014), and so on. Isolating single cells, typically in the size range of a 2-30μm, in a high throughput manner and analysis of those cells at the molecular level is problematic in bench-top methods. In general, the encapsulation process depends on Poisson distribution (Collins et al. 2015; Lagus and Edd 2013a). Thus, the probability of finding a certain number of cells inside a particular volume should follow the equation:

$$D_{k,Poisson} = \frac{\lambda^k e^{-\lambda}}{k!}$$

where λ is an average number of cells per volume. Mazutis et al. introduced a platform that encapsulated individual mouse hybriodma cells, fluorescent probes and single beads coated with anti-mouse IgG antibodies, in each droplet (Mazutis et al. 2013). Similarly, Schoeman et al. presented a droplet-based device for screening a heterogeneous hybridoma-cell population to obtain clones producing monoclonal-antibodies (mAbs) (Schoeman et al. 2014). Not only can single cells be encapsulated in a droplet, Lagus and Edd et al. demonstrated that inertial microfluidic flow enabled them to self-order cell trains in a micro-channel, leading to encapsulation of single or dual cells in droplets (Lagus and Edd 2013a; 2013b). However, they utilized high flow rates and high aspect ratio channel geometry to achieve the inertia self-ordering in microfluidics. This approach had drawbacks; for example, it requires a large footprint for making long/spiral channels and high flow rates that usually must be applied by syringe pumps causing fluctuation during droplet formation, etc. (X. Chen and Ren 2017b).

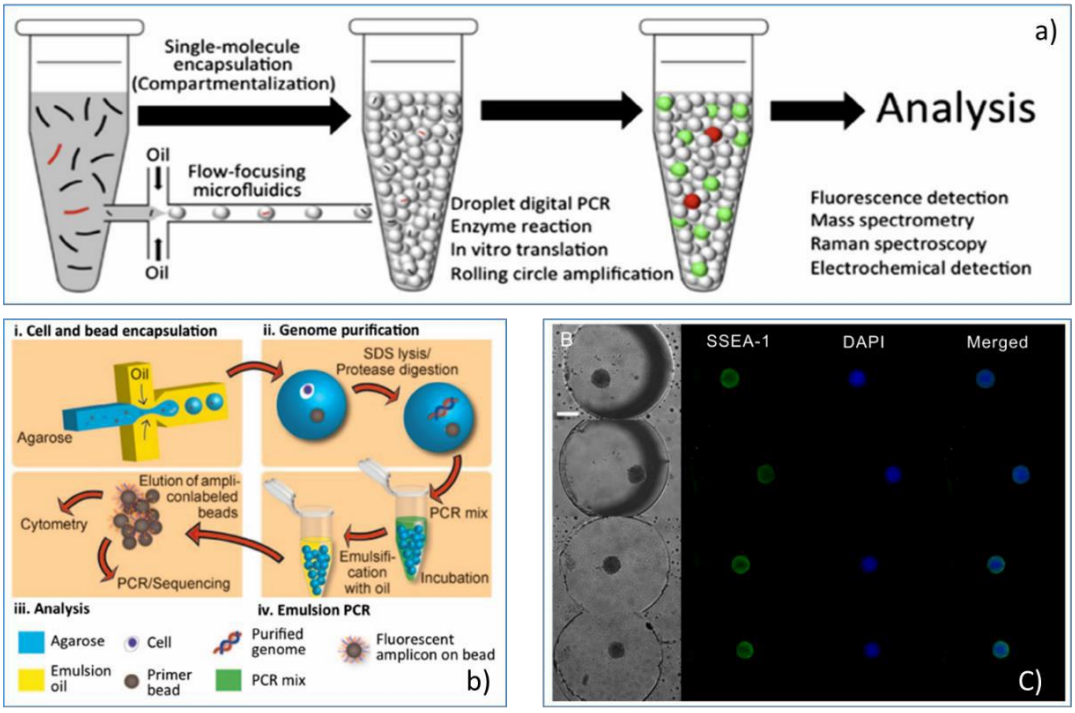

Figure 2-19. (a) Rare target molecules in complex biological sample are compartmentalized, amplified and analyzed using droplet microfluidics at the single- molecule level (Kang et al. 2014); (b) Agaros droplet based single cell ddPCR system (Novak et al. 2011); (c) Embryoid body formation on-chip (Wu et al. 2016)

Further research, presented by Yu et al., showed that bringing together the encapsulation of LCC6/Her2 breast tumor cells in droplets and trapping them in U-shaped drop-spots, facilitated the comprehensive study of multicellular tumor spheroid formation (L. Yu, Chen, and Cheung 2010). This approach was proposed as means for developing anti-cancer drug testing. Another investigation related to cancer therapeutics also presented the development of single-cell cytotoxicity assays with automated generation of optically-coded droplet libraries using a droplet-based microfluidic device. Brouzes et al. proved the concept of the possible cytotoxic effects of single leukemic monocyte U937 cells in the presence of mitomycin C at different concentrations (Brouzes et al. 2015). Over recent years, researchers have not only developed platforms for encapsulating single cells and studied them in 2D environments, but also established a PDMS-based microfluidic hanging drop for forming single embryo bodies (3D aggregates of pluripotent stem cells) (Bratt-Leal, Carpenedo, and McDevitt 2009; Y. Y. Choi et al. 2010; E. Kang et al. 2010; C. Kim et al. 2011; H. W. Wu et al. 2016). PDMS-based microfluidic hanging drop technology has opened up a new era of studying embryoid bodies on-chip. Compared to the conventional hanging drop technique, the device allowed for media exchange while the droplets were hanging on-chip, as well as for high throughput formation of EBs without using complex equipment. Thus, the study suggested that characterization of EBs and the study of immunochemistry could be accomplished on-chip, and offered the hope of growing mini-organs for further development of customized-drugs (Bratt-Leal, Carpenedo, and McDevitt 2009; H. W. Wu et al. 2016).

Taken together, all studies introduced above among the mass of literature suggest massive roles for droplet-based microfluidic technology in different research areas, from nanotechnology to biochemistry and pharmaceutical studies.

2.3 Personal perspective

Droplet based microfluidic technology is involved in many research areas, offering fast chemical mixing, homogeneous droplets generation for chemical synthesis, etc. The evidence also suggests that using droplet-based technology for the encapsulation of particles/cells, especially loading single cells/particles in droplets of controlled volume in the pL to nL range, is among the most important factors for microbiology (Rotem et al. 2015), single cell genomics (Gawad, Koh, and Quake 2016), drug discovery (Kalisky and Quake 2011), therapeutic research (Leeper, Hunter, and Cooke 2010), and material synthesis (Choe et al. 2018). Studying whole cell populations is difficult and misleading due to population heterogeneity and varied time dynamics within the sample; thus, molecular biology studies with single cell resolution are needed. Sizes of (bio) particles are typically varied from a few microns to hundreds of microns (1μm to 200 μm), such as functional magnetic beads, eukaryotic cells and embryoid bodies (Marshall et al. 2012). It is noted that the term (bio) particles mentioned throughout this thesis indicates cells, bio-functionalized particles, and embryoid bodies.

Single (bio) particle encapsulation, whether achieved by passive or active methods using droplet-based microfluidics devices has been explored in the last two decades. Overall, active methods provide users more flexibility and controllability to isolate droplets containing single (bio) particles from unwanted populations (Mazutis et al. 2013; Klein et al. 2015). Nevertheless, these methods have faced the difficulties and inconsistencies related to complex microfabrication and the need to integrate active sources into polymer devices. Current fabrication methods significantly increase the cost of devices, which limits the use of active methods in many applications. In addition, in some active methods, the heat applied to droplets to disturb their interfaces for sorting may influence real samples, such as cells, proteins, etc. Those active methods are rarely implemented in microfluidic devices unless necessary. In contrast, for passive droplet microfluidics, the inertial microfluidic technique to initially order cells/particles before the encapsulation is recommended (Edd et al. 2008; Clausell-Tormos et al. 2008; Je-

kyun Park 2008; Lagus and Edd 2013a; Kemna et al. 2012). Although this method provides high encapsulation efficiency, a major challenge arises in single cell encapsulation due to the high absolute flow rates required ($\geq$ 10 μL/min) and the enlarged device footprint needed for holding the curvy and long micro-channels required for cell-ordering. For instance, when using high volumetric flow rates to encapsulate single embryoid bodies within droplets, the induced high shear stress applied on the embryoid bodies would break the 3D cell aggregation structure into single cells. Moreover, co-encapsulation of single (bio) particles with another solution by injecting that solution downstream is challenging because of a lack of droplet synchronization. Additionally, integration of multiple components in one microfluidic device is difficult as it requires the understanding of coupling effects via the microfluidic network. These challenges limit the uses of passive droplet-based microfluidic devices in single (bio) particle encapsulation studies combined with multi-steps reactions. With these difficulties in mind, I realized the need to devise a microfluidic platform that:

- functions robustly during the multiple or single (bio) particle encapsulation processes, and does not require high flow rates to achieve the inertia needed for particle pre-ordering before encapsulation;
- enables the co-encapsulation of multiple reagents and these particles in one step, thus, minimizing the device footprint used for encapsulation and for the later injection of reagents into droplets;
- minimizes coupling effects induced by the integration of multiple components, such as merging, mixing, generating droplets in parallel, etc., in one platform;
- does not require costly and complex fabrication procedures.

Motivated by these criteria, I started by investigating a double-cross junction geometry and stratified flow structure, the latter of which is needed to generate hydrodynamic focusing between the two cross

junctions. Fine tuning the focusing width provides a new approach to align (bio) particles before encapsulation. The thesis's hypothesis is that using stratified flow structure occurring between the two cross junctions allows researchers to encapsulate either single or multiple (bio) particles with at least two reagents simultaneously in one step. Following chapters will demonstrate the immense impacts of this approach on the applications of interest. Chapter 6 will deliver a comprehensive experimental study to provide in depth knowledge of using a double-cross configuration with stratified flow to achieve hydrodynamic focusing with a viscosity contrast that assists the single encapsulation process.

Nomenclature

Acronyms:

1D one dimensional

2D two dimensional

3D three dimensional

DEP dielectrophoresis

DNA deoxyribonucleic acid

EWOD electrowetting on a dielectric

FACS fluorescence activated cell sorting

LOC lab on a chip

O/W oil-in-water

PDMS polydimethylsiloxane

PTFE polytetrafluoroethylene

Pe Peclet number

µ-PIV micro particle image velocimetry

UV ultra violet

W/O water-in-oil

Mathematical Symbols:

α fitting factor

β fitting factor

γ interfacial tension (N/m)

θ contact angle (rad)

κ curvature (1/m)

μ dynamic viscosity of fluid (Pa.s)

ρ density of fluid (kg/m^3)

φ ratio of dispersed to continuous phase flow rates

D diameter (m)

g_c geometric constant (dimensionless)

U velocity (m/s)

$Q_{d,c,m}$ flow rate of dispersed phase, continuous or main channel (m^3/s)

Chapter 3: Fabrication process and experiment setup

The section below describes the fabrication protocol and experimental facilities used to accomplish the experiments presented in this thesis.

3.1 Fabrication protocol

The microfabrication technique chosen for making microfluidic devices presented in this thesis is soft lithography technique. This approach is preferred in microfluidic *research* for its simplicity and cost-effectiveness (P. Kim et al. 2008). In addition, the polydimethylsiloxane (PDMS) material used to form microfluidic devices is inexpensive and compatible with most bio/chemical applications.

Soft lithography, first introduced in 1998 by Xia and Whitesides, has since been widely employed in many research groups (Xia and Whitesides 1998). In the Waterloo Microfluidic Laboratory, the fabrication protocol has been updated over the years and modified from the original to provide high-quality microfluidic masters. In detail, the process begins with designing a photo-mask that includes negative images of the microchannel layout designed by AutoCAD software and printed on Mylar film with 20k dpi resolution (CAD/Art Service, OR, USA). The minimum microchannel size that can be printed with good quality is 8um due to the limited resolution of printers. In detail, the fabrication can be separated into two steps: (1) making a master and (2) making a PDMS microfluidic device. Starting the fabrication correctly is essential. To prevent bubbles inside the dispensing tube transferring to a master, the preparation of a negative photoresist (SU8-2000 series) one day before is required. A suitable photoresist should be chosen for the desired thickness of micro-channels.

Masters are fabricated from the negative photoresist SU-8 on 4-inches silicon wafers. Firstly, a silicon wafer as a solid substrate on which to fabricate a master is dehydrated to remove moisture from the surface. Then, it is placed on the spin check of the spin coater, and aligned with the centering tool for

depositing photoresist. The thickness of the SU-8 defines the height of micro-channels; thus, it is controlled by different types of SU-8 and the spin coating process (adjusted for speed, acceleration, time). A thin layer of SU-8 2005 (5-10um) is deposited before the actual layer that defines the height of the channels is dispensed. The SU-8 layers are dynamically deposited using a precise pneumatic dispensing system (Ultra 1400, Engineered Fluid Dispensing). Next, soft baking is performed at 65ºC and 95ºC to evaporate the solvent in the photoresist and harden the layers. Subsequently, the wafer is exposed to UV light (Newport) while it is covered with the photo mask containing a design. UV light (~365nm) illuminates and photo-polymerizes the exposed regions, causing cross-linking to begin. Post baking is required to complete the cross linking. Depending on the thickness of the SU-8 layers, the required time varies from 2 to 30 minutes. To achieve multiple-layer lithography fabrication, the processes of spin coating, soft baking, UV-exposure and post baking should be repeated for other layers. Mask alignment is extremely important if a master requires the multi-layer fabrication process. It is recommended that the master containing SU-8 layers is placed in a dark place at least 2 hours before it is transferred into a large bath of SU-8 developer to dissolve unexposed regions. The fabrication process is completed after the wafer is washed with clean SU-8 developer, isopropyl alcohol, deionized water, and blown dry with nitrogen. Furthermore, the moisture in the SU-8 may affect the long-term quality of a master. Therefore, a master should be stored inside a clean and dry container. To keep the photoresist from peeling off, UV glue (Locitte 3311) can be used to cover the edges of the wafer. An overview of the soft lithography fabrication process is illustrated in Figure 3-1.

In the second step, after a developing process, a PDMS molding is prepared by mixing a 10:1 ratio of base to a curing agent, degassing it and pouring it onto a silicon master. According to Johnston and Tracey, the mechanical properties of bulk Sylard 184 PDMS were varied with curing temperature and time (Johnston et al. 2014). Compared to Dow Corning recommendation for the curing duration, their research provided a corrected tensile curing duration as well as compressive curing duration versus

temperatures. Our group recommends baking the PDMS mold on a hot plate at 95ºC for at least an hour and a half. The mold is peeled off and shaped after cooling. Fluidic access holes are made using a biopsy punch. Bonding PDMS micro-channels with a glass slide, already coated with a thin layer of PDMS (5-10μm), is the last step in achieving a PDMS microfluidic device. Both the glass slide and the trimmed PDMS mold are treated with oxygen plasma for 10 seconds at high power level. The plasma treatment temporarily makes the surface of PDMS hydrophilic against the natural hydrophobicity of PDMS. To generate water-in-oil droplets, in which oil phase wets the channels, hydrophobic micro-channels are required to prevent partial wetting issues, or droplets leaking. Hence, after an oxygen plasma treatment, a microfluidic device is placed on the hot plate at 120ºC for a least a day before use. Ideally, it should be baked for 2 days. In some applications, depending on the oil used, such as FC-40 and FC-70, surface treatments may be required to provide the perfect wetting condition for droplet generation. Surface treatment with Aquapel (PPG Industries) is usually applied to coat PDMS channels (Köster et al. 2008b; Bai et al. 2010; Lan et al. 2017). To use this method, the oxygen plasma treatment should be done for 1 to 2 minutes at high power instead of 10 seconds. During the treatment, Aquapel (PPG Industries) should be applied slowly into the microfluidic network using an air-tight syringe to prevent micro-bubbles being trapped at corners, leading to non-uniform coating. Furthermore, after 30 seconds to 1 minute treatment of micro-channels with Aquapel, a device should be baked at 95ºC for 1 minutes. Then, nitrogen should be injected into the channels to remove extra Aquapel. Especially after a treatment, devices should not be exposed to air before use.

Before running experiments, both the microfluidic device and a master need to be measured. The width of channels can be measured using a microscope and a CCD camera. By using the calibrated scale provided by NIS Element Advanced software, the number of pixels measured can be converted into distance on the image. The height of channels can be measured by adjusting the focusing to the top and the bottom planes respectively. The difference between two planes is the height of channels. To be more

accurate, five to 10 random points from a master are picked for measurement. The difference between those measured points should be less than 5 um to confirm that the microfluidic device has a uniform channel height.

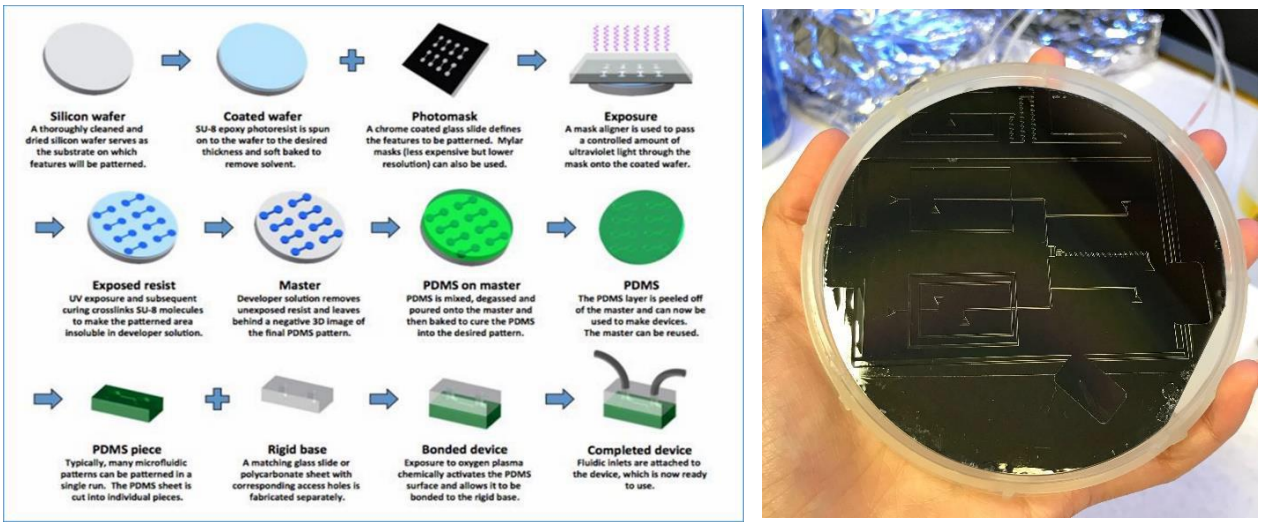

Figure 3-1.(Left) Soft lithography technique using for micro-fabrication (source: https://cleanroom.soe.ucsc.edu/microfluidics); (Right) Microfluidic design fabricated on a silicon wafer using Waterloo Microfluidics Laboratory facilities

3.2 Experimental setup

The experiment setup is illustrated in Figure 3-2. The general system used to run experiments consists of either a pressure system or a syringe pump, inverted epifluorescence microscope, high-speed camera, CCD camera, UV light hand held, mercury lamp and other connecting equipment.

Injecting and driving fluid flows requires a microfluidic pressure control system (Fluigent MFCS -4C/8C) and/or syringe pump (pump 33, Harvard Apparatus). In this thesis work, a pressure system is chosen to use as an applied pressure source because the syringe pump limits the number of inputs, and it takes up to 30 minutes for the system to reach steady state depending on the flow rate and the compliance of the system. Fluids are prepared in sterile vials (Simport), which are tightly screwed to the reservoir holders – Fluidwells (Fluigent). A pressure system can control up to 8 outputs at the same time and provide a

maximum of up to 1 bar (for Fluigent MFCS-8C) and up to 2 bars (for Fluigent MFCS-4C). ETFE (Ethyltrifluoroethylene) tubing (IDEX) is used to carry fluids from vials to microfluidic chips. The tubing has a large inner diameter (~ 500 um) in comparison to the channels, to minimize any pressure loss from the source-to-chip inlets. Pressures are tuned by using provided software. Furthermore, the liquid flow sensors (Sensirion) are also integrated with the pressure system to verify the flow rates during experiments.

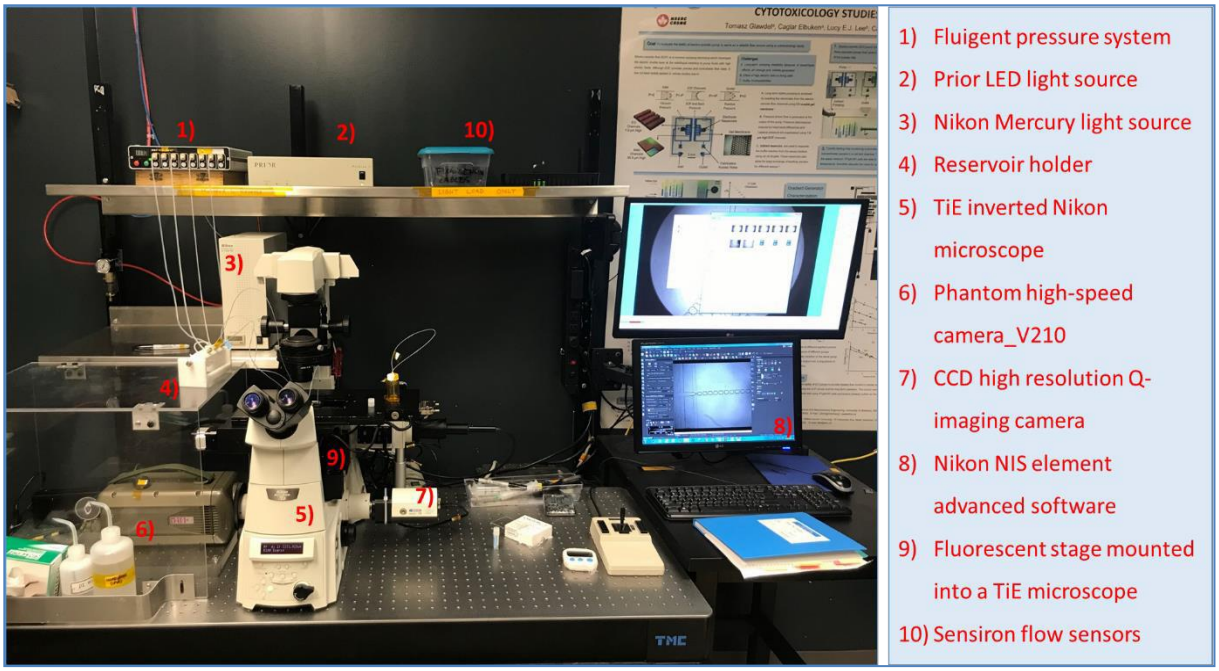

Figure 3-4. Overview of an experiment set up in the UW microfluidics laboratory (E3-3175B)

In addition to the pressure system, experiments are visualized using an inverted epifluorescence microscope system (Eclipse Ti, Nikon) and two cameras: (1) a highspeed camera (Phantom V210) and (2) a CCD camera (Retiga, Q-imaging). In detail, a CCD Retiga camera is excellent for fluorescence imaging because of its sensitivity and high resolution. However, the CCD camera can only capture up to 21 frames per second, which is not good enough to capture the dynamics of droplet generation in a few hundred hertz to kilohertz. Therefore, a high-speed camera, able to capture up to 2000 frames per second at full

resolution (1280x800 pixels), is installed with the microscope on the left port using a C-mount adapter (1X DXM, Nikon). Lowering the resolution, or scaling down the field of view means that the CMOS highspeed camera can easily capture 10,000 frames per second. The camera continuously records images until the trigger is activated. The microscope system mainly includes a programmable stage 3D (x, y, z), objective nosepiece, fluorescent turret and shutters. The lens objectives include CFI Plan fluor 4X, 10X, 20X, 40X and 60X. Available fluorescent filter cubes, installed inside the microscope, provide suitable working range emission and excitation wavelengths. The halogen lamp is used for bright field applications and phase contrast; whereas, a 100W mercury laide lamp (Intensilight, C-HGFIE) is used flor fluorescence. All videos and images are recorded and saved under the .TIFF format or .RAW format and analyzed using ImageJ software (National Institute of Health, MD, USA) and built-in MATLAB codes. Images and videos are recorded when the system is stable.

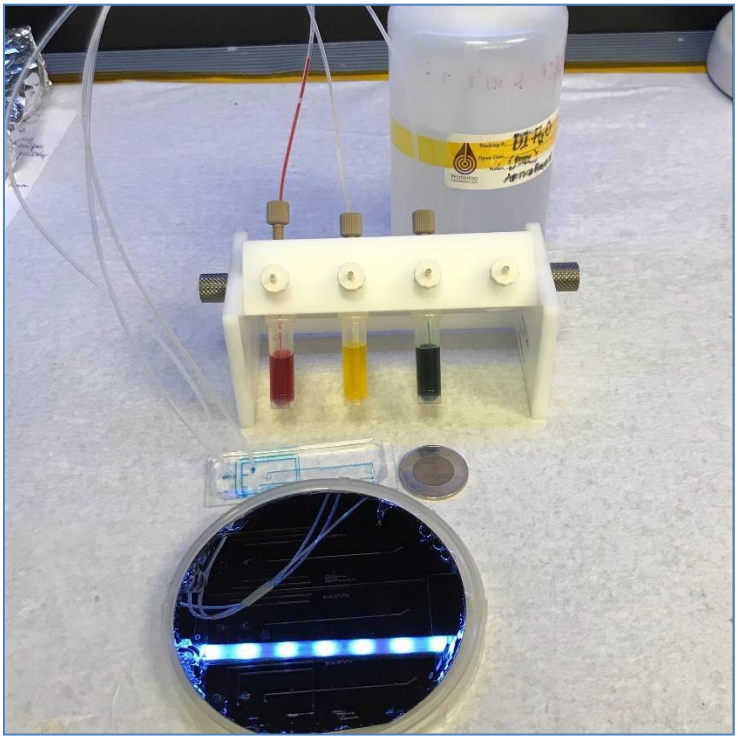

Figure 3-5. A reservoir holder, microtubes and PEEK tubing, silicon master holding microfluidic channel network, a PDMS microfluidic device (filled with food dye)

During the fabrication and experiments, several chemicals mentioned above, including SU-8 photoresists, PGMEA photoresist developers, acetone, PDMS base and curing agent, different types of oils, etc., are hazardous. Safety training is thus required, and all the appropriate safety procedures are followed based on the guidelines described in the MSDS. Chemical preparation must be conducted under a fume hood. Goggles, gloves, respiratory devices, and lab coats must be put on before handling chemicals. Chemical wastes are disposed of carefully following instructions written by the UW safety office.

Chapter 4: A droplet-based microfluidic platform for rapid immobilization of quantum dots on individual magnetic microbeads

The work presented in this chapter was published in the following article:

Thu H. Nguyen, Xiaoming Chen, Abootaleb Sedighi, Ulrich J. Krull, Carolyn L. Ren, "A droplet-based microfluidic platform for rapid immobilization of quantum dots on individual magnetic microbeads", Microfluidics and Nanofluidics, 2018, 22 (6), 1-11

This work was also presented in poster format at the following conference:

Thu H. Nguyen, Xiaoming Chen, Abootaleb Sedighi, Ulrich J. Krull, Carolyn L. Ren, " Development of co-encapsulating and well-mixing droplet microfluidic platform for rapid immobilizing semiconductor quantum dots onto micro-sized magnetic beads", Ontario-on-a-Chip Symposium, Toronto, Canada, May 25-26, 2017

Thu H. Nguyen (Ph.D. candidate, Department of Mechanical and Mechatronics Engineering) designed the final version of a microfluidic platform reported in this thesis chapter. She mainly performed experiments and analyzed experimental results. Xiaoming Chen (Post Doctoral Fellow in the Department of Mechanical Engineering, University of Waterloo) assisted in the first version of the platform design and provided fabrication training. Abootaleb Sedighi (Post Doctoral Fellow in the Department of Chemical and Physical Sciences, University of Toronto Mississauga) assisted in preparing chemical samples for the experiments. Prof. Ulrich Krull (Department of Chemical and Physical Sciences, University of Toronto Mississauga) and Prof. Carolyn Ren (Department of Mechanical Engineering, University of Waterloo) provided thoughtful discussions to accomplish the project.

4.1 The scope of this project

Quantum dots (QDs) provide opportunities for the development of bioassays, biosensors, and drug delivery strategies. Decoration of the surface of QDs offers unique functions such as resistance to non-specific adsorption, selective binding to target molecules, and cellular uptake. The quality of decoration has a substantial impact on the functionality of modified QDs. Single-phase microfluidic devices have been demonstrated for decorating QDs with biological molecules. The device substrate can serve as a solid phase reaction platform, but its uses is limited by difficulty in realizing reproducible decoration at a high density coverage of QDs. Magnetic beads (MBs) have been explored as an alternative form of solid phase reaction platform for decorating QDs. As one example, controlled decoration to achieve unusually high density can be realized by first coating MBs with QDs, followed by the addition of molecules such as DNA oligonucleotides. Uniformity and high density coatings on QDs have been obtained using MBs for solid phase reactions in bulk solution, with the further advantage that the MBs simplify procedural steps such as purification.

This chapter explores the use of a droplet microfluidic platform for achieving solid phase decoration of MBs with QDs, offering control of local reaction conditions beyond that available in bulk solution reactions. Initial testing was based on a similar design that was successful for encapsulation of 10μm microbeads, which received little success with extensive tuning of the flow rate ratios and viscosity contrast. The fundamental study of the flow focusing for ordering the 1 μm MB provided very structured guidance to shorten the optimization time. A microchannel network with a double-cross configuration is designed and optimized to co-encapsulate one single 1 μm MB and many QDs into individual droplets. Each micro droplet becomes a reaction vessel and enhance conjugation through its confined environment and fast mixing. A high density of QDs is coated onto the surface of a single MB even when using a low concentration of QDs. This approach quickly produces decorated MBs, and significantly reduces QD waste, ameliorating the need to remove excess QDs. The methodology offers a degree of precision to

control conjugation processes that cannot be attained in bulk synthesis methods. The proposed droplet microfluidic design can be widely adopted for nanomaterial synthesis using solid phase assays.

4.2 Introduction and project objectives

In the last two decades, a promising nanomaterial, comprised of semiconductor nanoparticles or quantum dots (QDs), has demonstrated tremendous potential for enhancing imaging. Examples include applications such as fixed cell labeling, imaging of live cell dynamics, sensing and *in vivo* animal imaging. QDs are chemically synthesized semiconductor nanocrystals with diameters of a few nanometers (2 to 10 nm) and quantum yields that routinely approach 50-80% (Bruchez Jr. 1998; C.-Y. Zhang et al. 2005; Xing and Rao 2008; Algar, Tavares, and Krull 2010; Sun and Gang 2013; Chou, Zagorovsky, and Chan 2014; He et al. 2014; Y. Cao et al. 2016; F. Yang et al. 2018). They are 100 times more resistant to photo-bleaching than molecular fluorescent dyes (Resch-Genger et al. 2008).

To endow QDs with selective binding capability, different biomolecules such as nucleic acids and antibodies that act as targeting agents or probes have been used to modify the surface of QDs via bioconjugation (Mattoussi et al. 2000; C.-Y. Zhang et al. 2005; Algar and Krull 2007; Resch-Genger et al. 2008). Such functionalized quantum dots have drawn a great deal of attention from both academia and industry because they enable the development of assays, *in vitro* diagnostics, and biosensors (Huo, Lytton-Jean, and Mirkin 2006; J. Kim et al. 2009; Prabhu et al. 2009; Chou, Zagorovsky, and Chan 2014; Inoue et al. 2016; B. Liu and Liu 2017; Godakhindi et al. 2017). For instance, QDs functionalized with DNA oligonucleotides have been successfully used for biological applications within *in vitro* and *in vivo* environments (Boeneman, Deschamps, Buckhout-white, Prasuhn, Goldman, et al. 2010; Lalander et al. 2010; Giri et al. 2011; Cutler, Auyeung, and Mirkin 2012; Noor, Tavares, and Krull 2013; Petryayeva, Algar, and Medintz 2013; Stanisavljevic et al. 2015). QD-based DNA hybridization assays can operate on the basis of fluorescence resonance energy transfer (FRET) which often involves the conjugation of

single-stranded DNA oligonucleotides (ssDNA) with QDs. A FRET pair can form where QDs are donors, and hybridization of the probe oligonucleotide with a target DNA strand that carries a fluorescent label serves as the acceptor (C.-Y. Zhang et al. 2005; Peng et al. 2007; Suzuki et al. 2008; Coopersmith, Han, and Maye 2015). The sensitivity and selectivity of the ssDNA-QD conjugates depends on the density and structural uniformity of the oligonucleotide strands at the surface of the QDs.

One method for increasing the deposition density is to first immobilize QDs on the surface of magnetic beads (MBs) via electrostatic reaction, and then continuously load oligonucleotides onto the surface of the QDs (Sedighi and Krull 2016). This solid phase conjugation strategy also offers the opportunity to concurrently decorate the QDs with different molecules, meaning that the exposed part of the QD surface is coated with a particular probe ssDNA, and on release from the MB, the other face of the QD can be coated with a different probe, or even a different class of molecule than an oligonucleotide. This strategy was implemented for a batch setting by using a bulk solution reaction. While functional, the batch operation imposes limitations. The batch approach does not allow multiple coating processes to be completed in a continuous manner. The reagent concentration is high to push reactions forward, but the consumption in each batch is small, resulting in high cost and large waste. The entire process is prone to variability due to changing conditions such as temperature, and to contamination (e.g. dust). Finally, yet importantly, purification is required to remove excess reagents and QD aggregates at each functionalization step in batch settings (Coopersmith, Han, and Maye 2015). Microfluidics has potential to address these challenges by offering continuous processing using a confined environment for enhancing reactions, reducing reagent consumption, offering sample management for purification and efficient NP collection.

Single phase microfluidics using miscible fluids to transport samples and perform reactions has been reported for decoration of QDs, where the channel surface serves as the solid substrate for immobilizing QDs (Noor, Shahmuradyan, and Krull 2013). This work demonstrated that microfluidic-based solid phase

reactions allowed nucleic acid hybridization within seconds to minutes due to small sample volumes, in contrast to bulk solution reactions where the identical hybridization reaction took hours to reach equilibrium. Despite its success, single phase microfluidics has some inherent limitations such as slow mixing, low throughput and high risk of cross contamination, which have largely limited the quantity and quality of the functionalized QDs and the opportunity to selectively decorate the surfaces of QDs. Droplet microfluidic methods that use an immiscible fluid to disperse the sample reagents into pico- to nano-liter droplets is capable of addressing these inherent limitations (Günther and Jensen 2006; Teh et al. 2008; Y. Zhu and Fang 2013; Rosenfeld et al. 2014; Tomasz S. Kaminski, Scheler, and Garstecki 2016), while maintaining the continuous flow advantage. First, benefiting from the confinement of microchannels, monodispersed droplets can be generated from Hz to kHz rates offering the potential to handle a reasonable quantity of decorated QDs even when the volume per droplet is quite small. Second, three-dimensional (3D) motion occurs within the droplets, which provides almost instantaneous mixing that enables faster and more homogeneous reactions. Finally, selective decoration of the surface of QDs is possible by merging, splitting, trapping and releasing droplets in a controllable manner. Droplet microfluidics allows the integration of multiple reactions, which is needed for the immobilization of QDs on solid substrates such as MBs, conjugation of biomolecules with the solution-facing surface of QDs, releasing the partially-decorated QDs from MBs, and conjugating other biomolecules onto the freshly exposed surface of QDs.

In this study, we target the first step of a process for selectively decorating the surface of QDs, as discussed in the study by Sedighi and Krull(Sedighi and Krull 2016), which demonstrated the feasibility of using a droplet microfluidics platform to enhance rapid, high-density immobilization of QDs onto *single* 1 μm MBs that serve as solid substrates. This step is critical to the subsequent processes and quality of bioconjugation, and thus to the performance of QDs for biosensing and imaging. The ability to manipulate one single MB that is coated with QDs offers a degree of control of the conjugation conditions

that is unattainable in batch settings. One question that arises is whether a droplet microfluidics approach is promising for ameliorating the need for QDs to reach uniform coating density on MBs. Therefore, efforts have been made to characterize the quality of deposition by physical inspection using fluorescence microscopy.

4.3 Working principle and Design of a microfluidic platform

4.3.1 Working principle

To ensure the coating of QDs onto a MB, co-encapsulation of many QDs with only one single MB in one droplet must be achieved which is one of the goals of the design of the microfluidic system. The conjugation between QDs and MBs is via electrostatic attraction, which tends to be rapid and can be facilitated by enhancing mixing in the reaction environment. It is expected that the conjugation occurs within seconds, benefiting from the fast mixing within the droplet due to 3D motion. Electrostatic conjugation requires QDs and MBs to have opposite charges. This is realized by coating QDs with glutathione (GSH) to render surfaces negatively charged, and functionalizing the MBs with positively charged diethyllaminoethyl (DEAE) groups. The association of a magnetic bead with many QDs is referred to as the MB-QD conjugate. This process is schematically illustrated in Figure 4-1.

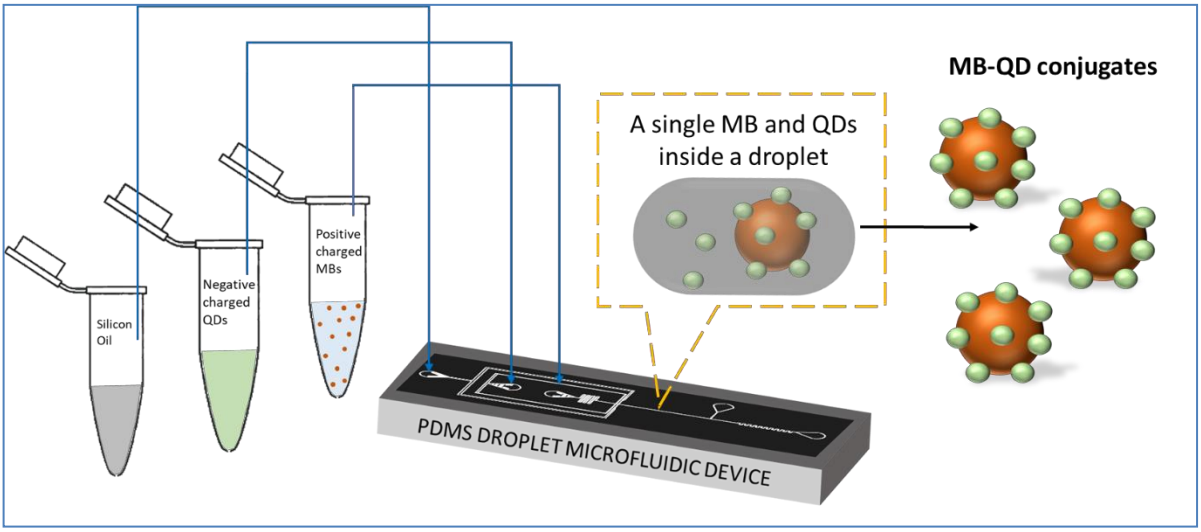

Figure 4-1. Schematic illustration of on-chip, in-droplet Magnetic Bead-Quantum Dots (MB-QD) conjugation via electrostatic adsorption

Monodispersed droplets can be generated using either passive or active methods(Teh et al. 2008; Chong, Tan, Gañán-Calvo, et al. 2016; Y. Zhu and Fang 2013), with each method offering opportunities and disadvantages. A passive method is chosen in this study to form monodispersed water-in-oil droplets because the design requires multiple pressure controls, which is simplified by operating with a multi-output pressure system (MFSC 4C, Fluent). To co-encapsulate one single magnetic bead and QDs, two junctions in series are designed. Two streams of aqueous buffer solutions with one carrying MBs and the other transporting QDs meet at the first junction, forming a stratified flow which is the dispersed phase. The continuous oil phase then interacts with the dispersed phase at the second junction forming monodispersed water-in-oil droplets. Details of this design are introduced later.

Encapsulation of single micron-sized MBs is challenging. In general, each bead should be physically directed and sequentially ordered by using a focused flow. Some strategies have explored the use of gel materials to first encapsulate the beads (B. W. Tan and Takeuchi 2007; Um et al. 2008; Edd et al. 2008; Velasco, Tumarkin, and Kumacheva 2012). Stratified flow with a viscosity contrast between the two fluids to focus the bead stream is proposed to achieve the single encapsulation particle. In the stratified

flow design used herein, the inner fluid has a higher viscosity than the outer focusing fluid. In the beginning, the inner fluid moves more slowly than the outer fluid, resulting in a shear force at the interface. The shear force will speed up the flow of the inner phase, until the velocity difference at the interface disappears. Under constant flow rates, the cross-section area of the inner fluid will decrease when the velocity increases, leading to a sharpened thin line of the inner phase ideal for focusing microbeads. In addition, the high viscosity inner fluid acts like a soft wall, largely reducing the vortex inside the inner fluid. It therefore prevents microbeads from moving out of the droplet during a droplet formation cycle.

The QD solution is used to focus the fluid carrying MBs at the first junction, resulting in a thin stream that allows one single MB of 1 μm diameter to enter a solution that contains many QDs. These two solutions form the total dispersed phase which is then formed into droplets, squeezed by the continuous oil phase at the second junction. Tuning of the flow and geometric parameters allows the encapsulation of single MBs into individual droplets as illustrated in Figure 4-2.

4.3.2 **Design a microfluidic platform**

Initial work explored the in-series two-junction design for manipulation of relatively large polystyrene (PS) beads that had nominal diameters of 10 μm and 4 μm. The design was demonstrated to operate successfully (Appendix B). Challenges arise when applying the same design and operational parameters for selecting individual 1 μm MBs. The MBs are more sensitive to disturbance of flow than the larger PS beads, and refinement of the design and precise control of all the parameters affecting flow is required. The key is to ensure that the focused bead stream between the two junctions is not disturbed by any event occurring downstream, such as droplet formation in the channel network, which causes changes in local and global flow resistance. Attention has also been paid to ensure homogenous mixing. Several

parameters that are widely applicable to single particle analysis influence this process.

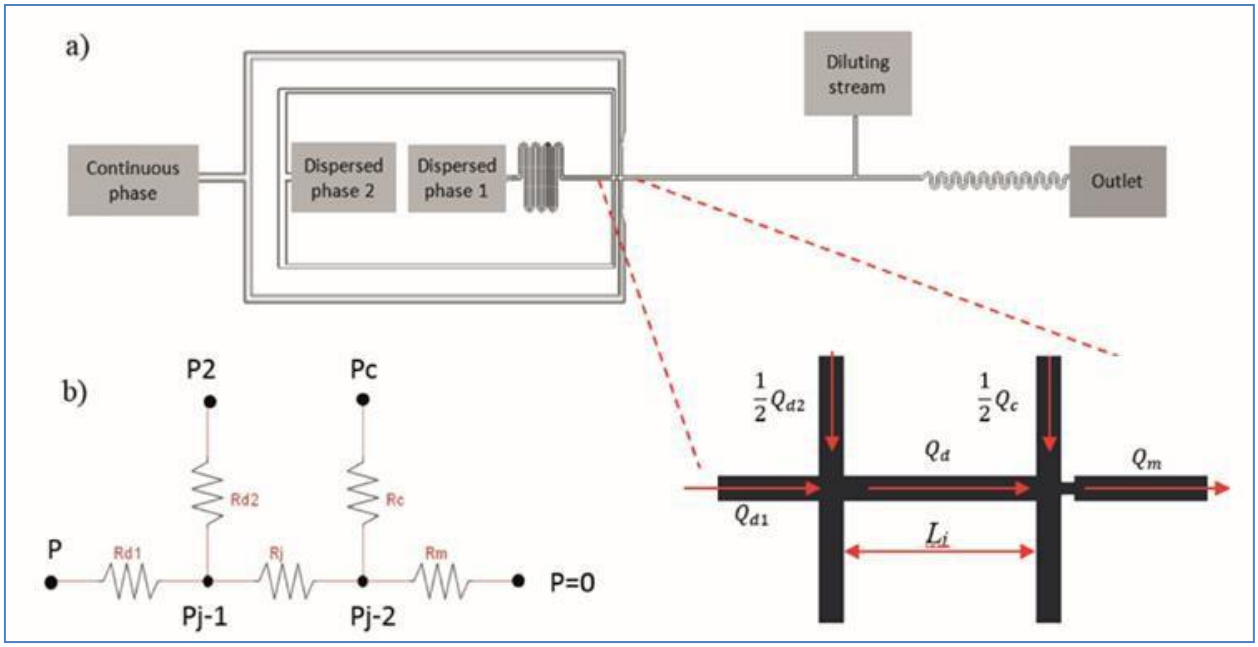

Figure 4-2. a) Layout of the droplet microfluidic platform for co-encapsulating a single MB and many QDs in individual droplets, with rapid mixing to enhance MB-QD conjugation, and b) The equivalent electrical circuit used to modify the microfluidic network.

The distance between the two junctions, L_j, is critical and should satisfy two main requirements: (1) allowing the stratified flow to fully develop, and (2) minimizing diffusion at the interface between the two miscible fluids. In addition, because the two junctions are coupled together, the hydrodynamic focusing at the first junction is also affected by the pressure change during the droplet formation cycle at the second junction(Garstecki et al. 2006; Glawdel and Ren 2012b; X. Chen et al. 2015). A design with the above concerns addressed is proposed using an electrical circuit analog method **(**Figure 4-2b**)**. The microfluidic network is treated as a 1D circuit where the pressures applied at the inlets and outlets are considered as applied voltages, hydrodynamic resistances act like electrical circuit resistors and the volumetric flow rate in each stream is treated as the electronic current. Kirchhoff's current law (KCL) and Kirchhoff's voltage

law (KVL) are applied to analyze the circuit, and thus the operating parameters for the microfluidic network.

In order to minimize the coupling effects caused by the pressure drop between the two junctions and maintain the hydrodynamic focusing of the bead stream, the length between the two junctions (L_j) in our design is set at 300 μm. Smaller channel dimensions provide for improved spatial control of smaller particles such as 1 μm MBs. However, the overall hydrodynamic resistance would increase dramatically, requiring much higher applied pressures to control the flow. In addition, smaller channels are prone to blockages. To balance these concerns, the channel height is set to 25 μm, the widths of the channels upstream and downstream are set to 40 μm and 50 μm, respectively. The microfluidic chip is made of polydimethylsiloxane (PDMS), which absorbs silicon oil. In practice, this absorption results in slight swelling of the polymer and provides smaller channel heights than stipulated (i.e. < 25 μm) – a problem that has been considered in the design. In this study, the channels are primed with silicon oil for 20 minutes to reach saturation, resulting in a channel height of ~18 μm (measured by using an optical microscope focused on the top plan and the bottom plan of the channel). An orifice is used at the second junction to better control and reduce droplet size (Um et al. 2008; Velasco, Tumarkin, and Kumacheva 2012; L. Wu et al. 2017) (Figure 4-2a). The total length of the mainstream after the orifice is adjusted to carry more than 50 droplets, so as to minimize fluctuations in the hydrodynamic resistance and flow rate caused by droplets entering and exiting the mainstream (Glawdel and Ren 2012c).

A long serpentine channel is placed after the orifice to provide homogeneous mixing. 3D motion occurs in each half of the droplet due to the symmetrical vortices created by droplets travelling through straight channels. Mixing between the two halves of the droplet is dominated by molecular diffusion. To ensure homogeneous mixing across the entire droplet, the symmetry must be disturbed by pumping droplets through serpentine channels(Shestopalov, Tice, and Ismagilov 2004; H. Song, Chen, and Ismagilov 2006;

Y. Song, Sauret, and Shum 2013). Non-axisymmetric vortexes inside droplets induced by the time periodic recirculating flow inside plug-shaped droplets results in chaotic advection. This recirculating flow is the result of shearing interaction between the channel wall and the fluid of the droplet. The chaotic flow happening inside the droplet can be interpreted by using Baker's transformation (Tice et al. 2003a; H. Song et al. 2003). The thickness of layers of fluids is calculated by:

$$\text{stl}\,(n) = \text{stl}\,(0) \times 2^{-n}$$

where n is the number of chaotic cycles. The mixing time is estimated by:

$$t_{mix}, \text{Ca} \sim \left(\frac{aw}{U}\right) \text{Log}\,(Pe) \qquad (2)$$

where a is the dimensionless length of the plug measured relative to the channel width, w, and Pe is the Peclet number. Based on the range of operating conditions, the serpentine channel is designed to have 20 turns, each with an inner and outer diameter of 150 and 200 μm respectively, so that the conjugation between QDs and MBs is guaranteed.

4.4 Experimental Validation

4.4.1 **Materials and Experimental setup**

4.4.1.1 Device Fabrication and Materials

Microfluidic devices are fabricated at the Waterloo Microfluidics Laboratory using standard soft-lithography. Briefly, SU8 -2015 negative photoresist (MicroChem) is used to form the micro-mold containing the microchannels. For replica molding, a PDMS (Sylgard 184, Dow Corning) base and a curing agent are mixed and de-gassed at a ratio of 1:9, poured on top of the mold and baked at 95^{o}C for 2 hours. The ratio is tuned so that the PDMS is harder than usual, ensuring that the small channels are not deformed easily through the bonding step. The PDMS substrate is then peeled and cleaned with isopropyl

alcohol before being bonded to a clean glass slide coated with a thin film of PDMS exposed to oxygen plasma treatment. Inlets and outlets are made using a 1.5 mm biopsy punch. To achieve wetting stability, the microfluidic chip is placed on a hot plate at 110^{o}C for 2 days, rendering its surface hydrophobic before the experiment.

The samples for this study were prepared by Dr. Sedighi (University of Toronto-Mississauga). The information on sample preparation is as follows. Green-emitting CdSe/ZnS core/shell quantum dots (photoluminescence, PL at 518 nm) are purchased from Cytodiagnostics (Burlington, ON, Canada). Diethylaminoethyl (DEAE)-functionalized magnetic beads (MB, 1 um) are from Bioclone Inc. (San Diego, CA). The capturing buffer for immobilizing QDs on MBs is a Tris-borate buffer (100 mM, pH 7.4) with 20 mM NaCl. The buffer for releasing QDs from MBs is borate buffer (100 mM, pH 10) with 1 M NaCl. The 5 cSt silicon oil is from Sigma Aldrich Canada. Water-soluble quantum dots have been prepared from the oleic acid-capped CdSe/ZnS quantum dots using a previously reported ligand exchange procedure with glutathione (GSH) (Noor, Shahmuradyan, and Krull 2013). Approximately 0.2 g GSH is dissolved in 600 μL of TMAH. Then 700 pmol of QDs is dissolved in 2 mL of chloroform that is gradually added to the GSH solution. Thereafter, the solution is briefly agitated and incubated overnight at room temperature. After incubation, the GSH-modified QDs (GSH-QDs) are extracted to a top layer of 200 μL of borate buffer (BB) containing 250 mM NaCl, at pH of 9.2. The organic layer is discarded and the aqueous layer is transferred to a 1.5 mL centrifuge tube. Ethanol is added to the QD solution until the solution becomes turbid. The mixtures are centrifuged at 8000 rpm for 7 min to obtain a pellet of QDs. The buffer addition, ethanol precipitation and centrifugation steps are repeated two more times. Finally, GSH-QDs are re-dispersed in a borate buffer at pH 9.2 without NaCl. The concentration of QDs is determined using UV-vis absorption spectroscopy.

4.4.1.2 Experimental setup

The experimental system consists of two main parts: 1) a pressure system (MSFC 4C, Fluigent) that is used to pump the fluids through microchannels, and 2) an inverted microscope (Nikon Ti-Eclipse) that is used to record the dynamic flow of droplets and detect luminescence. The conjugation processes are visualized using a microscope with 40 x (N/A: 0.75mm) and 20 x (N/A: 0.45mm) objectives. The excitation sources are a 100 W LED lamp (Nikon) for bright field images and 100 W mercury halide lamp (Nikon) for fluorescence images. All fluorescent images are captured using a CCD camera (Q-imaging R2000), and videos are recorded using a high-speed CMOS camera (Phantom v210, Vision Research). A fluorescein isothiocyanate (FITC) filter cube is used within the microscope.

4.4.2 **Experimental procedure**

4.4.2.1 Co-encapsulation of QDs and a single particle

The stock solution of QDs solution is diluted to 0.5 nM (unless noted otherwise) using the capturing buffer (Tris-borate, 100 mM, pH 7.4). Following the step-by-step protocol provided by Bioclone Inc., 1 μl (50 μg) of the MB solutions supplied by the manufacturer is washed two times with the releasing borate buffer (100 mM, pH 10), and then diluted by the capturing Tris-borate buffer (100 mM, pH 7.4) mixed with 80 % (wt %) glycerol. The viscosity of the mixture of glycerol buffer is ~44.1 mPa.s, while the viscosity of the mixture of quantum dots buffer is ~1.02 mPa.s. The resulting concentration of MBs is ~10^7 beads/mL. The microfluidic chip is primed with silicon oil for 20 minutes for good wetting condition and thus stable droplet formation. The encapsulation process is controlled by utilizing two side streams (dispersed phase 2) to squeeze the middle stream (dispersed phase 1), resulting in a focusing stream **(**Figure 4-3**).** The droplets were generated under the squeezing regime, which the Capillary is kept in the range from 0.002 to 0.006, and the ratio between the dispersed phase and continuous phase is tuned from 1/8 to 1/4. In details, the flow rate of the continuous phase was set at the range from 0.4 to 0.8 µl/min;

whereas, the total flow rate of the dispersed phase was kept as constant ~ 0.1 µl/min. The single encapsulation is efficient when the ratio of dispersed phase 1 and dispersed phase 2, (λ), is from 0.6 to 0.8. As a result, the 1 μm MBs are kept inside the inner stream since the highly viscous inner fluid acts as a soft wall, and encapsulation into a droplet with the QDs happens at the second junction.

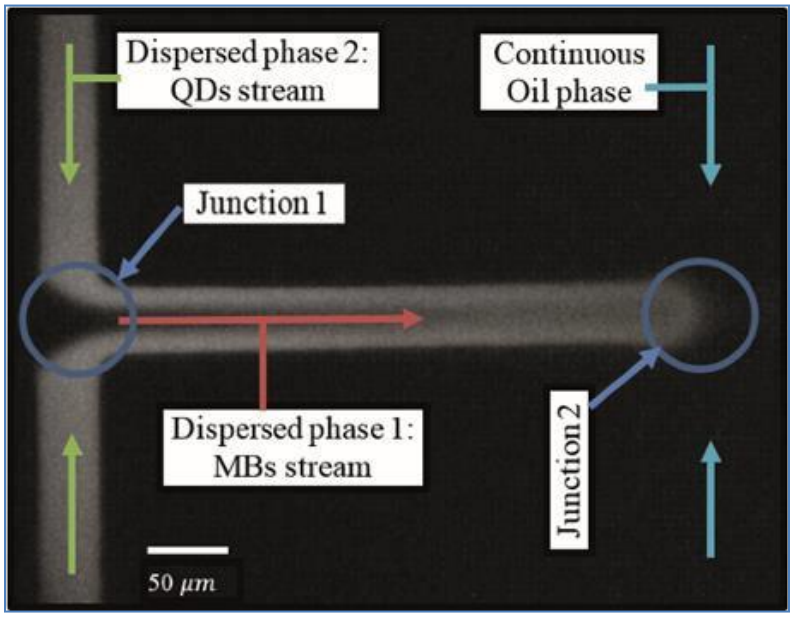

Figure 4-3. Using stratified flow with viscosity contrast in order to align a train of MBs and enhance co-encapsulation of a single MB and many QDs into a single droplet

Three bead sizes – 1 μm, 4 μm, and 10 μm – are used to test the effectiveness of the flow system. Results showing the single encapsulation of 4 μm, and 10 μm PS beads are presented in Appendix B. By counting the number of droplets and frames captured during a droplet generation cycle using the high-speed CMOS camera, the efficiency of encapsulation of a single 1 μm MB was determined to be up to 70 %. Miscounting of the beads that are not at the focal plane is possible but unlikely because the channel height is designed to be 25 μm before swelling and measured roughly 18 μm after swelling. It is observed that the majority of the beads are near the focal plane, which is close to the middle of the channel. Image processing, using ImageJ tool box, was necessary to remove background noise and clearly visualize the

single encapsulation of 1 μm MBs (Figure 4-4).

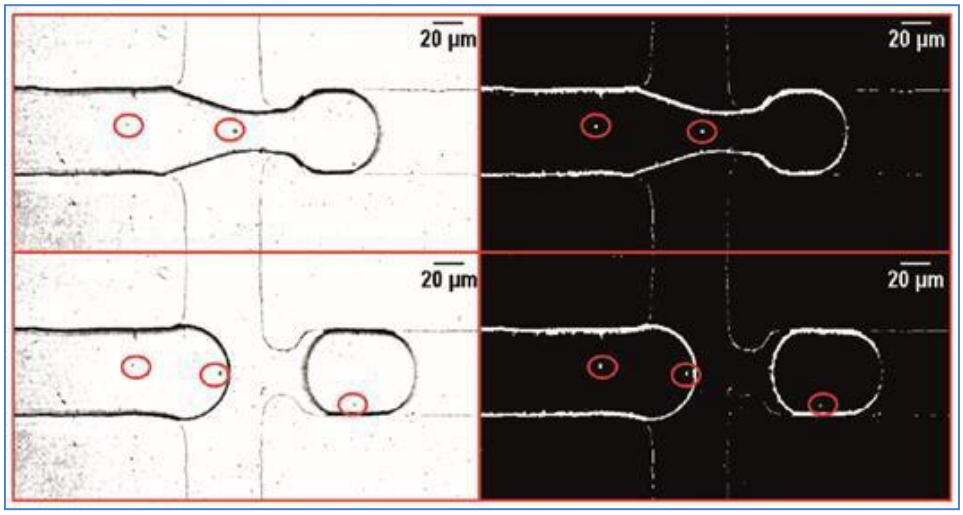

Figure 4-4. (Left) RGB images showing a single 1μm MB encapsulation. (Right) Binary images showing the single 1 um MB encapsulation.

4.4.2.2 Immobilization process

After a magnetic bead and a number of quantum dots are co-encapsulated into one single droplet, the electrostatic association occurs within ~ 10 seconds and continues while the droplet is travelling through the serpentine channel (Figure 5). By comparing the intensity contrast between the empty droplets and the droplets that have entrained a single MB, it is demonstrated that this microfluidic device enables rapid conjugation. One of the disadvantages of batch processing is the use of large quantities of QDs to ensure a high-density coating of QDs on MBs. The consequence is the need for extensive washing to remove unbound QDs before proceeding to the subsequent step of QD conjugation to biomolecules. It is found that a microfluidic droplet used as a reaction compartment facilitates coating of MBs with a high density of QDs, without the use of a large quantity of QDs. This finding is supported by two observations. First, the comparison of the fluorescent intensity between the inlet filled with the original solution containing QDs (before conjugation) and the outlet where there is a mixture of MB-QDs and excess QDs shows that the occurrence of excess QDs after conjugation is unlikely (Appendix A). Second, the fluorescent

intensity of the recovered QDs, detached from MBs using the releasing buffer is about 75 % that of the original QDs solution (Figure 4-6). There is some loss of QDs due to the multiple pipetting steps required for preparation of the samples for the fluorescence spectroscopy measurements, suggesting that the actual extraction of QDs on MBs can be higher than 75 % (Appendix A). Therefore, the proposed droplet-based microfluidic platform has potential to facilitate subsequent bio-conjugation of the MB-QDs (with biomolecules such as single stranded oligonucleotides), as it could be done by continuous flow without washing to remove excess QDs, simplifying the process of nanoparticle decoration. It is noteworthy that differences in the fluorescent intensity of the MB-QD conjugates between two adjacent droplets are primarily due to off-focus collection of the signal (Figure 4-5 and Appendix A-2).

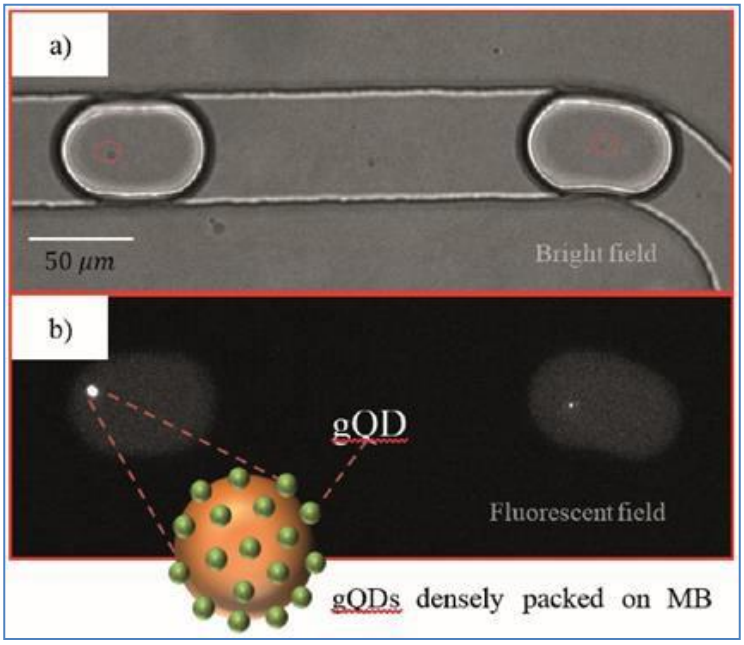

Figure 4-5. Zoom-in (40x magnification) images of fluorescence from QDs confirm the association with MBs in a 50 μm sized channel. a) The image was taken under the bright field, resulting in gray scale image. b) The QD-MB conjugate is luminescent in the fluorescent field

Improvement of the optical interrogation used to control focal position makes it possible to quantitatively evaluate the extent of QDs conjugation onto each single MB, offering a degree of quality control to adjust conjugation processes on-the-fly that is impossible with batch reactions. In order to

confirm that the electrostatic adsorption onto single MBs does not alter the optical properties of QDs, the fluorescence spectra of the recovered and original QDs are compared. The emission profiles of the QDs before and after interaction with MBs are identical **(**Figure 4-6**)**, confirming that the solid phase manipulation does not alter the spectral properties of the QDs. The indication that the QDs retain their excitation spectral characteristics which is essential for further applications, such as using QDs as donors in Forster resonance energy transfer (FRET)-based bioassays.

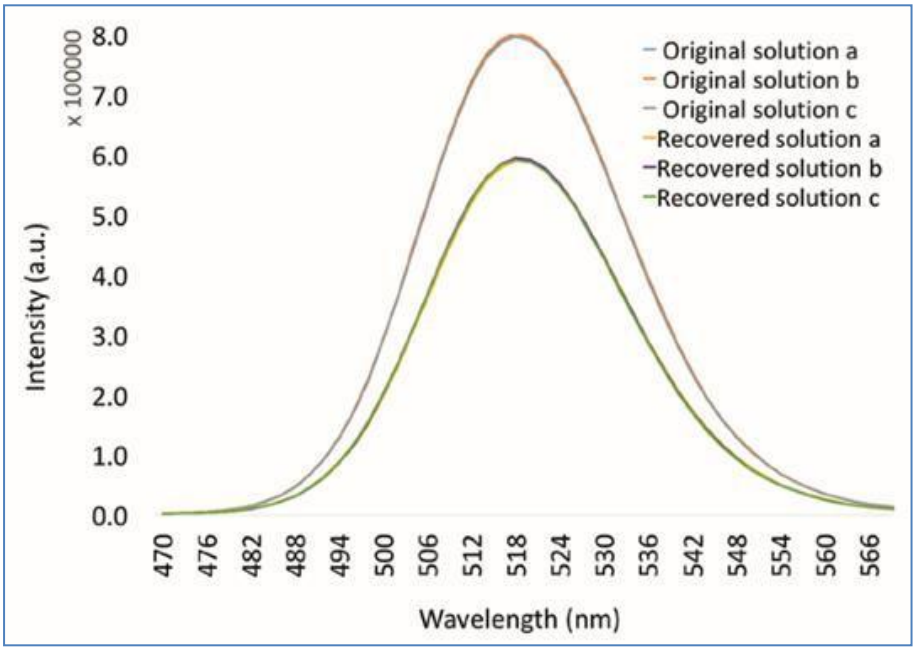

Figure 4-6. Comparison the intensity of original QDs solution before running experiment and the intensity of the recovery QDs.

4.5 Project summary

Droplet microfluidic methods are currently used in various fields such as biotechnology, pharmaceuticals, and biochemistry, for sample handling, synthetic reactions, and diagnostics. In this chapter, a droplet microfluidic platform has been explored as a platform that could eventually support processes for decorating quantum dots with biomolecules, which will be discussed in Chapter 5. The droplet microfluidic approach has been demonstrated to be capable of encapsulating a single 1 μm magnetic bead

with many quantum dots in one aqueous droplet. Furthermore, a rapid electrostatic association of the QDs onto the MB surface has been demonstrated, with speed being associated with the chaotic advection inside nanoliter sized droplets. The efficiency of sample consumption has been improved, and the aqueous droplets are extraordinarily uniform. Such precise of droplet formation enables quantitative control of the reaction environment. This methodology can be applicable to other types of nanoparticle (i.e, gold nanoparticles, up-conversion nanoparticles, etc.). The next step of this study is to integrate multiple components in one droplet microfluidic platform that allows researchers to decorate QDs with biomolecules in continuous flow production, suggesting a promising manufacturing approach.

Chapter 5: Integrating a double-cross geometry with other functionalities into a complex droplet microfluidic platform for rapid immobilization of oligonucleotides on semiconductor quantum dots

The work presented in this chapter was submitted as the following article:

Thu H. Nguyen, Abootaleb Sedighi, Ulrich J. Krull, Carolyn L. Ren, "A multifunctional droplet microfluidic platform for rapid immobilization of oligonucleotides on semiconductor quantum dots", ACS Sensors, 2019, *Submitted*

This work was also presented in poster format at the following conference:

Thu H. Nguyen, Abootaleb Sedighi, Ulrich J. Krull, Carolyn L. Ren, " A complex droplet-based microfluidic platform for rapid immobilization of oligonucleotides on semiconductor quantum dots", APS Division of Fluid Dynamics – November 18th-20th, 2018, Atlanta, Georgia (USA)

Thu H. Nguyen (Department of Mechanical and Mechatronics Engineering) mainly designed a microfluidic platform, conducted experiments and analyzed experimental results. Abootaleb Sedighi (Post Doctoral Fellow in the Department of Chemical and Physical Sciences, University of Toronto Mississauga) assisted in preparing chemical samples for experiments. Prof. Ulrich Krull (Department of Chemical and Physical Sciences, University of Toronto Mississauga) and Prof. Carolyn Ren (Department of Mechanical Engineering, University of Waterloo) provided thoughtful discussions to accomplish the project.

5.1 The scope of this project

Quantum dot-DNA oligonucleotide (QD-DNA) structures have been used in many fields such as nucleic acid bioassays, intracellular probes, and drug delivery systems. A typical solid-phase method that

achieves rapid loading of oligonucleotides on surfaces of QDs involves a two-step reaction and is performed using a batch-based approach. In contrast, droplet microfluidics offers numerous advantages that are unavailable when using batch processing, providing rapid and dense immobilized DNA oligonucleotides on QDs. However, integration of the two droplet generators with droplet merger and mixer raises challenges in design for robustness operation of co-encapsulation, which further enhances the need of fundamental knowledge for flow focusing towards controlled encapsulation. The two generators are designed for co-encapsulation of MBs and QDs, and oligonucleotides respectively to realize the two-step reaction assay. Specifically, in one section, a microfluidic device encapsulates QDs and magnetic beads (MBs) in droplets for the production of QD-MB conjugates. Each droplet is then merged with a section of different droplets that contain oligonucleotides. Subsequently, the merged droplets travel along a serpentine micro-channel for better mixing, resulting in QD-DNA conjugation structures of high quality. This multifunctional microfluidic device provides advantages such as improved control over the reaction conditions, minimized cross-contamination and impurities, reduced reagent consumption, while eliminating any need for external vortexing and pipetting. To evaluate the performance of the QD-DNA conjugates, they were used as Forster Resonance Energy Transfer (FRET) probes to quantify oligonucleic targets.

5.2 Introduction of the project

The semiconductor quantum dot-DNA oligonucleotide (QD-DNA) conjugate has emerged as a powerful platform for the development of nucleic acid bioassays, intracellular probes, and drug delivery (Chou, Zagorovsky, and Chan 2014; Coopersmith, Han, and Maye 2015; Inoue et al. 2016; Suzuki et al. 2008; Sun and Gang 2013; Pinaud et al. 2006; Y. Han et al. 2017; Medintz et al. 2005; Sedighi and Krull 2018; Das, Sedighi, and Krull 2018). Preparing the conjugate is challenging as the electrostatic repulsion between oligonucleotide strands and the surfaces of QDs limits the DNA packing densities and reduces nanoparticle stability. A conventional method for achieving high-density packing of oligonucleotides on QDs is known

as the salt-aging method, which is typically completed over two days (B. Liu and Liu 2017). Lately, the conjugation process has been reduced to minutes by a new approach consisting of a two-step reaction (Sedighi and Krull 2016). First, semiconductor quantum dots are adsorbed on the surface of positively charged magnetic beads, creating magnetic bead - quantum dot conjugates (MB-QD). Second, negatively charged oligonucleotides are electrostatically adsorbed onto the MB surface, accumulating in the vicinity of QD surfaces. Owing to the pre-concentration effect, the density of oligonucleotides on the surfaces of QDs increases significantly. Although this method promises fast preparation of high-quality QD-DNA conjugates, the current batch-based setting is prone to environmental effects and broad dispersity of coating, does not allow for the entire procedure to be monitored, and is difficult to integrate with other processes.

To address these drawbacks, a droplet microfluidics platform that offers a controllable reaction environment through monodispersed aqueous droplets in oil streams is an excellent alternative approach. In general, these droplets are generated and transported at Hz to kHz rates in microchannel networks making them ideal reactors for continuous production of decorated QDs with conjugate densities at speeds, rarely achieved with batch processing. With this approach, the bench-level reagents are now divided into multiple nano-liter or femto-liter volumes in order to take advantage of their high surface to volume ratio leading to rapid reactions, compartmentalization and decreased reagent use (Tomasz S. Kaminski, Scheler, and Garstecki 2016; J. Wang et al. 2017; Ganan-Calvo et al. 2013; Gruner et al. 2015; Rosenfeld et al. 2014; D. K. Kang et al. 2014; Zubaite et al. 2017; Shembekar et al. 2016). Droplet microfluidics has been applied in a wide range of areas such as biological analysis, drug screenings, material sciences, and many more (Y.-C. Tan et al. 2004; R. Dangla, Kayi, and Baroud 2013; Miller et al. 2012; Carroll 2008; R., Z., and A.J. 2016; Klein et al. 2015; Courtney et al. 2016; Schneider, Kreutz, and Chiu 2013). Despite the rapid growth of the field, its adoption as an enabling tool for high throughput screening analysis is rather slow. Among the many reasons, the integration of multiple droplet manipulation functions with robust performance as required by typical real-world assays is one of the key contributing factors. Lately, Chen et al. have introduced a

platform that integrate with droplet generation, pairing, trapping, merging, mixing and releasing (X. Chen and Ren 2017a) and demonstrated its performance for a drug screening assay towards treatment of Alzheimer's disease. This promising platform, however, is not suitable for the reaction of making QD-DNA conjugates because its main functions are to trap and screen droplets that encapsulate different concentrations of drug compounds.

In this study, we present a droplet microfluidic platform with a focus on realizing the two-step reactions needed for high-density immobilization of oligonucleotides onto the surfaces of QDs, while also considering production scale-up. This platform is also applicable to other assays that involve two steps of reactions. The quality of the produced QD-DNA conjugates is evaluated using an efficient fluorescence transduction of nucleic acid hybridization performed on a paper-based platform off-chip. The ratio-metric signal (Red/Green) before and after forming fluorescence resonance energy transfer (FRET) pairs is carefully characterized using an iPhone's camera. Nanoparticle-based FRETbioassay is considered to be a technique sufficient for fluorescence detection that provides for selective and sensitive quantification of biomarkers (Algar and Krull 2007; Kapanidis et al. 2015; Long et al. 2012; Crivat et al. 2010; Hsieh, Pan, and Lee 2009).

5.3 Rational Design

The general strategy for designing a chip suitable for the two-step reaction is to enable a "plug and collect" operation. Specifically, the platform is designed to allow users to inject their samples into the microfluidic device by means of a pressure system **(**Figure 1); then, collect the reaction product for further evaluation. To realize this strategy, the platform should consist of the following droplet operations working in an integrated and robust manner: i) parallel droplet generation with one stream of droplets containing MBs and QDs for the first step of the reaction, while the other encapsulating oligonucleotide DNA towards the second step of the reaction; ii) a merging chamber with controlled one-to-one droplet merging from the two streams of droplets respectively to initiate the second step of the reaction; iii)

thorough mixing to complete the second step of the reaction; and iv) ease of recovering the reaction product. Such a platform then presents several benefits over the batch-based method, including: i) a higher degree of control over the reaction conditions; ii) elimination of the need for external vortex mixing and pipetting, presenting the potential for high throughput analysis; iii) minimized cross-contamination and reduced influence from wall impurities; and iv) considerably reduced cost due to the order of magnitude lower reagent consumption. An additional benefit is its portability.

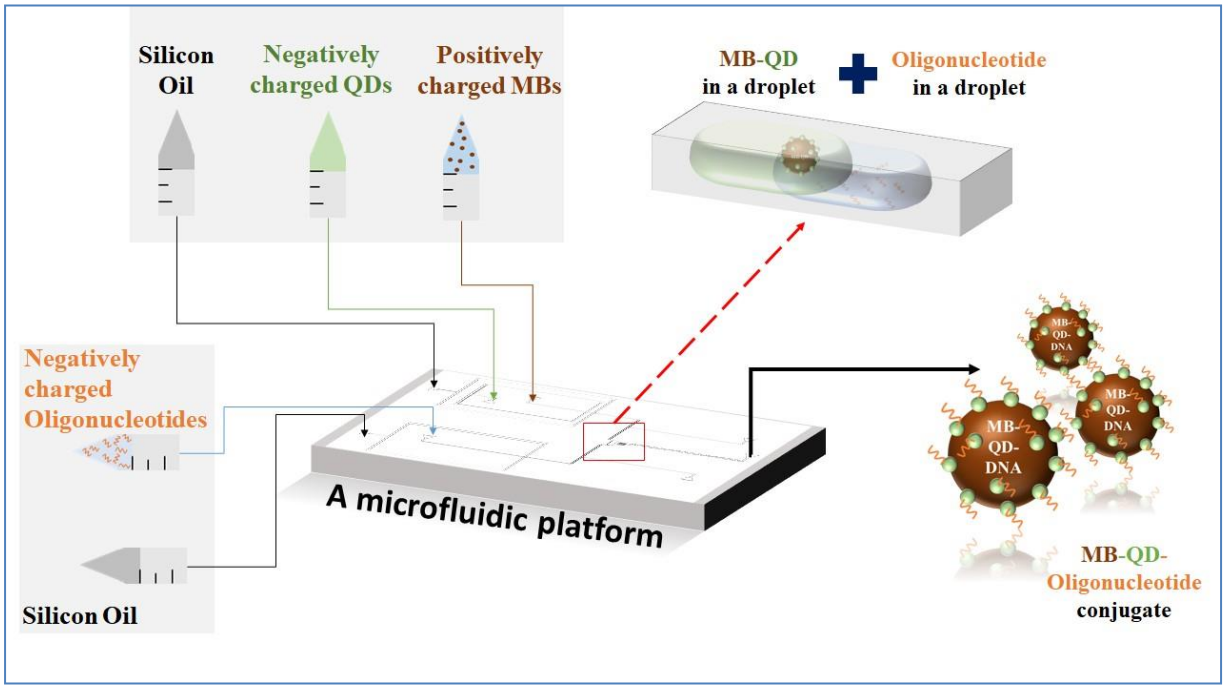

Figure 5-1. Schematic of a "plug and collect" droplet microfluidic platform for QD-oligonucleotide conjugate

5.3.1 **Design of microfluidic platform**

It is desirable to recover a relatively large amount of QD-DNA conjugates for further processes, such as in-vitro diagnostics, intracellular assays and DNA-programmed nanoparticle assembly (Chou, Zagorovsky, and Chan 2014; Bruchez Jr. 1998; Boeneman, Deschamps, Buckhout-white, Prasuhn, Blanco-canosa, et al. 2010; Y. Han et al. 2017), which requires a series of design concerns to be

considered. In this study, for instance, in order to quantify the quality of the QD-DNA conjugates, the required minimum volume is 50 µL. To produce this volume of conjugates, there are several options such as making large droplets and running the experiments for a long time. However, the size of droplets must be within a certain range to ensure that the one-to-one merging function is robust, which is $1.2 \leq \frac{V_{drop}}{w^2 h} \leq 1.8$, where W and h are the channel width and height, respectively. The operation time is also limited by reagents used, as some aggregate after a certain time period. In this study, it is observed that MBs tend to sink to the reservoir bottom and aggregate after one hour of operation.

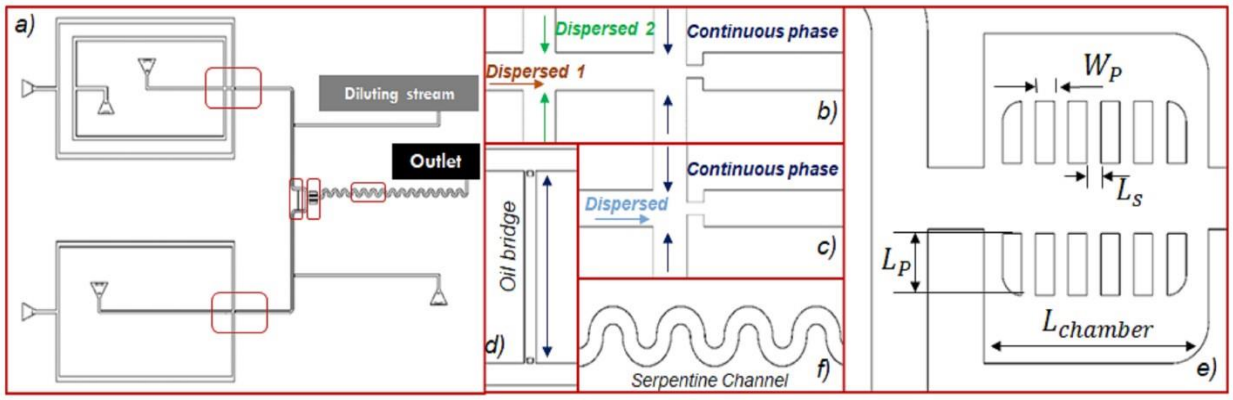

Figure 5-2. a) The general layout of the complex droplet microfluidic platform. b) The co-encapsulation component with two cross junctions in series. c) The flow focusing droplet generation geometry used for the generate droplet containing oligonucleotide DNA in parallel. d) The oil bridge used for balance the pressure between up and down streams, resulting in droplet synchronization. e) The merger chamber. f) The serpentine channel promotes the full-mixing inside droplets.

To accommodate all of the above features without sacrificing the quality of QD-DNA conjugates, a co-encapsulation component is designed in which the QD solution of 3 $pmol$ and the MBs prepared in a solution of ~ $4 \times 10^7 MBs/mL$ are co-encapsulated into nanoliter-sized droplets for the first step of the reaction (Figure 2b). The choice of concentrations is made to ensure a high density of immobilized QDs (Sedighi and Krull 2016; T. H. Nguyen et al. 2018). The mechanism for conjugating MBs and QDs is electrostatic attraction, which is enhanced with the small droplet volume. The conjugation is expected to happen in seconds, facilitated by the rapid mixing within the droplet caused by the 3D motion present in

droplets. Electrostatic conjugation requires QDs and MBs to have opposite charges. Thus, QD surfaces are modified with glutathione (GSH) to have negatively charged surfaces, whereas MBs are coated with positively charged diethylaminoethyl (DEAE) groups. The combination of a magnetic bead with many QDs is considered to be the QD-MB conjugate.

In parallel, another stream of droplets that contain oligonucleotide DNA are generated (Figure 2c). the platform design keeps these two streams of droplets separated until they merge in a chamber (Figure 2e) consisting of two arrays of pillars, at a one-to-one ratio, which is ensured by the bridge balancing the two streams (Figure 2d) (K. Song, Zhang, and Hu 2012; D.-H. Lee and Park 2010; Gershenfeld and Prakash 2007; Maddala and Rengaswamy 2014). The merging mechanism is the competition between hydrodynamic forces and interfacial tension (X. Chen, Brukson, and Ren 2017; X. Niu et al. 2008; Baroud, Gallaire, and Dangla 2010). In order to ensure the complete conjugation between the QD-MB conjugates and oligonucleotide DNA strands within the merged droplets, the reagents must be mixed well, which is achieved by pumping the merged droplets through a serpentine microchannel with 30 turns (Figure 2f). The number of turns was optimized to ensure homogeneous mixing induced by the 3D flow motion with asymmetric vortices inside the droplets (Tung, Li, and Yang 2009; H. Song, Chen, and Ismagilov 2006; Helen Song, Tice, and Ismagilov 2003; H. Song et al. 2003) without increasing the device footprint. This step of conjugation is via electrostatic attraction between the positively charged MBs covered by the QDs and the negatively charged oligonucleotide DNA strands, leading to the accumulation of DNA strands surrounding the QD-MB conjugate; thus, the QD-DNA conjugation occurs via the di-thiol group.

The two-step reaction can be realized only when all the functional components perform robustly in an integrated manner, which is ensured by the following strategies. First, the co-encapsulation of MBs and QDs is designed to occur using two junctions in series. The detailed design principles can be found elsewhere (X. Chen and Ren 2017b; T. H. Nguyen et al. 2018). Briefly, the MB solution with a higher

viscosity is injected into the middle stream that meets the low viscosity QDs solution coming from the two sides at the first junction. The viscosity ratio plays a key role in focusing the MB stream to a desired width before it enters the second junction to be dispersed into droplets by the oil stream (X. Chen and Ren 2017b). The level of control of the focusing width offers advantages of the concentration of each stream into the droplets eventually (Cubaud and Mason 2008). The other parallel generator for producing droplets encapsulating with DNA oligonucleotide employs a simple flow-focusing geometry, whereby the DNA solution is dispersed into droplets by the oil stream coming to the junction perpendicularly.

In this study, the width of all channels is 300 μm, unless specified otherwise. The width ratio between the droplet (dispersed phase) and carrier oil (continuous phase) ($\Lambda = \frac{W_d}{W_c}$) is 1 to minimize interface expansion during the droplet generation cycle, thereby reducing local fluctuations (Glawdel and Ren 2012c). The length between the two junctions is set as 900 μm which has optimized so that the focusing at the first junction is not influenced by the droplet generation at the second junction. Additionally, the generated droplets are transported in a channel of 25 mm long before they arrive at the merging section. This design minimizes the fluctuations in the hydrodynamic resistance and thus flow rate in the channels due to droplets entering and leaving the channel. The length after the droplet formation junction is adjusted to carry more than 30 droplets (Glawdel and Ren 2012c; Baroud, Gallaire, and Dangla 2010). That length has also been amended to guarantee that the conjugation between QDs and MBs is enhanced, as estimated from our previous work (T. H. Nguyen et al. 2018). To achieve the one-to-one droplet merging ratio, not only the frequencies of the two droplet generators but also the frequencies of two droplets moving to the merging chambers must be well synchronized. An oil bridge (figure 2d) is designed to connect the upper and lower streams of droplets before the merger to alter the sequence of alternating droplets that later flow to a merging chamber. This oil bridge is 100 μm wide and 2600 μm long. The hydrodynamic resistance difference in each channel is balanced automatically due to the

crossflow of carrier oil via the oil bridge (B. Ahn et al. 2011; K. Song, Zhang, and Hu 2012). Consequently, droplets from each stream are synchronized in turn.

The merger chamber is designed based on the numbers of input droplets to be merged, the length of input droplets, and the length of output droplets (Figure 2e)(X. Chen, Brukson, and Ren 2017). The length of each pillar (L_p) and the spacing between the pillars (L_s) are 300 μm and 75 μm respectively, to prevent droplets from entering the chamber's bypass channel (the region between the chamber walls and the pillars) while still allowing oil to bypass through the gaps between those pillars. To ensure the quality of individual pillars after fabrication, the pillar width (W_p) cannot be too small, and is 100 μm here. In addition, the length of the chamber should be equal or larger than the merged droplet's length (L_0), which is identified by the number of merged droplets (N = 2) multiplier of the input droplets length (L_d), such that $(N-1)L_d < L_{chamber} < NL_d$. Herein, the length of the chamber ($L_{chamber}$) is 1.2 mm. The details are explained in Appendix E.

Even though mixing between reagents occurs during droplet fusion, homogeneous mixing is not observed. The full-mixing is guaranteed by incorporating 30 turns after the merging chamber. The recirculating flow caused by the shearing between the channel wall and droplet fluid induces non-axisymmetric vortexes inside droplets. This chaotic flow happening inside droplets is inferred by using Baker's transformation (H. Song, Chen, and Ismagilov 2006; Helen Song, Tice, and Ismagilov 2003). Each turn has an inner and outer diameter of 200 μm and 500 μm, respectively. The entire platform design is fabricated using soft lithography technique to get a 100 μm channel height. In fact, the channel height could be reduced to as small as 85 μm because of oil swelling the polydimethylsiloxane (PDMS) chip material, which has been considered in the design.

5.3.2 **Device fabrication**

The microfluidic device is fabricated using standard soft-lithography technology. Briefly, two layers of SU-8 2025 negative photoresist (MicroChem) are employed to form the mold holding the microchannels

(h = 100 μm). For replica molding, a PDMS base and a curing agent are first mixed with a 1:10 ratio, degassed and poured on the top of the mold. Then, the mold with PDMS is baked at 95°C for 2 hours. The PDMS substrate is peeled off, cleaned with isopropyl alcohol and nitrogen dried, before being bonded with a clean glass slide coated with a thin layer of PDMS through oxygen plasma treatment. The inlets and outlets are made through the PDMS substrate using a 1.5 mm biopsy punch. Finally, a device is placed on a hot plate at 170°C for 2 days to recover its surface hydrophobic property before experiments for wetting oil.

5.3.3 **Material**

Green-emitting CdSe/ZnS core/shell quantum dots (PL = 518 nm) were obtained from Cytodiagnostics (Burlington, ON, Canada). Diethylaminoethyl (DEAE)-functionalized magnetic beads (MB, 1 μm) were from Bioclone Inc. (San Diego, CA). Sodium tetraborate, tris(2-carboxyethyl)phosphine hydrochloride (TCEP), l-glutathione (GSH, reduced, ≥98%), and tetramethylammonium hydroxide (TMAH) were from Sigma-Aldrich (Burlington, ON, Canada). Probe oligonucleotide (5′-DTPA-AATATCATCTTTGGTGTT-3′) and target oligonucleotides (5′-AACACCAAAGATGATATT-Cy3-3′) were synthesized and purified by Integrated DNA Technologies (Coralville, IA). All buffer solutions were prepared using deionized water (Milli-Q, 18 MΩ cm^{-1}) and were autoclaved prior to use. The buffer solutions included 100 mM tris-borate buffer (TB, pH 7.4), and 50 mM borate buffer (BB, pH 10).

5.3.4 **Experimental procedure**

To produce stable droplets, the chip material needs to preferably wet the continuous phase over the dispersed phase. Therefore, prior to each experiment, the microfluidic chip is primed with silicon oil for 30 minutes rendering a good wetting condition. After priming, the channel height and width are usually reduced due to oil swelling the chip material, and therefore must be carefully measured again.

Following the instruction provided by Bioclone Inc., 0.1 mg magnetic beads are washed twice with the borate buffer (100 mM, pH 10) and then diluted in the capture tris-borate buffer (50 mM, pH 7.4), which is mixed with 50% (wt %) glycerol. The viscosity of the mixture of glycerol buffer is ~5 mPa.s. The concentration of MBs is $\sim 4 \times 10^7$ beads/mL. GSH-QDs (3pmol) are also prepared in the capture buffer. The glutathione-capped quantum dots (GSH-QDs) are prepared using a previously reported protocols. The viscosity of the solution is approximately 1.02 mPa.s. Additionally, oligonucleotides DNA is incubated with 100 equiv of TCEP, and the solution is prepared an hour before starting the experiment.

Co-encapsulation function and droplet generation in parallel

As mentioned before, two streams of droplets are generated in parallel for the two-step reactions. Figure 3(a) shows the droplet generation for the first-step reaction producing MB-QD conjugates. The MB solution is injected into the horizontal channel whereas the QD solution is injected from the two perpendicular channels to focus the MB stream forming a stratified flow structure at the first junction. This stratified flow structure was designed to maintain its shape until being sheared into droplets co-encapsulating with QDs and MBs at the second junction. Droplets are generated in the squeezing to transition regime ($0.001 < Ca < 0.005$) (Gordon F. Christopher et al. 2008) where Ca is the capillary number comparing viscous force and interfacial tension force. The droplets generated within this regime generally have a very small size distribution with its interface touching the channel walls, which makes the prediction of droplet volume based on its length more accurately. Droplet length ranges from $1.2W_c$ to $1.8W_c$ for the flow rate ratio $0.6 \leq Q_{MD}/Q_{QD<} 0.8$ (T. H. Nguyen et al. 2018; X. Chen and Ren 2017b). A high-speed CMOS camera (Phantom V210) mounted to the fluorescent microscope (TiE, Nikon) is used to capture the co-encapsulation and droplet-generation cycles (Figure 3). The throughput of interest here is to have sufficient number of QD-MB conjugates for quantification which is achieved by

generating relatively large droplets (8 to 10 nL), each containing 268 to 407 well-dispersed MBs with 3nM QDs so as to cover the MBs' surfaces[37].

In parallel, droplets containing oligonucleotides are generated (Figure 3b) at a comparable frequency by tuning the flow rate ratios of the dispersed and continuous phases (Supplemental Video). To ensure that each droplet generator performs robustly, they are decoupled by using two separate oil streams and a long channel after the cross generators. To achieve a one-to-one merging ratio, the sizes of these two streams of droplets are tuned to stay as close to each other as possible.

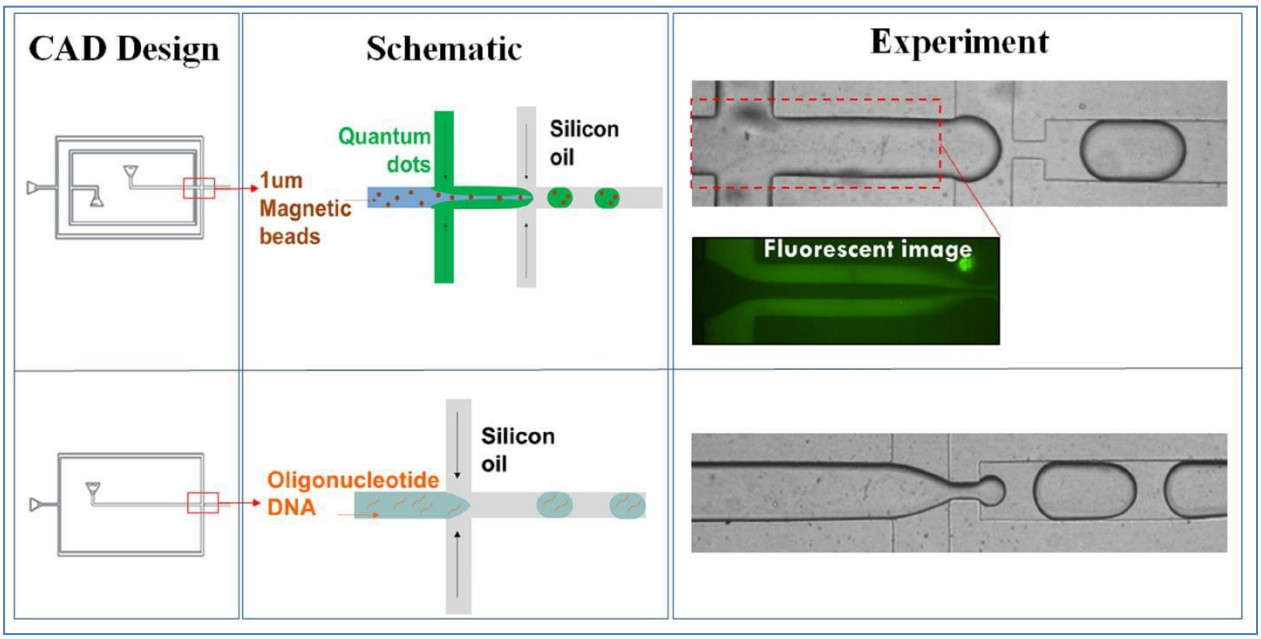

Figure 5-3. (Left) CAD design of two droplet generators in parallel (1) for the co-encapsulation of MBs and QDs and (2) for the encapsulation with Oligonucleotide DNA; (Mid) A schematic; (Right) Experiments of two droplet generators in parallel.

One-to-one droplet fusion and droplet full-mixing

As mentioned before, two streams of droplets are synchronized to enter the merger alternatively via the assistance of the oil bridge connecting the upper and lower parts (Figure 4). When a droplet from one stream arrives at the bridge location, it blocks one of its ends, pushing the oil into the other stream and thus increasing its flow rate and vice versa(Hong et al. 2010). The detailed working principle of the merger can be found in our previous work (X. Chen, Brukson, and Ren 2017). Briefly, the merger is

designed so that the droplet cannot flow into the bypass region. When the leading droplet enters the merger, it is temporarily trapped inside the two arrays of pillars increasing its resistance and causing the oil to flow through the bypass channels. The next droplet is then forced to enter the two arrays of pillars merging with the leading droplet.

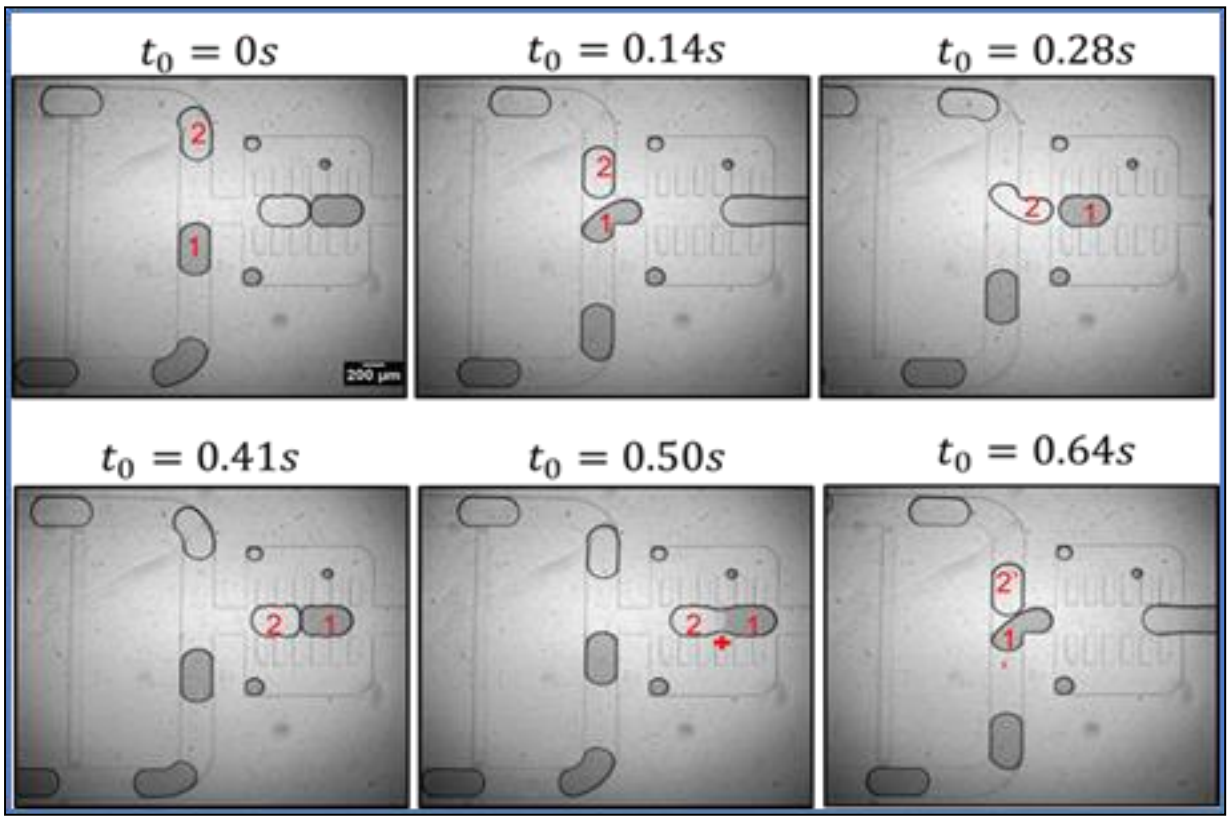

Figure 5-4. A cycle of one-to-one droplet fusion recorded by using a high-speed camera (frame rate: 1,000 frames/s)

To ensure one-to-one droplet fusion, the platform is operated under three main conditions. First, the droplet that enters the merger cannot flow through the bypass channels. Second, the ratio of droplet length relative to the chamber length ($L_{drop}/L_{chamber}$) is adjusted to be in the range of 0.23 to 0.6 (X. Chen, Brukson, and Ren 2017). Niu et al. mentioned that the relative ratio of droplet size to a central branch of a merger influences successful droplet merging (X. Niu et al. 2008). Last, the spacing between the droplets to be merged is $1.5 \leq \lambda < 2.5$ because too large a spacing makes the leading droplet leave the merger

before the following droplet enters it and too small a spacing tends to merge multiple droplets. A droplet merging cycle takes from 0.5s to 0.7s. In practice, there are some uncertainties, such as fabrication defects, imperfect wetting conditions, and bubbles trapped in a dead volume zone of the bypass channel, which together lead to approximately 20 % of droplets not merging with each other.

The merged droplets are pumped through a 30-turn serpentine channel to advance the QD-DNA conjugates on MBs' surfaces. The asymmetric vortices induced by shear force between the channel walls and droplets promote the rapid mixing of different reagents inside droplets (figure 5-5).

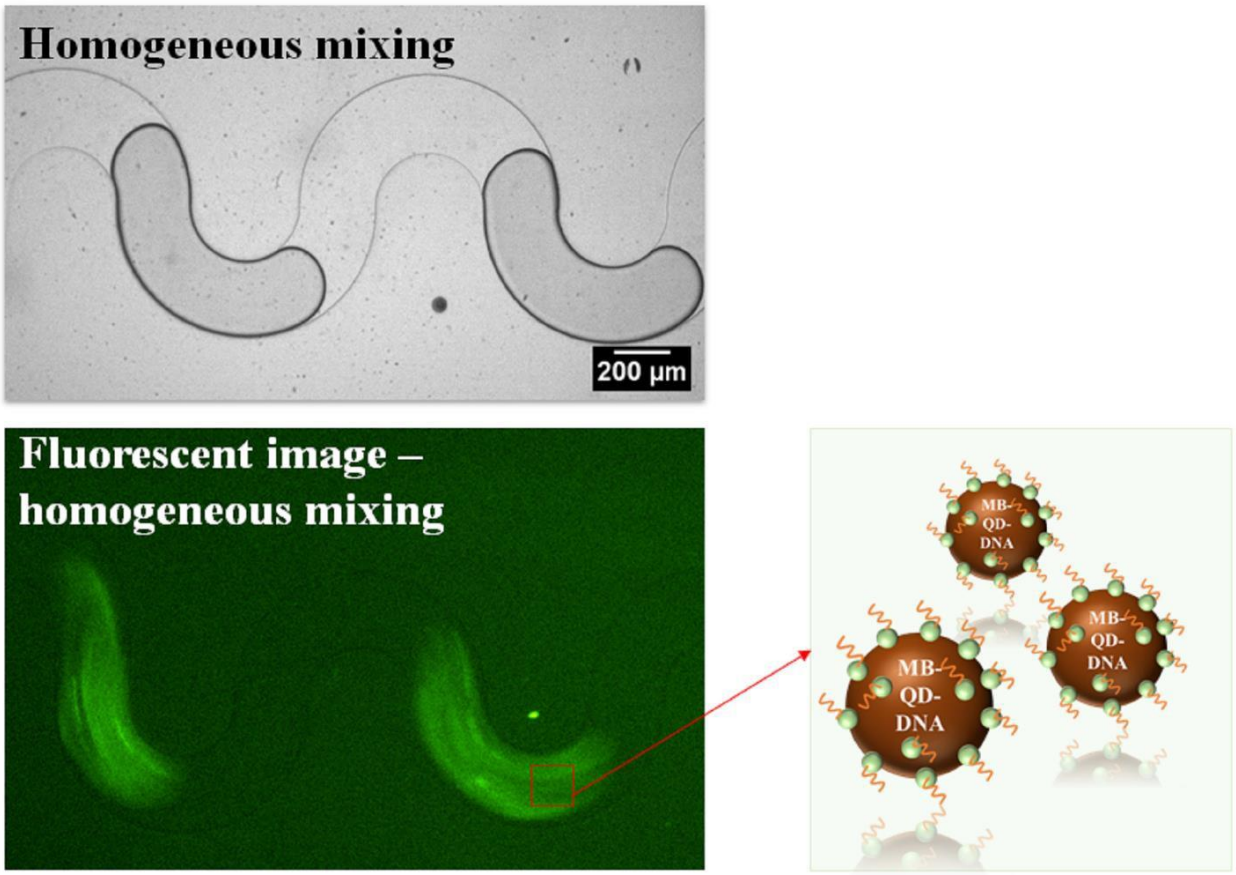

Figure 5-5. 3D chaotic mixing inside droplets promotes the QD-MB-DNA conjugates

Nucleic acid detection and validation of the QD-DNA conjugates

Oligonucleotide-QD conjugates are collected at the outlet and remobilized from the MBs' surfaces via a washing step. First, we remove the unbound QDs and oligonucleotide DNA strands from the collected solution using a magnet holder. Second, the collected MB-based conjugates are dispersed in the releasing buffer solution (EB) to release the QD-DNA conjugates, which are then transferred to a sterile microtube for the detection of nucleic acid using Forster resonance energy transfer (FRET) techniques (Figure 6). The FRET-based detection utilizes the QD-DNA as a probe to detect target oligonucleotides where the QDs serve as the donor and the Cy3-dye (attached to the 5-end of the target oligonucleotide) as the acceptor. The nucleic acid detection is conducted on built-in micro-paper-wells acquired using VSCO software on iPhone (Apple Inc., Cupertino, USA) as per an economic and efficient detection method developed by Noor and Krull (Noor, Shahmuradyan, and Krull 2013).

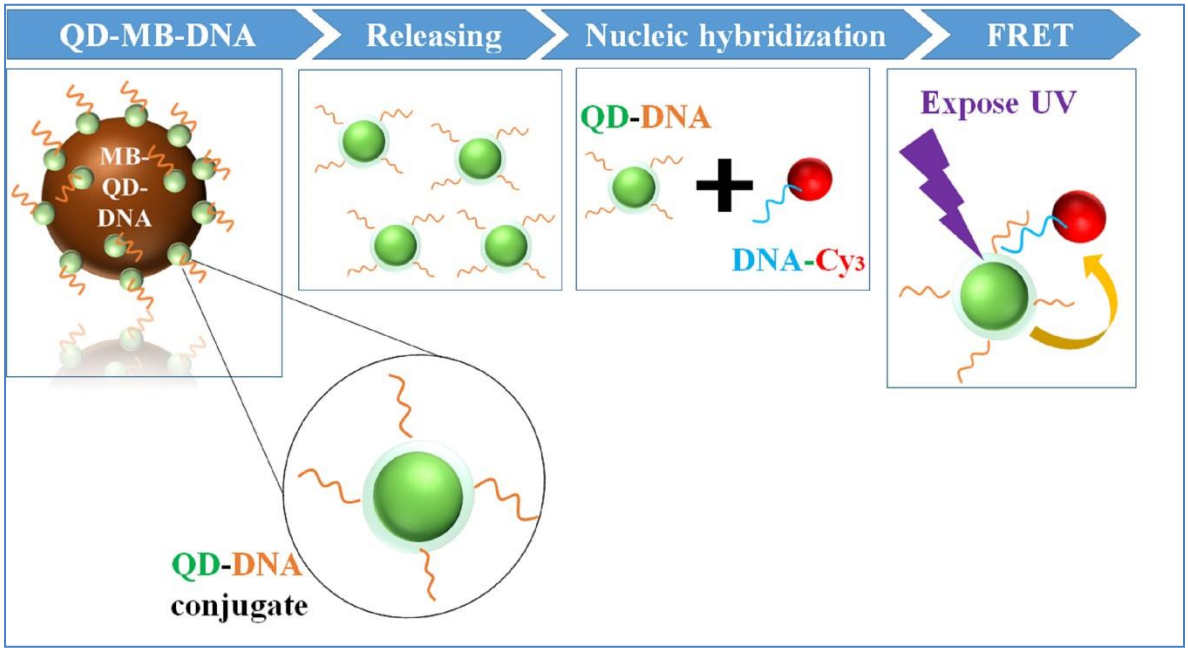

Figure 5-6. The schematic and experiments show the nucleic acid detection based on FRET technique

Following the protocol developed by the same group (Sedighi and Krull 2018), Whatman cellulose chromatography papers are patterned with wax using a Xerox ColorQube 8570DN solid ink printer. An array of 8 by 4 circular reaction zones 3 mm in diameter is printed in each 60 x 26 mm^2 paper. The printed papers are subsequently baked at 120^{oC} for 2.5 minutes. The reaction zones on the paper are used without chemical modification. First, 2 μL of QD-DNA conjugates are pipetted onto the circular reaction zones and allowed to distribute themselves in the paper pores for 1 minute. Next, the paper is exposed to UV light (120 W UV lamp, 356nm wavelength). Images shown before the hybridization are carefully recorded by taking out the color-balance function provided by CMOS sensor built in a phone camera. Subsequently, the same volume of target oligonucleotides is injected into the reaction zones. The hybridization reactions are allowed to proceed for 5-7 min. Thereafter, the post-hybridization image is captured under UV light. DNA hybridization between the QD-immobilized oligonucleotide and the target oligonucleotide places the Cy3 dye in the vicinity of QD, leading to the excitation of Cy3 dye through the FRET process. The camera setup was kept unchanged throughout the hybridization and imaging processes. Different concentrations of target strands (25 to 500 pmol) are allowed to hybridize to their complementary probe oligonucleotides immobilized on the QD surfaces.

The intensities of red and green channels are extracted using ImageJ software, and the Red-to-Green (R/G) ratio is obtained to represent the FRET signal. The background has been subtracted during the image processing and the final R/G ratio is calculated by

$$\frac{R}{G}\ Ratio = \left(\frac{I_r}{I_g}\right) DA - \left(\frac{I_r}{I_g}\right) D$$

where I_r and I_g correspond to the photoluminescence from each paper zone in the red and green channel, respectively (Noor, Shahmuradyan, and Krull 2013). DA is a subscript of the presence of donor and acceptor, whereas D stands for a measurement taken in the absence of an acceptor. Figure 7 shows the R/G ratio in the presence of 25 to 500pmol of target strands. The response linear increases in the range of

50 to 200 pmol, which illustrates the sensitivity of the QD-DNA conjugates (Appendix D). However, below 50 pmol of target oligonucleotide, the data cannot be quantified (limit of quantification). In both cases 175 pmol of oligonucleotides have conjugated with QDs and 300 pmol of oligonucleotides have conjugated with QDs. The bio-recognitivity of the probes that leads to creating FRET pairs is confirmed based on hybridization testing. Additionally, the reproducibility of the platform that integrates the solid-phase assay with a droplet microfluidic device for producing QD-DNA conjugates is evaluated. Each presented data point is a mean average of the data from five different experiments conducted in five different microfluidic chips using different batches of chemicals.

To test the number of oligonucleotides that can be immobilized onto the QD surfaces, the number of oligonucleotides is varied from 175 pmol to 300 pmol. From the R/G results, the ratio increases with the oligonucleotide strands, suggesting that there are more oligonucleotide strands captured onto the surfaces of quantum dots. Nevertheless, that ratio does not significantly change when the number of oligonucleotides is greater than 300 pmol, which is considered to be the saturation number for oligonucleotide strands that can be immobilized on the surfaces of QDs (Sedighi and Krull 2016).

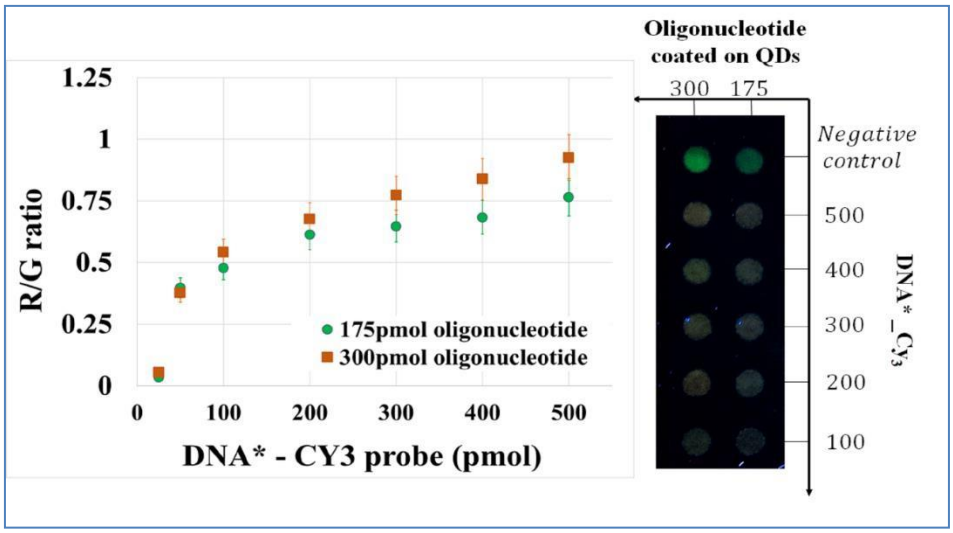

Figure 5-7. R/G ratios confirm the sensing capability of the produced QD-DNA

5.4 Project conclusion

One of the benefits of this droplet microfluidic platform is the integration of multiple functions enabled by the continuous flow nature. The platform can be used for conjugating not only oligonucleotide-QD, but also possibly for conjugating oligonucleotide-gold nanoparticles (Sedighi and Krull 2019). Furthermore, it can also be applied to bio/chemical assays requiring two-step reactions. The idea of "plug and collect" clearly demonstrated through this work allows oligonucleotide-QD conjugates to be produced without environmental effects and tedious manual processes. The quality of oligonucleotide-QD conjugation, validated using a FRET-based DNA hybridization technique, further confirms the feasibility of using the droplet microfluidic platform for functionalizing particles' surfaces. The washing steps for releasing the conjugates from MBs point to the direction of future work; for instance, integrating these steps and the detection onto one microfluidic device presenting a point-of-care bio-sensing opportunity.

Chapter 6: A hydrodynamic focusing formation considering viscosity contrast fluids integrated with droplet generation, and the effects on single cell encapsulation: an experimental study

The work presented in this chapter is in preparation for the following article:

Thu H. Nguyen, Carolyn L. Ren, "Hydrodynamic focusing formed by stratified flow of contrasting viscosity fluids, and its influence on the single (bio) particle encapsulation", *in preparation*

This work was presented in poster format at the following conference:

Thu H. Nguyen, Sarah Chan, Evelyn Yim, Carolyn L. Ren, "Encapsulation of single stem cell inside Gelatin Methacryloyl (GelMA) droplet using a stratified flow with viscosity contrast strategy", CSME – CFDSC Congress, June 2-3rd , 2019, London, Ontario

Thu H. Nguyen (Ph.D. candidate in the Department of Mechanical and Mechatronics Engineering) mainly investigated this study by designing a microfluidic platform, performed experiments and analyzed experimental data. Prof. Evelyn Yim (Department of Chemical Engineering, University of Waterloo) and Sarah Chan (Master's candidate in the Department of Chemical Engineering, University of Waterloo) assisted in preparing bio-chemical samples (mouse mesenchymal stem cells (mouse MSCs), Phosphate borate buffer solution, gelatin-methacryloyl (GelMA)). Prof. Carolyn Ren supported this study and provided fruitful discussions. I would also like to acknowledge Jeremy (a Co-op student working in the Waterloo Microfluidic Laboratory) for help provided in the experimental discussion section.

6.1 The scope of this project

Droplet microfluidics has become a powerful platform for multiple applications in not only biological and chemical applications but also in tissue and cell engineering. Indeed, the technology enables high-

throughput encapsulation of single cells inside separate droplets for further experimentation and analysis that would be very challenging in batch-based settings or in single-phase microfluidics. Currently, the encapsulation of single cells inside aqueous droplets using droplet-based microfluidic platforms has been achieved following two strategies: (1) inertial cell ordering in micro-channels, and (2) post-encapsulation, meaning isolating droplets containing only one cell after the encapsulation is required. Application of these strategies is limited by some practical constraints. For example, achieving the inertial cell self-ordering requires high flow rates and adequate space in a platform footprint for a curvature channel or a very long channel. Another way to achieve single encapsulation is by sorting the droplets containing only single cells downstream after the encapsulation process. To apply this method, cells are usually barcoded/labelled and specific cell concentrations should be determined. An external source must be used to detect and isolate the droplets of interest from the rest of the population. Most chemical/biological reactions in tissue engineering applications and biochemistry research require that multiple reagents be encapsulated with a single cell within individual droplets. Therefore, a platform is needed that not only enables encapsulation of single cells suspended in one fluid within another fluid, but that is also easy to implement in practice and does not require a large footprint.

Chapter 4 successfully demonstrated a process in which a hydrodynamically focused stream with a viscosity contrast and a simple double-cross configuration enables the encapsulation of a single 1μm magnetic bead within a quantum dot solution. Chen et al. previously used a similar strategy to successfully order 10 μm micro polystyrene beads and then encapsulate single micro bead in individual droplets with a high rate (>50%). As mentioned earlier, when a new need arises for example encapsulation of 150 μm embryoid body for tissue engineering studies, the entire channel network design fails and calls for redesign and optimization which requires extensive experience in droplet microfluidics and trial-and-error practice. To address this issue by providing a foundation for guiding the general design of double-cross for encapsulation of a wide range of particle sizes, a systematic fundamental study is

designed. The preliminary testing of encapsulation of 150 μm embryoid body and the knowledge gained through the above two projects suggest that this fundamental study should focus on the width of hydrodynamic focusing under different experimental conditions because the width affects the ordering of the particles. This chapter describes an experimental study conducted to further investigate parameters influencing the formation of a hydrodynamically focused stream before droplet generation.

6.2 Introduction of the project

The impacts of microfluidic technology have been emphasized in many bio-related applications over the last two decades (Whitesides 2006; Goddard and Erickson 2009; Y. Zhu and Fang 2013; D. K. Kang et al. 2014; Heath, Ribas, and Mischel 2016b; J. Wang et al. 2017; Scheler, Postek, and Garstecki 2019). In practice, compared to conventional multi-well plates, the dimensions of microchannels permit high-throughput and rapid manipulations, such as localizing, fusing, concentrating, and mixing reagents with cells (Breslauer, Lee, and Lee 2006; Stone and Kim 2001; J. Taylor, Stubley, and Ren 2008; Nan, Jiang, and Wei 2014). For example, by simply connecting a large channel (a few hundred micrometers in width) to many small channels (with widths of a few micrometers) oriented orthogonally to the large channel, the cell bodies of neurons can be placed in the large channel while cellular processes occur inside the small channels (A. M. Taylor et al. 2005). However, with single phase microfluidic methodologies, in some applications, cell stiction and adhesion to microchannel walls (PDMS channels) significantly limit the reusability of such devices (Ishikawa et al. 2011; Collins et al. 2015). Furthermore, evenly distributing bio-objects (polymer/bio-particles or cells) in drops for bioassays seems to be impossible using single phase microfluidic devices. In contrast, droplet microfluidic technology offers unique advantages (DeMello 2006; Baroud, Gallaire, and Dangla 2010; Dressler, Casadevall i Solvas, and DeMello 2017; Vladisavljević, Al Nuumani, and Nabavi 2017). For instance, single cells/particles can be enclosed inside pico-to-nanoliter droplets surrounded by an immiscible fluid. Thus, the chemical/biological reactions between cells and reagents are accommodated within a controlled micro-environment. Cells or bio-

particles are also kept inside droplets, preventing their adsorption to the micro-channel walls. Furthermore, with microfluidic technology, the droplets containing single cells/particles can further be merged with other droplets or sorted at the hertz to kilohertz rate (Lai, Bremond, and Stone 2009; Z. Cao et al. 2013; Dong et al. 2016; X. Chen and Ren 2017a). Some review articles underline how well droplet-based microfluidic technology has been recently applied in the chemical and biological sciences (C. Zhang and Van Noort 2011; Yin and Marshall 2012; Lecault et al. 2012; Heath, Ribas, and Mischel 2016b). This technology can potentially impact genetic and tissue engineering research consisting of gene expression (Spurgeon, Jones, and Ramakrishnan 2008), single cell genomics (Kalisky and Quake 2011), stem cell differentiation (Chung et al. 2005), cell sorting (Chabert and Viovy 2008; Johansson et al. 2009), and so on. This wide range of applications draws attention to the need for methodologies that provide high throughput encapsulation of bio-objects; specifically, the means to achieve single-cell encapsulation is urgently needed due to the importance of single-cell level data (Lecault et al. 2012).

Although there are methods for loading single cells/bio-particles into droplets, most are too limited for widespread adoption. For instance, bio-particles/cells that are well-dispersed in an aqueous phase can be enclosed in individual droplets following Poisson distribution. Therefore, the concentration of cells/bio-particles (#particles per volume) is usually diluted, generating many empty droplets (Köster et al. 2008a). As a result, reagent waste significantly increases. Another approach is using inertia flow to self-align cells/particles moving inside a high aspect ratio micro-channel (Edd et al. 2008; Lagus and Edd 2013a). This method is claimed to be superior to the Poisson distribution method. Another strategy is applying the secondary flow – a Dean flow induced inside a curved channel at high flow rate – to assist the self-ordering of cells/particles (Schoeman et al. 2014; Al-Halhouli et al. 2018). Despite the high encapsulation efficiency offered by these methods, they have the following limitations. First, to achieve cell self-ordering, a high flow rate (10 to 40 µL/min) must be used to induce inertia flow, which makes the droplet generation systems operate in the dripping to jetting regimes. Under these regimes, droplet sizes are not

homogeneous (C.V. > 5%) because of a series of tiny bubbles/droplets generated after the main droplets are pinched off (J K Nunes; S S H Tsai; J Wan; and H A Stone 2009; Kovalchuk et al. 2019). In contrast, droplets generated under the squeezing regime are highly monodispersed (C.V. < 5%) (X. Chen et al. 2015; van Loo et al. 2016). However, droplets generated under the squeezing regime are usually larger than ones generated under the dripping regime. Therefore, adding an orifice at the pinching junction would help to generate smaller droplets (Anna, Bontoux, and Stone 2003; Ong et al. 2007; L. Wu et al. 2017). Secondly, the requirement for high aspect ratio micro-channels would not be practical in reality because dust, or unwanted particles, etc. could not be removed and would block the channel. Moreover, the channel length required for cells/particles to reach their equilibrium positions is a function of the aspect ratio and diameter of those cells/particles. In some applications, to encapsulate single bio-particles/cells (ranging from 1 to 10 microns) inside droplets using the induced inertial flow approach, the length for focusing must be extended to 10cm, which is not practical in microfluidic chip designs (Dino Di Carlo et al. 2007; Dino Di Carlo 2009). If Dean flow is used to support self-ordering, the microfluidic device footprint must be enlarged to hold a curved (spiral) channel.

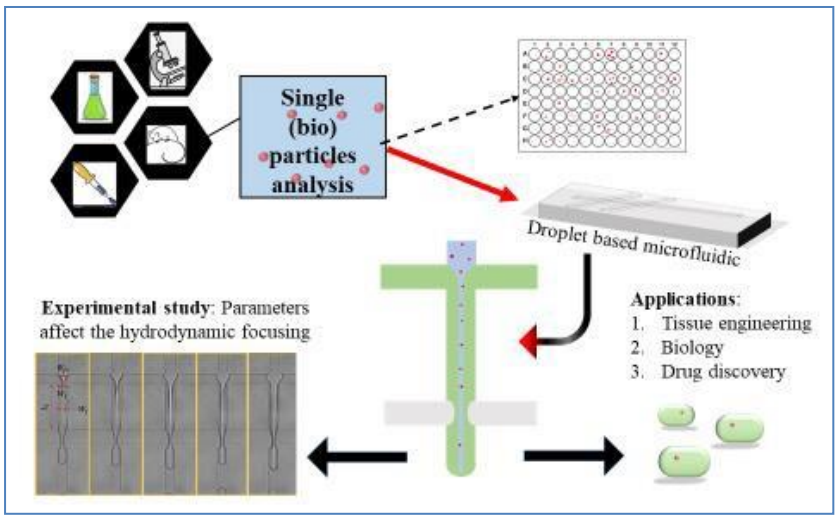

Figure 6-1. Hydrodynamic focusing formation considering viscosity contrast fluids integrated with droplet generation, and the effects on single cell encapsulation

Lately, another strategy, briefly mentioned in Chen et al.'s study, has shown the potential of using stratified flow formed between viscosity contrasting fluids in single encapsulation (X. Chen and Ren 2017b). This study mainly compares droplet generation between the cases of stratified flow dispersed phase and uniform dispersed phase. Different spanwise velocity distributions are formed between 10% Glycerol and 80% Glycerol, depending on whether the inner stream is the high or low viscosity fluid. However, this study does not focus on the experimental conditions for single encapsulation. In another study, the stratified flow structure in the dispersed phase has been applied to hold and align microbeads (1 micron) before they are enveloped within droplets containing quantum dots (T. H. Nguyen et al. 2018). Even though the criteria for designing a platform have been discussed and the single encapsulation process demonstrated, the study did not explore multiple parameters (i.e., flow rates between phases, viscosity contrast ratio, geometries) that alter the focusing width of the middle stream of the stratified flow.

This chapter experimentally studies the different parameters influencing the formation of hydrodynamic focusing integrated with droplet generation. The results section will discuss the optimized conditions for achieving the hydrodynamic focusing needed for single cell/(bio)particle encapsulation. This study provides information for researchers not only on the parameters affecting hydrodynamic focusing formation, which is coupled with droplet generation, but also on adopting this approach in other studies in biology, tissue engineering and drug discovery (Figure 6-1). As a demonstration, single mouse embryonic stem cells (mESCs) are encapsulated in droplets. Specifically, mESCs are prepared in a diluted gelatin-methacryloyl (GelMA) hydrogel and encapsulated within individual droplets containing a borate phosphate buffer (PBS). Stem cells have been chosen for this work because studying them potentially provides information needed by researchers and doctors in understanding diseases, developing drugs and creating diagnostic techniques (Pouton and Haynes 2007; Leeper, Hunter, and Cooke 2010; Herberts, Kwa, and Hermsen 2011). In general, stem cells can self-renew and differentiate into multiple lineages

consisting of pluripotent stem cells and multipotent stem cells. Even though the cell population is genetically homogenous, scientists often observe that individual cells behave differently when they are encapsulated in the same environment (Hood et al. 2004). The differences in how cells respond to the environment can provide information on the control mechanisms in biological systems. Hydrogels such as GelMA are used to provide tissue-like environments, acting as a means of stem cell transportation. Furthermore, cellular environments offered by micro-gel vesicles can be tuned to support research related to stem cell transplantation, thus, maximizing the advantages of stem cell therapeutic studies (Choe et al. 2018; Alkayyali et al. 2019; Castiaux, Spence, and Martin 2019)

6.3 Experimental Design

Before applying this approach in any application, we first explore the effects of parameters on the hydrodynamically focused stream forming between two dispersed fluids. This study uses a double-cross junction geometry, in which the first junction joins two dispersed phases and the second junction pinches droplets. Specifically, two miscible fluids of different viscosities are separately pumped into a microfluidic chip and meet at the first junction; where stratified flow is formed. The middle stream contains a mid-to-high viscosity fluid and is surrounded by a low viscosity fluid. A mixture of glycerol with different weight concentrations (30% w/w, 50% w/w, 70% w/w) is used as the mid-to-high viscosity fluid; whereas, pure de-ionized water is used as the low viscosity fluid stream. This stratified flow is then considered as the dispersed phase entering the second junction, where it is squeezed by a continuous phase to a critical point. Subsequently, droplets are generated. Silicon oil (20 cSt, surfactant free) is used for the continuous phase in all experiments. All fluids were purchased from Sigma Aldrich, Canada. The microfluidic device used in this study is designed to ensure that the channel network is not sensitive to any uncertainties, for instance, flow rate fluctuations during droplet generation, tubing compliance, materials for chip fabrication, etc. In brief, after fabrication, the cross-sectional shape of a microchannel is rectangular, and the channel height of each chip is assumed to be uniform. The actual channel width and

height are measured carefully before and after priming the micro-channels with oil following the method suggested by Glawdel et al. (Glawdel and Ren 2012a).

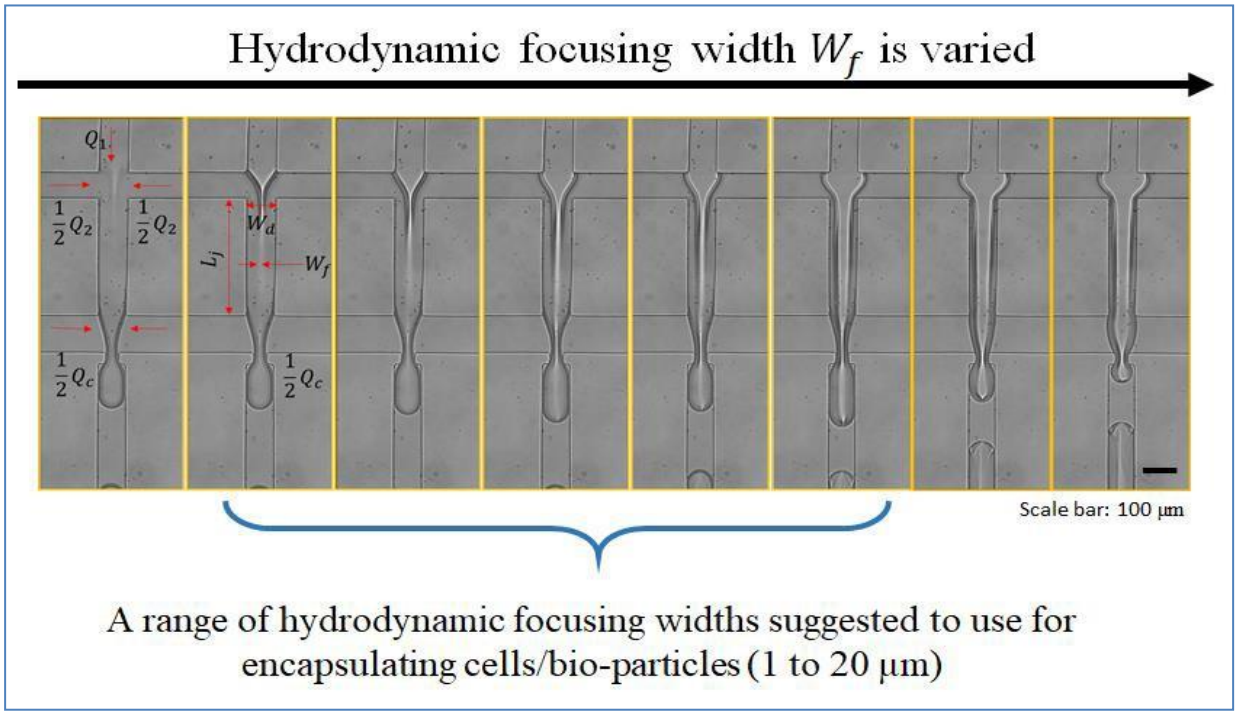

Figure 6-2. A range of hydrodynamic focusing widths suitable for achieving single encapsulation. Middle stream contains 50% glycerol mixture and the two side streams contain DI water; Silicon oil 20cSt is used for a continuous phase

There are three scenarios when two dispersed phases enter the first junction and form a stratified flow pattern before droplet generation, as mentioned in Chen et al.'s research (X. Chen and Ren 2017b). This present study focuses only on a case in which a mid-to-high viscosity fluid (DP1) is injected into a center stream, while a low viscosity fluid (DP2) is injected into the two side streams, as illustrated in Figure 6-3. The two fluid then form stratified flow inside the rectangular channel. This flow is driven by a pressure gradient along the microchannel under laminar conditions. In the beginning, when two dispersed phases join at the first junction and continuously flow downstream, a velocity contrast at the interface exists. Therefore, the mid-to-high viscosity fluid moves slower than the low viscosity fluid running along the two sides. Due to shear force presented at the interface, the axial velocity of DP1 tends to increase while that

of DP2 reduces until there is no velocity contrast between the two dispersed phases. Additionally, the width of each stream is inversely proportional to the average velocity of its respective fluid; thus, the width of DP1 is thinner when the axial velocity of DP1 increases, resulting in hydrodynamic focusing. This flow pattern is similar to the hydrodynamic focusing that has been indicated as the best choice for converging single cells/bio-particles in the middle of a micro-channel. This method is popular in developing flow-cytometry platforms (L. Wang et al. 2007; Mao et al. 2009; Di Carlo et al. 2010).

When coupled with droplet generation, the hydrodynamically focused stream occurring between two cross junctions is affected by multiple parameters: the dynamic viscosity of fluids (μ_1, μ_2, μ_c), the flow rates of different streams (Q_1, Q_2, Q_c), the geometries of micro-channels (width and height named $W_1, W_2, W_{DP}, W_{CP}, H, L_j$), and the interfacial tension of the dispersed and continuous phases ($\sigma_{DP/CP}$).

$$F_{focusing} = f(Q_1, Q_2, Q_c, \mu_1, \mu_2, \mu_c, \sigma_{DP/CP}, W_1, W_2, W_{DP}, W_{CP}, H, L_j) \quad (1)$$

where 1 & 2 are written as subscript for dispersed phase 1 and dispersed phase 2, respectively; DP & CP are subscript for the total dispersed phase and the continuous phase. The Buckingham π Theorem is employed to group the parameters involved together so as to understand their physical impacts on the focusing stream. Thus, the systematic non-dimensional function of hydrodynamic focusing is suggested to be:

$$W_f^* = f(\phi, \lambda, \eta, Ca) \quad (2)$$

where $\phi = Q_d/Q_c$ represents the flow rate ratio of a dispersed phase to a continuous phase;

$$\lambda = \frac{Q_2}{Q_1 + Q_2} = \frac{Q_2}{Q_d}$$

represents the flow rate ratio of the two dispersed phases corresponding to the total flow rate of a dispersed phase (Q_d); η is the viscosity ratio between two dispersed phases; and Ca is the capillary number representing the competition between the viscous force and the interfacial force.

Preliminary results also indicate that the combination of the flow rate of two dispersed phases and the viscosity contrast between them strongly influence the hydrodynamic focusing width. Additionally, the Capillary number and the flow rate ratio between the total dispersed phase and the continuous phase impact droplet generation (droplet size, generation regime). Hence, these four parameters are the main ones that will be studied throughout this chapter. Varying those key parameters will alter the hydrodynamic focusing width, making it compatible with the size of bio-objects and allowing them to be focused before encapsulation (Figure 6-2). Indeed, in most single cell encapsulation studies, cell sizes are in a range of 1 to 20 microns.

6.3.1 Microfluidic design

Overall, the length of the main channel is designed to be 5cm to hold 30 to 50 droplets so as to minimize uncertainties due to the existence of droplets. An orifice is added for two purposes: (1) to differentiate between the upstream and downstream parts, (2) to induce strong hydrodynamic focusing effects (Anna, Bontoux, and Stone 2003; Ong et al. 2007; L. Wu et al. 2017). The channel widths of all dispersed phases are set to be 100 μm, while the width of a continuous phase is slightly different (125 μm), so that the width ratio (Λ^*) at the second junction is 1.25. The aspect ratio of the channel is $H^* = \frac{H}{W_d} = \frac{3}{5}$. The length connecting two junctions is 500 μm. This length should be designed properly so that the flow of a dispersed phase can fully develop before it reaches the second junction. If this distance is too short, the pressure fluctuation during droplet generation can cause oscillation at the first junction, resulting in unstable hydrodynamic focusing. However, this distance should not be too long, so that the diffusion between the two dispersed phases is insignificant, which can be neglected.

From the work presented by Nishijima and Oster (1960), the diffusion in glycerol-water system is related to the weight percentage concentration of glycerol. Interestingly, the diffusion coefficient, approximately 1×10^{-5} (cm^2/s), does not depend on the glycerol concentration up to 70% w/w.

However, the dynamic viscosity of the glycerol-water mixture changes (Nishijima 1960). This conclusion has been confirmed by a recent work from Takamur et al. (Takamura, Fischer, and Morrow 2012). Therefore, in this study, the concentration of glycerol (% w/w) used in dispersed phase 1 is altered from 30% w/w (2.16 mPa.s) to 50% w/w (5.1 mPa.s) and up to 70% w/w (19.96 mPa.s). The dynamic viscosity is measured by using a rheometer (Brookfileld DV III). Glycerol has been chosen because of its uses in tissue engineering, serving as a potent inhibitor of cell proliferation (Wiebe and Dinsdale 1991).

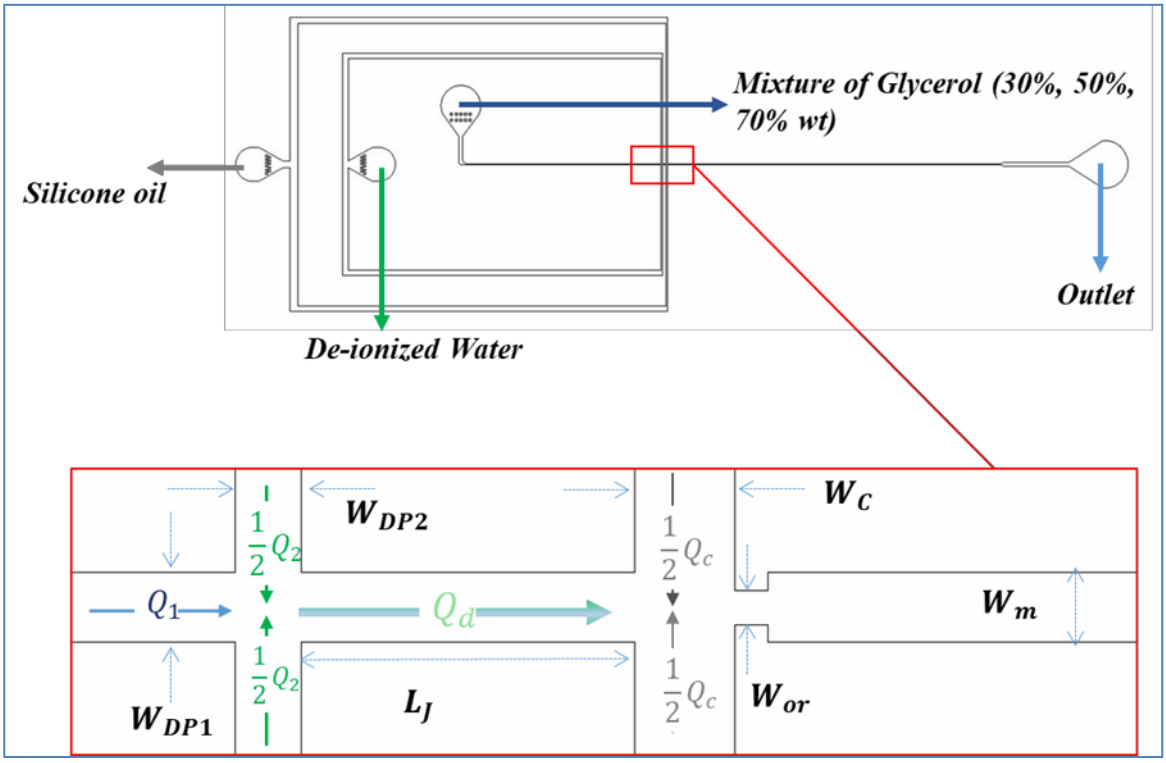

Figure 6-3. Design of a microfluidic chip

6.3.2 **Experimental validation**

6.3.2.1 Method for calibrating and measuring focusing width

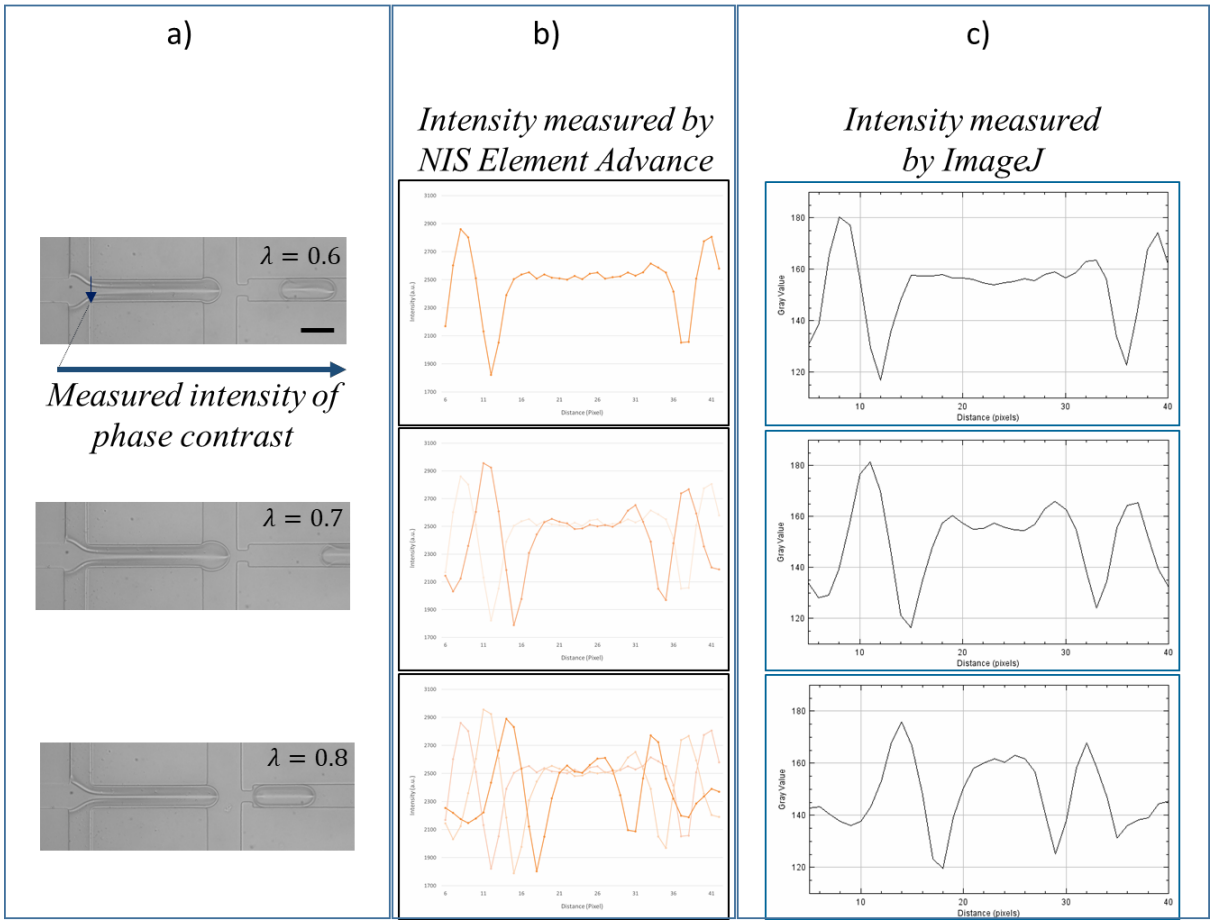

Figure 6-4. a) Hydrodynamic focusing widths taken using Q-imaging camera under different flow-rate-ratio conditions. b) Intensity recorded using NIS Element Advance. The bandwidth of the focusing narrows down when the flow rate ratio increases. c) ImageJ used to re-check the intensity measurement (presented in grayscale format).

All experiments are recorded using a CMOS high-speed camera (Phantom, V210) and a CCD camera (Qimaging) that are integrated with a phase contrast microscope (Nikon, Eclipse Ti). Images and videos are captured in 8-bits grey-scale format. The dynamics of droplet generation is recorded using a high-speed camera that offers a high frame rate (up to 2000s frames per second in full scale resolution).

However, the width of the focusing is retrieved by measuring the intensity differences between the phase contrasts induced by different fluids (Figure 6-4). During experiments, intensity variations are recorded by using a CCD camera and software (NIS Element Advance) (Figure 6-4b). The x-axis represents the number of pixels along the width of a channel, and the y-axis represents the intensity (a.u.) measured in real-time. To retrieve the width of the focusing in dimensional units (microns), both the number of pixels and size of each pixel must be calibrated. To ensure the focusing width can be analyzed based on the width of the contrast profile, representing the differences between two dispersed phases, images are also processed using ImageJ software (NIH, USA). The profile plots for each image agree well with the intensity plots taken by the NIS Element Advance software (Figure 6-4c).

6.3.2.2 The effect of viscosity contrast between two dispersed phases

To study the effect of the viscosity contrast between the two dispersed phases on the hydrodynamic focusing width, the viscosity contrast and the flow rate ratio between them are varied. Several experiments are performed under the same condition: fixed Ca and ϕ. In Figure 6-5, for each flow rate ratio between two dispersed phases associated with the total flow rate of the main dispersed phase, $\lambda = \frac{1}{1+\frac{Q_1}{Q_2}}$, the width of the hydrodynamic focusing (middle stream) slightly decreases when then the viscosity contrast between the two dispersed phases increases. From observation, the width under consideration is suggested to lie between two points showing minimal intensity around the stream. If a stratified flow is formed by two immiscible fluids (Cubaud and Notaro 2014), the edge between them is obviously recognized by their interface. However, in this work, a stratified flow between the two cross junctions is formed by two miscible fluids so that the edge between them is not as sharp as in Cubaud et al.'s study, especially when the viscosity contrast between two dispersed phases is low, $\eta = 2$. Therefore, the actual focusing width, as presented in Figure 6-5a, is computed by using the full half width maximum method. The focusing width is also presented in non-dimensional format by normalizing by the width of the

channel. Each data point is a mean average value taken from five different experiments using a new device for each test. By varying λ from 0.6 to 0.85, the normalized focusing width is realized to be within a range of $0.32 \geq W_f^* \geq 0.13$. Thus, the width ($\approx 32\ \mu m \geq W_f \geq \approx 13\ \mu m$) is considered to be suitable for aligning cells/bio-particles (in 1 to 10 microns) before their encapsulation. Interestingly, the normalized focusing width does not significantly change when $\lambda = 0.9$, even though the viscosity ratio is 10 times greater. This result suggests that the focusing width is mainly influenced by the flow rate ratio between two dispersed phases and is proportional to that ratio, $W_f^* \propto k\lambda$, where k is a constant related to the viscosity contrast, η, between the two dispersed phases.

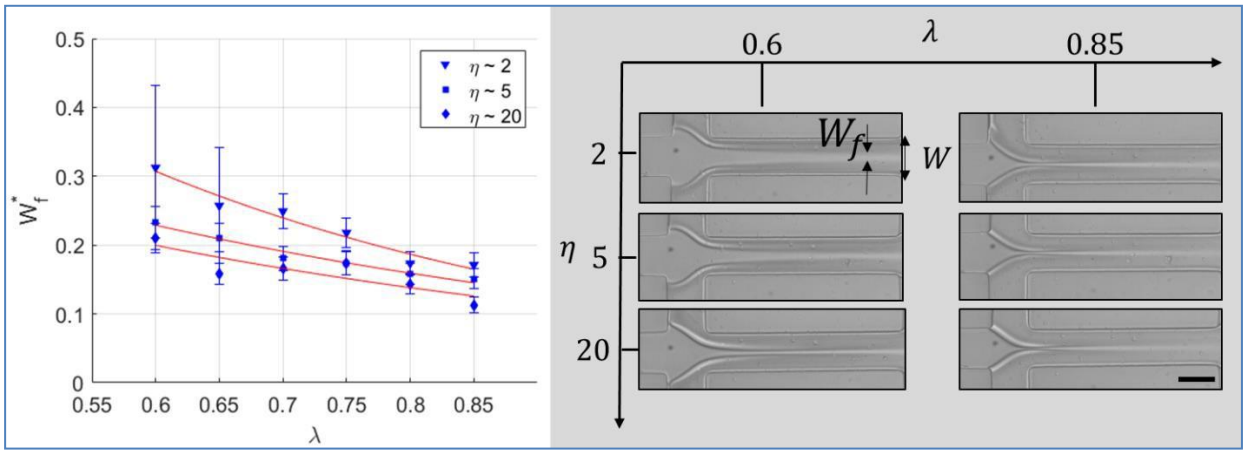

Figure 6-5. Normalized focusing width ($\boldsymbol{W_f^*}$) versus the flow rate ratio between two dispersed phases, corresponding to the total dispersed phase (fixed condition: $\boldsymbol{\phi \cong 1.4}$; $\boldsymbol{Ca \cong 1 \times 10^{-3}}$). Scale bar is 100 µm.

Moreover, the development of hydrodynamic focusing is monitored by measuring the width of the focusing stream from right after the first junction to before the droplet generation (Figure 6.6). As the formation of viscous hydrodynamic focusing begins, the velocities between the inner stream and the outer stream differ. When the stratified flow is formed and developed, the width of the focusing keeps varying when the flow is not fully developed. The induced shear stress at the barrier between two fluids balances

the velocity contrast between them so that the transverse velocity along the channel width is zero. After the flow is fully developed, and there is no variation in the focusing width. The transient length (L_s) is measured and normalized to the width of a dispersed phase instead the length of between two cross junctions. From experiments, at the low flow rate ratio, when the viscosity contrast between the two dispersed phase fluids has been varied, the transient length of the focusing width is different; however, that difference is only noticeable when the flow rate ratio between the two dispersed phases is high. These results indicate that the flow rate ratio between the two dispersed phases has a crucial influence on the width of the focusing and a greater impact the viscosity contrast. Additionally, it is noted that the viscosity ratio between the two fluids is not very high, $2 \leq \eta \leq 20$, resulting in the outer fluid (DI water) not fully lubricating the inner fluid (glycerol mixture).

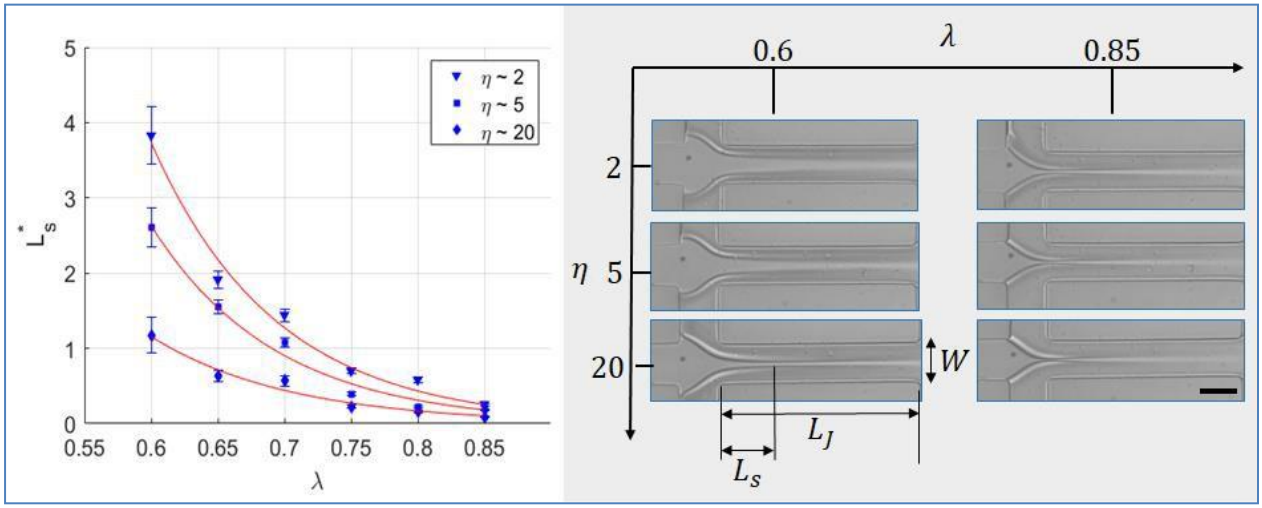

Figure 6-6. The formation of $\boldsymbol{L_S^*}$depending on the viscosity contrast between two miscible dispersed phases and the flow rate ratio between them (fixed condition: $\boldsymbol{\phi \cong 1.4}$; $\boldsymbol{Ca \cong 1 \times 10^{-3}}$). The scale bar is 100 µm.

6.3.2.3 The effects of flow rate ratio and Capillary number

As mentioned previously, this microfluidic network is designed to be insensitive to any induced uncertainties, so that the local pressure fluctuation during droplet generation at the second junction does

not influence the formation of the focusing width, as long as the flow rate ratio between the two dispersed phases is kept constant (Figure 6.7). Furthermore, the length between the two junctions should be long enough for the developed-flow. To vary the size of droplets, the flow rate ratio between the total dispersed phase and the continuous phase has been varied and the Capillary number is fixed in the range of $0.001 \leq$

$Ca \leq 0.005$ to ensure droplet generation in the squeezing regime. Figure 6.8 shows when the flow rate ratio between the total dispersed phase and the continuous phase is manipulated, droplet sizes respond accordingly, $2.65 \leq V_d^* \leq 3.75$. In addition, the flow rate ratio between two dispersed phases is also tuned from 0.65 to 0.85 to alter the focusing width.

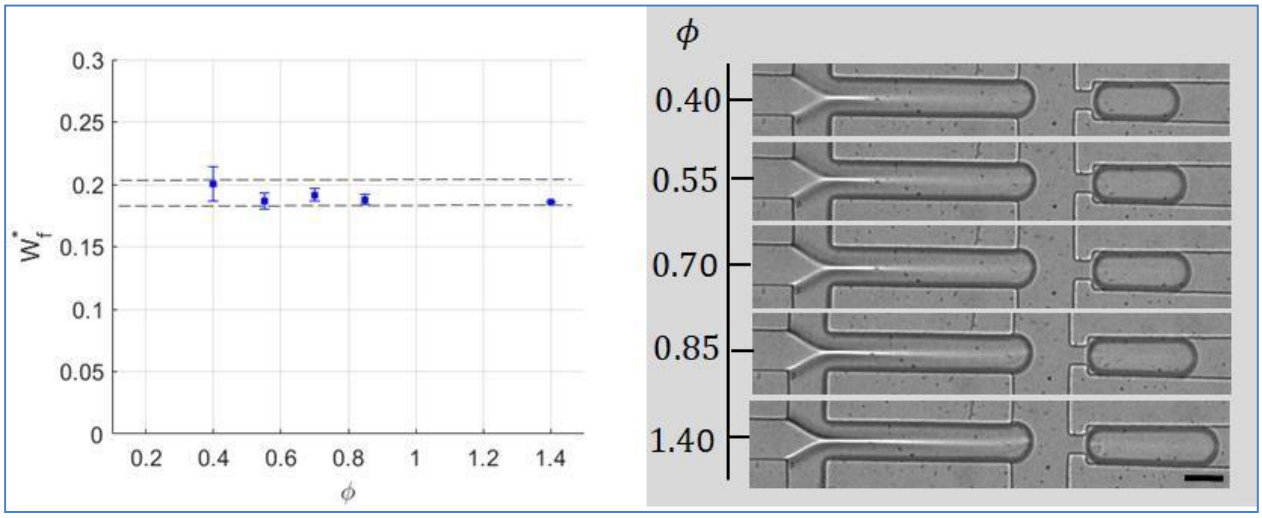

Figure 6-7. Stability of a normalized focusing width versus a variation of the flow rate ratio between a dispersed phase and a continuous phase (**fixed condition**: $\boldsymbol{\lambda \cong 0.8}$; $\boldsymbol{\eta = 5}$; $\boldsymbol{Ca \cong 1 \times 10^{-3}}$). The scale bar is 100 µm.

At the flow rate ratio λ from 0.6 to 0.65, the dispersed phase is considered to be filled with 26% to 32% of glycerol mixture, which is estimated based on the normalized focusing width (W^*) depending on the viscosity ratio between the two dispersed phases. In contrast, the dispersed phase is considered to filled with 10% to 12% when $\lambda \cong 0.85$. From experiments, although the total flow rate ratio between the

total dispersed phase and the continuous phase has been kept stable, the droplet size is slightly smaller when λ is close to 0.65 and larger when λ is close to 0.85 (Figure 6.8). This trend was also observed in the study by Chen et al. (X. Chen and Ren 2017b). Under the same ϕ condition, when a total dispersed phase is filled with only high viscosity fluid, a droplet is smaller than one that is generated when a total dispersed phase is filled with only water. In detail, the filling time equals the time it takes for the total dispersed phase to enter and fully block a cross junction. This time is influenced by the resistance of a dispersed phase experiencing this process, which is a combination between the interfacial force for holding the dispersed phase penetrating to a main channel and the pressure gradient along an interface. Therefore, a lower viscosity fluid has a longer filling time compared to a mid-to-high viscosity fluid. The viscosity ratio of the total dispersed phase depends on the variation of the flow rate ratio between two dispersed phases,

$\mu_D \propto \frac{Q_1}{Q_2}$. According to these results and the work by Chen et al., it takes a shorter time for the filling stage and a longer one for the necking stage when a dispersed phase is more occupied by mid-to-high viscosity fluid and vice versa.

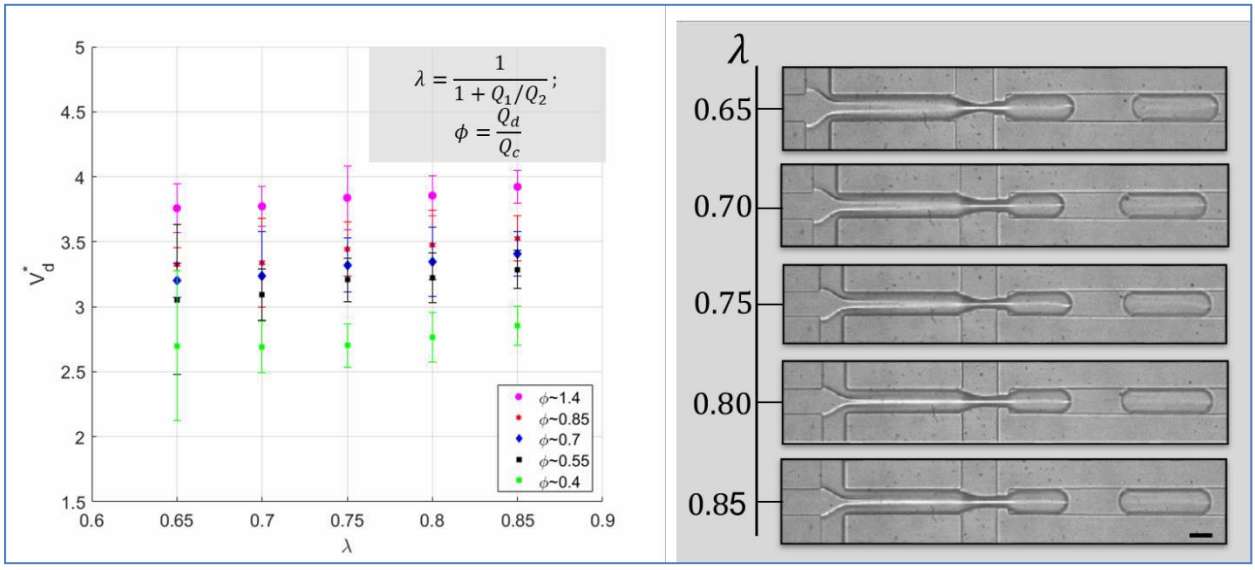

Figure 6-8. Normalized droplet volume versus a variation of flow rate ratio between a total dispersed phase and a continuous phase, at different flow rate ratios between the two dispersed phases (Fixed condition: $\boldsymbol{\eta = 2}$). The scale bar is 100 µm.

6.3.2.3.1 Role of local geometry

Several lines of evidence suggest that the geometry of a junction between two phases impacts droplet generation (Hashimoto et al. 2008; W. Lee, Walker, and Anna 2009; L. Wu et al. 2017). Specifically, at a low Capillary number (in the squeezing regime), the pinching off of droplets is affected by the dimensions of the orifice (Anna and Mayer 2006). According to Anna and Mayer, under a geometry-controlled regime – squeezing regime – droplets are highly uniform (monodispersity > 98%). In this work, an orifice configuration is located downstream, at the second junction, to provide highly monodispersed droplet generation. Furthermore, the escalating pressure of the continuous phase forces the dispersed phase to squeeze into a narrow gap, which maintains the high focus during droplet generation.

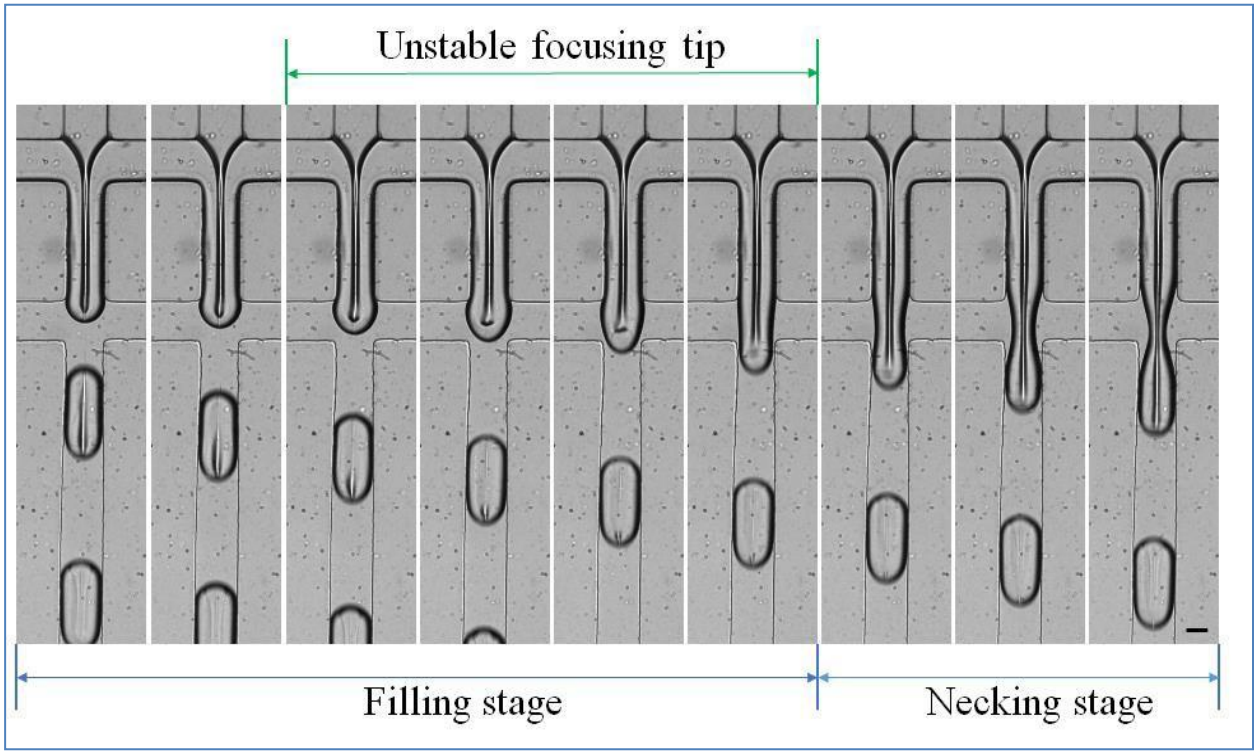

Figure 6-9. Unstable focusing tip during the filling stage in the case without an orifice. Experimental conditions: $\boldsymbol{Ca = 0.005}$, $\boldsymbol{\lambda = 0.85}$, $\boldsymbol{\phi \cong 0.4}$, $\boldsymbol{\eta = 5}$. The scale bar is 50 µm.

On the other hand, without an orifice, although the focusing tip is stable during the necking stage, it is not very stable during the filling stage. From observation, during the filling stage, while the focusing tip tends to continuously move forward, the surrounding flow tends to expand and cover the entire junction. At the end of the filling stage and before the necking stage, existent small vortices occur in the dispersed phase around the focusing tip. Thus, the tip has been disturbed (Figure 6.9). The disturbance happens only briefly and so might not affect the entire formation of the inner focusing stream. However, it might affect the single cell/bio-particle encapsulation process if cells/particles become trapped by the induced vortices.

6.3.2.4 Demonstration of single stem cell encapsulation

This section will describe the encapsulation of single stem cells in droplets following the optimized flow rate combinations and the viscosity contrast between two dispersed phases. In detail, mouse embryonic stem cells (5×10^6 cells/mL) are dispersed in a GelMA 2.5% wt solution and injected into dispersed phase 1. Phosphate buffered saline is injected into dispersed phase 2. Silicon oil is used for the continuous phase. Although the hydrogel has non-Newtonian fluid properties, by which the viscosity is varied with the shear rate, in this study, the GelMA solution has been diluted to 2.5% wt. Thus, the non-Newtonian fluid properties can be ignored.

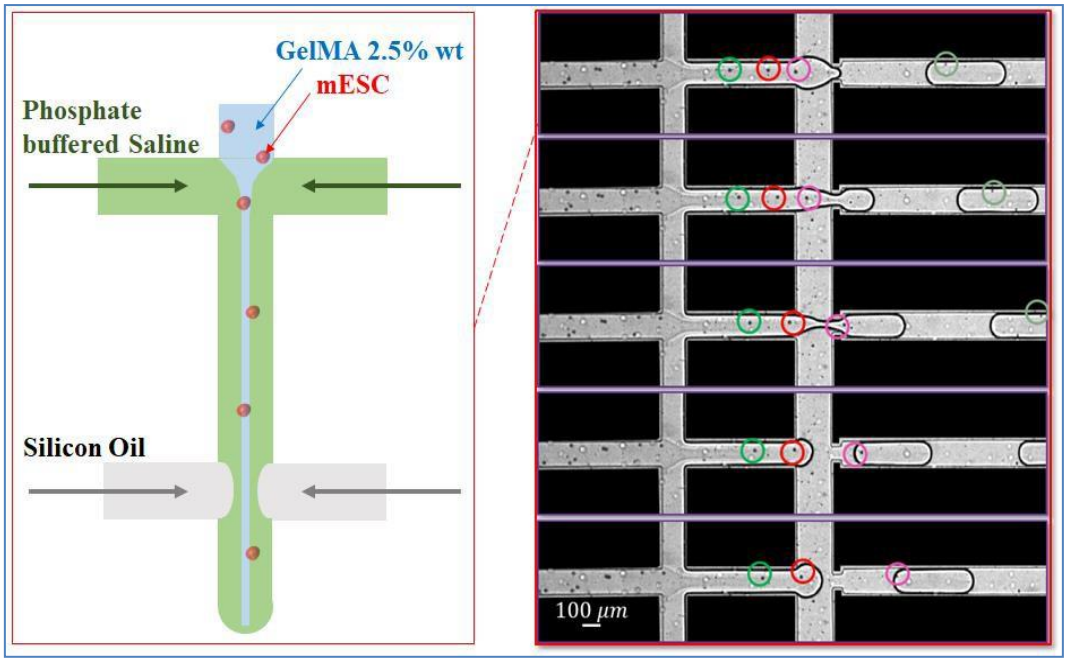

Figure 6-10. (Left) Schematic of single stem cell encapsulation. (Right) Experiment showing single stem cell within droplets under the conditions: $\boldsymbol{Ca = 0.002}$; $\boldsymbol{\phi = 1.4}$; $\boldsymbol{\eta \cong 5}$; $\boldsymbol{\lambda = 0.7}$

To encapsulate single stem cells inside droplets, the entire platform functions under a fixed condition: (1) droplets are generated in the squeezing regime ($Ca \cong 0.002$); (2) the flow rate ratio between two dispersed phases is varied in a range from 0.65 to 0.75; (3) the viscosity contrast between the two fluids is similar to that between 30% glycerol and water ($\eta \sim 2$). The flow rate of the continuous phase is kept constant $\cong 1.5\ \mu L/min$ and the flow rate of the total dispersed phase is $\cong 2.1\ \mu L/min$. In terms of geometry, the length between the two cross junctions is 500 μm, and the orifice width (W_{or}) is set at 50μm. Figure 6-10a shows that with this platform, single mouse stem cells can be successfully enveloped

inside droplets containing GelMA and phosphate buffered saline. Considering the number of droplets having one cell over the other droplet generated gives an efficiency for the process of up to 70%. In Figure 6-10, the focusing width between two fluids is not observed clearly due to the low contrast between the GelMA 2.5% wt and the phosphate buffered saline solution.

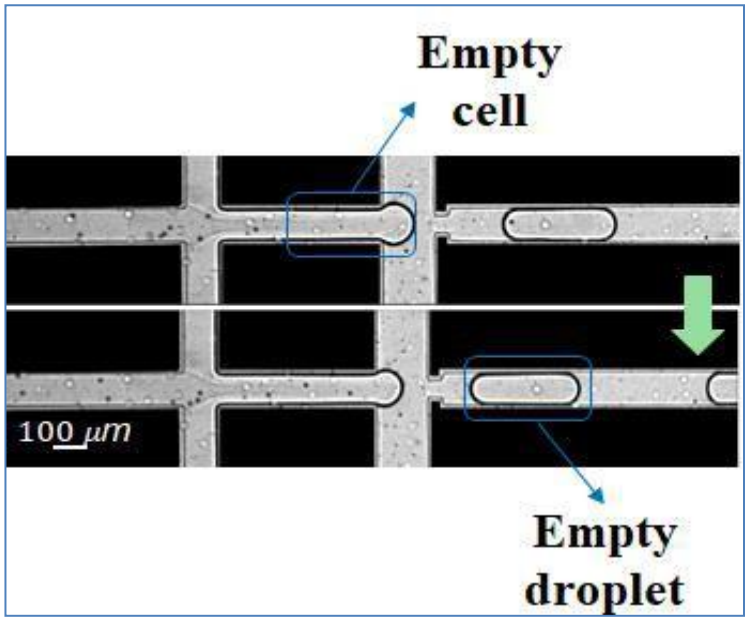

Figure 6-11. Cells aggregate upstream causing non-uniform cell distribution in dispersed phase 1, generating empty droplets downstream

The encapsulation process is successful at first; however, after one hour of experiments, cells start to aggregate at the inlet of dispersed phase 1. Hence, these cells are non-uniformly distributed in the prepared solution. As a result, many empty droplets are generated, decreasing the encapsulation efficiency of the single encapsulation process (Figure 6-11).

6.4 Conclusion of the project

In summary, the impacts of the flow rate ratios between phases and the viscosity contrast between two dispersed phases on the width focusing in between the two junctions have been systematically investigated. Moreover, the influence of the orifice on the focusing tip during droplet generation has been discussed. As a result, this study offers optimized experimental conditions for achieving a thin

f

hydrodynamic focusing width, $0.15 \leq W^{*} < 3.2$, which can be used for the single encapsulation that is useful in single cell studies. For instance, using the experimental conditions, described in this thesis, single mouse stem cells have been successfully encapsulated inside droplets containing two different reagents – GelMA and phosphate buffered saline, with the encapsulation efficiency of up to 70%. A double cross junction configuration is suggested not only for achieving single encapsulation of cells/bio-particles (in microns); but also for enveloping single embryoid bodies (3D aggregates of 1000 mESCs) within droplets to screen their development into mini-organs.

Chapter 7: Conclusion and recommendations for future work

7.1 Conclusion of the thesis

Droplet-based microfluidic devices are promising tools for advancing the performance of bio-chemical assays. Specifically, to be generated from low to high frequency (up to 10 kHz), each droplet (CV < 3%) acts as an individual vesicle carrying multiple reagents and bio-particles/cells. While these droplets are traveling inside microfluidic networks, they are enveloped by immiscible oil phase, which prevents the precipitating of substances and cross contamination between different droplets and between them and channel walls. Furthermore, the volume of droplets varies usually from nano-liter to femto-liter which advances the mass transfer inside droplets. Even though microfluidic systems function under low Reynold number conditions, the chaotic advection inside droplets is still achievable, particularly, when the droplets pass through serpentine micro-channels. As a result, the rapid and homogeneous mixing of bio-chemical components inside droplets is enhanced. Fast mixing is one of the key features making droplet-based microfluidic technology attractive to researchers and scientists. Additionally, generated droplets can be manipulated downstream, such as by merging them with other droplets; splitting them into daughter droplets to increase their capacities, trapping them in micro-wells for screening, and so on, enabling development of Lab-on-a-chip devices.

Despite extensive growth of this technology, its commercialization remains restricted due to limitations, such as a lack of robust designs that includes multiple compartments (to either actively or passively control droplets), plus, a scarcity of fabricating platforms and scaling up products. To expand the uses of droplet-based microfluidic platforms in multiple applications (i.e, cell studies, analytical chemistry and diagnostics) and narrow the gap between microfluidic research and other science studies, it is important (1) to make platforms easy to use and fabricate, (2) to be able to integrate them with other components so as to increase a platform's capabilities, and (3) to provide experimental guidelines for users. In response

to these three main requirements, the three projects discussed in this thesis have been designed and evaluated. In particular, this thesis focuses on investigating a strategy for encapsulating single/multiple (bio) particle/s within droplets containing multiple reagents. A double-cross configuration with viscosity contrast stratified flow is proposed. In detail, the first junction is where two dispersed fluids meet, then form stratified flow; and the second junction is used for generating droplets, as well as encapsulating (bio) particles inside droplets. Hypothetically, to hold and align the (bio) particles before they are loaded into droplets with other reagents, a middle stream of stratified flow formed by two miscible fluids, which contains a mid-to-high viscosity fluid, should be controlled to form a thin focusing stream.

In the first project, as discussed in Chapter 4, this strategy has been applied for encapsulating single magnetic bead (1 micron) with quantum dots that are prepared in aqueous solution. A double-cross junction is coupled with a series of serpentine channel downstream to provide a rapid mixing mechanism inside droplets, resulting in homogeneously coating the beads with quantum dots. Overall, this strategy cannot only can be applied to achieve the immobilization of quantum dots in micron magnetic beads, but also used in other one-step coating (bio) particle applications. Continuing the first project, the second project, as described in Chapter 5, indicates the ability to combine the existent platform having a double-cross junction configuration with more complex compartments, such as another droplet generator, a merging chamber, and a series of serpentine channels downstream. This project successfully achieved a main goal of providing a “plug and collect” microfluidic platform for biochemists to use in the two-step conjugating of oligonucleotide strands with nanoparticles, which are immobilized on solid magnetic beads. In addition to the capacities to separately generate two chains of droplets in parallel, merge them alternatively, and mix reagents inside droplets uniformly, this platform is driven by a pressure system and can be easily fabricated using a standard soft-lithography technique. Therefore, this approach presents one step towards narrowing the gap between the academic research and commercialization products. As presented in Chapter 6, the experimental study offers an experimental guideline for achieving a thin

focusing stream. The impacts of parameters on the formation of hydrodynamic focusing coupled with droplet generation are investigated throughout this study. With the optimized experimental conditions provided, single mouse embryonic stem cells have been successfully encapsulated inside droplets that contain diluted GelMA solution and phosphate buffered saline solution. Compared to other methodologies, this strategy is attainable because of the design simplicity that allows researchers to inject multiple reagents and simultaneously encapsulate (bio) particles inside droplets. Furthermore, this method does not need a high flow rate to order cells/particles before the encapsulation, which could potentially affect cell membrane rates; as well as, a large footprint for long straight/curvy channels are not required.

7.2 Recommendations for future work

The results from this thesis's research have shown that a double-cross junction and hydrodynamic focusing stream formed in between are possible. However, many aspects should be further studied. For instance, the experimental study, as presented in Chapter 6, does not fully cover the impacts of geometries (i.e, the angle created in between streams, the aspect ratio and the width ratio) on the hydrodynamic focusing width. Especially; at the second junction, the droplet generation is a function of multiple parameters, including the aspect ratio and the width ratio. Moreover, the influences of surfactant and its concentration have not been investigated in this study.

In this thesis, the two-sided flow (dispersed phase 2) surrounding the hydrodynamic focusing is only filled with one type of fluid (DI water). In future work, the inlet of the dispersed phase 2 could be split into two so that researchers can inject three different reagents and envelope them with (bio) particles within individual droplets. In the current study, the width ratios between dispersed phases are proportional to the flow rate ratio between them. This ratio can be considered to estimate the volume fraction of reagents inside a single droplet, suggesting a volume concentration of each fluid inside a droplet.

However, a model to precisely estimate the concentration of each reagent that is loaded into individual droplets should be further investigated.

The approach discussed in this thesis for encapsulating single cells/particles in droplets can be further employed for encapsulating single embryoid bodies in droplets. The materials that are encapsulated with embryoid bodies need not only be aqueous solutions but could also be hydrogel, mimicking the tissue environment for cell and mini-organ studies. Some preliminary experiments have been conducted (Figure 7-1). Nevertheless, the current challenges are listed as follows: (1) injecting embryoid bodies into a microfluidic device without breaking them; (2) working with different polymer solution to create different tissue environments, incomplete understanding of polymer fluid properties (i.e, non-Newtonian fluid behaviors, viscoelasticity, etc.). Thus, efforts to discover a model for generating droplets considering non-Newtonian fluid, to explore a stratified flow formed with viscoelastic fluids, and to employ these models in tissue engineering applications are crucial. Furthermore, densities and shapes of embryoid bodies should also be concerned in an updated study.

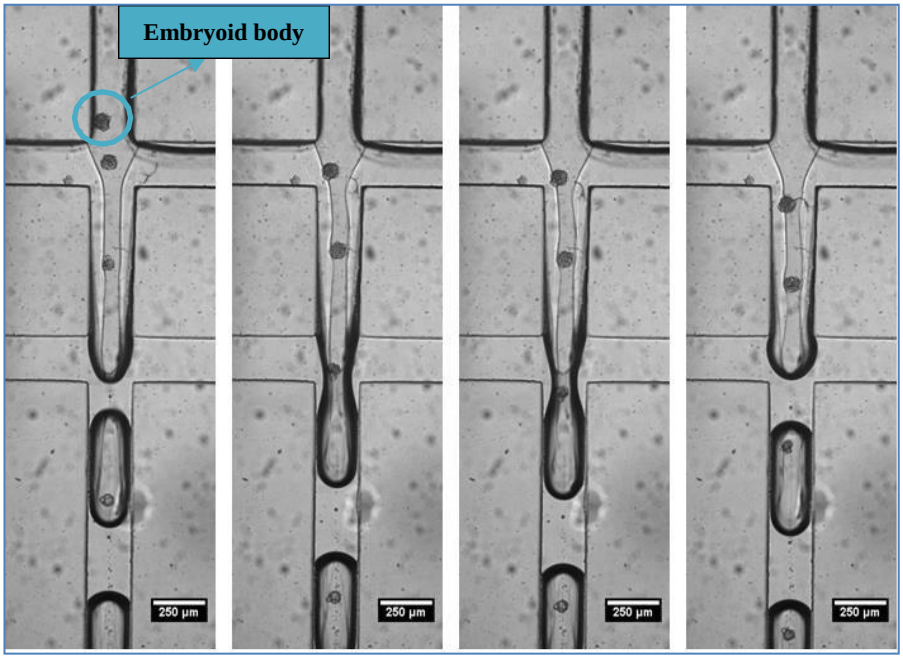

Figure 7-1. Embryoid bodies encapsulated within hydrogel droplets

Lastly, before ending this thesis, I would like to suggest another method to enhance commercialized microfluidic products. Compared to the other traditional methods to fabricate microfluidic devices (hot embossing, hard-lithography, silicon wafer etching), soft-lithography is the best option. Nonetheless, this technique is not feasible for using in scaling up microfluidic products. Another inexpensive but sufficient method to fabricate microfluidic devices, such as the low force stereo-lithography technique (a 3D printer), should be carried out. Compared to the soft-lithography technique, the stereo-lithography technique is promising for manufacturing microfluidic devices. It would also allow researchers to explore initial ideas with low-risk. For instance, a microfluidic device with multiple channel heights would be easy to fabricate using a 3D printer, instead of a soft-lithography technique which actually requires control in coating multiple photoresist layers (Figure 7-2). Moreover, microfluidic devices can be made with different materials by replacing different resins. However, the current problem with this technique is the printing resolution, resulting in significant surface roughness. The roughness can lead to a non-uniform surface property that could potentially cause partial wetting issues, influencing droplet generation and droplet transportation. Thus, a sufficient coating method to treat surface of micro-channels, fabricated using this technique, should be carefully characterized.

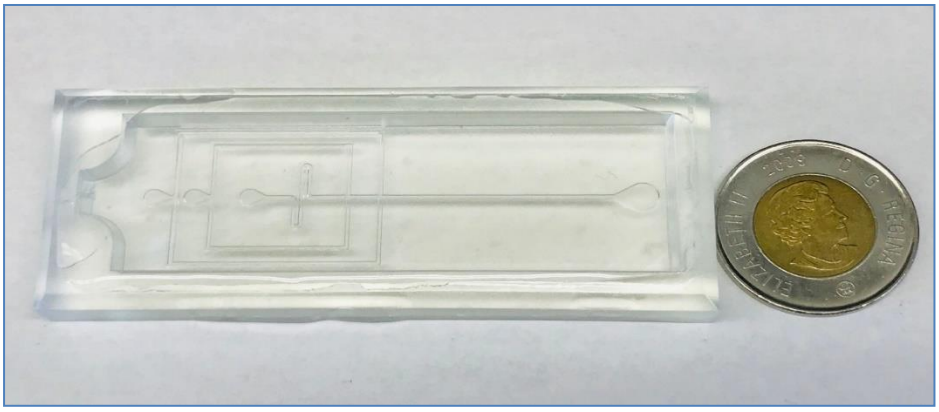

Figure 7-2. A microfluidic platform printed using a Formlab3 3D printer

Bibliography

Aarts, Dirk G A L, Henk N W Lekkerkerker, Hua Guo, Gerard H. Wegdam, and Daniel Bonn. 2005. "Hydrodynamics of Droplet Coalescence." *Physical Review Letters* 95 (16): 1–4. https://doi.org/10.1103/PhysRevLett.95.164503.

Abgrall, P., and A. M. Gué. 2007. "Lab-on-Chip Technologies: Making a Microfluidic Network and Coupling It into a Complete Microsystem - A Review." *Journal of Micromechanics and Microengineering* 17 (5). https://doi.org/10.1088/0960-1317/17/5/R01.

Agresti, Jeremy J. 2010. "Correction for Agresti et Al., Ultrahigh-Throughput Screening in Drop-Based Microfluidics for Directed Evolution." *Proceedings of the National Academy of Sciences* 107 (14): 6550–6550. https://doi.org/10.1073/pnas.1002891107.

Ahn, Byungwook, Kangsun Lee, Hun Lee, Rajagopal Panchapakesan, and Kwang W. Oh. 2011. "Parallel Synchronization of Two Trains of Droplets Using a Railroad-like Channel Network." *Lab on a Chip* 11 (23): 3956. https://doi.org/10.1039/c1lc20690g.

Ahn, Keunho, Charles Kerbage, Tom P. Hunt, R. M. Westervelt, Darren R. Link, and D. A. Weitz. 2006. "Dielectrophoretic Manipulation of Drops for High-Speed Microfluidic Sorting Devices." *Applied Physics Letters* 88 (2): 1–3. https://doi.org/10.1063/1.2164911.

Al-Halhouli, Ala'aldeen, Wisam Al-Faqheri, Baider Alhamarneh, Lars Hecht, and Andreas Dietzel. 2018. "Spiral Microchannels with Trapezoidal Cross Section Fabricated by Femtosecond Laser Ablation in Glass for the Inertial Separation of Microparticles." *Micromachines* 9 (4). https://doi.org/10.3390/mi9040171.

Algar, W. Russ, and Ulrich J. Krull. 2007. "Towards Multi-Colour Strategies for the Detection of Oligonucleotide Hybridization Using Quantum Dots as Energy Donors in Fluorescence Resonance Energy Transfer (FRET)." *Analytica Chimica Acta* 581 (2): 193–201. https://doi.org/10.1016/j.aca.2006.08.026.

Algar, W. Russ, Anthony J. Tavares, and Ulrich J. Krull. 2010. "Beyond Labels: A Review of the Application of Quantum Dots as Integrated Components of Assays, Bioprobes, and Biosensors Utilizing Optical Transduction." *Analytica Chimica Acta* 673 (1): 1–25. https://doi.org/10.1016/j.aca.2010.05.026.

Alkayyali, T., T. Cameron, B. Haltli, R. G. Kerr, and A. Ahmadi. 2019. "Microfluidic and Cross-Linking

Methods for Encapsulation of Living Cells and Bacteria - A Review." *Analytica Chimica Acta* 1053: 1–21. https://doi.org/10.1016/j.aca.2018.12.056.

Amstad, Esther, Xiaoming Chen, Max Eggersdorfer, Noa Cohen, Thomas E. Kodger, Carolyn L. Ren, and David A. Weitz. 2017. "Parallelization of Microfluidic Flow-Focusing Devices." *Physical Review E* 95 (4): 1–6. https://doi.org/10.1103/PhysRevE.95.043105.

Anna, Shelley L., Nathalie Bontoux, and Howard A. Stone. 2003. "Formation of Dispersions Using 'Flow Focusing' in Microchannels." *Applied Physics Letters* 82 (3): 364–66. https://doi.org/10.1063/1.1537519.

Anna, Shelley L., and Hans C. Mayer. 2006. "Microscale Tipstreaming in a Microfluidic Flow Focusing Device." *Physics of Fluids* 18 (12). https://doi.org/10.1063/1.2397023.

Bai, Yunpeng, Ximin He, Dingsheng Liu, Santoshkumar N. Patil, Dan Bratton, Ansgar Huebner, Florian Hollfelder, Chris Abell, and Wilhelm T.S. Huck. 2010. "A Double Droplet Trap System for Studying Mass Transport across a Droplet-Droplet Interface." *Lab on a Chip* 10 (10): 1281–85. https://doi.org/10.1039/b925133b.

Balasuriya, Sanjeeva. 2015. "Dynamical Systems Techniques for Enhancing Microfluidic Mixing." *Journal of Micromechanics and Microengineering* 25: 94005. https://doi.org/10.1088/0960-1317/25/9/094005.

Baret, Jean-Christophe. 2012. "Surfactants in Droplet-Based Microfluidics." *Lab Chip* 12 (3): 422–33. https://doi.org/10.1039/C1LC20582J.

Baret, Jean-Christophe, Oliver J. Miller, Valerie Taly, Michaël Ryckelynck, Abdeslam El-Harrak, Lucas Frenz, Christian Rick, et al. 2009. "Fluorescence-Activated Droplet Sorting (FADS): Efficient Microfluidic Cell Sorting Based on Enzymatic Activity." *Lab on a Chip* 9 (13): 1850–58. https://doi.org/10.1039/b902504a.

Baroud, Charles N., Francois Gallaire, and Rémi Dangla. 2010. "Dynamics of Microfluidic Droplets." *Lab on a Chip* 10 (16): 2032. https://doi.org/10.1039/c001191f.

Baroud, Charles N., Matthieu Robert de Saint Vincent, and Jean-Pierre Delville. 2007. "An Optical Toolbox for Total Control of Droplet Microfluidics." *Lab on a Chip* 7 (8): 1029. https://doi.org/10.1039/b702472j.

Basu, Amar S., and Yogesh B. Gianchandani. 2008. "Virtual Microfluidic Traps, Filters, Channels and

Pumps Using Marangoni Flows." *Journal of Micromechanics and Microengineering* 18 (11). https://doi.org/10.1088/0960-1317/18/11/115031.

Baume, Maud, Astrid Cariou, Adélaïde Leveau, Noémie Fessy, Frédéric Pastori, Sophie Jarraud, and Sophie Pierre. 2019. "Quantification of Legionella DNA Certified Reference Material by Digital Droplet PCR." *Journal of Microbiological Methods* 157 (October 2018): 50–53. https://doi.org/10.1016/j.mimet.2018.12.019.

Blauch, Lucas R., Ya Gai, Jian Wei Khor, Pranidhi Sood, Wallace F. Marshall, and Sindy K. Y. Tang. 2017. "Microfluidic Guillotine for Single-Cell Wound Repair Studies." *Proceedings of the National Academy of Sciences* 114 (28): 7283–88. https://doi.org/10.1073/pnas.1705059114.

Boeneman, Kelly, Jeffrey R Deschamps, Susan Buckhout-white, Duane E Prasuhn, R Goldman, Mario Ancona, and Igor L Medintz. 2010. "Quantum Dot DNA Biocojugates: Attachment Chemistry Strongly Influences the Resulting Composite Architecture." *ACS Nano* 4 (12): 7253–66. https://doi.org/10.1021/nn1021346.Quantum.

Boeneman, Kelly, Jeffrey R Deschamps, Susan Buckhout-white, Ḱ Duane E Prasuhn, Juan B Blanco-canosa, Philip E Dawson, Michael H Stewart, et al. 2010. "Quantum Dot DNA Bioconjugates : Architecture." *ACS Nano* 4 (12): 7253–66.

Boruah, Manash Protim, Anik Sarker, Pitambar R. Randive, Sukumar Pati, and Suman Chakraborty. 2018. "Wettability-Mediated Dynamics of Two-Phase Flow in Microfluidic T-Junction." *Physics of Fluids* 30 (12). https://doi.org/10.1063/1.5054898.

Bratt-Leal, Andres M., Richard L. Carpenedo, and Todd C. McDevitt. 2009. "Engineering the Embryoid Body Microenvironment to Direct Embryonic Stem Cell Differentiation." *Biotechnology Progress* 25 (1): 43–51. https://doi.org/10.1021/bp.139.

Bremond, Nicolas, Abdou R. Thiam, and J??r??me Bibette. 2008. "Decompressing Emulsion Droplets Favors Coalescence." *Physical Review Letters* 100 (2): 1–4. https://doi.org/10.1103/PhysRevLett.100.024501.

Breslauer, David N., Philip J. Lee, and Luke P. Lee. 2006. "Microfluidics-Based Systems Biology." *Molecular BioSystems* 2 (2): 97–112. https://doi.org/10.1039/b515632g.

Brouzes, Eric, Travis Kruse, Robert Kimmerling, and Helmut H. Strey. 2015. "Rapid and Continuous Magnetic Separation in Droplet Microfluidic Devices." *Lab on a Chip* 15 (3): 908–19.

https://doi.org/10.1039/c4lc01327a.

Bruchez Jr., M. 1998. “Semiconductor Nanocrystals as Fluorescent Biological Labels.” *Science* 281 (5385): 2013–16. https://doi.org/10.1126/science.281.5385.2013.

Cao, Yiming, Alexandros Stavrinadis, Tania Lasanta, David So, and Gerasimos Konstantatos. 2016. “The Role of Surface Passivation for Efficient and Photostable PbS Quantum Dot Solar Cells.” *Nature Energy* 1 (4): 16035. https://doi.org/10.1038/nenergy.2016.35.

Cao, Zhenning, Fangyuan Chen, Ning Bao, Huacheng He, Peisheng Xu, Saikat Jana, Sunghwan Jung, Hongzhen Lian, and Chang Lu. 2013. “Droplet Sorting Based on the Number of Encapsulated Particles Using a Solenoid Valve.” *Lab on a Chip* 13 (1): 171–78. https://doi.org/10.1039/C2LC40950J.

Carlo, Di, Soojung Claire Hur, Tat Kwong, and Dino Di. 2010. “Sheathless Inertial Cell Ordering for Extreme Throughput Flow Cytometry †.” *Lab Chip* 10 (3): 274–80. https://doi.org/10.1039/b919495a.

Carlo, Dino Di. 2009. “Inertial Microfluidics.” *Lab on a Chip* 9 (21): 3038. https://doi.org/10.1039/b912547g.

Carlo, Dino Di, Daniel Irimia, Ronald G Tompkins, and Mehmet Toner. 2007. “Continuous Inertial Focusing, Ordering, and Separation of Particles in Microchannels.” *Proceedings of the National Academy of Sciences of the United States of America* 104 (48): 18892–97. https://doi.org/10.1073/pnas.0704958104.

Carlson, A., M. Do-Quang, and G. Amberg. 2010. “Droplet Dynamics in a Bifurcating Channel.” *International Journal of Multiphase Flow* 36 (5): 397–405. https://doi.org/10.1016/j.ijmultiphaseflow.2010.01.002.

Carroll, N J Et Al. 2008. “Droplet-Based Microfluids for Emulsion and Solvent Evaporation Synthesis of Monodisperse Mesoporous Silica Microspheres.” *Langmuir* 24 (18): 658–61. https://doi.org/10.1021/la7032516.

Casadevall I Solvas, Xavier, and Andrew Demello. 2011. “Droplet Microfluidics: Recent Developments and Future Applications.” *Chemical Communications* 47 (7): 1936–42. https://doi.org/10.1039/c0cc02474k.

Castiaux, Andre D., Dana M. Spence, and R. Scott Martin. 2019. “Review of 3D Cell Culture with

Analysis in Microfluidic Systems." *Analytical Methods* 11 (33): 4220–32. https://doi.org/10.1039/c9ay01328h.

Castro-Hernández, Elena, Wim Van Hoeve, Detlef Lohse, and José M. Gordillo. 2011. "Microbubble Generation in a Co-Flow Device Operated in a New Regime." *Lab on a Chip* 11 (12): 2023–29. https://doi.org/10.1039/c0lc00731e.

Chabert, Max, Kevin D. Dorfman, and Jean Louis Viovy. 2005. "Droplet Fusion by Alternating Current (AC) Field Electrocoalescence in Microchannels." *Electrophoresis* 26 (19): 3706–15. https://doi.org/10.1002/elps.200500109.

Chabert, Max, and Jean-Louis Viovy. 2008. "Microfluidic High-Throughput Encapsulation and Hydrodynamic Self-Sorting of Single Cells." *Proceedings of the National Academy of Sciences of the United States of America* 105 (9): 3191–96. https://doi.org/10.1073/pnas.0708321105.

Chen, Hong, Qun Fang, Xue Feng Yin, and Zhao Lun Fang. 2005. "Microfluidic Chip-Based Liquid-Liquid Extraction and Preconcentration Using a Subnanoliter-Droplet Trapping Technique." *Lab on a Chip* 5 (7): 719–25. https://doi.org/10.1039/b416964f.

Chen, Michael C W, Madhuja Gupta, and Karen C. Cheung. 2010. "Alginate-Based Microfluidic System for Tumor Spheroid Formation and Anticancer Agent Screening." *Biomedical Microdevices* 12 (4): 647–54. https://doi.org/10.1007/s10544-010-9417-2.

Chen, Xiaoming, Alexander Brukson, and Carolyn L. Ren. 2017. "A Simple Droplet Merger Design for Controlled Reaction Volumes." *Microfluidics and Nanofluidics* 21 (3): 34. https://doi.org/10.1007/s10404-017-1875-x.

Chen, Xiaoming, Tomasz Glawdel, Naiwen Cui, and Carolyn L. Ren. 2015. "Model of Droplet Generation in Flow Focusing Generators Operating in the Squeezing Regime." *Microfluidics and Nanofluidics* 18 (5–6): 1341–53. https://doi.org/10.1007/s10404-014-1533-5.

Chen, Xiaoming, and Carolyn L. Ren. 2017a. "A Microfluidic Chip Integrated with Droplet Generation, Pairing, Trapping, Merging, Mixing and Releasing." *RSC Advances* 7 (27): 16738–50. https://doi.org/10.1039/c7ra02336g.

Chen, Xiaoming, and Carolyn L Ren. 2017b. "Experimental Study on Droplet Generation in Flow Focusing Devices Considering a Stratified Flow with Viscosity Contrast." *Chemical Engineering Science* 163: 1–10. https://doi.org/10.1016/j.ces.2017.01.029.

Cheng-Tso Chen, and Gwo-Bin Lee. 2006. “A New Microfluidic Chip for Formation of Micro-Droplets in Liquids Utilizing Active Pneumatic Choppers” 15 (6): 494–97. https://doi.org/10.1109/memsys.2006.1627844.

Cho, Sung Kwon, Yuejun Zhao, and Chang-Jin Cj Kim. 2007. “Concentration and Binary Separation of Micro Particles for Droplet-Based Digital Microfluidics.” *Lab on a Chip* 7 (4): 490–98. https://doi.org/10.1039/b615665g.

Choe, Goeun, Junha Park, Hansoo Park, and Jae Young Lee. 2018. “Hydrogel Biomaterials for Stem Cell Microencapsulation.” *Polymers* 10 (9): 1–17. https://doi.org/10.3390/polym10090997.

Choi, Kihwan, Alphonsus H.C. Ng, Ryan Fobel, and Aaron R. Wheeler. 2012. “Digital Microfluidics.” *Annual Review of Analytical Chemistry* 5 (1): 413–40. https://doi.org/10.1146/annurev-anchem-062011-143028.

Choi, Yoon Young, Bong Geun Chung, Dae Ho Lee, Ali Khademhosseini, Jong Hoon Kim, and Sang Hoon Lee. 2010. “Controlled-Size Embryoid Body Formation in Concave Microwell Arrays.” *Biomaterials* 31 (15): 4296–4303. https://doi.org/10.1016/j.biomaterials.2010.01.115.

Chong, Zhuang Zhi, Say Hwa Tan, Alfonso M. Gañán-Calvo, Shu Beng Tor, Ngiap Hiang Loh, and Nam Trung Nguyen. 2016. “Active Droplet Generation in Microfluidics.” *Lab on a Chip* 16 (1): 35–58. https://doi.org/10.1039/c5lc01012h.

Chong, Zhuang Zhi, Say Hwa Tan, Alfonso M Ganan-Calvo, Shu Beng Tor, Ngiap Hiang Loh, and Nam-Trung Nguyen. 2016. “Active Droplet Generation in Microfluidics.” *Lab Chip* 16 (1): 35–58. https://doi.org/10.1039/C5LC01012H.

Chou, Leo Y. T., Kyryl Zagorovsky, and Warren C. W. Chan. 2014. “DNA Assembly of Nanoparticle Superstructures for Controlled Biological Delivery and Elimination.” *Nature Nanotechnology* 9 (2): 148–55. https://doi.org/10.1038/nnano.2013.309.

Christopher, G F, and S L Anna. 2007. “Microfluidic Methods for Generating Continuous Droplet Streams.” *Journal of Physics D: Applied Physics* 40 (19): R319–36. https://doi.org/10.1088/0022-3727/40/19/R01.

———. 2009. “Passive Breakup of Viscoelastic Droplets and Filament Self-Thinning at a Microfluidic T-Junction.” *Journal of Rheology Appl. Phys. Lett* 53 (10): 164107–41102. https://doi.org/10.1122/1.3086871.

Christopher, G F, J Bergstein, N B End, M Poon, C Nguyen, and S L Anna. 2009. “Coalescence and Splitting of Confined Droplets at Microfluidic Junctions.” *Lab on a Chip* 9 (8): 1102–9. https://doi.org/10.1039/b813062k.

Christopher, Gordon F., N. Nadia Noharuddin, Joshua A. Taylor, and Shelley L. Anna. 2008. “Experimental Observations of the Squeezing-to-Dripping Transition in T-Shaped Microfluidic Junctions.” *Physical Review E - Statistical, Nonlinear, and Soft Matter Physics* 78 (3): 1–12. https://doi.org/10.1103/PhysRevE.78.036317.

Chung, Bong Geun, Lisa A. Flanagan, Seog Woo Rhee, Philip H. Schwartz, Abraham P. Lee, Edwin S. Monuki, and Noo Li Jeon. 2005. “Human Neural Stem Cell Growth and Differentiation in a Gradient-Generating Microfluidic Device.” *Lab on a Chip* 5 (4): 401–6. https://doi.org/10.1039/b417651k.

Clausell-Tormos, Jenifer, Diana Lieber, Jean Christophe Baret, Abdeslam El-Harrak, Oliver J. Miller, Lucas Frenz, Joshua Blouwolff, et al. 2008. “Droplet-Based Microfluidic Platforms for the Encapsulation and Screening of Mammalian Cells and Multicellular Organisms.” *Chemistry and Biology* 15 (5): 427–37. https://doi.org/10.1016/j.chembiol.2008.04.004.

Collins, David J., Adrian Neild, Andrew deMello, Ai-Qun Liu, and Ye Ai. 2015. “The Poisson Distribution and beyond: Methods for Microfluidic Droplet Production and Single Cell Encapsulation.” *Lab Chip*, 3439–59. https://doi.org/10.1039/C5LC00614G.

Coopersmith, Kaitlin, Hyunjoo Han, and Mathew M. Maye. 2015. “Stepwise Assembly and Characterization of DNA Linked Two-Color Quantum Dot Clusters.” *Langmuir* 31 (27): 7463–71. https://doi.org/10.1021/acs.langmuir.5b01130.

Courtney, Matthew, Xiaoming Chen, Sarah Chan, Tarek Mohamed, Praveen P. N. Rao, and Carolyn L. Ren. 2016. “A Droplet Microfluidic System with On-Demand Trapping and Releasing of Droplet for Drug Screening Applications.” *Analytical Chemistry*, acs.analchem.6b04039. https://doi.org/10.1021/acs.analchem.6b04039.

Courtois, Fabienne, Luis F. Olguin, Graeme Whyte, Daniel Bratton, Wilhelm T.S. Huck, Chris Abell, and Florian Hollfelder. 2008. “An Integrated Device for Monitoring Time-Dependent in Vitro Expression from Single Genes in Picolitre Droplets.” *ChemBioChem* 9 (3): 439–46. https://doi.org/10.1002/cbic.200700536.

Cramer, Carsten, Peter Fischer, and Erich J. Windhab. 2004. “Drop Formation in a Co-Flowing Ambient Fluid.” *Chemical Engineering Science* 59 (15): 3045–58. https://doi.org/10.1016/j.ces.2004.04.006.

Cristobal, Galder, Jean Philippe Benoit, Mathieu Joanicot, and Armand Ajdari. 2006. “Microfluidic Bypass for Efficient Passive Regulation of Droplet Traffic at a Junction.” *Applied Physics Letters* 89 (3): 3–5. https://doi.org/10.1063/1.2221929.

Crivat, Georgeta, S. M D Silva, Darwin R. Reyes, Laurie E. Locascio, Michael Gaitan, Nitsa Rosenweig, and Zeev Rosenzweig. 2010. “Quantum Dot FRET-Based Probes in Thin Films Grown in Microfluidic Channels.” *Journal of the American Chemical Society* 132 (5): 1460–61. https://doi.org/10.1021/ja908784b.

Cubaud, Thomas, and Thomas G. Mason. 2008. “Capillary Threads and Viscous Droplets in Square Microchannels.” *Physics of Fluids* 20 (5): 1–11. https://doi.org/10.1063/1.2911716.

Cubaud, Thomas, and Sara Notaro. 2014. “Regimes of Miscible Fluid Thread Formation in Microfluidic Focusing Sections.” *Physics of Fluids* 26 (12). https://doi.org/10.1063/1.4903534.

Cutler, Joshua I., Evelyn Auyeung, and Chad A. Mirkin. 2012. “Spherical Nucleic Acids.” *Journal of the American Chemical Society* 134 (3): 1376–91. https://doi.org/10.1021/ja209351u.

Dangla, R., S. C. Kayi, and C. N. Baroud. 2013. “Droplet Microfluidics Driven by Gradients of Confinement.” *Proceedings of the National Academy of Sciences* 110 (3): 853–58. https://doi.org/10.1073/pnas.1209186110.

Dangla, Rémi, Etienne Fradet, Yonatan Lopez, and Charles N. Baroud. 2013. “The Physical Mechanisms of Step Emulsification.” *Journal of Physics D: Applied Physics* 46 (11). https://doi.org/10.1088/0022-3727/46/11/114003.

Dangla, Rémi, Franois Gallaire, and Charles N. Baroud. 2010. “Microchannel Deformations Due to Solvent-Induced PDMS Swelling.” *Lab on a Chip* 10 (21): 2972–78. https://doi.org/10.1039/c003504a.

Darmakkolla, Srikar Rao, Hoang Tran, Atul Gupta, and Shankar B. Rananavare. 2016. “A Method to Derivatize Surface Silanol Groups to Si-Alkyl Groups in Carbon-Doped Silicon Oxides.” *RSC Advances* 6 (95): 93219–30. https://doi.org/10.1039/c6ra20355h.

Das, Pradip, Abootaleb Sedighi, and Ulrich J. Krull. 2018. “Cancer Biomarker Determination by Resonance Energy Transfer Using Functional Fluorescent Nanoprobes.” *Analytica Chimica Acta*

1041: 1–24. https://doi.org/10.1016/j.aca.2018.07.060.

DeMello, Andrew J. 2006. “Control and Detection of Chemical Reactions in Microfluidic Systems.” *Nature* 442 (7101): 394–402. https://doi.org/10.1038/nature05062.

Derzsi, Ladislav, Marta Kasprzyk, Jan Philip Plog, and Piotr Garstecki. 2013. “Flow Focusing with Viscoelastic Liquids.” *Physics of Fluids* 25 (9). https://doi.org/10.1063/1.4817995.

Dong, Libing, Dong-Wei Chen, Shuang-Jiang Liu, and Wenbin Du. 2016. “Automated Chemotactic Sorting and Single-Cell Cultivation of Microbes Using Droplet Microfluidics.” *Scientific Reports* 6 (April): 24192. https://doi.org/10.1038/srep24192.

Doonan, Steven R, and Ryan C. Bailey. 2017. “The K-Channel: A Multi-Functional Architecture for Dynamically Re-Configurable Sample Processing in Droplet Microfluidics.” *Analytical Chemistry*, acs.analchem.6b05041. https://doi.org/10.1021/acs.analchem.6b05041.

Dressler, Oliver J., Xavier Casadevall i Solvas, and Andrew J. DeMello. 2017. “Chemical and Biological Dynamics Using Droplet-Based Microfluidics.” *Annual Review of Analytical Chemistry* 10 (1): 1–24. https://doi.org/10.1146/annurev-anchem-061516-045219.

Dreyfus, Remi, Patrick Tabeling, and Herve Willaime. 2003. “Ordered and Disordered Patterns in Two-Phase Flows in Microchannels.” *Physical Review Letters* 90 (14): 144505. https://doi.org/10.1103/PhysRevLett.90.144505.

Duraiswamy, Suhanya, and Saif A. Khan. 2009. “Droplet-Based Microfluidic Synthesis of Anisotropic Metal Nanocrystals.” *Small* 5 (24): 2828–34. https://doi.org/10.1002/smll.200901453.

Edd, Jon F, Dino Di Carlo, Katherine J Humphry, Sarah Köster, Daniel Irimia, David a Weitz, and Mehmet Toner. 2008. “Controlled Encapsulation of Single-Cells into Monodisperse Picolitre Drops.” *Lab on a Chip* 8 (8): 1262–64. https://doi.org/10.1039/b805456h.

Edel, Joshua B., Robin Fortt, John C. DeMello, and Andrew J. DeMello. 2002. “Microfluidic Routes to the Controlled Production of Nanoparticles.” *Chemical Communications* 2 (10): 1136–37. https://doi.org/10.1039/b202998g.

El-Ali, Jamil, Peter K Sorger, and Klavs F Jensen. 2006. “Cells on Chips.” *Nature* 442 (7101): 403–11. https://doi.org/10.1038/nature05063.

Faustino, Vera, Susana O. Catarino, Rui Lima, and Graça Minas. 2016. “Biomedical Microfluidic Devices by Using Low-Cost Fabrication Techniques: A Review.” *Journal of Biomechanics* 49 (11): 2280–

92. https://doi.org/10.1016/j.jbiomech.2015.11.031.

Feng, Qiang, Jiashu Sun, and Xingyu Jiang. 2016. “Microfluidics-Mediated Assembly of Functional Nanoparticles for Cancer-Related Pharmaceutical Applications.” *Nanoscale* 8 (25): 12430–43. https://doi.org/10.1039/C5NR07964K.

Fernandes, Tiago G., Maria Margarida Diogo, Douglas S. Clark, Jonathan S. Dordick, and Joaquim M.S. Cabral. 2009. “High-Throughput Cellular Microarray Platforms: Applications in Drug Discovery, Toxicology and Stem Cell Research.” *Trends in Biotechnology* 27 (6): 342–49. https://doi.org/10.1016/j.tibtech.2009.02.009.

Fidalgo, Luis M., Chris Abell, and Wilhelm T.S. Huck. 2007. “Surface-Induced Droplet Fusion in Microfluidic Devices.” *Lab on a Chip* 7 (8): 984–86. https://doi.org/10.1039/b708091c.

Frenz, Lucas, Kerstin Blank, Eric Brouzes, and Andrew D Griffiths. 2009. “Reliable Microfluidic On-Chip Incubation of Droplets in Delay-Lines.” *Lab on a Chip* 9 (10): 1344–48. https://doi.org/10.1039/b816049j.

Frenz, Lucas, Abdeslam El Harrak, Matthias Pauly, Sylvie Bégin-Colin, Andrew D. Griffiths, and Jean Christophe Baret. 2008. “Droplet-Based Microreactors for the Synthesis of Magnetic Iron Oxide Nanoparticles.” *Angewandte Chemie - International Edition* 47 (36): 6817–20. https://doi.org/10.1002/anie.200801360.

Fu, Taotao, Yining Wu, Youguang Ma, and Huai Z. Li. 2012. “Droplet Formation and Breakup Dynamics in Microfluidic Flow-Focusing Devices: From Dripping to Jetting.” *Chemical Engineering Science* 84: 207–17. https://doi.org/10.1016/j.ces.2012.08.039.

Gai, Ya, Chia Min Leong, Wei Cai, and Sindy K.Y. Tang. 2016. “Spatiotemporal Periodicity of Dislocation Dynamics in a Two-Dimensional Microfluidic Crystal Flowing in a Tapered Channel.” *Proceedings of the National Academy of Sciences of the United States of America* 113 (43): 12082–87. https://doi.org/10.1073/pnas.1606601113.

Ganan-Calvo, A. M., J. M. Montanero, L. Martin-Banderas, and M. Flores-Mosquera. 2013. “Building Functional Materials for Health Care and Pharmacy from Microfluidic Principles and Flow Focusing.” *Advanced Drug Delivery Reviews* 65 (11–12): 1447–69. https://doi.org/10.1016/j.addr.2013.08.003.

Garstecki, Piotr, Michael J Fuerstman, Howard a Stone, and George M Whitesides. 2006. “Formation of

Droplets and Bubbles in a Microfluidic T-Junction-Scaling and Mechanism of Break-Up." *Lab on a Chip* 6 (3): 437–46. https://doi.org/10.1039/b510841a.

Garstecki, Piotr, Howard A Stone, and George M Whitesides. 2005. "Mechanism for Flow-Rate Controlled Breakup in Confined Geometries : A Route to Monodisperse Emulsions" 164501 (April): 1–4. https://doi.org/10.1103/PhysRevLett.94.164501.

Gawad, Charles, Winston Koh, and Stephen R. Quake. 2016. "Single-Cell Genome Sequencing: Current State of the Science." *Nature Reviews Genetics* 17 (3): 175–88. https://doi.org/10.1038/nrg.2015.16.

Gershenfeld, Neil, and Manu Prakash. 2007. "Microfluidic Bubble Logic." *Science* 315 (February): 832–35. https://doi.org/DOI 10.1126/science.1136907.

Giri, Supratim, Edward A. Sykes, Travis L. Jennings, and Warren C W Chan. 2011. "Rapid Screening of Genetic Biomarkers of Infectious Agents Using Quantum Dot Barcodes." *ACS Nano* 5 (3): 1580–87. https://doi.org/10.1021/nn102873w.

Giuffrida, Maria Chiara, Giovanni Cigliana, and Giuseppe Spoto. 2018. "Ultrasensitive Detection of Lysozyme in Droplet-Based Microfluidic Devices." *Biosensors and Bioelectronics* 104 (December 2017): 8–14. https://doi.org/10.1016/j.bios.2017.12.042.

Glawdel, Tomasz, Caglar Elbuken, and Carolyn Ren. 2011. "Passive Droplet Trafficking at Microfluidic Junctions under Geometric and Flow Asymmetries." *Lab on a Chip* 11 (22): 3774–84. https://doi.org/10.1039/c1lc20628a.

Glawdel, Tomasz, Caglar Elbuken, and Carolyn L Ren. 2012. "Droplet Formation in Microfluidic T-Junction Generators Operating in the Transitional Regime . II . Modeling." *Physical Review E - Statistical, Nonlinear, and Soft Matter Physics* 016323: 1–12. https://doi.org/10.1103/PhysRevE.85.016323.

Glawdel, Tomasz, and Carolyn L. Ren. 2012a. "Droplet Formation in Microfluidic T-Junction Generators Operating in the Transitional Regime. I. Experimental Observation." *Physical Review E - Statistical, Nonlinear, and Soft Matter Physics* 85 (2): 016322. https://doi.org/10.1103/PhysRevE.86.026308.

———. 2012b. "Droplet Formation in Microfluidic T-Junction Generators Operating in the Transitional Regime. III. Dynamic Surfactant Effects." *Physical Review E - Statistical, Nonlinear, and Soft Matter Physics* 86 (2): 1–12. https://doi.org/10.1103/PhysRevE.86.026308.

———. 2012c. "Global Network Design for Robust Operation of Microfluidic Droplet Generators with

Pressure-Driven Flow." *Microfluidics and Nanofluidics* 13 (3): 469–80. https://doi.org/10.1007/s10404-012-0982-y.

Godakhindi, Varsha Sanjay, Peiyuan Kang, Maud Serre, Naga Aravind Revuru, Jesse Minghao Zou, Michael R. Roner, Ruth Levitz, Jeffrey S. Kahn, Jaona Randrianalisoa, and Zhenpeng Qin. 2017. "Tuning the Gold Nanoparticle Colorimetric Assay by Nanoparticle Size, Concentration, and Size Combinations for Oligonucleotide Detection." *ACS Sensors* 2 (11): 1627–36. https://doi.org/10.1021/acssensors.7b00482.

Goddard, Julie M., and David Erickson. 2009. "Bioconjugation Techniques for Microfluidic Biosensors." *Analytical and Bioanalytical Chemistry* 394 (2): 469–79. https://doi.org/10.1007/s00216-009-2731-y.

Gruner, Philipp, Birte Riechers, Laura Andreina Chacòn Orellana, Quentin Brosseau, Florine Maes, Thomas Beneyton, Deniz Pekin, and Jean Christophe Baret. 2015. "Stabilisers for Water-in-Fluorinated-Oil Dispersions: Key Properties for Microfluidic Applications." *Current Opinion in Colloid and Interface Science* 20 (3): 183–91. https://doi.org/10.1016/j.cocis.2015.07.005.

Gu, Hao, Michel H G Duits, and Frieder Mugele. 2011. "Droplets Formation and Merging in Two-Phase Flow Microfluidics." *International Journal of Molecular Sciences* 12 (4): 2572–97. https://doi.org/10.3390/ijms12042572.

Guillot, Pierre, Armand Ajdari, Julie Goyon, Mathieu Joanicot, and Annie Colin. 2009. "Droplets and Jets in Microfluidic Devices." *Comptes Rendus - Chimie* 12 (1–2): 247–57. https://doi.org/10.1016/j.crci.2008.07.005.

Guillot, Pierre, and Annie Colin. 2005. "Stability of Parallel Flows in a Microchannel after a T Junction." *Physical Review E - Statistical, Nonlinear, and Soft Matter Physics* 72 (December): 1–4. https://doi.org/10.1103/PhysRevE.72.066301.

Günther, Axel, and Klavs F Jensen. 2006. "Multiphase Microfluidics: From Flow Characteristics to Chemical and Materials Synthesis." *Lab Chip* 6 (12): 1487–1503. https://doi.org/10.1039/B609851G.

Gupta, Amit, and Ranganathan Kumar. 2010. "Effect of Geometry on Droplet Formation in the Squeezing Regime in a Microfluidic T-Junction." *Microfluidics and Nanofluidics* 8: 799–812. https://doi.org/10.1007/s10404-009-0513-7.

Gupta, Amit, S. M Sohel Murshed, and Ranganathan Kumar. 2009. “Droplet Formation and Stability of Flows in a Microfluidic T-Junction.” *Applied Physics Letters* 94 (16): 1–4. https://doi.org/10.1063/1.3116089.

Gupta, Amit, S M Sohel Murshed, Ranganathan Kumar, Amit Gupta, S M Sohel Murshed, and Ranganathan Kumar. 2011. “Droplet Formation and Stability of Flows in a Microfluidic T-Junction Droplet Formation and Stability of Flows in a Microfluidic T-Junction.” *Applied Physics Letters* 164107 (2009): 1–4. https://doi.org/10.1063/1.3116089.

Hadwen, B., G. R. Broder, D. Morganti, A. Jacobs, C. Brown, J. R. Hector, Y. Kubota, and H. Morgan. 2012. “Programmable Large Area Digital Microfluidic Array with Integrated Droplet Sensing for Bioassays.” *Lab on a Chip* 12 (18): 3305–13. https://doi.org/10.1039/c2lc40273d.

Han, Wenbo, Xueye Chen, Zhongli Wu, and Yue Zheng. 2019. “Three-Dimensional Numerical Simulation of Droplet Formation in a Microfluidic Flow-Focusing Device.” *Journal of the Brazilian Society of Mechanical Sciences and Engineering* 41 (6): 1–10. https://doi.org/10.1007/s40430-019-1767-y.

Han, Yi, M. Omair Noor, Abootaleb Sedighi, Uvaraj Uddayasankar, Samer Doughan, and Ulrich J. Krull. 2017. “Inorganic Nanoparticles as Donors in Resonance Energy Transfer for Solid-Phase Bioassays and Biosensors.” *Langmuir*, acs.langmuir.7b01483. https://doi.org/10.1021/acs.langmuir.7b01483.

Hashimoto, Michinao, Sergey S. Shevkoplyas, Beata Zasońska, Tomasz Szymborski, Piotr Garstecki, and George M. Whitesides. 2008. “Formation of Bubbles and Droplets in Parallel, Coupled Flow-Focusing Geometries.” *Small* 4 (10): 1795–1805. https://doi.org/10.1002/smll.200800591.

Hatch, Andrew C., Apurva Patel, N. Reginald Beer, and Abraham P. Lee. 2013. “Passive Droplet Sorting Using Viscoelastic Flow Focusing.” *Lab on a Chip* 13 (7): 1308. https://doi.org/10.1039/c2lc41160a.

He, Xuewen, Zhi Li, Muzi Chen, and Nan Ma. 2014. “DNA-Programmed Dynamic Assembly of Quantum Dots for Molecular Computation.” *Angewandte Chemie - International Edition* 53 (52): 14447–50. https://doi.org/10.1002/anie.201408479.

Heath, James R., Antoni Ribas, and Paul S. Mischel. 2016a. “Single-Cell Analysis Tools for Drug Discovery and Development.” *Nature Reviews Drug Discovery* 15 (3): 204–16. https://doi.org/10.1038/nrd.2015.16.

———. 2016b. “Single-Cell Analysis Tools for Drug Discovery and Development.” *Nature Reviews*

Drug Discovery 15 (3): 204–16. https://doi.org/10.1038/nrd.2015.16.

Hébert, Marie, Matthew Courtney, and Carolyn L. Ren. 2019. "Semi-Automated on-Demand Control of Individual Droplets with a Sample Application to a Drug Screening Assay." *Lab on a Chip* 19 (8): 1490–1501. https://doi.org/10.1039/c9lc00128j.

Hejazian, Majid, Weihua Li, and Nam-Trung Nguyen. 2015. "Lab on a Chip for Continuous-Flow Magnetic Cell Separation." *Lab Chip* 15 (4): 959–70. https://doi.org/10.1039/C4LC01422G.

Herberts, Carla A., Marcel S.G. Kwa, and Harm P.H. Hermsen. 2011. "Risk Factors in the Development of Stem Cell Therapy." *Journal of Translational Medicine* 9 (1): 29. https://doi.org/10.1186/1479-5876-9-29.

Hindson, Benjamin J, Kevin D Ness, Donald A Masquelier, Phillip Belgrader, Nicholas J Heredia, Anthony J Makarewicz, Isaac J Bright, et al. 2011. "High-Throughput Droplet Digital PCR System for Absolute Quantitation of DNA Copy Number," 8604–10.

Hoeve, W. Van, B. Dollet, J. M. Gordillo, M. Versluis, L. Van Wijngaarden, and D. Lohse. 2011. "Bubble Size Prediction in Co-Flowing Streams." *Epl* 94 (6). https://doi.org/10.1209/0295-5075/94/64001.

Holtze, Christian, Sebastian A. Weisse, and Marcel Vranceanu. 2017. "Commercial Value and Challenges of Drop-Based Microfluidic Screening Platforms-An Opinion." *Micromachines* 8 (6). https://doi.org/10.3390/mi8060193.

Hong, Jongin, Minsuk Choi, Joshua B. Edel, and Andrew J. Demello. 2010. "Passive Self-Synchronized Two-Droplet Generation." *Lab on a Chip* 10 (20): 2702–3. https://doi.org/10.1039/c005136e.

Hood, Leroy, James R. Heath, Michael E. Phelps, and Biaoyang Lin. 2004. "Systems Biology and New Technologies Enable Predictive and Preventative Medicine." *Science* 306 (5696): 640–43. https://doi.org/10.1126/science.1104635.

Hsieh, Albert Tsung Hsi, Patrick Jen Hao Pan, and Abraham Phillip Lee. 2009. "Rapid Label-Free DNA Analysis in Picoliter Microfluidic Droplets Using FRET Probes." *Microfluidics and Nanofluidics* 6 (3): 391–401. https://doi.org/10.1007/s10404-009-0406-9.

Huebner, Ansgar, Dan Bratton, Graeme Whyte, Min Yang, Andrew J. Demello, Chris Abell, and Florian Hollfelder. 2009. "Static Microdroplet Arrays: A Microfluidic Device for Droplet Trapping, Incubation and Release for Enzymatic and Cell-Based Assays." *Lab on a Chip* 9 (5): 692–98.

https://doi.org/10.1039/b813709a.

Hung, Lung-Hsin, Kyung M. Choi, Wei-Yu Tseng, Yung-Chieh Tan, Kenneth J. Shea, and Abraham Phillip Lee. 2006. “Alternating Droplet Generation and Controlled Dynamic Droplet Fusion in Microfluidic Device for CdS Nanoparticle Synthesis.” *Lab on a Chip* 6 (2): 174. https://doi.org/10.1039/b513908b.

Hunt, Thomas P., David Issadore, and R. M. Westervelt. 2007. “Integrated Circuit/Microfluidic Chip to Programmably Trap and Move Cells and Droplets with Dielectrophoresis.” *Lab on a Chip* 8 (1): 81–87. https://doi.org/10.1039/b710928h.

Huo, Fengwei, Abigail K R Lytton-Jean, and Chad A. Mirkin. 2006. “Asymmetric Functionalization of Nanoparticles Based on Thermally Addressable DNA Interconnects.” *Advanced Materials* 18 (17): 2304–6. https://doi.org/10.1002/adma.200601178.

Inoue, Asuka, Hiroshi Sugimoto, Hidenobu Yaku, and Minoru Fujii. 2016. “DNA Assembly of Silicon Quantum Dots/Gold Nanoparticle Nanocomposites.” *RSC Adv.* 6 (68): 63933–39. https://doi.org/10.1039/C6RA13565J.

Ishikawa, Takuji, Hiroki Fujiwara, Noriaki Matsuki, Takefumi Yoshimoto, Yohsuke Imai, Hironori Ueno, and Takami Yamaguchi. 2011. “Asymmetry of Blood Flow and Cancer Cell Adhesion in a Microchannel with Symmetric Bifurcation and Confluence.” *Biomedical Microdevices* 13 (1): 159–67. https://doi.org/10.1007/s10544-010-9481-7.

J K Nunes; S S H Tsai; J Wan; and H A Stone. 2009. “Dripping and Jetting in Microfluidic Multiphase Flows Applied to Particle and Fiber Synthesis.” *J Phys D Appl Phys.* 6 (11): 247–53. https://doi.org/10.1111/j.1743-6109.2008.01122.x.Endothelial.

Jacobson, Stephen C., Timothy E. McKnight, and J. Michael Ramsey. 1999. “Microfluidic Devices for Electrokinetically Driven Parallel and Serial Mixing.” *Analytical Chemistry* 71 (20): 4455–59. https://doi.org/10.1021/ac990576a.

Jayaraj, S., S.M. Kang, and Y.K. Suh. 2007. “A Review on the Analysis and Experiment of Fluid Flow and Mixing in Micro-Channels.” *Journal of Mechanical Science and Technology* 21 (3): 536–48.

Jin, B-J, Y W Kim, Y Lee, and J Y Yoo. 2010. “Droplet Merging in a Straight Microchannel Using Droplet Size or Viscosity Difference.” *Journal of Micromechanics and Microengineering* 20 (3): 035003. https://doi.org/10.1088/0960-1317/20/3/035003.

Johansson, Linda, Fredrik Nikolajeff, Stefan Johansson, and Sara Thorslund. 2009. “On-Chip Fluorescence-Activated Cell Sorting by an Integrated Miniaturized Ultrasonic Transducer.” *Analytical Chemistry* 81 (13): 5188–96. https://doi.org/10.1021/ac802681r.

Johnston, I. D., D. K. McCluskey, C. K.L. Tan, and M. C. Tracey. 2014. “Mechanical Characterization of Bulk Sylgard 184 for Microfluidics and Microengineering.” *Journal of Micromechanics and Microengineering* 24 (3). https://doi.org/10.1088/0960-1317/24/3/035017.

Jose, Bibin M., and Thomas Cubaud. 2012. “Droplet Arrangement and Coalescence in Diverging/Converging Microchannels.” *Microfluidics and Nanofluidics* 12 (5): 687–96. https://doi.org/10.1007/s10404-011-0909-z.

Jullien, M. C., M. J. Tsang Mui Ching, C. Cohen, L. Menetrier, and P. Tabeling. 2009. “Droplet Breakup in Microfluidic T-Junctions at Small Capillary Numbers.” *Physics of Fluids* 21 (7): 1–7. https://doi.org/10.1063/1.3170983.

Jung, Jin Ho, Ghulam Destgeer, Byunghang Ha, Jinsoo Park, and Hyung Jin Sung. 2016. “On-Demand Droplet Splitting Using Surface Acoustic Waves.” *Lab Chip* 77: 977–1026. https://doi.org/10.1039/C6LC00648E.

Jung, Jin Ho, Kyung Heon Lee, Ghulam Destgeer, Kang Soo Lee, Hyunjun Cho, Byung Hang Ha, and Hyung Jin Sung. 2015. “In Situ Seriate Droplet Coalescence under an Optical Force.” *Microfluidics and Nanofluidics* 18 (5–6): 1247–54. https://doi.org/10.1007/s10404-014-1522-8.

Kalisky, Tomer, and Stephen R Quake. 2011. “Single-Cell Genomics.” *Nature Methods*. https://doi.org/10.1038/nmeth0411-311.

Kaminski, T. S., and P. Garstecki. 2017. “Controlled Droplet Microfluidic Systems for Multistep Chemical and Biological Assays.” *Chemical Society Reviews* 46 (20): 6210–26. https://doi.org/10.1039/c5cs00717h.

Kaminski, Tomasz S., Ott Scheler, and Piotr Garstecki. 2016. “Droplet Microfluidics for Microbiology: Techniques, Applications and Challenges.” *Lab Chip* 16 (12). https://doi.org/10.1039/C6LC00367B.

Kang, Dong Ku, M. Monsur Ali, Kaixiang Zhang, Egest J. Pone, and Weian Zhao. 2014. “Droplet Microfluidics for Single-Molecule and Single-Cell Analysis in Cancer Research, Diagnosis and Therapy.” *TrAC - Trends in Analytical Chemistry* 58: 145–53. https://doi.org/10.1016/j.trac.2014.03.006.

Kang, Edward, Yoon Young Choi, Yesl Jun, Bong Geun Chung, and Sang Hoon Lee. 2010. "Development of a Multi-Layer Microfluidic Array Chip to Culture and Replate Uniform-Sized Embryoid Bodies without Manual Cell Retrieval." *Lab on a Chip* 10 (20): 2651–54. https://doi.org/10.1039/c0lc00005a.

Kapanidis, Achillefs, Devdoot Majumdar, Mike Heilemann, Eyal Nir, and Shimon Weiss. 2015. "Alternating Laser Excitation for Solution-Based Single-Molecule FRET." *Cold Spring Harbor Protocols* 2015 (11): 979–87. https://doi.org/10.1101/pdb.top086405.

Kemna, Evelien W. M., Rogier M. Schoeman, Floor Wolbers, Istvan Vermes, David a. Weitz, and Albert van den Berg. 2012. "High-Yield Cell Ordering and Deterministic Cell-in-Droplet Encapsulation Using Dean Flow in a Curved Microchannel." *Lab on a Chip* 12 (16): 2881. https://doi.org/10.1039/c2lc00013j.

Khater, Asmaa, Mehdi Mohammadi, Abdulmajeed Mohamad, and Amir Sanati Nezhad. 2019. "Dynamics of Temperature-Actuated Droplets within Microfluidics." *Scientific Reports* 9 (1): 1–11. https://doi.org/10.1038/s41598-019-40069-9.

Khor, Jian Wei, Neal Jean, Eric S. Luxenberg, Stefano Ermon, and Sindy K.Y. Tang. 2019. "Using Machine Learning to Discover Shape Descriptors for Predicting Emulsion Stability in a Microfluidic Channel." *Soft Matter* 15 (6): 1361–72. https://doi.org/10.1039/c8sm02054j.

Kim, Choong, Kang Sun Lee, Jae Hoon Bang, Young Eyn Kim, Min Cheol Kim, Kwang Wook Oh, Soo Hyun Lee, and Ji Yoon Kang. 2011. "3-Dimensional Cell Culture for on-Chip Differentiation of Stem Cells in Embryoid Body." *Lab on a Chip* 11 (5): 874–82. https://doi.org/10.1039/c0lc00516a.

Kim, Haejune, Dawei Luo, Darren Link, David A. Weitz, Manuel Marquez, and Zhengdong Cheng. 2007. "Controlled Production of Emulsion Drops Using an Electric Field in a Flow-Focusing Microfluidic Device." *Applied Physics Letters* 91 (13): 1–3. https://doi.org/10.1063/1.2790785.

Kim, Jungkyu, Michael Junkin, Deok Ho Kim, Seunglee Kwon, Young Shik Shin, Pak Kin Wong, and Bruce K. Gale. 2009. "Applications, Techniques, and Microfluidic Interfacing for Nanoscale Biosensing." *Microfluidics and Nanofluidics* 7 (2): 149–67. https://doi.org/10.1007/s10404-009-0431-8.

Kim, Pilnam, Keon Woo Kwon, Min Cheol Park, Sung Hoon Lee, and Sun Min Kim. 2008. "Soft Lithography for Microfluidics : A Review." *Biochip Journal* 2 (1): 1–11. http://s-

space.snu.ac.kr/handle/10371/9558.

Kinoshita, Haruyuki, Shohei Kaneda, Teruo Fujii, and Marie Oshima. 2007. “Three-Dimensional Measurement and Visualization of Internal Flow of a Moving Droplet Using Confocal Micro-PIV.” *Lab on a Chip* 7 (3): 338–46. https://doi.org/10.1039/b617391h.

Klein, Allon M., Linas Mazutis, Ilke Akartuna, Naren Tallapragada, Adrian Veres, Victor Li, Leonid Peshkin, David A. Weitz, and Marc W. Kirschner. 2015. “Droplet Barcoding for Single-Cell Transcriptomics Applied to Embryonic Stem Cells.” *Cell* 161 (5): 1187–1201. https://doi.org/10.1016/j.cell.2015.04.044.

Köhler, J. M., Th Henkel, A. Grodrian, Th Kirner, M. Roth, K. Martin, and J. Metze. 2004. “Digital Reaction Technology by Micro Segmented Flow - Components, Concepts and Applications.” *Chemical Engineering Journal* 101 (1–3): 201–16. https://doi.org/10.1016/j.cej.2003.11.025.

Korczyk, Piotr M., Ladislav Derzsi, Sławomir Jakieła, and Piotr Garstecki. 2013. “Microfluidic Traps for Hard-Wired Operations on Droplets.” *Lab on a Chip* 13 (20): 4096–4102. https://doi.org/10.1039/c3lc50347j.

Köster, Sarah, Francesco E. Angilè, Honey Duan, Jeremy J. Agresti, Anton Wintner, Christian Schmitz, Amy C. Rowat, et al. 2008a. “Drop-Based Microfluidic Devices for Encapsulation of Single Cells.” *Lab on a Chip* 8 (7): 1110–15. https://doi.org/10.1039/b802941e.

Köster, Sarah, Francesco E Angilè, Honey Duan, Jeremy J Agresti, Anton Wintner, Christian Schmitz, Amy C Rowat, et al. 2008b. “Drop-Based Microfluidic Devices for Encapsulation of Single Cells.” *Lab on a Chip* 8 (7): 1110–15. https://doi.org/10.1039/b802941e.

Kovalchuk, Nina M., Masanobu Sagisaka, Kasparas Steponavicius, Daniele Vigolo, and Mark J.H. Simmons. 2019. “Drop Formation in Microfluidic Cross-Junction: Jetting to Dripping to Jetting Transition.” *Submitted* 23 (8): 1–14. https://doi.org/10.1007/s10404-019-2269-z.

Labrot, Vincent, Michael Schindler, Pierre Guillot, Annie Collin, and Mathieu Joanicot. 2009. “Extracting the Hydrodynamic Resistance of Droplets from Their Behavior in Microchannel Networks.” *Biomicrofluidics* 3 (1): 1–16. https://doi.org/10.1063/1.3109686.

Lagus, Todd P., and Jon F. Edd. 2013a. “High-Throughput Co-Encapsulation of Self-Ordered Cell Trains: Cell Pair Interactions in Microdroplets.” *RSC Advances* 3 (43): 20512. https://doi.org/10.1039/c3ra43624a.

Lagus, Todd P, and Jon F Edd. 2013b. “A Review of the Theory, Methods and Recent Applications of High-Throughput Single-Cell Droplet Microfluidics.” *Journal of Physics D: Applied Physics* 46 (11): 114005. https://doi.org/10.1088/0022-3727/46/11/114005.

Lagus, Todd P, Jon F Edd, Ryan T Davies, Donghwan Kim, Jaesung Park, Martin Urbanski, Catherine G Reyes, et al. 2012. “Droplet Based Microfluidics.” *Reports on Progress in Physics* 75: 016601. https://doi.org/10.1088/0034-4885/75/1/016601.

Lai, Ann, Nicolas Bremond, and Howard A. Stone. 2009. “Separation-Driven Coalescence of Droplets: An Analytical Criterion for the Approach to Contact.” *Journal of Fluid Mechanics* 632: 97–107. https://doi.org/10.1017/S0022112009007320.

Lalander, Cecilia H., Yuanhui Zheng, Scott Dhuey, Stefano Cabrini, and Udo Bach. 2010. “DNA-Directed Self-Assembly of Gold Nanoparticles onto Nanopatterned Surfaces: Controlled Placement of Individual Nanoparticles into Regular Arrays.” *ACS Nano* 4 (10): 6153–61. https://doi.org/10.1021/nn101431k.

Lan, Freeman, Benjamin Demaree, Noorsher Ahmed, and Adam R. Abate. 2017. “Single-Cell Genome Sequencing at Ultra-High-Throughput with Microfluidic Droplet Barcoding.” *Nature Biotechnology* 35 (7): 640–46. https://doi.org/10.1038/nbt.3880.

Laval, Philippe, Nicolas Lisai, Jean-Baptiste Salmon, Mathieu Joanicot, G. H. W. Sanders, A. Manz, J. R. Luft, et al. 2007. “A Microfluidic Device Based on Droplet Storage for Screening Solubility Diagrams.” *Lab on a Chip* 7 (7): 829. https://doi.org/10.1039/b700799j.

Lecault, Véronique, Adam K. White, Anupam Singhal, and Carl L. Hansen. 2012. “Microfluidic Single Cell Analysis: From Promise to Practice.” *Current Opinion in Chemical Biology* 16 (3–4): 381–90. https://doi.org/10.1016/j.cbpa.2012.03.022.

Lee, D.-H., and J.-K. Park. 2010. “Controllable Droplet Synchronization Module for Temporal Control of Microdroplets.” *14th International Conference on Miniaturized Systems for Chemistry and Life Sciences 2010, MicroTAS 2010* 2 (October): 1097–99. http://www.scopus.com/inward/record.url?eid=2-s2.0-84884409990&partnerID=40&md5=569db352448338ada7ba0257d193d98e.

Lee, Wingki, Lynn M. Walker, and Shelley L. Anna. 2009. “Role of Geometry and Fluid Properties in Droplet and Thread Formation Processes in Planar Flow Focusing.” *Physics of Fluids* 21 (3).

https://doi.org/10.1063/1.3081407.

Leeper, Nicholas, Arwen Hunter, and John Cooke. 2010. “Stem Cell Therapy for Vasuclar Regeneration: Adult, Embryonic, and Induced Pluripoten Stem Cells.” *Circulation* 122 (5): 517–26. https://doi.org/10.1038/jid.2014.371.

Leshansky, A. M., and Pismen L. M. 2009. “Breakup of Drops in a Microfluidic T Junction.” *Physics of Fluids* 21: 023303. https://doi.org/10.1103/PhysRevLett.108.264502.

Li, Huajun, Yining Wu, Xiaoda Wang, Chunying Zhu, Taotao Fu, and Youguang Ma. 2016. “Magnetofluidic Control of the Breakup of Ferrofluid Droplets in a Microfluidic Y-Junction.” *RSC Advances* 6: 778–85. https://doi.org/10.1039/C5RA21802K.

Li, Xiao-bin, Feng-chen Li, Juan-cheng Yang, and Haruyuki Kinoshita. 2012. “Study on the Mechanism of Droplet Formation in T-Junction Microchannel.” *Chemical Engineering Science* 69 (1): 340–51. https://doi.org/10.1016/j.ces.2011.10.048.

Liau, Albert, Rohit Kamik, Arun Majumdar, and Jamie H.Doudna Cate. 2005. “Mixing Crowded Biological Solutions in Milliseconds.” *Analytical Chemistry* 77 (23): 7618–25. https://doi.org/10.1021/ac050827h.

Lindken, Ralph, Massimiliano Rossi, Sebastian Große, and Jerry Westerweel. 2009. “Micro-Particle Image Velocimetry (PIV): Recent Developments, Applications, and Guidelines.” *Lab on a Chip* 9 (17): 2551–67. https://doi.org/10.1039/b906558j.

Link, D R, S L Anna, D A Weitz, and H A Stone. 2004. “Geometrically Mediated Breakup of Drops in Microfluidic Devices.” *Physical Review Letters* 92 (5): 054503. https://doi.org/10.1103/PhysRevLett.92.054503.

Link, Darren R., Erwan Grasland-Mongrain, Agnes Duri, Flavie Sarrazin, Zhengdong Cheng, Galder Cristobal, Manuel Marquez, and David A. Weitz. 2006. “Electric Control of Droplets in Microfluidic Devices.” *Angewandte Chemie - International Edition* 45 (16): 2556–60. https://doi.org/10.1002/anie.200503540.

Liu, Biwu, and Juewen Liu. 2017. “Methods for Preparing DNA-Functionalized Gold Nanoparticles, a Key Reagent of Bioanalytical Chemistry.” *Anal. Methods* 9 (18): 2633–43. https://doi.org/10.1039/C7AY00368D.

Liu, Chunchen, Xiaonan Xu, Bo Li, Bo Situ, Weilun Pan, Yu Hu, Taixue An, Shuhuai Yao, and Lei

Zheng. 2018. “Single-Exosome-Counting Immunoassays for Cancer Diagnostics.” *Nano Letters* 18 (7): 4226–32. https://doi.org/10.1021/acs.nanolett.8b01184.

Liu, Kan, Huijiang Ding, Yong Chen, and Xing Zhong Zhao. 2007. “Droplet-Based Synthetic Method Using Microflow Focusing and Droplet Fusion.” *Microfluidics and Nanofluidics* 3 (2): 239–43. https://doi.org/10.1007/s10404-006-0121-8.

Liu, Yong, and Xingyu Jiang. 2017. “Why Microfluidics? Merits and Trends in Chemical Synthesis.” *Lab on a Chip* 17 (23): 3960–78. https://doi.org/10.1039/c7lc00627f.

Loizou, Katerina, Voon-Loong Wong, and Buddhika Hewakandamby. 2018. “Examining the Effect of Flow Rate Ratio on Droplet Generation and Regime Transition in a Microfluidic T-Junction at Constant Capillary Numbers.” *Inventions* 3 (3): 54. https://doi.org/10.3390/inventions3030054.

Lombardo, Teo, Lidia Lancellotti, Christelle Souprayen, Catherine Sella, and Laurent Thouin. 2019. “Electrochemical Detection of Droplets in Microfluidic Devices: Simultaneous Determination of Velocity, Size and Content.” *Electroanalysis*, 1–10. https://doi.org/10.1002/elan.201900293.

Long, Feng, Chunmei Gu, April Z. Gu, and Hanchang Shi. 2012. “Quantum Dot/Carrier-Protein/Haptens Conjugate as a Detection Nanobioprobe for FRET-Based Immunoassay of Small Analytes with All-Fiber Microfluidic Biosensing Platform.” *Analytical Chemistry* 84 (8): 3646–53. https://doi.org/10.1021/ac3000495.

Loo, Stéphanie van, Serguei Stoukatch, Michael Kraft, and Tristan Gilet. 2016. “Droplet Formation by Squeezing in a Microfluidic Cross-Junction.” *Microfluidics and Nanofluidics* 20 (10): 1–12. https://doi.org/10.1007/s10404-016-1807-1.

Ma, Shou-Yu, Yu-Cheng Chiang, Chia-Hsien Hsu, Jyh-Jian Chen, Chin-Chi Hsu, An-Chong Chao, and Yung-Sheng Lin. 2019. “Peanut Detection Using Droplet Microfluidic Polymerase Chain Reaction Device.” *Journal of Sensors* 2019: 1–9. https://doi.org/10.1155/2019/4712084.

Maddala, Jeevan, and Raghunathan Rengaswamy. 2014. “Design of Multi-Functional Microfluidic Ladder Networks to Passively Control Droplet Spacing Using Genetic Algorithms.” *Computers and Chemical Engineering* 60: 413–25. https://doi.org/10.1016/j.compchemeng.2013.09.009.

Maddala, Jeevan, William S. Wang, Siva A. Vanapalli, and Raghunathan Rengaswamy. 2013. “Traffic of Pairs of Drops in Microfluidic Ladder Networks with Fore-Aft Structural Asymmetry.” *Microfluidics and Nanofluidics* 14 (1–2): 337–44. https://doi.org/10.1007/s10404-012-1054-z.

Mao, Xiaole, Sz Chin Steven Lin, Cheng Dong, and Tony Jun Huang. 2009. “Single-Layer Planar on-Chip Flow Cytometer Using Microfluidic Drifting Based Three-Dimensional (3D) Hydrodynamic Focusing.” *Lab on a Chip* 9 (11): 1583–89. https://doi.org/10.1039/b820138b.

Marshall, Wallace F., Kevin D. Young, Matthew Swaffer, Elizabeth Wood, Paul Nurse, Akatsuki Kimura, Joseph Frankel, et al. 2012. “What Determines Cell Size?” *BMC Biology* 10. https://doi.org/10.1186/1741-7007-10-101.

Mashaghi, Samaneh, Alireza Abbaspourrad, David A. Weitz, and Antoine M. van Oijen. 2016. “Droplet Microfluidics: A Tool for Biology, Chemistry and Nanotechnology.” *TrAC - Trends in Analytical Chemistry* 82: 118–25. https://doi.org/10.1016/j.trac.2016.05.019.

Mashaghi, Samaneh, and Antoine M van Oijen. 2015. “External Control of Reactions in Microdroplets.” *Scientific Reports* 5: 11837. https://doi.org/10.1038/srep11837.

Mattoussi, Hedi, J Matthew Mauro, Ellen R Goldman, George P Anderson, Vikram C Sundar, Frederic V Mikulec, and Moungi G Bawendi. 2000. “Self-Assembly of CdS-ZnS Quantum Dot Bioconjugates Using an Engineered Recombinant Protein.” *Journal of the American Chemical Society* 122 (49): 12142–50. https://doi.org/10.1021/ja002535y.

Mazutis, Linas, John Gilbert, W Lloyd Ung, David A Weitz, Andrew D Griffiths, and John A Heyman. 2013. “Single-Cell Analysis and Sorting Using Droplet-Based Microfluidics.” *Nat. Protocols* 8 (5): 870–91. https://doi.org/10.1038/nprot.2013.046\rhttp://www.nature.com/nprot/journal/v8/n5/abs/nprot.2013.046.html#supplementary-information.

Mcdermott, P, Duc Do, Claudia M Litterst, Dianna Maar, Christopher M Hindson, Erin R Steenblock, Tina C Legler, et al. 2013. “Multiplexed Target Detection Using DNA-Binding Dye Chemistry in Droplet Digital PCR.”

MCGloin, David. 2017. “Droplet Lasers: A Review of Current Progress.” *Reports on Progress in Physics* 80 (5). https://doi.org/10.1088/1361-6633/aa6172.

Medintz, Igor L, H Tetsuo Uyeda, Ellen R Goldman, and Hedi Mattoussi. 2005. “Quantum Dot Bioconjugates for Imaging, Labelling and Sensing.” *Nature Materials* 4: 435–46. https://doi.org/10.1038/nmat1390.

Mench, M. De, P. Garstecki, F. Jousse, and H. A. Stone. 2008. “Transition from Squeezing to Dripping in

a Microfluidic T-Shaped Junction." *Journal of Fluid Mechanics* 595: 1–17. https://doi.org/10.1017/S002211200700910X.

Miller, Oliver J, Abdeslam El, Thomas Mangeat, Jean-christophe Baret, Lucas Frenz, Bachir El, Estelle Mayot, et al. 2012. "High-Resolution Dose – Response Screening Using Droplet-Based Microfluidics." *Proceedings of the National Academy of Sciences* 109 (2): 378–83. https://doi.org/10.1073/pnas.1113324109/-/DCSupplemental.www.pnas.org/cgi/doi/10.1073/pnas.1113324109.

Mukhopadhyay, Rajendrani. 2007. "When PDMS Isn't the Best." *Analytical Chemistry* 79 (9): 3248–53. https://doi.org/10.1021/ac071903e.

Murshed, S. M Sohel, Say Hwa Tan, Nam Trung Nguyen, Teck Neng Wong, and Levent Yobas. 2009. "Microdroplet Formation of Water and Nanofluids in Heat-Induced Microfluidic T-Junction." *Microfluidics and Nanofluidics* 6 (2): 253–59. https://doi.org/10.1007/s10404-008-0323-3.

Nan, Lang, Zhuangde Jiang, and Xueyong Wei. 2014. "Emerging Microfluidic Devices for Cell Lysis: A Review." *Lab on a Chip* 14 (6): 1060–73. https://doi.org/10.1039/c3lc51133b.

Nguyen, Nam Trung, Teck Hui Ting, Yit Fatt Yap, Teck Neng Wong, John Chee Kiong Chai, Wee Liat Ong, Junlong Zhou, Say Hwa Tan, and Levent Yobas. 2007. "Thermally Mediated Droplet Formation in Microchannels." *Applied Physics Letters* 91 (8): 89–92. https://doi.org/10.1063/1.2773948.

Nguyen, Thu H, Xiaoming Chen, Abootaleb Sedighi, Ulrich J Krull, and Carolyn L Ren. 2018. "A Droplet-Based Microfluidic Platform for Rapid Immobilization of Quantum Dots on Individual Magnetic Microbeads." *Microfluidics and Nanofluidics* 22 (6): 1–11. https://doi.org/10.1007/s10404-018-2085-x.

Nishijima, Yasunori. 1960. "Diffusion in Glycerol-Water Mixture." *Bulletin of the Chemical Society of Japan* 33 (12): 1649–51.

Nisisako, Takasi, Toru Torii, Takanori Takahashi, and Yoichi Takizawa. 2006. "Synthesis of Monodisperse Bicolored Janus Particles with Electrical Anisotropy Using a Microfluidic Co-Flow System." *Advanced Materials* 18 (9): 1152–56. https://doi.org/10.1002/adma.200502431.

Niu, X. Z., B. Zhang, R. T. Marszalek, O. Ces, J. B. Edel, D. R. Klug, and A. J. deMello. 2009. "Droplet-Based Compartmentalization of Chemically Separated Components in Two-Dimensional

Separations." *Chemical Communications*, no. 41: 6159. https://doi.org/10.1039/b918100h.

Niu, Xize, Shelly Gulati, Joshua B Edel, and Andrew J deMello. 2008. "Pillar-Induced Droplet Merging in Microfluidic Circuits." *Lab on a Chip* 8 (11): 1837–41. https://doi.org/10.1039/b813325e.

Niu, Xize, Mengying Zhang, Suili Peng, Weijia Wen, and Ping Sheng. 2007. "Real-Time Detection, Control, and Sorting of Microfluidic Droplets." *Biomicrofluidics* 1 (4): 1–12. https://doi.org/10.1063/1.2795392.

Noor, M. Omair, Anna Shahmuradyan, and Ulrich J. Krull. 2013. "Paper-Based Solid-Phase Nucleic Acid Hybridization Assay Using Immobilized Quantum Dots as Donors in Fluorescence Resonance Energy Transfer." *Analytical Chemistry* 85 (3): 1860–67. https://doi.org/10.1021/ac3032383.

Noor, M. Omair, Anthony J. Tavares, and Ulrich J. Krull. 2013. "On-Chip Multiplexed Solid-Phase Nucleic Acid Hybridization Assay Using Spatial Profiles of Immobilized Quantum Dots and Fluorescence Resonance Energy Transfer." *Analytica Chimica Acta* 788: 148–57. https://doi.org/10.1016/j.aca.2013.06.017.

Noor, M Omair, and Ulrich J Krull. 2014. "Camera-Based Ratiometric Fluorescence Transduction of Nucleic Acid Hybridization with Reagentless Signal Ampli Fi Cation on a Paper- Based Platform Using Immobilized Quantum Dots as Donors." *Analytical Chemistry*.

Novak, Richard; Zeng, Yong; Shuga, Joe; Venugopalan, Gautham; Fletcher, Daniel; Smith, Martyn; Mathies, Richard. 2011. "Single Cell Multiplex Gene Detection and Sequencing Using Microfluidically Generated Agarose Emulsion." *Angew Chem Int Ed Engl.* 50 (June 2000): 390–95. https://doi.org/10.1002/anie.201006089.Single.

Ong, Wee Liat, Jinsong Hua, Baili Zhang, Teng Yuan Teo, Junlong Zhuo, Nam Trung Nguyen, Nagarajan Ranganathan, and Levent Yobas. 2007. "Experimental and Computational Analysis of Droplet Formation in a High-Performance Flow-Focusing Geometry." *Sensors and Actuators, A: Physical* 138 (1): 203–12. https://doi.org/10.1016/j.sna.2007.04.053.

Paik, Phil, Vamsee K. Pamula, Michael G. Pollack, and Richard B. Fair. 2003. "Electrowetting-Based Droplet Mixers for Microfluidic SystemsElectronic Supplementary Information (ESI) Available: Six Mpeg Videos Showing Some Mixing Schemes Used in Fig. 7. See Http://Www.Rsc.Org/Suppdata/Lc/B2/B210825a/." *Lab on a Chip* 3 (1): 28. https://doi.org/10.1039/b210825a.

Pamme, Nicole. 2006. “Magnetism and Microfluidics.” *Lab Chip* 6 (1): 24–38. https://doi.org/10.1039/B513005K.

Papautsky, Ian, and a Bruno Frazier. 2001. “A Review of Laminar Single-Phase Flow in Microchannels.” *2001 ASME International Mechanical Enginnering Congress and Exposition*, no. January: 1–9.

Park, Je-kyun. 2008. “Continuous Generation of Hydrogel Beads and Encapsulation of Biological Materials Using a Microfluidic Droplet-Merging Channel,” 541–49. https://doi.org/10.1007/s10404-008-0268-6.

Park, Jinsoo, Jin Ho Jung, Kwangseok Park, Ghulam Destgeer, Husnain Ahmed, Raheel Ahmad, and Hyung Jin Sung. 2018. “On-Demand Acoustic Droplet Splitting and Steering in a Disposable Microfluidic Chip.” *Lab on a Chip* 18 (3): 422–32. https://doi.org/10.1039/c7lc01083d.

Parthiban, Pravien, and Saif A. Khan. 2013. “Bistability in Droplet Traffic at Asymmetric Microfluidic Junctions.” *Biomicrofluidics* 7 (4): 24–27. https://doi.org/10.1063/1.4819276.

Peng, Hui, Lijuan Zhang, Tanja H M Kjällman, Christian Soeller, and Jadranka Travas-Sejdic. 2007. “DNA Hybridization Detection with Blue Luminescent Quantum Dots and Dye-Labeled Single-Stranded DNA.” *Journal of the American Chemical Society* 129 (11): 3048–49. https://doi.org/10.1021/ja0685452.

Perozziello, G., P. Candeloro, F. Gentile, A. Nicastri, A. Perri, M. L. Coluccio, A. Adamo, et al. 2014. “Microfluidics & Nanotechnology: Towards Fully Integrated Analytical Devices for the Detection of Cancer Biomarkers.” *RSC Advances* 4 (98): 55590–98. https://doi.org/10.1039/C4RA10486B.

Petralia, Salvatore, and Sabrina Conoci. 2017. “PCR Technologies for Point of Care Testing: Progress and Perspectives.” https://doi.org/10.1021/acssensors.7b00299.

Petryayeva, Eleonora, W. Russ Algar, and Igor L. Medintz. 2013. “Quantum Dots in Bioanalysis: A Review of Applications across Various Platforms for Fluorescence Spectroscopy and Imaging.” *Applied Spectroscopy* 67 (3): 215–52. https://doi.org/10.1366/12-06948.

Pinaud, Fabien, Xavier Michalet, Laurent A. Bentolila, James M. Tsay, Soren Doose, Jack J. Li, Gopal Iyer, and Shimon Weiss. 2006. “Advances in Fluorescence Imaging with Quantum Dot Bio-Probes.” *Biomaterials* 27 (9): 1679–87. https://doi.org/10.1016/j.biomaterials.2005.11.018.

Pit, Arjen M., Michèl H.G. Duits, and Frieder Mugele. 2015. “Droplet Manipulations in Two Phase Flow Microfluidics.” *Micromachines* 6 (11): 1768–93. https://doi.org/10.3390/mi6111455.

Pouton, Colin W., and John M. Haynes. 2007. “Embryonic Stem Cells as a Source of Models for Drug Discovery.” *Nature Reviews Drug Discovery* 6 (8): 605–16. https://doi.org/10.1038/nrd2194.

Prabhu, Vivek M, Steven D Hudson, Nathaniel S. Green, Michael L. Norton, Rajni Garg, Naba Dutta, Namita Choudhury, et al. 2009. “Nanoparticle Assembly: DNA Provides Control.” *Nature Materials* 8 (5): 365–66. https://doi.org/10.1038/nmat2436.

Priest, Craig, Stephan Herminghaus, and Ralf Seemann. 2006a. “Controlled Electrocoalescence in Microfluidics: Targeting a Single Lamella.” *Applied Physics Letters* 89 (13): 2004–7. https://doi.org/10.1063/1.2357039.

———. 2006b. “Generation of Monodisperse Gel Emulsions in a Microfluidic Device.” *Applied Physics Letters* 88 (2): 1–3. https://doi.org/10.1063/1.2164393.

Puigmartí-Luis, Josep. 2014. “Microfluidic Platforms: A Mainstream Technology for the Preparation of Crystals.” *Chemical Society Reviews* 43: 2253–71. https://doi.org/10.1039/c3cs60372e.

R., Gao, Cheng Z., and Demello A.J. 2016. “Wash-Free Magnetic Immunoassay of the PSA Cancer Marker Using SERS and Droplet Microfluidics.” *Lab on a Chip - Miniaturisation for Chemistry and Biology* 16 (6): 1022–29. https://doi.org/10.1039/C5LC01249J.

Ren, Kangning, Jianhua Zhou, and Hongkai Wu. 2013. “Materials for Microfluidic Chip Fabrication.” *Accounts of Chemical Research* 46 (11): 2396–2406. https://doi.org/10.1021/ar300314s.

Resch-Genger, Ute, Markus Grabolle, Sara Cavaliere-Jaricot, Roland Nitschke, and Thomas Nann. 2008. “Quantum Dots versus Organic Dyes as Fluorescent Labels.” *Nature Methods* 5 (9): 763–75. https://doi.org/10.1038/nmeth.1248.

Reyes, Darwin R, Dimitri Iossifidis, Pierre-Alain Auroux, and Andreas Manz. 2002. “Micro Total Analysis Systems. 1. Introduction, Theory, and Technology.” *Analytical Chemistry* 74 (12): 2623–36. https://doi.org/10.1021/ac0202435.

Rivet, Catherine, Hyewon Lee, Alison Hirsch, Sharon Hamilton, and Hang Lu. 2011. “Microfluidics for Medical Diagnostics and Biosensors.” *Chemical Engineering Science* 66 (7): 1490–1507. https://doi.org/10.1016/j.ces.2010.08.015.

Rosenfeld, Liat, Tiras Lin, Ratmir Derda, and Sindy K Y Tang. 2014. “Review and Analysis of Performance Metrics of Droplet Microfluidics Systems.” *Microfluidics and Nanofluidics* 16 (5): 921–39. https://doi.org/10.1007/s10404-013-1310-x.

Rotem, Assaf, Oren Ram, Noam Shoresh, Ralph A. Sperling, Michael Schnall-Levin, Huidan Zhang, Anindita Basu, Bradley E. Bernstein, and David A. Weitz. 2015. “High-Throughput Single-Cell Labeling (Hi-SCL) for RNA-Seq Using Drop-Based Microfluidics.” *PLoS ONE* 10 (5): 1–14. https://doi.org/10.1371/journal.pone.0116328.

Sackmann, Eric K., Anna L. Fulton, and David J. Beebe. 2014. “The Present and Future Role of Microfluidics in Biomedical Research.” *Nature* 507 (7491). https://doi.org/10.1038/nature13118.

Saqib, Muhammad, O. Berkay Şahinoğlu, and E. Yegân Erdem. 2018. “Alternating Droplet Formation by Using Tapered Channel Geometry.” *Scientific Reports* 8 (1): 1–9. https://doi.org/10.1038/s41598-018-19966-y.

Scheler, Ott, Witold Postek, and Piotr Garstecki. 2019. “Recent Developments of Microfluidics as a Tool for Biotechnology and Microbiology.” *Current Opinion in Biotechnology* 55: 60–67. https://doi.org/10.1016/j.copbio.2018.08.004.

Schneider, Thomas, Jason Kreutz, and Daniel T. Chiu. 2013. “The Potential Impact of Droplet Microfluidics in Biology.” *Analytical Chemistry* 85 (7): 3476–82. https://doi.org/10.1021/ac400257c.

Schoeman, Rogier M., Evelien W M Kemna, Floor Wolbers, and Albert van den Berg. 2014. “High-Throughput Deterministic Single-Cell Encapsulation and Droplet Pairing, Fusion, and Shrinkage in a Single Microfluidic Device.” *Electrophoresis* 35 (2–3): 385–92. https://doi.org/10.1002/elps.201300179.

Sedighi, Abootaleb, and Ulrich J. Krull. 2016. “Rapid Immobilization of Oligonucleotides at High Density on Semiconductor Quantum Dots and Gold Nanoparticles.” *Langmuir* 32 (50): 13500–509. https://doi.org/10.1021/acs.langmuir.6b03840.

———. 2018. “Enzymatic Amplification of Oligonucleotides in Paper Substrates.” *Talanta* 186 (March): 568–75. https://doi.org/10.1016/j.talanta.2018.02.107.

———. 2019. “Enhanced Immunoassay Using a Rotating Paper Platform for Quantitative Determination of Low Abundance Protein Biomarkers.” Research-article. *Analytical Chemistry* 91 (8): 5371–79. https://doi.org/10.1021/acs.analchem.9b00502.

Sesen, Muhsincan, Tuncay Alan, and Adrian Neild. 2014. “Microfluidic On-Demand Droplet Merging Using Surface Acoustic Waves.” *Lab on a Chip* 14 (17): 3325. https://doi.org/10.1039/c4lc00456f.

———. 2017. “Droplet Control Technologies for Microfluidic High Throughput Screening (MHTS).” *Lab on a Chip* 17 (14): 2372–94. https://doi.org/10.1039/c7lc00005g.

Shang, Luoran, Yao Cheng, and Yuanjin Zhao. 2017. “Emerging Droplet Microfluidics.” *Chemical Reviews* 117 (12): 7964–8040. https://doi.org/10.1021/acs.chemrev.6b00848.

Shembekar, Nachiket, Chawaree Chaipan, Ramesh Utharala, and Christoph A. Merten. 2016. “Droplet-Based Microfluidics in Drug Discovery, Transcriptomics and High-Throughput Molecular Genetics.” *Lab Chip* 16: 1314–31. https://doi.org/10.1039/C6LC00249H.

Shestopalov, Ilya, Joshua D Tice, and Rustem F Ismagilov. 2004. “Multi-Step Synthesis of Nanoparticles Performed on Millisecond Time Scale in a Microfluidic Droplet-Based System.” *Lab on a Chip* 4 (4): 316–21. https://doi.org/10.1039/b403378g.

Shi, Weiwei, Jianhua Qin, Nannan Ye, and Bingcheng Lin. 2008. “Droplet-Based Microfluidic System for Individual Caenorhabditis Elegans Assay.” *Lab on a Chip* 8 (9): 1432–35. https://doi.org/10.1039/b808753a.

Shui, Lingling, Albert Van Den Berg, and Jan C.T. Eijkel. 2009. “Interfacial Tension Controlled W/O and O/W 2-Phase Flows in Microchannel.” *Lab on a Chip* 9 (6): 795–801. https://doi.org/10.1039/b813724b.

Shui, Lingling, Jan C T Eijkel, and Albert van den Berg. 2007. “Multiphase Flow in Microfluidic Systems - Control and Applications of Droplets and Interfaces.” *Advances in Colloid and Interface Science* 133 (1): 35–49. https://doi.org/10.1016/j.cis.2007.03.001.

Shui, Lingling, Sumita Pennathur, Jan C.T. Eijkel, and Albert Van Den Berg. 2008. “Multiphase Flow in Lab on Chip Devices: A Real Tool for the Future?” *Lab on a Chip* 8 (7): 1010–14. https://doi.org/10.1039/b808974b.

Singh, Kirat, Alan O Neill, Carl Jackson, Jan Kr, Alan Morrison, and Peter O Brien. 2002. “Development of a Microfluidic Device for Fluorescence Activated Cell Sorting.” *Journal of Micromechanics and Microengineering*, no. 12: 486–94.

Song, H., M. R. Bringer, Joshua D. Tice, C. J. Gerdts, and Rustem F. Ismagilov. 2003. “Experimental Test of Scaling of Mixing by Chaotic Advection in Droplets Moving through Microfluidic Channels.” *Applied Physics Letters* 83 (12): 4664–66. https://doi.org/10.1097/OPX.0b013e3182540562.The.

Song, H., D. L. Chen, and Rustem F. Ismagilov. 2006. “Reactions in Droplets in Microfluidic Channels.” *Angew Chem Int Ed Engl.* 45 (44): 7336–56. https://doi.org/10.1097/OPX.0b013e3182540562.The.

Song, Helen, Joshua D Tice, and Rustem F Ismagilov. 2003. “A Microfluidic System for Controlling Reaction Networks in Time - Song - 2003 - Angewandte Chemie - Wiley Online Library.” *Angewandte Chemie* 115 (7): 792–96. https://doi.org/10.1002/ange.19350483406.

Song, J. H., R. Evans, Y. Y. Lin, B. N. Hsu, and R. B. Fair. 2009. “A Scaling Model for Electrowetting-on-Dielectric Microfluidic Actuators.” *Microfluidics and Nanofluidics* 7 (1): 75–89. https://doi.org/10.1007/s10404-008-0360-y.

Song, Kui, Li Zhang, and Guoqing Hu. 2012. “Modeling of Droplet Traffic in Interconnected Microfluidic Ladder Devices.” *Electrophoresis* 33 (3): 411–18. https://doi.org/10.1002/elps.201100320.

Song, Yang, Alban Sauret, and Ho Cheung Shum. 2013. “All-Aqueous Multiphase Microfluidics.” *Biomicrofluidics* 7 (6): 1–12. https://doi.org/10.1063/1.4827916.

Spurgeon, Sandra L., Robert C. Jones, and Ramesh Ramakrishnan. 2008. “High Throughput Gene Expression Measurement with Real Time PCR in a Microfluidic Dynamic Array.” *PLoS ONE* 3 (2). https://doi.org/10.1371/journal.pone.0001662.

Squires, Todd M., and Stephen R. Quake. 2005. “Microfluidics: Fluid Physics at the Nanoliter Scale.” *Reviews of Modern Physics* 77 (3): 977–1026. https://doi.org/10.1103/RevModPhys.77.977.

Stanisavljevic, Maja, Sona Krizkova, Marketa Vaculovicova, Rene Kizek, and Vojtech Adam. 2015. “Quantum Dots-Fluorescence Resonance Energy Transfer-Based Nanosensors and Their Application.” *Biosensors and Bioelectronics* 74: 562–74. https://doi.org/10.1016/j.bios.2015.06.076.

Steinke, Mark E, and Satish G Kandlikar. 2004. “Single-Phase Heat Transfer Enhancement Techniques in Microchannel and Minichannel Flows.” In *The 2nd International Conference on Microchannels and Minichannels*, 2328.

Stone, H. A., and S. Kim. 2001. “Microfluidics: Basic Issues, Applications, and Challenges.” *AIChE Journal* 47 (6): 1250–54. https://doi.org/10.1002/aic.690470602.

Stone, H A, A D Stroock, and A Ajdari. 2004. “ENGINEERING FLOWS IN SMALL DEVICESMicrofluidics Toward a Lab-on-a-Chip.” *Annual Review of Fluid Mechanics* 36 (1): 381–411. https://doi.org/doi:10.1146/annurev.fluid.36.050802.122124.

Sun, Dazhi, and Oleg Gang. 2013. “DNA-Functionalized Quantum Dots : Fabrication , Structural , and Physicochemical Properties.” https://doi.org/10.1021/la4000186.

Suzuki, M, Y Husimi, H Komatsu, K Suzuki, and a. K T Douglas. 2008. “Quantum Dot FRET Biosensors That Respond to PH, to Proteolytic or Nucleolytic Cleavage, to DNA Synthesis, or to a Multiplexing Combination.” *J. Am. Chem. Soc.* 130 (20): 5720–25. https://doi.org/10.1021/ja710870e.

Taassob, Arsalan, Mohammad Karim Dehghan Manshadi, Alireza Bordbar, and Reza Kamali. 2017. “Monodisperse Non-Newtonian Micro-Droplet Generation in a Co-Flow Device.” *Journal of the Brazilian Society of Mechanical Sciences and Engineering* 39 (6): 2013–21. https://doi.org/10.1007/s40430-016-0699-z.

Takamura, Koichi, Herbert Fischer, and Norman R. Morrow. 2012. “Physical Properties of Aqueous Glycerol Solutions.” *Journal of Petroleum Science and Engineering* 98–99: 50–60. https://doi.org/10.1016/j.petrol.2012.09.003.

Tan, By Wei-heong, and Shoji Takeuchi. 2007. “Monodisperse Alginate Hydrogel Microbeads for Cell Encapsulation **.” *Advanced Materials* 19: 2696–2701. https://doi.org/10.1002/adma.200700433.

Tan, Yung-Chieh, Jeffrey S Fisher, Alan I Lee, Vittorio Cristini, and Abraham Phillip Lee. 2004. “Design of Microfluidic Channel Geometries for the Control of Droplet Volume, Chemical Concentration, and Sorting.” *Lab on a Chip* 4 (4): 292–98. https://doi.org/10.1039/b403280m.

Tan, Yung Chieh, Yao Li Ho, and Abraham Phillip Lee. 2007. “Droplet Coalescence by Geometrically Mediated Flow in Microfluidic Channels.” *Microfluidics and Nanofluidics* 3 (4): 495–99. https://doi.org/10.1007/s10404-006-0136-1.

———. 2008. “Microfluidic Sorting of Droplets by Size.” *Microfluidics and Nanofluidics* 4 (4): 343–48. https://doi.org/10.1007/s10404-007-0184-1.

Taylor, Anne M., Mathew Blurton-Jones, Seog Woo Rhee, David H. Cribbs, Carl W. Cotman, and Neon Li Jeon. 2005. “A Microfluidic Culture Platform for CNS Axonal Injury, Regeneration and Transport.” *Nature Methods* 2 (8): 599–605. https://doi.org/10.1038/nmeth777.

Taylor, Jay, G. D. Stubley, and Carolyn L. Ren. 2008. “Experimental Determination of Sample Stream Focusing with Fluorescent Dye.” *Electrophoresis* 29 (14): 2953–59. https://doi.org/10.1002/elps.200700931.

Taylor, Sean C., Genevieve Laperriere, and Hugo Germain. 2017. “Droplet Digital PCR versus QPCR for

Gene Expression Analysis with Low Abundant Targets: From Variable Nonsense to Publication Quality Data." *Scientific Reports* 7 (1): 1–8. https://doi.org/10.1038/s41598-017-02217-x.

Teh, Shia-Yen, Robert Lin, Lung-Hsin Hung, and Abraham P Lee. 2008. "Droplet Microfluidics." *Lab on a Chip* 8 (2): 198–220. https://doi.org/10.1039/b715524g.

Teste, Bruno, Nicolas Jamond, Davide Ferraro, Jean Louis Viovy, and Laurent Malaquin. 2015. "Selective Handling of Droplets in a Microfluidic Device Using Magnetic Rails." *Microfluidics and Nanofluidics* 19 (1): 141–53. https://doi.org/10.1007/s10404-015-1556-6.

Theberge, Ashleigh B., Estelle Mayot, Abdeslam El Harrak, Felix Kleinschmidt, Wilhelm T.S. Huck, and Andrew D. Griffiths. 2012. "Microfluidic Platform for Combinatorial Synthesis in Picolitre Droplets." *Lab on a Chip* 12 (7): 1320–26. https://doi.org/10.1039/c2lc21019c.

Tice, Joshua D., Helen Song, Adam D. Lyon, and Rustem F. Ismagilov. 2003a. "Formation of Droplets and Mixing in Multiphase Microfluidics at Low Values of the Reynolds and the Capillary Numbers." *Langmuir* 19 (22): 9127–33. https://doi.org/10.1021/la030090w.

———. 2003b. "Formation of Droplets and Mixing in Multiphase Microfluidics at Low Values of the Reynolds and the Capillary Numbers." *Langmuir* 19 (22): 9127–33. https://doi.org/10.1021/la030090w.

Ting, Teck Hui, Yit Fatt Yap, Nam Trung Nguyen, Teck Neng Wong, John Chee Kiong Chai, and Levent Yobas. 2006. "Thermally Mediated Breakup of Drops in Microchannels." *Applied Physics Letters* 89 (23): 2006–8. https://doi.org/10.1063/1.2400200.

Tran, Thanh Huyen, Chi Thanh Nguyen, Dong-Pyo Kim, Yong-kyu Lee, and Kang Moo Huh. 2012. "Microfluidic Approach for Highly Efficient Synthesis of Heparin-Based Bioconjugates for Drug Delivery." *Lab on a Chip* 12: 589. https://doi.org/10.1039/c1lc20769e.

Trivedi, Varun, Ankur Doshi, G. K. Kurup, E. Ereifej, P. J. Vandevord, and Amar S. Basu. 2010. "A Modular Approach for the Generation, Storage, Mixing, and Detection of Droplet Libraries for High Throughput Screening." *Lab on a Chip* 10 (18): 2433–42. https://doi.org/10.1039/c004768f.

Tung, Kai Yang, Chih Chieh Li, and Jing Tang Yang. 2009. "Mixing and Hydrodynamic Analysis of a Droplet in a Planar Serpentine Micromixer." *Microfluidics and Nanofluidics* 7 (4): 545–57. https://doi.org/10.1007/s10404-009-0415-8.

Um, Eujin;, Dae-Sik; Lee, Hyeon-Bong; Pyo, and Je-Kyun Park. 2008. "Continuous Generation of

Hydrogel Beads and Encapsulation of Biological Materials Using a Microfluidic Droplet-Merging Channel." *Microfluidics and Nanofluidics* 5: 541–49. https://doi.org/10.1007/s10404-008-0268-6.

Umbanhowar, P. B., V. Prasad, and D. A. Weitz. 2000. "Monodisperse Emulsion Generation via Drop Break off in a Coflowing Stream." *Langmuir* 16 (2): 347–51. https://doi.org/10.1021/la990101e.

Utada, Andrew S., Alberto Fernandez-Nieves, Jose M. Gordillo, and David A. Weitz. 2008. "Absolute Instability of a Liquid Jet in a Coflowing Stream." *Physical Review Letters* 100 (1): 1–4. https://doi.org/10.1103/PhysRevLett.100.014502.

Valencia, Pedro M., Omid C. Farokhzad, Rohit Karnik, and Robert Langer. 2012. "Microfluidic Technologies for Accelerating the Clinical Translation of Nanoparticles." *Nature Nanotechnology* 7 (10): 623–29. https://doi.org/10.1038/nnano.2012.168.

Velasco, Diego, Ethan Tumarkin, and Eugenia Kumacheva. 2012. "Microfluidic Encapsulation of Cells in Polymer Microgels," no. 11: 1633–42. https://doi.org/10.1002/smll.201102464.

Verguet, Stéphane, Chuanhua Duan, Albert Liau, Veysel Berk, Jamie H.D. Cate, Arun Majumdar, and Andrew J. Szeri. 2010. "Mechanics of Liquid-Liquid Interfaces and Mixing Enhancement in Microscale Flows." *Journal of Fluid Mechanics* 652: 207–40. https://doi.org/10.1017/S0022112009994113.

Vladisavljević, Goran, Ruqaya Al Nuumani, and Seyed Nabavi. 2017. "Microfluidic Production of Multiple Emulsions." *Micromachines* 8 (3): 75. https://doi.org/10.3390/mi8030075.

Vreeland, Wyatt N., Samuel M. Stavis, Michael Gaitan, Don L. DeVoe, Andreas Jahn, and Jennifer S. Hong. 2010. "Microfluidic Mixing and the Formation of Nanoscale Lipid Vesicles." *ACS Nano* 4 (4): 2077–87. https://doi.org/10.1021/nn901676x.

Walsh, David I., David S. Kong, Shashi K. Murthy, and Peter A. Carr. 2017. "Enabling Microfluidics: From Clean Rooms to Makerspaces." *Trends in Biotechnology* 35 (5): 383–92. https://doi.org/10.1016/j.tibtech.2017.01.001.

Wang, Jianmei, Yan Li, Xueying Wang, Jianchun Wang, Hanmei Tian, Pei Zhao, Ye Tian, Yeming Gu, Liqiu Wang, and Chengyang Wang. 2017. "Droplet Microfluidics for the Production of Microparticles and Nanoparticles." *Micromachines* 8 (1): 1–23. https://doi.org/10.3390/mi8010022.

Wang, Lisen, Lisa a Flanagan, Edwin Monuki, Noo Li Jeon, and Abraham P Lee. 2007. "Dielectrophoresis Switching with Vertical Sidewall Electrodes for Microfluidic Flow Cytometry."

Lab on a Chip 7 (9): 1114–20. https://doi.org/10.1039/b705386j.

Wang, Mark M, Eugene Tu, Daniel E Raymond, Joon Mo Yang, Haichuan Zhang, Norbert Hagen, Bob Dees, et al. 2005. "Microfluidic Sorting of Mammalian Cells by Optical Force Switching." *Nature Biotechnology* 23 (1): 83–87. https://doi.org/10.1038/nbt1050.

Wang, Xiang, Zhaomiao Liu, and Yan Pang. 2018. "Droplet Breakup in an Asymmetric Bifurcation with Two Angled Branches." *Chemical Engineering Science* 188: 11–17. https://doi.org/10.1016/j.ces.2018.05.003.

Wang, Xiaoguang, Emre Bukusoglu, and Nicholas L. Abbott. 2016. "A Practical Guide to the Preparation of Liquid Crystal-Templated Microparticles." *Chemistry of Materials,* no. TBD: TBD. https://doi.org/10.1021/acs.chemmater.6b02668.

Ward, Kevin, and Z. Hugh Fan. 2015a. "Mixing in Microfluidic Devices and Enhancement Methods." *Journal of Micromechanics and Microengineering* 25 (9). https://doi.org/10.1088/0960-1317/25/9/094001.

———. 2015b. "Mixing in Microfluidic Devices and Enhancement Methods." *Journal of Micromechanics and Microengineering* 25 (9): 094001. https://doi.org/10.1088/0960-1317/25/9/094001.

Wharton, C.F. Chen; K. 2017. "Characterization and Failure Mode Analyses of Air Plasma Oxidized PDMS-PDMS Bonding by Peel Testing." *RSC Advances* 7 (3): 1286–89. https://doi.org/10.1039/C6RA25947B.

Whitesides, George M. 2006. "The Origins and the Future of Microfluidics." *Nature* 442 (7101): 368–73. https://doi.org/10.1038/nature05058.

Wiebe, J.P., and C.J. Dinsdale. 1991. "Inhibition of Cell Proliferation by Glycerol." *Life Sciences* 48 (16): 1511–17.

Wong, David, and Carolyn L Ren. 2016. "Microfluidics Droplet Trapping, Splitting and Merging with Feedback Controls and State Space Modelling." *Lab on a Chip* 16: 1–14. https://doi.org/10.1039/C6LC00626D.

Wu, Huei Wen, Yi Hsing Hsiao, Chih Chen Chen, Shaw Fang Yet, and Chia Hsien Hsu. 2016. "A Pdms-Based Microfluidic Hanging Drop Chip for Embryoid Body Formation." *Molecules* 21 (7): 1–11. https://doi.org/10.3390/molecules21070882.

Wu, Liangyu, Xiangdong Liu, Yuanjin Zhao, and Yongping Chen. 2017. “Role of Local Geometry on Droplet Formation in Axisymmetric Microfluidics.” *Chemical Engineering Science* 163: 56–67. https://doi.org/10.1016/j.ces.2017.01.022.

Xi, Heng Dong, Hao Zheng, Wei Guo, Alfonso M. Gañán-Calvo, Ye Ai, Chia Wen Tsao, Jun Zhou, et al. 2017a. “Active Droplet Sorting in Microfluidics: A Review.” *Lab on a Chip* 17 (5): 751–71. https://doi.org/10.1039/c6lc01435f.

———. 2017b. “Active Droplet Sorting in Microfluidics: A Review.” *Lab on a Chip* 17 (5): 751–71. https://doi.org/10.1039/c6lc01435f.

Xia, Younan, and George M Whitesides. 1998. “SOFT LITHOGRAPHY.” *Annu. Rev. Mater. Sci* 28: 153–84.

Xing, Yun, and Jianghong Rao. 2008. “Quantum Dot Bioconjugates for in Vitro Diagnostics & in Vivo Imaging.” *Cancer Biomarkers : Section A of Disease Markers* 4 (6): 307–19.

Yang, Fan, Qian Li, Lihua Wang, Guo Jun Zhang, and Chunhai Fan. 2018. “Framework-Nucleic-Acid-Enabled Biosensor Development.” Review-article. *ACS Sensors* 3 (5): 903–19. https://doi.org/10.1021/acssensors.8b00257.

Yang, Lu, Kai Wang, Jing Tan, Yangcheng Lu, and Guangsheng Luo. 2012. “Experimental Study of Microbubble Coalescence in a T-Junction Microfluidic Device.” *Microfluidics and Nanofluidics* 12 (5): 715–22. https://doi.org/10.1007/s10404-011-0912-4.

Yeap, Eunice W.Q., Andrew J. Acevedo, and Saif A. Khan. 2019. “Microfluidic Extractive Crystallization for Spherical Drug/Drug-Excipient Microparticle Production.” Review-article. *Organic Process Research and Development* 23 (3): 375–81. https://doi.org/10.1021/acs.oprd.8b00432.

Yesiloz, Gurkan, Muhammed S. Boybay, and Carolyn L. Ren. 2017. “Effective Thermo-Capillary Mixing in Droplet Microfluidics Integrated with a Microwave Heater.” *Analytical Chemistry*, acs.analchem.6b04520. https://doi.org/10.1021/acs.analchem.6b04520.

Yin, Huabing, and Damian Marshall. 2012. “Microfluidics for Single Cell Analysis.” *Current Opinion in Biotechnology* 23 (1): 110–19. https://doi.org/10.1016/j.copbio.2011.11.002.

Yoon, Dong Hyun, Afshan Jamshaid, Junichi Ito, Asahi Nakahara, Daiki Tanaka, Takashiro Akitsu, Tetsushi Sekiguchi, and Shuichi Shoji. 2014. “Active Microdroplet Merging by Hydrodynamic Flow

Control Using a Pneumatic Actuator-Assisted Pillar Structure." *Lab on a Chip* 14 (16): 3050–55. https://doi.org/10.1039/c4lc00378k.

Yu, Linfen, Michael C.W. Chen, and Karen C. Cheung. 2010. "Droplet-Based Microfluidic System for Multicellular Tumor Spheroid Formation and Anticancer Drug Testing." *Lab on a Chip* 10 (18): 2424–32. https://doi.org/10.1039/c004590j.

Yu, Wei, Xiangdong Liu, Yuanjin Zhao, and Yongping Chen. 2019. "Droplet Generation Hydrodynamics in the Microfluidic Cross-Junction with Different Junction Angles." *Chemical Engineering Science* 203: 259–84. https://doi.org/10.1016/j.ces.2019.03.082.

Zagnoni, Michele, Charles N. Baroud, and Jonathan M. Cooper. 2009. "Electrically Initiated Upstream Coalescence Cascade of Droplets in a Microfluidic Flow." *Physical Review E - Statistical, Nonlinear, and Soft Matter Physics* 80 (4): 1–9. https://doi.org/10.1103/PhysRevE.80.046303.

Zagnoni, Michele, Guillaume Le Lain, and Jonathan M. Cooper. 2010. "Electrocoalescence Mechanisms of Microdroplets Using Localized Electric Fields in Microfluidic Channels." *Langmuir* 26 (18): 14443–49. https://doi.org/10.1021/la101517t.

Zeng, Yong, Mimi Shin, and Tanyu Wang. 2013. "Programmable Active Droplet Generation Enabled by Integrated Pneumatic Micropumps." *Lab on a Chip* 13 (2): 267–73. https://doi.org/10.1039/c2lc40906b.

Zhang, Chi, and Danny Van Noort. 2011. *Cells in Microfluidics*. *Topics in Current Chemistry*. Vol. 304. https://doi.org/10.1007/128_2011_147.

Zhang, Chun-Yang, Hsin-Chih Yeh, Marcos T Kuroki, and Tza-Huei Wang. 2005. "Single-Quantum-Dot-Based DNA Nanosensor." *Nature Materials* 4 (11): 826–31. https://doi.org/10.1038/nmat1508.

Zhao, Chun Xia, and Anton P J Middelberg. 2011. "Two-Phase Microfluidic Flows." *Chemical Engineering Science* 66 (7): 1394–1411. https://doi.org/10.1016/j.ces.2010.08.038.

Zheng, B.; Tice J. D.; Ismagilov R. F. 2004. "Formation of Droplets of Alternating Composition in Microfluidic Channels and Applications to Indexing of Concentrations in Droplet-Based Assays." *Anal Chem.* 76 (17): 4977–82. https://doi.org/10.1038/jid.2014.371.

Zhou, Chunfeng, Pengtao Yue, and James J. Feng. 2006. "Formation of Simple and Compound Drops in Microfluidic Devices." *Physics of Fluids* 18 (9): 1–14. https://doi.org/10.1063/1.2353116.

Zhu, Pingan, Xin Tang, and Liqiu Wang. 2016. "Droplet Generation in Co - Flow Microfluidic Channels

with Vibration." *Microfluidics and Nanofluidics* 20 (3): 1–10. https://doi.org/10.1007/s10404-016-1717-2.

Zhu, Pingan, and Liqiu Wang. 2017. "Passive and Active Droplet Generation with Microfluidics: A Review" 17: 34–75. https://doi.org/10.1039/C6LC01018K.

Zhu, Ying, and Qun Fang. 2013. "Analytical Detection Techniques for Droplet Microfluidics-A Review." *Analytica Chimica Acta*. https://doi.org/10.1016/j.aca.2013.04.064.

Ziaie, Babak, Antonio Baldi, Ming Lei, Yuandong Gu, and Ronald A. Siegel. 2004. "Hard and Soft Micromachining for BioMEMS: Review of Techniques and Examples of Applications in Microfluidics and Drug Delivery." *Advanced Drug Delivery Reviews* 56 (2): 145–72. https://doi.org/10.1016/j.addr.2003.09.001.

Zubaite, Greta, Karolis Simutis, Robertas Galinis, Valdemaras Milkus, Vaidotas Kiseliovas, and Linas Mazutis. 2017. "Droplet Microfluidics Approach for Single-DNA Molecule Amplification and Condensation into DNA-Magnesium-Pyrophosphate Particles." *Micromachines* 8 (2): 62. https://doi.org/10.3390/mi8020062.

Appendix A

Comparing fluorescent intensity at the inlet and outlet to confirm conjugation yield

A – 1. Evaluating the conjugate yield

To evaluate conjugtion yield, the fluorecent intensity of QDs at the inlet (prior to conjugation) and outlet (post conjugation) are compared. Conjugation-yield efficiency is estimated as:

$$Efficiency = \left(1 - \frac{\#\ of\ white\ pixels\ of\ the\ MBQD\ conjugate\ images}{\#\ of\ white\ pixels\ of\ the\ original\ QDs\ images}\right) \times 100 \qquad \text{(A-1)}$$

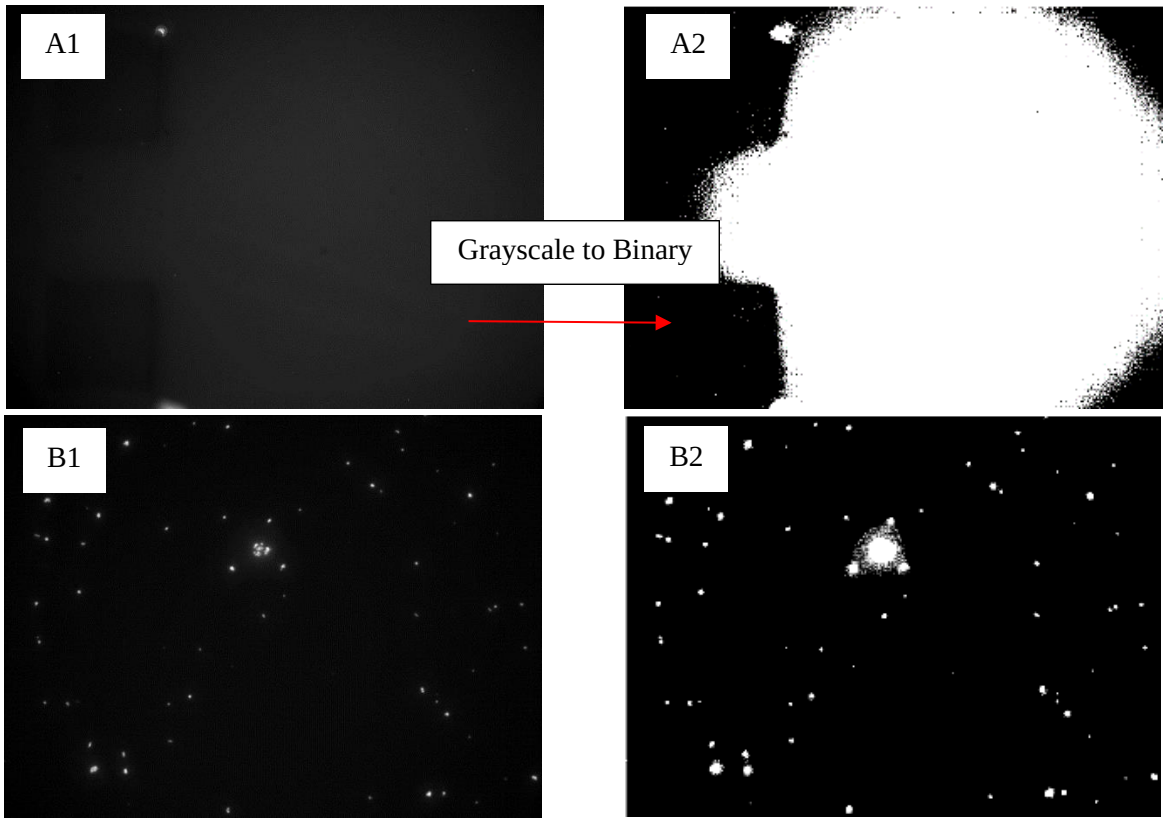

Figure A-1. A1) A grayscale image of the inlet with QDs well dispersed, A2) The binary image converted from A1 using the developed MATLAB code. B1) A grayscale image of the outlet with QD-MB conjugates. B2) The binary image converted from B1 using the developed MATLAB code.

where white pixels represent the concentration of QDs shown in binary images. Equation (A-1) indicates

the concentration of the excess QDs after conjugation.A higher determined value means a lower concentration of excess QDs after conjugation, indicating a higher conjugation yield. The image directly obtained from the microscope is in gray scale and is converted to a binary image using an in-house written MATLAB code with a treshold of 18 for white pixels **(Figure A-1)**. The total number of pixels for all images is 480000 pixels (600x800).

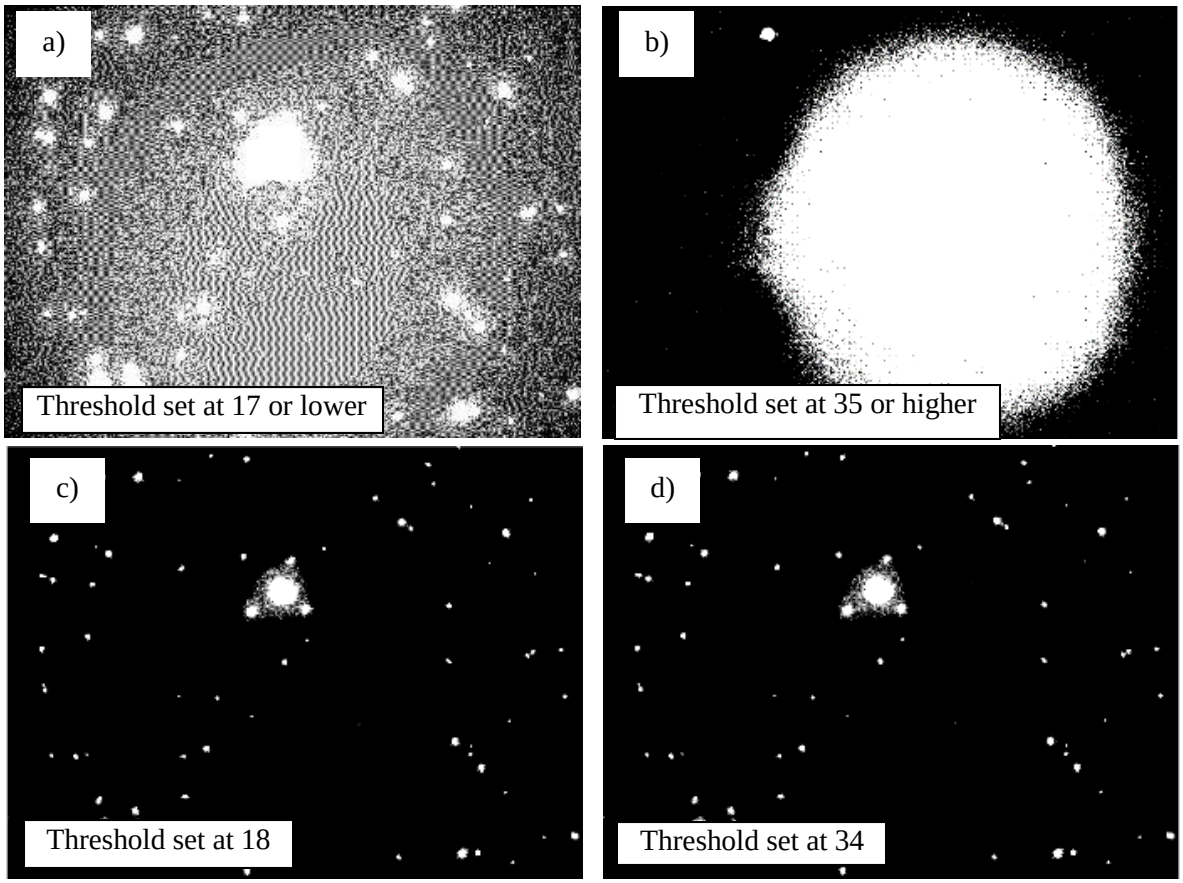

Figure A-2. a) When the threshold is set at 17 and below, the binary image of the outlet shows more white pixels (a higher concentration of MB-QDs conjugates) than is observed in the corresponding gray scale image; b) when the threshold is set at 35 or higher, the binary image of the inlet with QDs well dispersed presents a lower number of white pixels than is desirable supposed to be, i.e, the original

The threshold of 18 is chosen because the value of the gray pixel is 17, and when a threshold of 17 or below is chosen, the binary image of the outlet shows many more MB-QDs conjugates than what are observed in the corresponding gray scale image (Figure A-1(a)). The threshold cannot be too high

because that might result in the loss of white pixels representing QDs (Figure A-2(b)). In this study, the maximum threshold is set up as 35. In order to ensure that choosing a threshold within the range of 18-35 does not influence the efficiency determined for Equation (A-1), the same image was processed based on different threshold values, including 18, 20, 25, 28, 30 and 34, which all produce the same results. The images processed with the threshold values of 18 and 34 are presented in Figure A-2(c) and (d) respectively.

Table A1 provides information for the binary images of a typical inlet with QDs well dispersed before conjugation, and the corresponding outlet where both MB-QD conjugates and excess QDs exist. The efficiency is around 98.4 based on the information provided in Table A-1.

Table A-1: Information on the binary images for the QD solution prior and post conjugation

	QDs at the inlet (binary image)	MB-QD conjugate (binary image)
Size of image (pixels)	600x800	600x800
Threshold value of white pixel	18	18
# of white pixels	394859	6198

A – 2. Method for evaluating intensity of the conjugation inside droplets

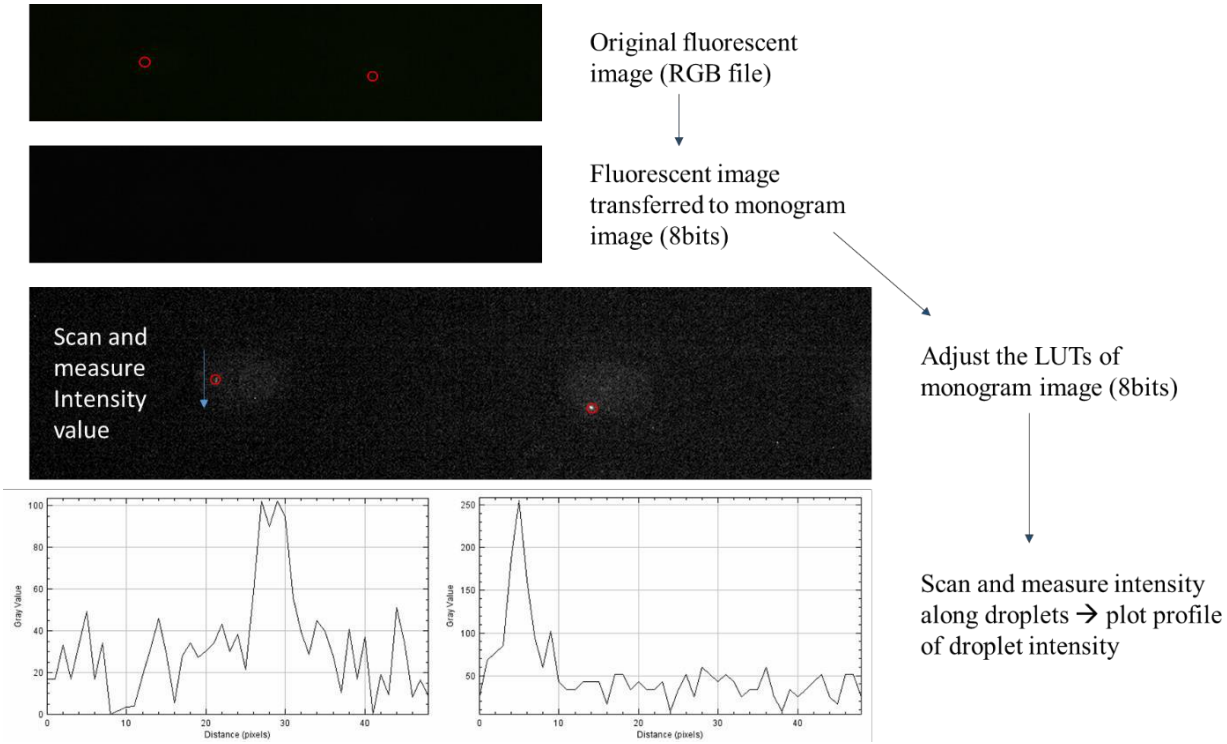

Figure A-3. Steps to evaluate conjugation occuring inside droplets

The fluorescent image taken in the RGB format is transferred to the monogram image (8 bits) for image processing. Under the monogram 8-bits image, the pixel value varies from 0 to 255. The conjugation is confirmed by processing the images, as in Figure A-3. When droplets contain a single MB-QD conjugate, the highest peak value (> 100) of the intensity profile plot is induced due to the full coverage of QDs on MB surfaces; whereas, the highest value for the background is 60.

Appendix B

Single encapsulation 10 um sized polystyrene bead

Similarly to the designed discussed in Chapter 4, this design is used to encapsulate micro-beads, ~4 to 10 μm in diameter, in aqueous droplets. The channel widths of all fluidic streams are consistently set at 100 um, and channel height is 60 um (before the PDMS swelling). The encapsulation of large micro-particles is tested to confirm the hypothesis that a double cross-junction and a hydrodynamic focusing induced by viscosity contrast fluids can be used as an approach for single encapsulation of particles. Figure B-1 illustrated the encapsulation of polystyrene (PS) particles ($\rho = 1.055\ g/cm^3$) in aqueous droplets, in which the PS particles are prepared in a mixture of 80% wt glycerol. The droplet generation frequency is 95 to 110 Hz. Using this approach, single encapsulation is enhanced when a droplet is generated.

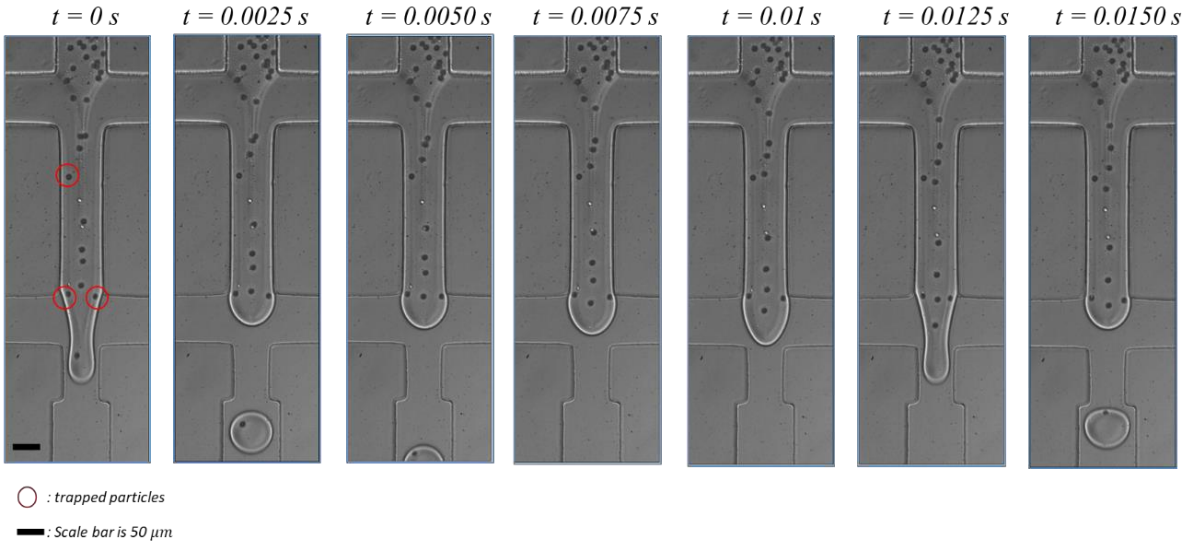

Figure B-1. Experimental result showing the single encapsulation of 10 um polystyrene bead inside droplets using a double cross junctions approach and stratified flow with viscosity contrast fluids

Appendix C

A complex microfluidic circuit to an electric circuit analysis

The functional performance of passive microfluidic designs mainly depends on channel dimensions and the precision of fabrication. The entire microfluidic network is well-connected, so any event happening in this network will change local and global hydrodynamic resistance. Thus, the microfluidic network, specifically a complex one, should be designed to be insensitive to multiple uncertainties, such as fabrication defects or local resistance changes, etc. The numerical simulation – Computational Fluid Dynamics (CFD) – can help to illustrate the fluid flow in detail and accurately; however, the high level of physical details as well as multiple parts integrated in one design will cause high computational cost.

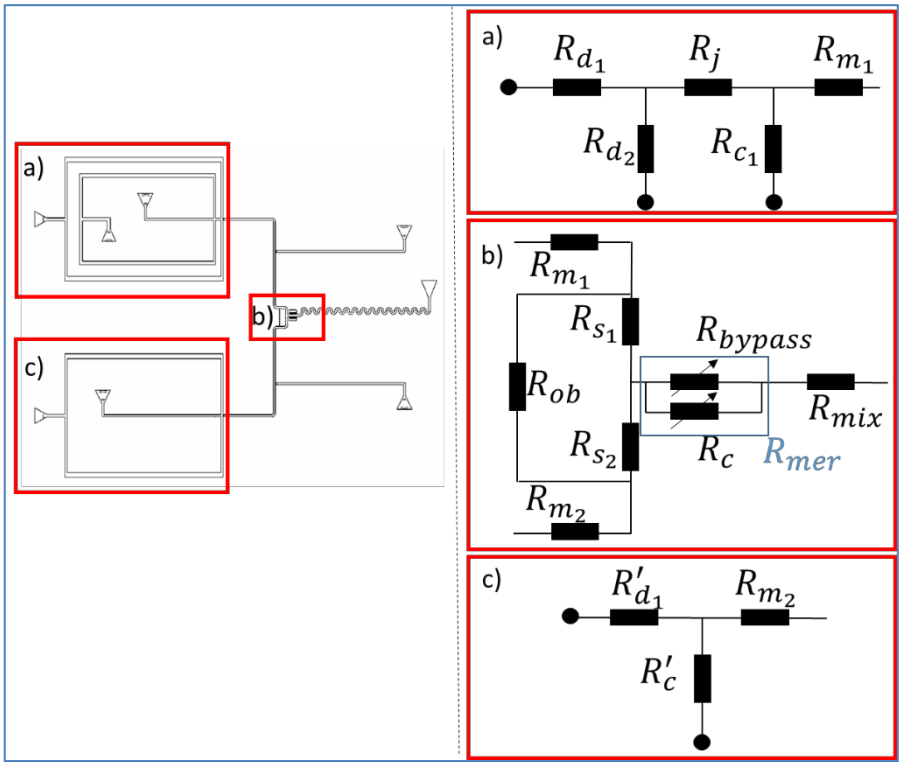

Figure C-1. Electric circuit analysis is used to simplify a complex droplet microfluidic system.

As discussed in Chapter 5, based on the analogous behavior of hydraulic and electric circuits with the associations of parameters (i.e, pressure to voltage, volumetric flow rate to current, hydraulic resistance to electric resistance, etc.), the applications of circuit methods are used to simplify a complex microfluidic design with multiple functions. The circuit analysis offers rapid adjustments of pressure-driven laminar flow in micro-channels; therefore, the prognosis for the microfluidic design and the system's performance can be predicted in advance of fabrication. Particularly, this design includes three main parts, illustrated in Figure C-1. Part a) and c) represent the electric circuits that are used to simplify the encapsulation coupling with the droplet generator and another separate droplet generator, respectively. Details of design criteria for a double cross-junction for the encapsulation as well as the one for a flow-focusing droplet generator are discussed in Chapter 4 and also in Dr. Xiaoming Chen's thesis (UWspace). Meanwhile, the alternative droplet merging component is illustrated in Part b). In detail, since the hydraulic resistances upstream are designed to be almost similar, as well as the flow conditions and the droplet generation frequencies of both generators are also maintained during the experiment, it will be valid to assume that $Q_{m_1} = Q_{m_2}$ is equivalent. Additionally, droplets are assumed to follow the flows of each branch. Therefore, there are 2 possible scenarios (Figure C-2).

1. Designing the two side branches to be symmetrical, $R_{S_1} = R_{S_2}$, leads to equivalent flow rates in the two side branches, $Q_{m_1'} = Q_{m_2'}$. Thus, the droplets from both sides will arrive at the junction at the same time and fuse into each other before they enter the chamber (R_{mer}). (Figure C-2-1)
2. Designing the two side branches to be asymmetrical achieves alternating merging when the hydraulic resistance of one branch is slightly greater than that of the other, $R_{S_2} \leq R_{S_1} + R_{drop}$. At the beginning of a merging cycle, when both branches are filled with droplets, $R_{S_2} + 1R_{drop} \leq R_{S_1} + 2R_{drop}$,

- At the left note, $Q_{m_{1'}} = Q_{m_1} - Q_{ob}$ (1)
- At the right note, $Q_{m_2'} = Q_{m_2} + Q_{ob}$ (2)

Equations (1) & (2) lead to $Q_{m_{1'}} < Q_{m_{2'}}$, resulting in the droplet from the right branch, which follows $Q_{m_2'}$, moving faster than the ones from the left branch. Therefore, the right droplets will enter the chamber first and be partially trapped inside the pillar arrays (Figure C-2-2). Subsequently, when a droplet leaves the right branch, the resistance of the right branch can be described as $R_{S_2} < R_{S_1} + R_{drop}$. The oil keeps draining from the left branch to the right branch, increasing $Q_{m_2'}$so that another droplet staying in the right branch tends to move forward to where it has higher flow rate. Meanwhile, the first droplet, staying in the left branch, also moves forward and temporarily blocks the junction, inducing built-up pressure. Continuously, another droplet from the right branch comes and blocks the node right where the oil bridge and the main right channel meet. The flow in the oil bridge reverses its direction from right to left (Figure C-2-3). Now, the flow at the left branch increases through the addition of flow from the oil bridge (3), pushing remain droplets in the left branch to move forward until another coming droplet blocks a left node. A new merging cycle begins.

- At the left note, $Q_{m_{1'}} = Q_{m_1} + Q_{ob}$ (3)

- At the right note, $Q_{m_2'} = Q_{m_2} - Q_{ob}$ (4)

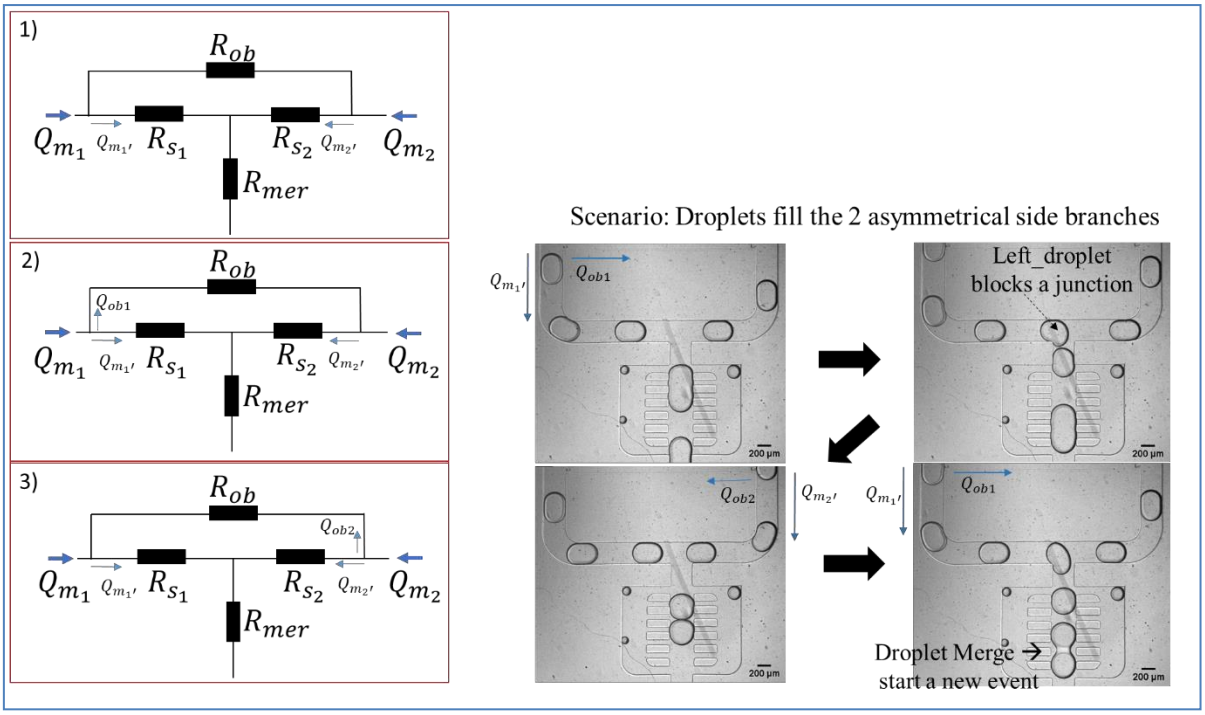

Figure C-2. The two scenarios show one-to-one droplet merging. (1) 2 side branches are symmetrical, (2) 2 side branches are asymmetrical

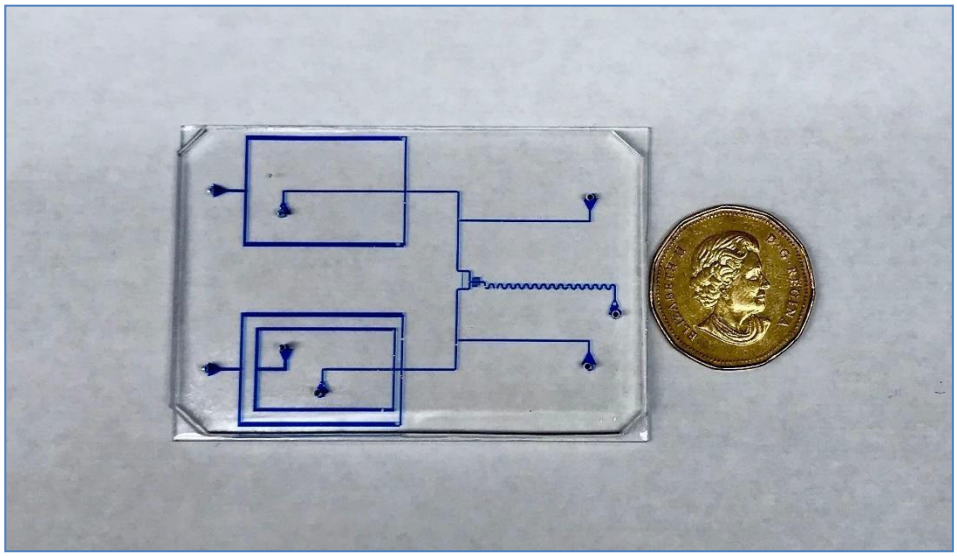

Figure C-3. The multifunctional droplet based microfluidic device fabricated using the standard soft-lithography technique and PDMS substrate

The similarities between the physical parameters used in microfluidics and electronic parameters, which are useful in electric circuit analysis, are presented in Table C-1.

Microfluidics	**Electronics**
Fluid molecules	Electrons
Flow of fluid	Flow of fluid
Volumetric flow rate $Q\ [\frac{m^3}{s}]$	Electric current $I[Amp]$
Pressure drop $\Delta P[Pa]$	Voltage drop $\Delta V[Volt]$
Hydraulic resistance $R_H = \frac{12\mu L}{wh^3}$ (for cases that w/h <1and for a rectangular channel)	Electric resistance $R = \frac{\rho . L}{A}$
Hagen-Poiseuille's law $\Delta P = Q.R_H$	Ohm's law $\Delta V = I.R$
Equivalent fluidic resistor in series $R_{eq} = R_{H_1} + R_{H_2} + \cdots.$	Equivalent electronic resistor in series $R_{eq} = R_1 + R_2 + \cdots.$
Equivalent fluidic resistor in parallel $1/R_{eq} = \frac{1}{R_{H_1}} + \frac{1}{R_{H_2}} + \cdots.$	Equivalent electronic resistor in parallel $1/R_{eq} = \frac{1}{R_1} + \frac{1}{R_2} + \cdots.$
Atmospheric pressure	Floating ground (GND)
Conservation of mass	Kirchhoff's current law
Conservation of energy	Kirchhoff's votage law in a closed path
Pressure division	Voltage division
Flow division	Current division

Table C-2. Physical similarities between microfluidics and electronics

Appendix D

Measurement R/G ratio by using ImageJ tool

Generally, the ratio-metric detection presented in Chapter 5 is achieved by detecting two detection color channels from digital images. In this work, the photoluminescence (PL) of gQDs and Cy3 are associated with the G and R channels. Each photosensitive element (pixel) is related to either a red, green, or blue filter to pass certain wavelengths, such as long, middle and short wavelengths of visible white light. A digital image, captured using an IPhone camera, is split into R-G-B color channels using ImageJ software (Figure D-1). A ratio of the mean PL intensity of the R channel to one of the G channel for a given spot is used to confirm optical transduction, which is based on the ratio metric detection requiring concurrent detection of two wavelength bands. The R/G ratio achieved using the simple method could also represent the FRET signal (Noor and Krull 2014). However, the automatic image contrast adjustments can potentially cause the reproducibility of digitization of the color intensity response. Therefore, firstly, to minimize the influences of the automatic exposure time, variations in the ambient light, a white balance of images, all images are captured in RAW format using the VSCO photography mobile app for iOS (Visual Supply Company, CA, USA). Furthermore, the distances between a UV light source and paper-based substrates are maintained, and all pictures are imaged in a dark room. Last but not least, the background of paper-based substrates is printed in black; thus, the control spots serves as the brightest spots in the field

of view. As a result, the imaging contrast adjustment also increases.

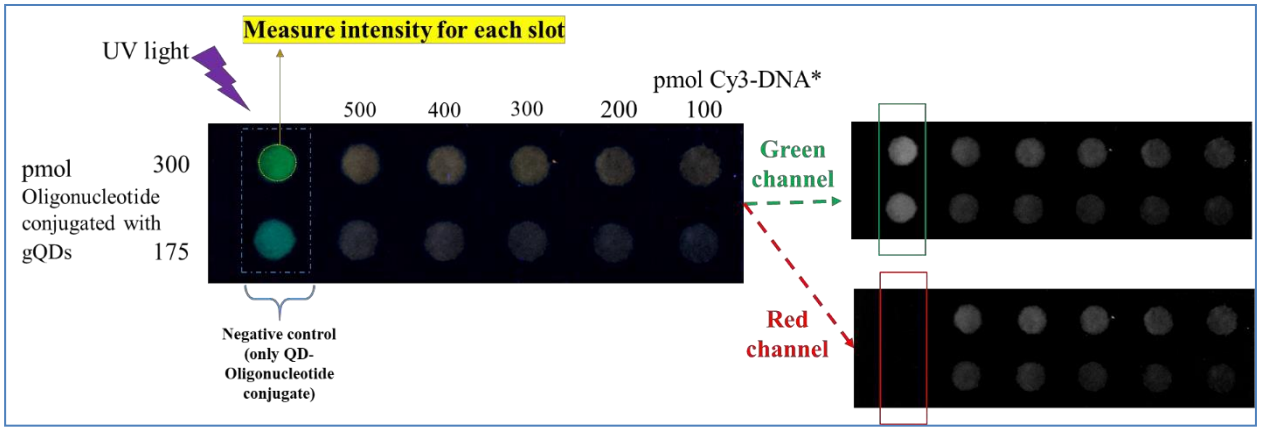

Figure D-1. The RGB photo is split into the G channel and R channel for image processing by using the imageJ software

Step-to-step to confirm optical transduction from a digital image:

1. Drop the same volume of QD-Oligonucleotide solution (1.5 μL) , release from the surfaces of MBs, to individual control spot on paper-based substrate.
2. Wait for 1 min before capturing image – initial stage: before FRET pair is created
3. Drop the same volume of Cy3-DNA* solution (1.5 μL) with different concentration to different control spots
4. Wait for 3 to 5 minutes for the hybridization – creating FRET pair between Cy3-DNA. During this time, the UV light is covered (although the light source is on).
5. Shine the UV light onto a paper-based substrate
6. Capture image – end stage: FRET pair created achieving optical transduction
7. Image processing:

   Process the initial stage to retrieve the $(\frac{R}{G})_D$

a. ImageJ (NIH, USA) is used and images (RAW format) are loaded.

b. Measure and record the mean intensity of the background of each control spot

c. Under the toolbar, choose Image > Color > Slit channel

d. Measure and record the mean intensity of each control spot corresponding to the R channel

e. Similarly, the mean intensity of G signal is achieved

f. Process the end stage to retrieve the $(\frac{R}{G})_{DA}$, follow all steps discussed above

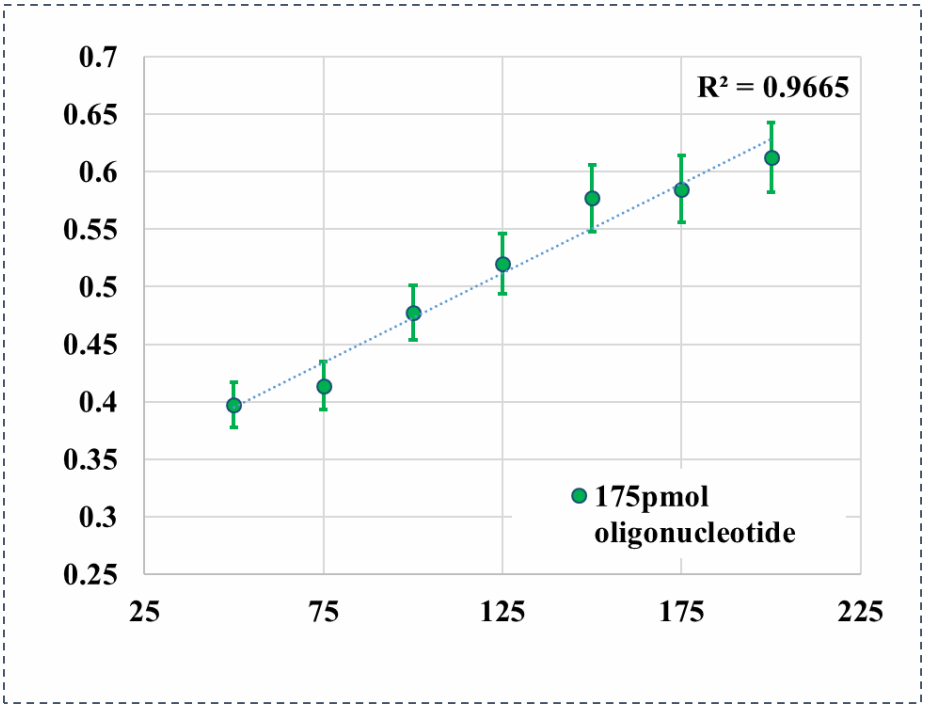

Figure D-2. The R/G ratio, the case that 175 pmol of oligonucleotide conjugating with QDs using this microfluidic platform, responses linearly in the presence of 50 pmol to 200 pmol Cy3-target DNA*.

Appendix E

Detail of merging chamber design

As discussed in the main text, the geometry of the merger has influenced the droplet fusion. The length of the chamber must be equal or larger than a merged droplet length (L_0), identified by the number of merger droplets (N = 2) multiplier of the input droplet length (L_d). Herein, the merger is evaluated using the ratio (BRR) between the total bypass flow resistance (R_{Bybass}) and the one of the mid-channel (R_c) where the droplets fuses. Since that ratio is proportional to the ratio of oil flowing through each branch, BRR must be smaller than 1 to ensure that a droplet will enter the central channel when it arrives at the chamber. In this work, the dimensionless of all parameters used to design a merger chamber are as follows:

$$L_p^* = \frac{L_p}{W} = 1;\ L_s^* = \frac{\mathrm{L_s}}{W} = 0.25; W_p^* = \frac{W_p}{W} = 0.33;$$

$$L_{relative}^* = \frac{L_d}{L_{chamber}};$$

$$BRR = \frac{R_{bypass}}{R_C} = \frac{R\left(h, S_p, L_p\right) + \frac{1}{2}(h, W_{bypass}, L_{chamber})}{R(h, W_c, L)}$$

where L_p is the length of each pillar, L_s is the spacing between each pillar, W_p is the width of each pillar, L_d is the length of each droplet before merging, W is the width of a main channel and h is the height of an entire microfluidic network.